

Single cell transcriptomic analysis reveals the impact of elevating neurogenic factor expression on human retinal organoid development

Xiangmei Zhang¹, Igor Mandric², Kevin H. Nguyen¹, Thao T. T. Nguyen¹, Matteo Pellegrini², James C. R. Grove¹, Steven Barnes^{1,3}, *Xian-Jie Yang^{1,4}

¹Department of Ophthalmology, Stein Eye Institute

²Department of Molecular, Cell, and Developmental Biology

³Doheny Eye Institute, ⁴Molecular Biology Institute,

University of California, Los Angeles, CA, USA

*Corresponding author: Xian-Jie Yang

Address: Stein Eye Institute
UCLA School of Medicine
100 Stein Plaza
Los Angeles, CA 90095, USA

Tel: 1-310-825-7020

Fax: 1-310-825-6992

Email: yang@jsei.ucla.edu

Running title:

Sc RNA-seq analysis of neurogenic factor function in human retinal organoids

Zhang, X. et al

Abstract

Multiple transcription factors containing the bHLH motif are expressed during retinogenesis. Their precise functions and interactions in uncommitted retinal progenitors remain to be fully elucidated. Here, we investigate the roles of bHLH factors in human ES cell-derived 3D retinal organoids by elevating ATOH7 and Neurog2 expression. Single cell transcriptome analyses identify three progenitor states in retinal organoids: neural stem cell-like, neurogenic, and cell cycle-exiting progenitors, which feed into a postmitotic neuroblast pool that gives rise to early born neuronal lineages. Both ATOH7 and Neurog2 accelerate the transition from the stem cell to the neurogenic state, expand the exiting progenitor and neuroblast populations, and significantly enhance retinal ganglion cell production. However, ATOH7 and Neurog2 differentially promote neuronal types with distinct molecular characteristics. Moreover, single cell transcriptome analyses reveal novel insight that ATOH7 and Neurog2 modulate an intricate interactive gene network, thus impacting the competence states and fate choices of uncommitted progenitors.

Introduction

As an integral component of the central nervous system, the vertebrate neural retina retains a highly conserved laminar structure that senses, processes, and delivers visual information to the brain. Classic cell birth dating and lineage tracing studies have established that the seven major neuronal cell types constituting the retinal network are generated in a temporal order from a common ocular progenitor pool during development¹⁻³. The ensuing research has ruled out a rigid deterministic cell fate specification mechanism, but instead supports a view that multipotent progenitors progressively evolve through different competence states to enable the sequential production of distinct cell types^{1,4}. Cumulative molecular genetic studies have uncovered important roles of cell intrinsic factors involved in retinal development⁵. Among these, transcription factors containing the basic helix-loop-helix (bHLH) motif have emerged as important players regulating the production and differentiation of various retinal cell types⁶. Multiple bHLH factors are expressed during retinogenesis either in proliferating progenitors or in postmitotic neurons; however, their dynamic regulation and function in specific cellular contexts remain to be fully elucidated.

The bHLH factors Atoh7 and Neurog2 are both expressed early in the developing retinal epithelium. Atoh7 plays a critical role in the development of an early born retinal neuronal type, the retinal ganglion cells (RGCs), which project axons through the optic nerve to multiple higher visual centers^{2,7}. Both Atoh7 and Neurog2 mRNAs are expressed by subsets of early retinal progenitors, with some co-expression at the protein level during certain time windows⁸⁻¹⁰. Loss of Atoh7 function in mouse, zebrafish, and humans results in a severe reduction of RGCs leading to a diminished optic nerve and blindness¹¹⁻¹⁵. Atoh7 deficiency also causes a minor abnormality in the production of cone photoreceptors, another early-born cell type in the retina¹¹. In contrast, genetic ablation of Neurog2 yields a transient stall of neurogenesis but without severe lasting deficits¹⁶. In the mouse retina, Atoh7 protein is not detected in fully differentiated RGCs^{9,10}, suggesting that its main biological activity is transiently required in uncommitted early progenitors. Ectopic expression of Atoh7 in different late stage retinal progenitors either redirects progenitors towards an RGC fate¹⁷ or fails to specify the RGC fate¹⁸. Therefore, Atoh7 is thought to confer a competent state of progenitors to adopt early cell fates¹⁹. In the absence of Atoh7, co-expression of two downstream transcription factors Islet1 and Pou4f2 is sufficient to rescue the RGC production deficit and ensure full execution of the RGC differentiation program in the mouse retina²⁰⁻²⁴. We have shown previously that viral mediated expression of human ATOH7 in the developing chicken retina results in precocious neurogenesis and a significant increase in RGC production²⁵, supporting a hypothesis that a critically high threshold of ATOH7 expression triggers uncommitted early progenitors to exit the cell cycle and predominantly adopt the RGC fate²⁶.

In the human retina, RGC development occurs during the first trimester and remains a minor cell population in the mature retina²⁷⁻²⁹. This scarcity of human RGCs has hindered research on human RGC development as well as blinding diseases caused by RGC loss. The advancements of pluripotent stem cell technologies in the preceding decade have led to robust stem cell based retinal organoid culture systems³⁰⁻³³, which provide an excellent opportunity to produce and study human RGCs in vitro. A series of recent studies have applied powerful single cell transcriptomic analyses to characterize the molecular features of cell types in the mature retina and to analyze developmental processes of mammalian, including human retinas³⁴⁻³⁹. In this study, we have used human embryonic stem cell (ESC)-derived 3D retinal organoids to test whether elevating ATOH7 expression levels enhances human RGC production. In addition, we have performed single cell transcriptomic analysis to investigate the effects of modulating neurogenic factor ATOH7 and Neurog2 expression levels on early human retinogenesis. Results of this study further validate that expression levels of these neurogenic factors critically impact human retinal cell production. Moreover, our findings provide new insights into the

Zhang, X. et al

function of ATOH7 and Neurog2 in uncommitted progenitors to modulate an interactive gene network that plays important roles during cell cycle withdrawal and cell fate determination.

Results

Viral mediated bHLH factor expression affects progenitor proliferation in 3D human retinal organoids.

To investigate the roles of bHLH neurogenic factors during development of the human retina, we established H9 embryonic stem cell (ESC)-derived 3D retinal organoid cultures^{30,40}. These human retinal organoids showed typical morphology of the retinal neural epithelium and co-expressed PAX6 and VSX2 transcription factors (Supplementary Fig. 1), a characteristic feature specific to retinal progenitors. To regulate gene expression during retinogenesis, we constructed lentiviral vectors that encode the doxycycline (Dox) inducible TetO promoter upstream of the human ATOH7 cDNA fused with the Flag epitope tag (LV-ATOH7f) or co-expressing EGFP and puromycin resistant genes (LV-AEP) (Fig. 1a). We also produced a previously described lentiviral TetO vector co-expressing the mouse Neurog2, EGFP, and puromycin resistant genes (LV-NEP)⁴¹(Fig. 1a). Immunohistochemistry confirmed Dox-induced bHLH protein expression following in vitro co-infections of H9 ESCs with LV-rtTA and either LV-ATOH7f, LV-AEP, or LV-NEP (Fig. 1b). We next carried out co-infection of retinal organoids with LV-rtTA and either LV-AEP or LV-NEP at the onset of retinogenesis followed by Dox inductions (Fig. 1c). Live imaging of the EGFP reporter showed that at 24 hours post Dox induction, significant numbers of LV-AEP or LV-NEP infected cells had already migrated towards the inner retina compared to cells from the control LV-GFP infected organoids. This trend continued and became more obvious as the Dox induction times lengthened (Supplementary Fig. 2). By 6-days after Dox induction, the majority of LV-AEP and LV-NEP infected cells were located in the inner layer of the organoids (Fig. 1d, 1e), indicating that viral mediated ATOH7 and Neurog2 expression impacted retinal organoid development.

To investigate whether virally expressed bHLH factors affected retinal progenitor proliferation, we performed BrdU pulse-labeling and examined progenitor marker expression by immunohistochemistry. In the control LV-GFP infected retinal organoids, BrdU-labeled and the proliferating cell nuclear antigen (PCNA)-labeled progenitors occupied the ventricular zone, whereas phospho-histone 3 (PH3) labeled M phase cells were detected at the ventricular surface of the organoids (Fig. 2a, 2b, 2c). Furthermore, PCNA showed co-labeling with PAX6-expressing progenitors in the ventricular zone, but was absent from the PAX6⁺ cells located in the inner layer, where postmitotic POU4F⁺ RGCs resided (Fig. 2b, 2c). In contrast to LV-GFP infected retinal organoids, in which GFP⁺ cells were distributed throughout the neural epithelium, the majority of GFP⁺ cells in LV-AEP and LV-NEP infected organoids were located in the inner retinal layer and devoid of co-labeling with BrdU or PCNA (Fig. 2d, 2e). Quantification of dissociated retinal organoids confirmed that percentages of GFP⁺PCNA⁺ double labeled cells were reduced significantly from 52.7 ± 8.0 % for LV-GFP infection to 9.0 ± 3.8 % and 2.0 ± 1.9 % for LV-AEP and LV-NEP infections, respectively (Fig. 2f). These results demonstrate that viral driven ATOH7 or Neurog2 expression promoted cell cycle exit.

Elevated neurogenic factor expression promotes RGC production in 3D retinal organoids.

The retinal projection neurons (RGCs) are among the earliest neuronal cells produced during retinogenesis^{2,28}. In our human retinal organoid cultures, RGC genesis was detected as early as Day 25 and continued through Day 60 (Fig. 2c). By Day 40, retinal organoid-derived neurons exhibited voltage-gated Na⁺, K⁺ and Ca²⁺ channels as well as spontaneous and provoked electrophysiological excitability in vitro during whole cell patch clamp recording, characteristic of native RGCs (Supplementary Fig. 3). TTX-sensitive Na⁺ channels, TEA-sensitive K⁺ channels, and Cd²⁺-sensitive Ca²⁺ channel currents were recorded. Average Na⁺ current amplitude was 219 ± 76 pA (n=12) but in cells with large Na⁺ currents (~1

Zhang, X. et al

nA), multiple action potentials were observed, while cells expressing smaller Na⁺ currents (200-400 pA) typically produced a single spike. Average K⁺ current amplitude at +40 mV was 438 ± 49 pA (n=40).

To determine whether viral mediated ATOH7 or Neurog2 expression promoted RGC production, we performed immunohistochemical analyses of retinal organoid sections using known RGC markers (Fig. 3). In LV-ATOH7f infected retinal organoids, signals of the viral reporter Flag closely correlated with POU4F-expressing RGCs in the inner retina as detected by a pan-POU4F/BRN3 antibody (Fig. 3a). Compared to control LV-GFP infected organoids, both LV-AEP and LV-NEP infected cells showed increased co-labeling with the RGC markers NF145, NeuN, and DCX in the inner retina (Fig. 3b). Similarly, in attached organoid cultures that displayed extensive neurite outgrowth, the ATOH7f-expressing cells showed extensive co-labeling for the RGC markers POU4F, NF145, and RBPMs (Fig. 4a).

We also performed flow cytometry analyses of dissociated retinal organoid cells to quantify the effects of viral mediated ATOH7 or Neurog2 expression on RGC genesis (Fig. 4b, 4c, 4d). After 4 days of Dox induction at Day 39, ATOH7 expression led to a 2-fold increase of POU4F⁺ cells, from 6.6 ± 0.68 % of total cells in LV-GFP infected organoids to 13.7 ± 0.59 % of total cells in LV-ATOH7f infected organoids (Fig. 4c). Among LV-ATOH7f infected cells, 57.1 ± 1.9 % were POU4F⁺ compared to 6.1 ± 1.1 % among LV-GFP infected cells (Fig. 4d). However, LV-ATOH7f did not increase expression of the RGC marker ISLET1 at this stage (Fig. 4c). In the parallel analysis, LV-NEP infection did not significantly promote POU4F⁺ cells, but instead increased ISLET⁺ cells from 5.9 ± 0.95 % to 11.1 ± 0.89 % of total cells (Fig. 4c), and from 4.4 ± 1.1 % to 18.4 ± 1.6 % among viral infected cells (Fig. 4d). Similar analyses at Day 47 following a 7-day Dox induction showed significantly increased co-labeling with the RGC markers ISLET1 (> 10-fold of 6.3%), DCX (>4-fold of 21%), and NeuN (>20-fold of 4%) of LV-AEP and LV-NEP infected cells compared with the control LV-GFP infected cells (Fig. 4e). These results demonstrate that elevated ATOH7 or Neurog2 expression promoted human RGC production in retinal organoids.

Single cell RNA-sequencing analysis reveals accelerated neurogenesis.

To elucidate the influences asserted by viral driven ATOH7 and Neurog2 expression on transcriptome, we performed single cell RNA-sequencing (sc RNA-seq) analysis. We first used fluorescent activated cell sorting to enrich for LV-GFP, LV-AEP, and LV-NEP infected retinal organoid cells between Day 45 to Day 48 (Supplementary Fig.4), followed by 10X Genomics automated single-cell capture, mRNA barcoding, and cDNA library preparation. The high throughput DNA sequencing resulted in 192,932, 153,154, and 132,651 mean readings per cell for LV-GFP, LV-AEP, and LV-NEP samples, respectively. After aligning to the reference human genome and eliminating poor quality cells, the final single cell datasets had a mean gene range between 2935-3079 per cell, and consisted of 3004 cells for LV-GFP, 2063 cells for LV-AEP, and 3909 cells for LV-NEP infected samples.

The sc RNA-seq datasets were subjected to Seurat cell clustering analysis ⁴², which resolved into 12-15 clusters, and visualized as 2-dimensional UMAPs (Fig. 5a). We applied dot plot analysis using known genes to assign various cell clusters into seven categories or states; each was represented with one or two highly or uniquely expressed genes (Fig.5b; Supplementary Fig. 5). The neural stem cell, neurogenic progenitor, and cell cycle-exiting progenitor categories all expressed CCDN1, encoding cyclin D1, indicating that they all belonged to proliferative cells. However, the neural stem cell clusters showed distinctively high levels of PLOD2 transcripts (procollagen-lysine,2-oxoglutarate 5-dioxygenase 2), whereas the exiting progenitors exhibited upregulation of GADD45A (growth arrest and DNA damage inducible alpha) and downregulation of the retinal progenitor marker VSX2. The exiting progenitors and postmitotic neuroblasts were the main populations expressing ATOH7 mRNA (see Fig. 9). Markers identifying the early born retinal neuronal types included ISL1 and POU4F2 for RGCs, CRX and RCVRN for photoreceptors, and PRDM13 and TFAP2A for horizontal and amacrine cells (HC/AC) (Fig. 5b; Supplementary Fig. 5). These sc RNA-seq analyses thus not only allowed identification of the early

Zhang, X. et al

postmitotic neuronal types in the human retinal organoids at the time of analysis, but also revealed subclasses of neural progenitors with distinct molecular signatures, and transitional states including cell cycle exiting progenitors and postmitotic neuroblasts.

Next, we combined different cell clusters assigned to each of the seven cell categories (Fig. 6a) and performed a pseudotime trajectory analysis (Fig. 6b). Without defining the starting and ending points, the trajectory of LV-GFP infected cells revealed that the neural stem cells were closely related to the neurogenic progenitors, which in turn produced exiting progenitors that developed into the postmitotic neuroblasts and a single trajectory including three types of retinal neurons. In both LV-AEP and LV-NEP infected samples, the pseudotime trajectory displayed a more clearly defined progression from the neurogenic progenitors toward the exiting progenitors, which in turn gave rise to neuroblasts. The postmitotic neuroblasts showed a single node for bifurcated trajectories separating the RGC and HC/AC branch from the photoreceptor branch (Fig. 6b). Quantification of the different cell categories/states further demonstrated that LV-AEP and LV-NEP infection significantly reduced the percentage cells in the neural stem cell category from 25.2 % to less than 4% (Fig. 6c). Neurog2 expression also caused a significant reduction of neurogenic progenitors from 45 % to 26.9 %. Concomitantly, ATOH7f and Neurog2 induction increased the percentage of exiting progenitors from 2.2 % to 4.5 % as well as the percentage of neuroblasts from 5.0 % to 14.9 % and 20.2 %, respectively. Moreover, consistent with marker analysis, elevated ATOH7f and Neurog2 expression resulted in increased proportion of RGCs from 7.0 % to 22.1 % and 27.7 % of total cells, respectively (Fig. 6c). Interestingly, Neurog2, but not ATOH7f, enhanced the photoreceptor population from 3.4 % to 9.8 %; whereas ATOH7f, but not Neurog2, promoted HC/AC proportions from 3.1 % to 4.6 %; (Fig. 6c). These sc RNA-seq data demonstrated that elevating ATOH7f and Neurog2 expression promoted transitions from the pre-neurogenic to the neurogenic state and enhanced neurogenesis of early retinal cell types in retinal organoids.

Neurogenic factors promote transitions of distinct developmental states.

Since viral mediated expression of ATOH7 and Neurog2 affected transitions between developmental states, we explored the key characteristics of each cell state. We compiled differentially expressed genes (DEGs, adjusted p values <0.05) of each cell category for LV-GFP, LV-AEP and LV-NEP samples (Supplement Tables 1-3), and constructed heatmaps for the top 10 DEGs displaying more than Log 1.5-fold change of expression levels (Fig. 7a) (Supplement Tables 4-6). In the control LV-GFP infected sample, the top 10 DEGs in the neural stem cell category included SLC2A1, encoding glucose transporter protein type 1 (GLUT1), and GPI, glucose-6 phosphate isomerase, and were quite distinct from those of the neurogenic progenitors. In LV-AEP and LV-NEP infected retinal organoids, the neural stem cells were not only reduced, but also shared genes, such as SFRP2, IFITM3, and VIM with the neurogenic progenitors. In all three virus infected samples, the exiting progenitors shared top DEGs, including HES6, a suppressor of HES1⁴³, and HMGB2, a member of the chromosomal high mobility group of proteins⁴⁴, indicating common processes involved in cell cycle exit. The heatmaps also revealed that neuroblasts in each virus infected sample expressed some genes associated with the RGC, photoreceptor, and HC/AC cell lineages, suggesting that the newly postmitotic neuroblasts were poised at an intermediate developmental state and in the process of committing to specific cell fates.

To further decipher the changes of gene expression and the key biological processes that occur during normal developmental transitions, we constructed volcano plots (Fig. 7b) and performed gene ontology (GO) analyses (Fig. 7c) using significant DEGs from the LV-GFP infected cell categories. The neural stem cell state was associated with higher levels of transcripts for several glycolytic pathway enzymes such as SLC2A1, GPI, ENO1, and PGK1, as well as low levels of mitochondrial respiratory chain components and proteins required for rapid cell proliferation such as PCNA and TOP2A (Fig. 7b). This

Zhang, X. et al

was consistent with the dominant GO pathways for the neural stem cell state (Fig. 7c). In contrast, cells in the neurogenic progenitor state expressed high levels of SFRP2, FGF19, and SOX2 (Fig. 7b), correlating with the biological responses to growth stimulation and the mitotic cell cycle (Fig. 7c). The dominant GO terms associated with the exiting progenitors included cell cycle arrest and Notch signaling (Fig. 7c). The exiting progenitor to neuroblast transition was marked by elevated expression of the Notch signaling inhibitor HES6 and the antiproliferation factors BTG1⁴⁵, BTG2, and GADD45A⁴⁶ (Fig. 7b), consistent with the GO pathway analysis (Fig. 7c). The predominant GO pathways for the three neuronal types reflected their phenotypic differentiation with high axonal growth and light transduction processes associated with RGCs and photoreceptors, respectively (Fig. 7c).

ATOH7 and Neurog2 assert differential effects on cell cycle and neuronal differentiation.

To examine the potential impact of neurogenic factor expression on the cell cycle, we combined the LV-GFP, LV-AEP, and LV-NEP sc-RNA-seq datasets and carried out Seurat cell clustering analysis (Fig. 8a). Based on feature plots of known genes (Supplementary Fig. 6), cell clusters in the combined UMAP were identified as distinct cell categories. Furthermore, the progenitor cell clusters were assigned to different phases of the cell cycle (Fig. 8a) based on known functions of cell cycle genes, including CDK2 associated with G1/S phase⁴⁷, MCM4 as a DNA replication licensing factor⁴⁸, CCNB2 encoding M phase cyclin B2⁴⁹, and PLK1 involved in spindle assembly and cytokinesis⁵⁰ (Supplementary Fig. 6). Slingshot analysis performed for the combined dataset illustrated the developmental trajectory of cell clusters from the neural stem cell state through the different phases of the cell cycle toward cell cycle exit (Fig. 8a). Although cell clusters 5 and 6 both expressed M phase genes, they clearly had distinct transcript profiles since cluster 6 was poised to exit the cell cycle (Fig. 8a). As expected, individual UMAPs of ATOH7 and Neurog2 infected samples displayed significantly reduced neural stem cell populations (Fig. 8b; Fig. 6c). In addition, quantitative analyses showed that ATOH7 and Neurog2 infection altered cell cycle distributions among progenitors compared to controls (Fig. 8c). For example, LV-AEP increased G1 distribution by 5 % while decreasing S phase cells by 3.7 %, whereas LV-NEP caused a 7 % S phase cell reduction and a 4.5% increase of M phase cells, which included the exiting progenitors (Fig. 8c).

The Slingshot analysis demonstrated that the postmitotic neuroblast pool, cluster 7, served as the root source giving rise to three neuronal cell lineages (Fig. 8a). Interestingly, UMAPs of individual virus infected retinal organoids revealed differential effects of ATOH7 and Neurog2 on neuronal fate specification. ATOH7 elevation resulted in clear enhancement of the RGC cluster 8, without affecting the photoreceptor cluster 10 (Fig. 8b, also see Fig. 6c). In contrast, Neurog2 overexpression not only significantly enhanced the production of photoreceptor cluster 10 and RGC cluster 8, but also generated a distinct RGC cluster 9, which was largely absent in LV-GFP and LV-AEP infected retinal organoids (Fig. 8b, also see Fig. 6c). Comparison analyses revealed that the two RGC clusters consisted of cells with differential gene expression levels. For example, GAP43 and NSG1 were expressed by cells in both clusters, however, they were frequently detected at higher levels in cluster 8 (Fig. 8d, 8e). Although both clusters expressed ISL1 and POU4F2 (Supplementary Fig. 6), we often observed lower levels of POU4F2 and SNCG in many cluster 9 cells (Fig. 8d). These results suggest that ATOH7 and Neurog2 might differentially influence neuroblast fate specification and/or neuronal differentiation.

Neurogenic factors modulate early retinal gene network.

Next, we examined the effects of viral mediated ATOH7f and Neurog2 elevation on endogenous bHLH gene expression. Since the lentiviral vectors did not contain poly-A sequences associated with ATOH7 and Neurog2 cDNAs, and the single cell cDNA libraries were constructed using oligo dT priming, we were able to analyze expression of the endogenous genes using the sc RNA-seq datasets, while

Zhang, X. et al

excluding genes encoded by the viruses. We first examined expression of ASCL1, an early onset bHLH neurogenic factor. Consistent with previous studies^{34,36}, feature plots showed that ASCL1 was predominantly expressed in neural stem cells and progenitors (Fig. 9a). Viral mediated ATOH7f and Neurog2 expression resulted in significant reduction of ASCL1⁺ cell from 29.7 % to 17.1 % and 13.2 %, respectively (Fig. 9c); but neither affected the median levels of ASCL1 expression (Fig. 9b). In retinal organoids, ATOH7 and NEUROG2 were detected in exiting progenitors, neuroblasts, and some postmitotic neurons (Fig. 9a). Both virally expressed ATOH7f and Neurog2 increased the number of endogenous ATOH7-expressing cells from 9.1 % to 22.0 % among total cells (Fig. 9c), and LV-NEP infection also increased the median ATOH7 expression level (Fig. 9b). Interestingly, LV-NEP but not LV-AEP infection caused a 2-fold increase of endogenous NEUROG2-expressing cells as well as elevated the median expression level (Fig. 9b, 9c), suggesting that Neurog2 positively regulates endogenous NEUROG 2. In addition, elevated levels of ATOH7f and Neurog2 both correlated with the increased percentages of cells expressing OLIG2, another bHLH gene in retinal organoids⁵¹ (Fig. 9c).

In addition to ASCL1, ATOH7, NEUROG2, and OLIG2, sc RNA-seq analysis identified additional Notch signaling pathway genes and bHLH genes affected by ATOH7f and Neurog2 expression (Supplementary Table 1-3; Supplementary Fig. 7). Violin plots and quantification showed that the Notch ligands DLL1 and DLL4 were upregulated, especially by Neurog2 (Fig. 9d, 9e). In addition, the percentage of cells expressing the Notch signaling effector HES1 was significantly reduced compared to the control LV-GFP infected cells (Fig. 9e), while changes in median expression levels were mild (Fig. 9d). In contrast, not only the percentages of HES6 and HEY1 expressing cells were increased (Fig. 9e), the median HES6 expression levels were significantly elevated by bot LV-AEP and LV-NEP (Fig. 9d). Since HES1 was predominantly expressed by progenitors, whereas HES6 and HEY1 were upregulated in exiting progenitors and neuroblasts (Supplementary Fig. 7), these changes reflected the trend of enhanced neurogenesis. Data from sc RNA-seq also showed that viral expression of ATOH7f or Neurog2 caused substantial increases of several bHLH genes involved in neuronal fate specification or differentiation, including NEUROD1, NEUROD4, NHLH1 and NHLH2 (Fig. 9d, 9e; Supplementary Fig. 7). In all cases, elevated Neurog2 strongly impacted both the number of cells expressing these genes as well as their expression levels.

Together, these results suggested that viral mediated ATOH7f and Neurog2 expression in the developing retinal organoids affected an interactive gene network. We therefore performed STRING network analysis by inputting bHLH genes and a few selected genes known to be involved in RGC development. The resulting network model included previously reported molecular interactions as well as novel regulatory relationships revealed in this study (Fig. 9f). We also summarize the observed temporal progression of gene expression as retinal organoid cells advanced through the developmental states as defined by sc RNA-seq analysis (Fig. 9g).

Discussion

In this study we have used human ESC-derived organoid cultures as a model system to investigate embryonic retinal development. The 3D retinal organoids retain the unique molecular signature and correct tissue polarity of the embryonic retinal epithelium *in vivo*, and generate the expected early retinal cell lineages and functional neurons. By transducing human retinal organoids with inducible viral vectors, we were able to determine whether elevating ATOH7 or Neurog2 affected neuronal production, and examine the biological processes and the gene network involving these neurogenic factors.

We have identified three classes of retinal progenitors by performing single cell transcriptome analysis. The neural stem cells express PAX6, VSX2, LHX2, and SOX2, and thus clearly possess the

Zhang, X. et al

identity of the retinal primordium. Their main GO pathways show cellular metabolic characteristics common to stem cells⁵², with prominently featured DEGs of the glycolytic pathway, including SLC2A1, GPI, PGK1, and PLOD2, and low mitochondrial respiratory chain genes. This state likely represents a naïve pre-neurogenic status found in the retinal primordium before the onset of neurogenesis or later at the ciliary margin of the retina. These neural stem cells express cyclin D1, but have relatively low levels of PCNA and TOP2A, suggesting that they might be slow cycling cells. The neural stem cell category was significantly reduced in LV-AEP and LV-NEP transduced retinal organoids, indicating that expression of these neurogenic factors promotes the transition from the pre-neurogenic to the neurogenic state. This finding is consistent with our previous observation in the chicken retina, where ectopic ATOH7 expression in the pre-neurogenic peripheral retina induces precocious neurogenesis ahead of the neurogenic wave front²⁵. These results indicate that the onset of neurogenic factor expression among naïve retinal progenitors can trigger or accelerate the transition into a neurogenic state in the context of the ocular primordium. Noticeably, the transition from the stem cell state to the neurogenic state is also accompanied by upregulation of the chromosomal high mobility group genes, such as HMGB2 and HMGN2, reflecting the underlying epigenetic changes accompanying this transition.

Our sc RNA-seq analysis also identified a distinct progenitor state among the proliferating neurogenic progenitor population, the cell cycle exiting progenitors. This group of cells still express the characteristic M phase genes such as CDC20 that interacts with the mitosis complex, and MZT1 and PLK1 which organize the mitotic spindles. However, the exiting progenitors show significant upregulation of the Notch ligands DLL1 and DLL4, as well as the bHLH genes ATOH7 and NEUROD1. Both viral mediated ATOH7 and Neurog2 elevation caused expansion of the exiting progenitor state. The developmental trajectory analysis points to a progression from the exiting progenitors to the postmitotic neuroblasts, which exhibit a transcriptome profile partially overlapping with all three early neuronal lineages, including VSX1, NHLH1, ATOH7, ONECUT2, NEUROD1, and the growth arrest gene GADD45A. Thus, the neuroblasts appear to serve as a transitional cell pool poised for terminal cell fate choices and differentiation. Interestingly, we have observed that relative to ATOH7, elevating Neurog2 asserted more potent effects in promoting cell cycle withdrawal, neuroblast expansion, and neuronal differentiation in retinal organoids.

Among the early bHLH factors detected by sc RNA-seq in retinal organoids, a higher percentage of cells expressed ATOH7 (9%) than NEUROG2 (3.2%) endogenously. Although elevating either ATOH7 or Neurog2 caused enhanced neurogenesis, we also detected differential effects of these two factors. For example, at Day 39, ATOH7 promoted POU4F⁺ cells, whereas Neurog2 increased ISL1⁺ cells; but both factors enhanced ISL1⁺ cells by Day 47. Furthermore, the RGC cluster enhanced by ATOH7 elevation shared transcriptomic signatures with RGCs from the control organoids. In contrast, Neurog2 induction promoted two distinct groups of RGCs, but only one of the two matched the expression profile of RGCs in the control organoids. Further analyses showed that although both RGC groups expressed ISLET1 and POU4F2, they exhibited different levels of known RGC markers such as SNCG, POU4F2, and GAP43. The promotion of the two RGC subtypes may reflect the more potent neurogenic effect of Neurog2, which might have accelerated the RGC differentiation program to acquire additional subtype features. In addition, the effect of elevated Neurog2 to induce ISL1⁺ neurons preferentially earlier on may also influence outcomes of neuronal differentiation. Alternatively, the viral induced exogenous Neurog2 could have promoted the production of a hybrid neuronal cell type, which does not naturally occur during retinogenesis. Future research using long term cultures may provide data to address these possibilities. In addition to the RGC phenotypes, ATOH7 increased the HA/AC lineage without impacting cone photoreceptor genesis, consistent with the developmental trajectory. In contrast, Neurog2 significantly enhanced photoreceptor production without affecting the HC/AC lineage, likely reflecting the effect of Neurog2 induced NEUROD1 upregulation.

Zhang, X. et al

Expression of cell intrinsic factors can be profoundly influenced by extrinsic signaling events during neural development⁵³. Notch mediated cell-to-cell signaling plays important roles during retinogenesis, and disruption of Notch signaling can influence RGC and cone photoreceptor development^{6,54-57}. In addition, differentiated RGCs have been shown to produce secreted signals that modulate progenitor behaviors. Among the signaling molecules released by differentiated RGCs are Shh, GDF11, and VEGF, all of which promote retinal progenitor proliferation while simultaneously suppressing RGC production⁵⁸⁻⁶¹. Accumulating evidence indicate that the Notch signaling downstream effector Hes1 may serve as an important integration node for distinct signaling pathways that converge upon retinal progenitors to influence cell proliferation and control neurogenesis. Hes1 is known to directly control cell proliferation by repressing the CDK inhibitor p27(Kip1)⁴³. The negative feedback of extrinsic signals on RGC genesis is in part mediated by Hes1 suppression of ATOH7⁶²⁻⁶⁴. At the present time, the temporal expression sequence and the complex regulatory relationships among the various early bHLH factors in the retina are not fully understood but their elucidation is likely crucial for a better understanding of cell fate selection and the progressive changes in progenitor competent states. The single cell RNA-seq technology has provided a tool to decipher gene regulatory networks at the transcription level on a global scale.

As demonstrated by sc RNA-seq data, HES1 is predominantly expressed by neural stem cells and neurogenic progenitors, and is down regulated among exiting progenitors. The sc RNA-seq data also show that ASCL1 is present at low levels in retinal organoid neural stem cells, and is mainly expressed by neurogenic progenitors, suggesting that it could play a role in establishing competence for the neurogenic state. This is consistent with the potent regeneration effects of ASCL1 in mature retinal Muller glial cells which promote reentry into the cell cycle and the generation of new neurons⁶⁵⁻⁶⁷. Intriguingly, viral mediated ATOH7 and Neurog2 expression decrease both HES1 and ASCL1 expression. Concomitantly, ATOH7 and Neurog2 significantly upregulate the expression of the HES1 inhibitor HES6⁴³ among exiting progenitors. Interestingly, Atoh7 has been shown to promote another Notch effector Hes5.3^{68,69}. These data suggest that ATOH7 and NEUROG2 comprise a select group of neurogenic factors that can dampen the positive effect of HES1 on cell proliferation and relieve the inhibitory effect of HES1 on neurogenesis. Moreover, viral mediated ATOH7 and Neurog2 expression significantly increase NEUROD1, which initiates its expression in exiting progenitors, as well as several other factors including NEUROD4, NHLH1 and NHLH4, which are expressed predominantly by postmitotic neurons. We summarize our analysis of these newly uncovered regulatory relationships together with previously validated data in a gene network model focusing on RGC development (Fig. 9f, 9g). Future investigations are necessary to determine whether the regulatory effects asserted by ATOH7 and Neurog2 are direct or indirect, and if the gene network is indeed interactive as proposed.

Expression of the HES1 gene in developing cortical progenitors is oscillatory due to autorepression by its own product, and as a consequence, the levels of its target Neurog2 also oscillate in cortical progenitors⁷⁰⁻⁷³. However, it has not yet been demonstrated if autorepression induced HES1 oscillations occur in the developing retina, and the modes of regulation between HES1 and bHLH neurogenic genes in the retina remain largely unknown. Results from this study support the hypothesis that high levels of ATOH7 or NEUROG2 trigger a withdrawal from the cell cycle which leads to the birth of a neuroblast. Critical questions remain regarding how the level of ATOH7 is regulated in neurogenic progenitors to result in a stochastic expression pattern. It has been shown that the ATOH7 gene contains enhancers that mediate direct positive regulation by Pax6⁷⁴. In Hes1 mutants, Atoh7 is precociously expressed along with the formation of RGC and HC/AC⁷⁵, supporting that Hes1 negatively regulates Atoh7 expression. Our sc RNA-seq analysis reveals that viral mediated ATOH7 expression elevates endogenous ATOH7 without affecting endogenous NEUROG2 expression, whereas Neurog2 induction leads to increases in both ATOH7 and NEUROG2 expression. These results suggest positive

Zhang, X. et al

autoregulation of ATOH7 and NEUROG2, as well as cross-regulation of ATOH7 by NEUROG2. This conclusion is consistent with previous reports that suggest cross regulation between Atoh7 and Neurog2^{16,76}. Since only a fraction of ATOH7 protein expressing cells appear to co-express Neurog2 protein during a given window of time⁹, progenitors that have coincidental expression of both factors are more likely to reach or exceed a threshold level of Atoh7, which may effectively counteract the negative impact of Notch and secreted signals, and lead to a terminal cell division and neurogenic event. We therefore propose that integrated cell extrinsic signals and interacting cell-intrinsic factors could converge, resulting in stochastic expression of the ATOH7 gene, and thus enabling a limited subset of progenitors that have reached this threshold to exit the cell cycle and initiate downstream RGC and/or cone photoreceptor differentiation programs. Similar explanations can be extended to the observed stochastic expression patterns of multiple neurogenic bHLH factors among neurogenic progenitors^{77,78}. The sc RNA-seq approach enables us to survey multiple genes simultaneously, thus allowing us to construct a gene regulatory network model (Fig. 9f) that integrates previous findings and can be further interrogated. This model focuses on bHLH factors expressed during early retinogenesis, but does not exclude other genes involved in the developmental process. In fact, RGC and other neuronal fate determinations are known to be regulated by multiple transcription factors⁷⁹⁻⁸⁵, which together coordinate epigenetic changes and orchestrate transcriptomic responses required for neuronal differentiation.

In summary, we have shown that elevating neurogenic factor expression in ESC-derived retinal organoids significantly enhances retinogenesis, which can serve as a useful approach to produce authentic human RGCs for studying development and degenerative diseases. Our single cell transcriptome analysis provides novel insights into the interactive network of neurogenic factors and their functions during human retinogenesis.

Materials and Methods

Lentiviral construction and production

The inducible lentiviral vector plasmids LV-GFP and LV-NEP (YS-TetO-FUW-Ng2-P2A-EGFP-T2A-Puro) were generous gifts from Dr. Thomas Sudhof⁴¹. The human ATOH7 cDNA was obtained as described previously²⁵. The LV-ATOH7f vector was constructed by replacing the EGFP gene in the LV-GFP vector with ATOH7 cDNA fused to the Flag epitope tag at the c-terminus. The LV-AEP vector was constructed by custom synthesizing the continuous open reading frame of ATOH7f-P2A-EGFP-T2A-Puro by GenScript, and replacing the EGFP gene in the LV-GFP vector. All lentiviral vector plasmids were verified by DNA sequencing. The LV-rtTA lentiviral vector (FUW-M2rtTA) with the Ubi promoter was obtained from AddGene (Plasmid #20342).

Lentiviral stocks were produced by co-transfection of HEK 293T cells with a given viral vector DNA and the third-generation lentiviral helper plasmids with VSVG pseudotyping as described⁸⁶⁻⁸⁸. The 293T cell medium DMEM containing 10% fetal bovine serum (SigmaAldrich, 12103C) was changed to serum free CD293 (ThermoFisher, 11913) one day post transfection, and viral supernatants were harvested every 24 hours. Combined viral stocks were concentrated by ultracentrifugation as previously described⁸⁸.

Human retinal organoid derivation

Human H9 ES cells were cultured and passaged on Matrigel (Corning, 356231) coated dishes in mTeSR1 medium (Stemcell Technologies, 05850). Retinal organoids were generated based on a previously described protocol³⁰ with modifications. At the start of the culture (Day 0), H9 ES cells (at 80-90% confluence) were enzymatic detached using dispase (1 mg/ml, Stemcell Technologies, 07923).

Zhang, X. et al

Detached cells were transferred into medium at 3:1 ratio of mTeSR1 to Neural Induction Medium (NIM) that consists of DMEM/F12 with 1x N2 supplement (ThermoFisher, 17502048), 1x non-essential amino acid (NEAA; ThermoFisher, 11140050), 2 µg/ml Heparin (ThermoFisher, H7482), and 1x Antibiotic-Antimycotic (Anti-Anti; ThermoFisher, 15240112) in low-attachment plates (Corning, 3471) to allow the formation of embryonic bodies (EBs). During the next three days, the medium was replaced daily with the ratio of NIM to mTeSR1 increased to 100%. At Day 6, human BMP4 (R&D Systems, 314-BP-010) was added to the NIM medium to a final concentration of 55 ng/ml ⁴⁰. At Day 7, EBs were collected and seeded in NIM as adherent cultures in 6-well dishes (Corning, 3516) till Day 16. At Day 16, the visible neural rosettes formed from attached EBs were manually lifted, collected, and further cultured as suspensions in Retinal Differentiation Medium (RDM) consisting of DMEM to F12 at 3:1, 1x B27 supplement (ThermoFisher, 1754044), 1x NEAA, and 1x Anti-Anti. During the 7 days after lifting neural rosettes, 5 µM SU-5402 (SigmaMillipore, SML0443) and 3 µM GSK inhibitor CHIR99021 (Stemgent, 04-0004) were added to RDM. At Day 20, the translucent optic vesicle-like structures were manually separated from the rest of the suspension culture, collected, and cultured as retinal organoids in RDM. From Day 24, 10 % FBS (SigmaAldrich, 12103C), 100 µM Taurine (SigmaAldrich, 0625), and 500 µM retinoic acid (SigmaAldrich, R2625) were added, and the medium was changed twice a week.

Lentiviral Infection and transgene induction

Retinal organoids were infected by different lentiviruses in conjunction with LV-rtTA three times between Day 23 and Day 40. TetO promoter induction was carried out by adding doxycycline (Dox) to a final concentration of 2 µg/ml (SigmaAldrich, D3072) according to experimental designs as indicated in the results.

Attached and dissociated retinal organoid cultures

Retinal organoids between Day 30-35 were cut into small pieces (0.1- 0.5 mm) and plated on Matrigel coated culture dishes, or dissociated with Trypsin (SigmaAldrich, T9935) to single cells and plated on poly-D-lysine and laminin coated glass coverslips (Corning, 354087). After attachment, retinal organoid cells were cultured in RDM or BrainPhys neuronal medium (Stemcell Technologies, 05790) with SM1 (Stemcell Technologies, 05711) and N2 supplements (ThermoFisher, 17502048), 20 ng/ml BDNF (PeproTech, 450-02), 20 ng/ml GDNF (Stemcell Technologies, 78058), 1 mM dibutyryl cyclic-AMP (Stemcell Technologies, 73882), and 200 nM ascorbic acid (Stemcell Technologies, 72132) till desired time, followed by immunofluorescent labeling or electrophysiological recordings.

Electrophysiological recording

Electrophysiological recordings were performed using dissociated retinal organoid cells cultured as a monolayer on glass coverslips between Day 40-45 using previously described methodologies ⁸⁹⁻⁹². Whole cell patch clamp was performed at room temperature using an Axopatch 200B amplifier controlled by pClamp 11 data acquisition software (Molecular Devices). The pipette solution contained 20 mM KCl, 120 mM K-gluconate 0.1 mM CaCl₂, 1 mM EGTA, 10 mM HEPES, 3 mM Mg-ATP, 0.2 mM Li-GTP, and 8 mM phosphocreatine, at pH7.2. The bathing solution (for recording K⁺ currents, Na⁺ currents and for current clamp) contained 125 mM NaCl, 3 mM KCl, 2 mM CaCl₂, 1.25 mM NaH₂PO₄, 1 mM MgCl₂, 25 mM NaHCO₃ and 10 mM glucose bubbled continuously with 95% O₂ – 5% CO₂. A high barium external solution for Ca²⁺ channel current recordings containing 110 mM choline chloride, 5 mM KCl, 1 mM MgCl₂, 7 mM BaCl₂, 15 mM TEACl, 0.1 mM 4-aminopyridine, 20 mM glucose, 10 mM HEPES and 1 µM tetrodotoxin, adjusted to pH 7.4, was used with a CsCl intracellular solution containing 140 mM CsCl, 1 mM CaCl₂, 11 mM EGTA, 2 mM MgCl₂, and 10 mM HEPES, at pH7.2.

Zhang, X. et al

Immunohistochemistry and imaging

For live imaging of whole mounts retinal organoids, EGFP signals were first captured using a Leica MZ10F fluorescent dissecting microscope, followed by image acquisition using an Olympus Flowview FV1000-IX81 (inverted) scanning laser confocal microscope. For whole mount immunolabeling, retinal organoids were fixed with 4% paraformaldehyde (PFA) in PBS for 30 minutes, followed by primary and secondary antibody incubations overnight at 4°C, with extensive washes in between²⁵. Cryosections (14 µm) or attached cultures were processed for immunolabeling as previously described²⁵.

The following primary antibodies were used: mouse anti-GFP (1:200; Millipore, MAB#3580); goat anti-GFP (1:200; Rockland Inc, 600-101-215); rabbit anti-GFP (1:200; Rockland Inc, 400-401-215); mouse anti-FLAG (Clone M2) (1:500; SigmaAldrich, F3165); rabbit anti-ATOH7 (1:100; NovusBio, NBP1-88639); goat anti-Ngn2 (1:200; Santa Cruz Biotechnology, sc-19233); mouse anti-BrdU (1:1; GE Healthcare, RPN202); mouse anti-PCNA (1:500; SigmaAldrich, P3825); rabbit anti-phospho-histone 3 (ser10) (1:3000; Upstate Biotechnology, 06-570); rabbit anti-Pax6 (1:200; Chemicon, ab5409); goat anti-CHX10/VSX2 (N-18) (1:50; Santa Cruz Biotechnology, sc-21690); goat anti-BRN3a (1:100; Santa Cruz Biotechnology, sc-31984); goat anti-pan BDNF (1:50; Santa Cruz Biotechnology, sc-6026); mouse anti-Islet1 (1:10; Developmental Study Hybridoma Bank, 39.4D5); mouse anti-doublecortin (E-6) (1:50; Santa Cruz Biotechnology, sc-271390); rabbit anti-NeuN (1:200; Abcam, ab177487); rabbit anti-NF145 (1:750; Millipore, AB1987); rabbit anti-RBPMS (1:200;⁹³). Secondary antibodies used were: Alexa Fluor 488 donkey anti-mouse (1:500; ThermoFisher, A32766); Alexa Fluor 488 donkey anti-rabbit (1:500; ThermoFisher, A32790); Alexa Fluor 488 donkey anti-goat (1:500; ThermoFisher, A32814); Alexa Fluor 594 donkey anti-mouse (1:500; ThermoFisher, A32744); Alexa Fluor 594 donkey anti-rabbit (1:500; ThermoFisher, A32754); Alexa Fluor 594 donkey anti-goat (1:500; ThermoFisher, A32758); Alexa Fluor 647 donkey anti-mouse (1:500; ThermoFisher, A32787); Alexa Fluor 647 donkey anti-rabbit (1:500; ThermoFisher, A32795); Alexa Fluor 647 donkey anti-goat (1:500; ThermoFisher, A32849).

Slides were mounted with Fluoro-Gel (Electron Microscopy Sciences, 17985-10) after staining with DAPI (SigmaAldrich, D9542). Confocal images were acquired using an Olympus Flowview FV1000-BX61 (upright) scanning laser microscope with Plan-APO objectives. Images were arranged using Adobe Photoshop.

Cell marker quantification and statistics

Lentivirus infected retinal organoids at Day 39 were pooled (10-15 organoids in each sample n), dissociated into single cell suspensions using trypsin (SigmaAldrich, T-9935), and immunolabeled as previously described⁶⁰. Flow cytometry was performed using LSRII Analytic Flow Cytometer for cell marker analyses. Quantification of FACS data was performed using FlowJo software (Tree Star, Inc.). In addition, pooled retinal organoids at Day 47 were dissociated with trypsin and plated as a monolayer for 3 hours followed by immunolabeling for the various cell markers listed above. Monolayer cell quantification was performed by counting marker-positive cells in multiple fields of independent samples (n=3) using captured confocal images. Bar graphs were constructed using Prism (Graphic Pad). Ordinary one-way ANOVA with Tukey's multiple comparison test was used for statistical analysis of cell marker quantifications, with p value < 0.05 considered significant.

Single cell cDNA library preparation and sequencing

Distinct pools of H9 ES cell-derived retinal organoids (12-20 retinal organoids/pool) co-infected by LV-rtTA and LV-EGFP, LV-AEP, or LV-NEP were induced by Dox and dissociated between Day 45 and Day 48 using trypsin and manual trituration. Dissociated cell suspensions were subjected to fluorescence activated cell sorting using FACSAriall (BD Biosciences). Non-infected retinal organoid cells

Zhang, X. et al

were used to set thresholds for selecting EGFP-positive cells. Sorted EGFP-positive cells were collected in HBSS without Ca²⁺ and Mg²⁺ (ThermoFisher, 14170-112) containing 1% FBS and 0.4% BSA. The cells were washed with PBS containing 0.04% BSA, then counted with Countess II Cell Counter (ThermoFisher).

Automated single-cell capture, barcoding, and cDNA library preparation were carried out using 10X Genomics Chromium Controller with Chromium Single Cell 3' Library & Gel Bead Kit v2 reagents, with 12 cycles of cDNA amplification and 12 cycles of library amplification, following the manufacturer's instructions. Qubit dsDNA Assay kit (Life Technologies) and TapeStation 4200 (Agilent) were used to assess the quality and concentration of the libraries. Illumina NovaSeq6000 S2 paired-end 2x50bp mode was used to sequence the libraries.

Single cell RNA-sequencing data processing and quality control

10X Genomics Cell Ranger version 2.1.1 was used to demultiplex the raw base calls into FASTQ files (cellranger mkfastq). Spliced Transcripts Alignment to a Reference (STAR) version 2.5.1b (cellranger count) was used to perform sequence alignments to the reference human genome (GRCh38), barcode counts, and UMI counts to yield summary reports and t-Stochastic Neighboring Embedding (t-SNE) dimensionality reduction. For downstream analyses, cells with a number of unique molecular identifiers (UMI) > 2500 per cell and < 0.1 % mitochondrial gene expression were used. For LV-GFP, LV-AEP, LV-NEP samples, the mean reads per cell ranged from 139,000-195,000, with mean gene per cell ranging from 2935-3079. The resulting total single cell counts used for analysis were 3004 for LV-EGFP, 2063 for LV-AEP, and 3909 for LV-NEP infected samples.

Single cell RNA-sequencing data analysis and visualization

The analysis of sc RNA-seq data was performed using Seurat R package (<https://satijalab.org/seurat/v2.2>)^{42,94}. Clustering of cells was performed by using Seurat FindCluster function (top 20 principal components, resolution 0.8) that implements the shared nearest neighbor modularity optimization algorithm. Nonlinear dimensionality reduction using UMAP (Uniform Manifold Approximation and Projection) was applied for the visualization of cells in two-dimensional space. Feature plots of known genes were used to designate clusters observed in the UMAP space into six major cell categories/states. Cell counts of each category were obtained using custom R code.

Pseudotime developmental progression of cell states was obtained by using the Monocle R package (version 2) to process the datasets with cell labels corresponding to the six cell categories and visualized as UMAPs. Pseudotime cell cycle progression and cell fate adoption analysis was performed using Slingshot R (version1.6.1) by combining the LV-GFP, LV-AEP, and LV-NEP sc RNA-seq datasets and assigning the start point as neural stem cells and end points as differentiated neuronal cell types.

Differentially expressed genes (DEGs) were identified using edgeR with significantly enriched genes in each cell category defined as those with adjusted *p* values < 0.05 for LV-GFP, LV-AEP, and LV-NEP data sets (Supplementary Tables 1-3). The top 10 enriched DEGs in each cell category were defined as those with adjusted *p*-value < 0.05, and log fold change >1.5 (Supplementary Tables 4-6). Heatmaps of the top 10 DEGs were generated using the Seurat package. Volcano plots were generated using EnhancedVolcano R package to show *p* values and fold changes of DEGs between two datasets. Gene Ontology (GO) Enrichment analysis was performed using ShinyGO v0.61 (<http://bioinformatics.sdsstate.edu/go>)⁹⁵ and the Homo Sapiens background using *p*-value (FDR) cutoff at 0.05. The top 25 DEGs from each cell category within the LV-GFP dataset were used as inputs, and the redundancy of the output biological processes was manually reduced to the most predominant GO terms.

Zhang, X. et al

Feature plots of individual gene expression patterns in different cell clusters were presented as UMAPs. Violin plots for individual genes in all cell clusters were constructed to show expression levels and cell distributions. Kruskal-Wallis one-way ANOVA rank sum test and Tukey-Kramer-Nemenyi all-pairs test were used for statistical analysis, taken into consideration of both gene expression levels and cell numbers between different samples, with p value < 0.05 considered significant. The statistical tests were performed on R Studio using ‘PMCMRPlus’⁹⁶ and ‘FSA’⁹⁷ packages. Data were plotted using R Studio ‘ggplot2’⁹⁸ and ‘ggsignif’⁹⁹ packages. Cells with gene expression level < 0.2 were exclude from the violin plots and statistical analyses.

STRING analysis exploring protein-protein association network was performed using human protein database (version 11.0; <https://string-db.org/>) by inputting relevant genes involved in retinal development. The schematic network model shows known molecular interactions reported previously and new regulatory relationships described in this study.

Acknowledgments

This work was supported by NIH grant R01EY026319 to XJY, NIH core grant P30EY000331, and an unrestricted grant from the Research to Prevent Blindness to the Department of Ophthalmology at University of California Los Angeles.

Author Contributions

X-J Y. conceived the project and designed lentiviral vectors; X.Z. carried out human retinal organoid and neuronal cultures, performed immunohistochemistry and imaging, and FACS analysis; X.Z. and K.H.N. prepared viral stocks and sc RNA-seq libraries; T.T.T.N, I.M., and M.P. performed bioinformatic analysis; T.T.T.N. performed statistical analysis; J.C.R.G and S.B. performed electrophysiological recordings; X.Z, T.T.T.N., and X-J Y. prepared the figures, and analyzed the data; X-J Y. wrote the manuscript. All authors reviewed and commented on the manuscript.

Competing Interests

The authors declare no competing interests.

Supplementary information

Description of additional supplementary files, and Supplementary Figures and Tables.

References

- 1 Livesey, F. J. & Cepko, C. L. Vertebrate neural cell-fate determination: lessons from the retina. *Nature reviews. Neuroscience* **2**, 109-118, doi:10.1038/35053522 (2001).
- 2 Young, R. W. Cell differentiation in the retina of the mouse. *Anat Rec* **212**, 199-205 (1985).
- 3 Wong, L. L. & Rapaport, D. H. Defining retinal progenitor cell competence in *Xenopus laevis* by clonal analysis. *Development* **136**, 1707-1715, doi:10.1242/dev.027607 (2009).
- 4 Cepko, C. L., Austin, C. P., Yang, X., Alexiades, M. & Ezzeddine, D. Cell fate determination in the vertebrate retina. *Proceedings of the National Academy of Sciences of the United States of America* **93**, 589-595, doi:10.1073/pnas.93.2.589 (1996).
- 5 Xiang, M. Intrinsic control of mammalian retinogenesis. *Cell Mol Life Sci* **70**, 2519-2532, doi:10.1007/s00018-012-1183-2 (2013).
- 6 Akagi, T. et al. Requirement of multiple basic helix-loop-helix genes for retinal neuronal subtype specification. *The Journal of biological chemistry* **279**, 28492-28498, doi:10.1074/jbc.M400871200 (2004).
- 7 Hoon, M., Okawa, H., Della Santina, L. & Wong, R. O. Functional architecture of the retina: development and disease. *Progress in retinal and eye research* **42**, 44-84, doi:10.1016/j.preteyeres.2014.06.003 (2014).
- 8 Brown, N. L. et al. Math5 encodes a murine basic helix-loop-helix transcription factor expressed during early stages of retinal neurogenesis. *Development* **125**, 4821-4833 (1998).
- 9 Miesfeld, J. B., Glaser, T. & Brown, N. L. The dynamics of native Atoh7 protein expression during mouse retinal histogenesis, revealed with a new antibody. *Gene expression patterns : GEP* **27**, 114-121, doi:10.1016/j.gep.2017.11.006 (2018).
- 10 Fu, X. et al. Epitope-tagging Math5 and Pou4f2: new tools to study retinal ganglion cell development in the mouse. *Developmental dynamics : an official publication of the American Association of Anatomists* **238**, 2309-2317, doi:10.1002/dvdy.21974 (2009).
- 11 Brown, N. L., Patel, S., Brzezinski, J. & Glaser, T. Math5 is required for retinal ganglion cell and optic nerve formation. *Development* **128**, 2497-2508 (2001).
- 12 Wang, S. W. et al. Requirement for math5 in the development of retinal ganglion cells. *Genes Dev* **15**, 24-29 (2001).
- 13 Kay, J. N., Finger-Baier, K. C., Roeser, T., Staub, W. & Baier, H. Retinal ganglion cell genesis requires lakritz, a Zebrafish atonal Homolog. *Neuron* **30**, 725-736, doi:10.1016/s0896-6273(01)00312-9 (2001).
- 14 Ghiasvand, N. M. et al. Deletion of a remote enhancer near ATOH7 disrupts retinal neurogenesis, causing NCRNA disease. *Nature neuroscience* **14**, 578-586, doi:10.1038/nn.2798 (2011).
- 15 Miesfeld, J. B. et al. The Atoh7 remote enhancer provides transcriptional robustness during retinal ganglion cell development. *Proceedings of the National Academy of Sciences of the United States of America* **117**, 21690-21700, doi:10.1073/pnas.2006888117 (2020).
- 16 Hufnagel, R. B., Le, T. T., Riesenber, A. L. & Brown, N. L. Neurog2 controls the leading edge of neurogenesis in the mammalian retina. *Developmental biology* **340**, 490-503, doi:10.1016/j.ydbio.2010.02.002 (2010).
- 17 Mao, C. A. et al. Reprogramming amacrine and photoreceptor progenitors into retinal ganglion cells by replacing Neurod1 with Atoh7. *Development* **140**, 541-551, doi:10.1242/dev.085886 (2013).
- 18 Prasov, L. & Glaser, T. Pushing the envelope of retinal ganglion cell genesis: context dependent function of Math5 (Atoh7). *Developmental biology* **368**, 214-230, doi:10.1016/j.ydbio.2012.05.005 (2012).

Zhang, X. et al

- 19 Brzezinski, J. A. t., Prasov, L. & Glaser, T. Math5 defines the ganglion cell competence state in a subpopulation of retinal progenitor cells exiting the cell cycle. *Developmental biology* **365**, 395-413, doi:10.1016/j.ydbio.2012.03.006 (2012).
- 20 Wu, F. et al. Two transcription factors, Pou4f2 and Isl1, are sufficient to specify the retinal ganglion cell fate. *Proceedings of the National Academy of Sciences of the United States of America* **112**, E1559-1568, doi:10.1073/pnas.1421535112 (2015).
- 21 Mu, X., Fu, X., Beremand, P. D., Thomas, T. L. & Klein, W. H. Gene regulation logic in retinal ganglion cell development: Isl1 defines a critical branch distinct from but overlapping with Pou4f2. *Proceedings of the National Academy of Sciences of the United States of America* **105**, 6942-6947, doi:10.1073/pnas.0802627105 (2008).
- 22 Liu, W., Mo, Z. & Xiang, M. The Ath5 proneural genes function upstream of Brn3 POU domain transcription factor genes to promote retinal ganglion cell development. *Proceedings of the National Academy of Sciences of the United States of America* **98**, 1649-1654, doi:10.1073/pnas.98.4.1649 (2001).
- 23 Pan, L., Deng, M., Xie, X. & Gan, L. ISL1 and BRN3B co-regulate the differentiation of murine retinal ganglion cells. *Development* **135**, 1981-1990, doi:10.1242/dev.010751 (2008).
- 24 Li, R. et al. Isl1 and Pou4f2 form a complex to regulate target genes in developing retinal ganglion cells. *PloS one* **9**, e92105, doi:10.1371/journal.pone.0092105 (2014).
- 25 Zhang, X. M., Hashimoto, T., Tang, R. & Yang, X. J. Elevated expression of human bHLH factor ATOH7 accelerates cell cycle progression of progenitors and enhances production of avian retinal ganglion cells. *Scientific reports* **8**, 6823, doi:10.1038/s41598-018-25188-z (2018).
- 26 Prasov, L., Nagy, M., Rudolph, D. D. & Glaser, T. Math5 (Atoh7) gene dosage limits retinal ganglion cell genesis. *Neuroreport* **23**, 631-634, doi:10.1097/WNR.0b013e328355f260 (2012).
- 27 Hendrickson, A. Development of Retinal Layers in Prenatal Human Retina. *American journal of ophthalmology* **161**, 29-35 e21, doi:10.1016/j.ajo.2015.09.023 (2016).
- 28 Hoshino, A. et al. Molecular Anatomy of the Developing Human Retina. *Developmental cell* **43**, 763-779 e764, doi:10.1016/j.devcel.2017.10.029 (2017).
- 29 Mellough, C. B. et al. An integrated transcriptional analysis of the developing human retina. *Development* **146**, doi:10.1242/dev.169474 (2019).
- 30 Ohlemacher, S. K. et al. Stepwise Differentiation of Retinal Ganglion Cells from Human Pluripotent Stem Cells Enables Analysis of Glaucomatous Neurodegeneration. *Stem cells* **34**, 1553-1562, doi:10.1002/stem.2356 (2016).
- 31 Nakano, T. et al. Self-formation of optic cups and storable stratified neural retina from human ESCs. *Cell stem cell* **10**, 771-785, doi:10.1016/j.stem.2012.05.009 (2012).
- 32 Reichman, S. et al. From confluent human iPS cells to self-forming neural retina and retinal pigmented epithelium. *Proceedings of the National Academy of Sciences of the United States of America* **111**, 8518-8523, doi:10.1073/pnas.1324212111 (2014).
- 33 Meyer, J. S. et al. Optic vesicle-like structures derived from human pluripotent stem cells facilitate a customized approach to retinal disease treatment. *Stem cells* **29**, 1206-1218, doi:10.1002/stem.674 (2011).
- 34 Lu, Y. et al. Single-Cell Analysis of Human Retina Identifies Evolutionarily Conserved and Species-Specific Mechanisms Controlling Development. *Developmental cell* **53**, 473-491 e479, doi:10.1016/j.devcel.2020.04.009 (2020).
- 35 Lukowski, S. W. et al. A single-cell transcriptome atlas of the adult human retina. *EMBO J* **38**, e100811, doi:10.15252/embj.2018100811 (2019).

Zhang, X. et al

- 36 Sridhar, A. *et al.* Single-Cell Transcriptomic Comparison of Human Fetal Retina, hPSC-Derived Retinal Organoids, and Long-Term Retinal Cultures. *Cell reports* **30**, 1644-1659 e1644, doi:10.1016/j.celrep.2020.01.007 (2020).
- 37 Menon, M. *et al.* Single-cell transcriptomic atlas of the human retina identifies cell types associated with age-related macular degeneration. *Nature communications* **10**, 4902, doi:10.1038/s41467-019-12780-8 (2019).
- 38 Lo Giudice, Q., Leleu, M., La Manno, G. & Fabre, P. J. Single-cell transcriptional logic of cell-fate specification and axon guidance in early-born retinal neurons. *Development* **146**, doi:10.1242/dev.178103 (2019).
- 39 Hoang, T. *et al.* Gene regulatory networks controlling vertebrate retinal regeneration. *Science*, doi:10.1126/science.abb8598 (2020).
- 40 Kuwahara, A. *et al.* Generation of a ciliary margin-like stem cell niche from self-organizing human retinal tissue. *Nature communications* **6**, 6286, doi:10.1038/ncomms7286 (2015).
- 41 Zhang, Y. *et al.* Rapid single-step induction of functional neurons from human pluripotent stem cells. *Neuron* **78**, 785-798, doi:10.1016/j.neuron.2013.05.029 (2013).
- 42 Butler, A., Hoffman, P., Smibert, P., Papalexi, E. & Satija, R. Integrating single-cell transcriptomic data across different conditions, technologies, and species. *Nature biotechnology* **36**, 411-420, doi:10.1038/nbt.4096 (2018).
- 43 Bae, S., Bessho, Y., Hojo, M. & Kageyama, R. The bHLH gene Hes6, an inhibitor of Hes1, promotes neuronal differentiation. *Development* **127**, 2933-2943 (2000).
- 44 Bianchi, M. E. & Agresti, A. HMG proteins: dynamic players in gene regulation and differentiation. *Current opinion in genetics & development* **15**, 496-506, doi:10.1016/j.gde.2005.08.007 (2005).
- 45 Liu, C. *et al.* BTG1 potentiates apoptosis and suppresses proliferation in renal cell carcinoma by interacting with PRMT1. *Oncol Lett* **10**, 619-624, doi:10.3892/ol.2015.3293 (2015).
- 46 Barreto, G. *et al.* Gadd45a promotes epigenetic gene activation by repair-mediated DNA demethylation. *Nature* **445**, 671-675, doi:10.1038/nature05515 (2007).
- 47 Horiuchi, D. *et al.* Chemical-genetic analysis of cyclin dependent kinase 2 function reveals an important role in cellular transformation by multiple oncogenic pathways. *Proceedings of the National Academy of Sciences of the United States of America* **109**, E1019-1027, doi:10.1073/pnas.1111317109 (2012).
- 48 Yabuta, N. *et al.* Mammalian Mcm2/4/6/7 complex forms a toroidal structure. *Genes Cells* **8**, 413-421, doi:10.1046/j.1365-2443.2003.00645.x (2003).
- 49 Liu, J. H. *et al.* Functional association of TGF-beta receptor II with cyclin B. *Oncogene* **18**, 269-275, doi:10.1038/sj.onc.1202263 (1999).
- 50 Lee, K. S., Oh, D. Y., Kang, Y. H. & Park, J. E. Self-regulated mechanism of Plk1 localization to kinetochores: lessons from the Plk1-PBIP1 interaction. *Cell Div* **3**, 4, doi:10.1186/1747-1028-3-4 (2008).
- 51 Hafler, B. P. *et al.* Transcription factor Olig2 defines subpopulations of retinal progenitor cells biased toward specific cell fates. *Proceedings of the National Academy of Sciences of the United States of America* **109**, 7882-7887, doi:10.1073/pnas.1203138109 (2012).
- 52 Gu, W. *et al.* Glycolytic Metabolism Plays a Functional Role in Regulating Human Pluripotent Stem Cell State. *Cell stem cell* **19**, 476-490, doi:10.1016/j.stem.2016.08.008 (2016).
- 53 Gouti, M., Metzis, V. & Briscoe, J. The route to spinal cord cell types: a tale of signals and switches. *Trends Genet* **31**, 282-289, doi:10.1016/j.tig.2015.03.001 (2015).
- 54 Jadhav, A. P., Cho, S. H. & Cepko, C. L. Notch activity permits retinal cells to progress through multiple progenitor states and acquire a stem cell property. *Proceedings of the National*

Zhang, X. et al

- Academy of Sciences of the United States of America **103**, 18998-19003, doi:10.1073/pnas.0608155103 (2006).
- 55 Jadhav, A. P., Mason, H. A. & Cepko, C. L. Notch 1 inhibits photoreceptor production in the developing mammalian retina. *Development* **133**, 913-923, doi:10.1242/dev.02245 (2006).
- 56 Riesenbergs, A. N., Liu, Z., Kopan, R. & Brown, N. L. Rbpj cell autonomous regulation of retinal ganglion cell and cone photoreceptor fates in the mouse retina. *The Journal of neuroscience : the official journal of the Society for Neuroscience* **29**, 12865-12877, doi:10.1523/JNEUROSCI.3382-09.2009 (2009).
- 57 Yaron, O., Farhy, C., Marquardt, T., Applebury, M. & Ashery-Padan, R. Notch1 functions to suppress cone-photoreceptor fate specification in the developing mouse retina. *Development* **133**, 1367-1378, doi:10.1242/dev.02311 (2006).
- 58 Wang, Y., Dakubo, G. D., Thurig, S., Mazerolle, C. J. & Wallace, V. A. Retinal ganglion cell-derived sonic hedgehog locally controls proliferation and the timing of RGC development in the embryonic mouse retina. *Development* **132**, 5103-5113, doi:10.1242/dev.02096 (2005).
- 59 Zhang, X. M. & Yang, X. J. Regulation of retinal ganglion cell production by Sonic hedgehog. *Development* **128**, 943-957 (2001).
- 60 Sakagami, K., Gan, L. & Yang, X. J. Distinct effects of Hedgehog signaling on neuronal fate specification and cell cycle progression in the embryonic mouse retina. *The Journal of neuroscience : the official journal of the Society for Neuroscience* **29**, 6932-6944, doi:10.1523/JNEUROSCI.0289-09.2009 (2009).
- 61 Kim, J. et al. GDF11 controls the timing of progenitor cell competence in developing retina. *Science* **308**, 1927-1930, doi:10.1126/science.1110175 (2005).
- 62 Miesfeld, J. B. et al. Rbpj direct regulation of Atoh7 transcription in the embryonic mouse retina. *Scientific reports* **8**, 10195, doi:10.1038/s41598-018-28420-y (2018).
- 63 Hashimoto, T., Zhang, X. M., Chen, B. Y. & Yang, X. J. VEGF activates divergent intracellular signaling components to regulate retinal progenitor cell proliferation and neuronal differentiation. *Development* **133**, 2201-2210, doi:10.1242/dev.02385 (2006).
- 64 Maurer, K. A., Riesenbergs, A. N. & Brown, N. L. Notch signaling differentially regulates Atoh7 and Neurog2 in the distal mouse retina. *Development* **141**, 3243-3254, doi:10.1242/dev.106245 (2014).
- 65 Pollak, J. et al. ASCL1 reprograms mouse Muller glia into neurogenic retinal progenitors. *Development* **140**, 2619-2631, doi:10.1242/dev.091355 (2013).
- 66 Ramachandran, R., Fausett, B. V. & Goldman, D. Ascl1a regulates Muller glia dedifferentiation and retinal regeneration through a Lin-28-dependent, let-7 microRNA signalling pathway. *Nature cell biology* **17**, 532, doi:10.1038/ncb3144 (2015).
- 67 Jorstad, N. L. et al. Stimulation of functional neuronal regeneration from Muller glia in adult mice. *Nature* **548**, 103-107, doi:10.1038/nature23283 (2017).
- 68 Chiodini, F. et al. A positive feedback loop between ATOH7 and a Notch effector regulates cell-cycle progression and neurogenesis in the retina. *Cell reports* **3**, 796-807, doi:10.1016/j.celrep.2013.01.035 (2013).
- 69 Akazawa, C., Sasai, Y., Nakanishi, S. & Kageyama, R. Molecular characterization of a rat negative regulator with a basic helix-loop-helix structure predominantly expressed in the developing nervous system. *The Journal of biological chemistry* **267**, 21879-21885 (1992).
- 70 Kageyama, R., Shimojo, H. & Isomura, A. Oscillatory Control of Notch Signaling in Development. *Advances in experimental medicine and biology* **1066**, 265-277, doi:10.1007/978-3-319-89512-3_13 (2018).

Zhang, X. et al

- 71 Kageyama, R., Shimojo, H. & Ohtsuka, T. Dynamic control of neural stem cells by bHLH factors. *Neurosci Res* **138**, 12-18, doi:10.1016/j.neures.2018.09.005 (2019).
- 72 Imaiishi, I. et al. Oscillatory control of factors determining multipotency and fate in mouse neural progenitors. *Science* **342**, 1203-1208, doi:10.1126/science.1242366 (2013).
- 73 Ochi, S., Imaizumi, Y., Shimojo, H., Miyachi, H. & Kageyama, R. Oscillatory expression of Hes1 regulates cell proliferation and neuronal differentiation in the embryonic brain. *Development* **147**, doi:10.1242/dev.182204 (2020).
- 74 Riesenbergs, A. N. et al. Pax6 regulation of Math5 during mouse retinal neurogenesis. *Genesis* **47**, 175-187, doi:10.1002/dvg.20479 (2009).
- 75 Lee, H. Y. et al. Multiple requirements for Hes 1 during early eye formation. *Developmental biology* **284**, 464-478, doi:10.1016/j.ydbio.2005.06.010 (2005).
- 76 Matter-Sadzinski, L., Matter, J. M., Ong, M. T., Hernandez, J. & Ballivet, M. Specification of neurotransmitter receptor identity in developing retina: the chick ATH5 promoter integrates the positive and negative effects of several bHLH proteins. *Development* **128**, 217-231 (2001).
- 77 Boije, H., Rulands, S., Dudczig, S., Simons, B. D. & Harris, W. A. The Independent Probabilistic Firing of Transcription Factors: A Paradigm for Clonal Variability in the Zebrafish Retina. *Developmental cell* **34**, 532-543, doi:10.1016/j.devcel.2015.08.011 (2015).
- 78 He, J. et al. How variable clones build an invariant retina. *Neuron* **75**, 786-798, doi:10.1016/j.neuron.2012.06.033 (2012).
- 79 Jiang, Y. et al. Transcription factors SOX4 and SOX11 function redundantly to regulate the development of mouse retinal ganglion cells. *The Journal of biological chemistry* **288**, 18429-18438, doi:10.1074/jbc.M113.478503 (2013).
- 80 Chang, K. C. et al. Novel Regulatory Mechanisms for the SoxC Transcriptional Network Required for Visual Pathway Development. *The Journal of neuroscience : the official journal of the Society for Neuroscience* **37**, 4967-4981, doi:10.1523/JNEUROSCI.3430-13.2017 (2017).
- 81 Koike, C. et al. Functional roles of Otx2 transcription factor in postnatal mouse retinal development. *Molecular and cellular biology* **27**, 8318-8329, doi:10.1128/MCB.01209-07 (2007).
- 82 Yamamoto, H., Kon, T., Omori, Y. & Furukawa, T. Functional and Evolutionary Diversification of Otx2 and Crx in Vertebrate Retinal Photoreceptor and Bipolar Cell Development. *Cell reports* **30**, 658-671 e655, doi:10.1016/j.celrep.2019.12.072 (2020).
- 83 Rehmtulla, A. et al. The basic motif-leucine zipper transcription factor Nrl can positively regulate rhodopsin gene expression. *Proceedings of the National Academy of Sciences of the United States of America* **93**, 191-195, doi:10.1073/pnas.93.1.191 (1996).
- 84 Oh, E. C. et al. Transformation of cone precursors to functional rod photoreceptors by bZIP transcription factor NRL. *Proceedings of the National Academy of Sciences of the United States of America* **104**, 1679-1684, doi:10.1073/pnas.0605934104 (2007).
- 85 Wu, F. et al. Onecut1 is essential for horizontal cell genesis and retinal integrity. *The Journal of neuroscience : the official journal of the Society for Neuroscience* **33**, 13053-13065, 13065a, doi:10.1523/JNEUROSCI.0116-13.2013 (2013).
- 86 Dull, T. et al. A third-generation lentivirus vector with a conditional packaging system. *Journal of virology* **72**, 8463-8471 (1998).
- 87 Zufferey, R. et al. Self-inactivating lentivirus vector for safe and efficient in vivo gene delivery. *Journal of virology* **72**, 9873-9880 (1998).
- 88 Hashimoto, T. et al. Lentiviral gene replacement therapy of retinas in a mouse model for Usher syndrome type 1B. *Gene Ther* **14**, 584-594, doi:10.1038/sj.gt.3302897 (2007).

Zhang, X. et al

- 89 Hartwick, A. T., Lalonde, M. R., Barnes, S. & Baldridge, W. H. Adenosine A1-receptor modulation
of glutamate-induced calcium influx in rat retinal ganglion cells. *Investigative ophthalmology &*
visual science **45**, 3740-3748, doi:10.1167/iovs.04-0214 (2004).
- 90 Hirooka, K. et al. T-Type calcium channel alpha1G and alpha1H subunits in human retinoblastoma
cells and their loss after differentiation. *Journal of neurophysiology* **88**, 196-205 (2002).
- 91 Lalonde, M. R., Jollimore, C. A., Stevens, K., Barnes, S. & Kelly, M. E. Cannabinoid receptor-
mediated inhibition of calcium signaling in rat retinal ganglion cells. *Molecular vision* **12**, 1160-
1166 (2006).
- 92 Sargoy, A., Sun, X., Barnes, S. & Brecha, N. C. Differential calcium signaling mediated by voltage-
gated calcium channels in rat retinal ganglion cells and their unmyelinated axons. *PLoS one* **9**,
e84507, doi:10.1371/journal.pone.0084507 (2014).
- 93 Ye, L., Gu, L., Caprioli, J. & Piri, N. RNA-binding protein Rbpms is represented in human retinas by
isoforms A and C and its transcriptional regulation involves Sp1-binding site. *Mol Genet Genomics*
293, 819-830, doi:10.1007/s00438-018-1423-8 (2018).
- 94 Stuart, T. et al. Comprehensive Integration of Single-Cell Data. *Cell* **177**, 1888-1902 e1821,
doi:10.1016/j.cell.2019.05.031 (2019).
- 95 Ge, S. X., Jung, D. & Yao, R. ShinyGO: a graphical gene-set enrichment tool for animals and plants.
Bioinformatics **36**, 2628-2629, doi:10.1093/bioinformatics/btz931 (2020).
- 96 Kessler, S., Pohlert, T., Breitung, V., Wilcsek, K. & Bierl, R. Comparative evaluation of four
suspended particulate matter (SPM) sampling devices and their use for monitoring SPM quality.
Environ Sci Pollut Res Int **27**, 5993-6008, doi:10.1007/s11356-019-07314-0 (2020).
- 97 FSA: Fisheries Stock Analysis v. R package version 0.8.30 (2020).
- 98 Hadley, W. *Ggplot2*. (Springer Science+Business Media, LLC, 2016).
- 99 ggsignif: Significane Brackets for 'ggplot2' v. R package version 0.6.0 (2019).

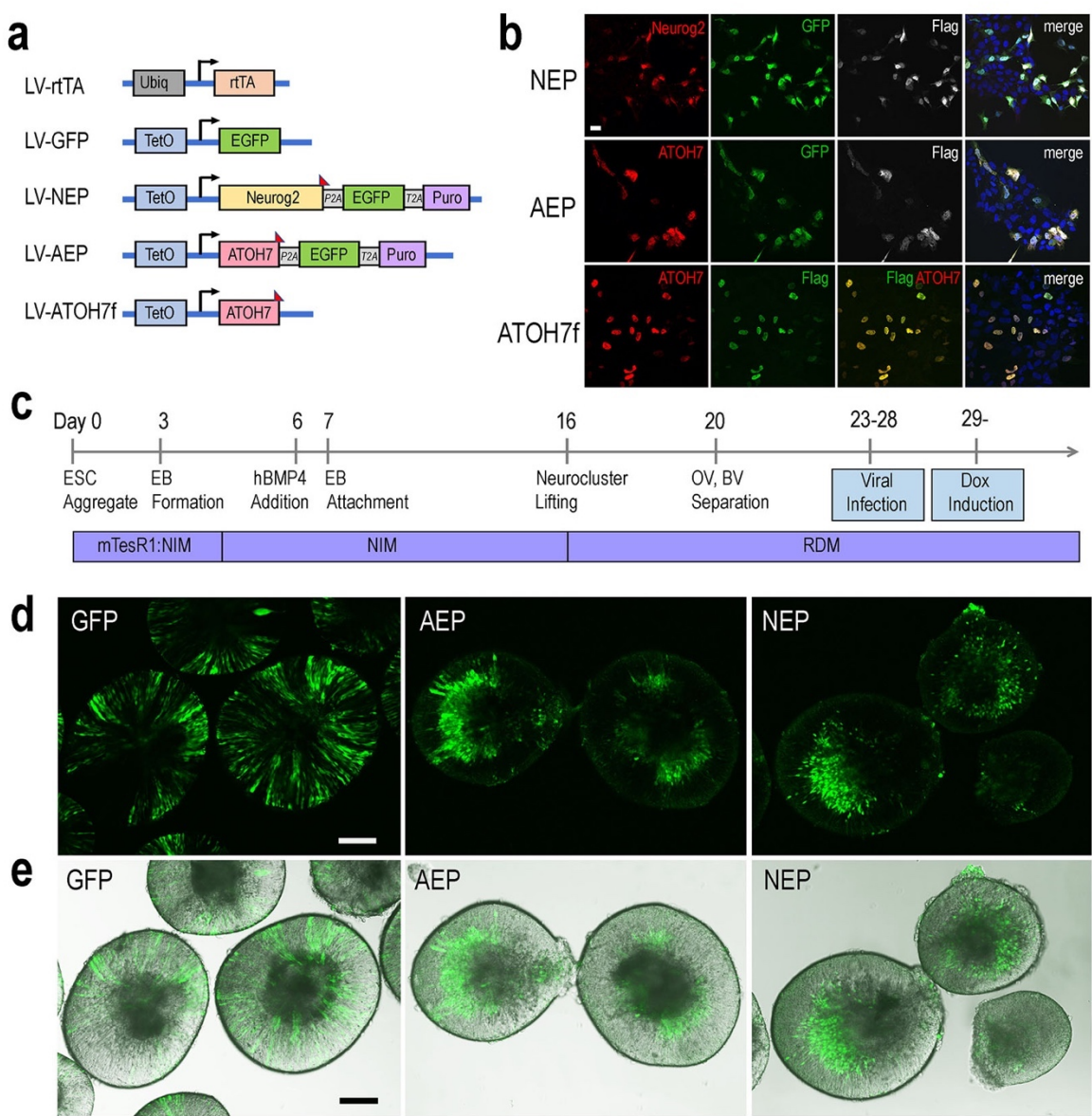


Fig. 1 Inducible lentivirus-mediated gene expression in human ES cell-derived retinal organoids.

a Schematics of lentiviral vectors used in the study. A vector expressing rtTA under the control of the constitutive Ubiq promoter was used to co-infect human ES cells with lentiviral vectors encoding the inducible TetO promoter. Puro, puromycin-resistant gene; P2A and T2A, intervening 2T sequences in frame with the coding sequences of the other genes in LV-NEP and LV-AEP. The Flag epitope tag was fused to the c-terminus of Neurog2 and ATOH7 coding regions. **b** Expression of Neurog2 and ATOH7 proteins as detected by immunofluorescent microscopy in H9 ES cells co-infected with LV-rtTA and either LV-NEP, LV-AEP, or LV-ATOH7f after 36 hours of Dox induction. Scale Bar for all, 20 μ m. **c** Experimental time course of human retinal organoid derivation and lentiviral infection. **d, e** Confocal images (**d**) and merged confocal and bright field images (**e**) show distribution of viral infected GFP $^{+}$ cells in live retinal organoids at Day 36 after 6 days of Dox induction. Names of lentiviruses are abbreviated as: GFP for LV-GFP, NEP for LV-NEP, AEP for LV-AEP. Scale Bars, 100 μ m.

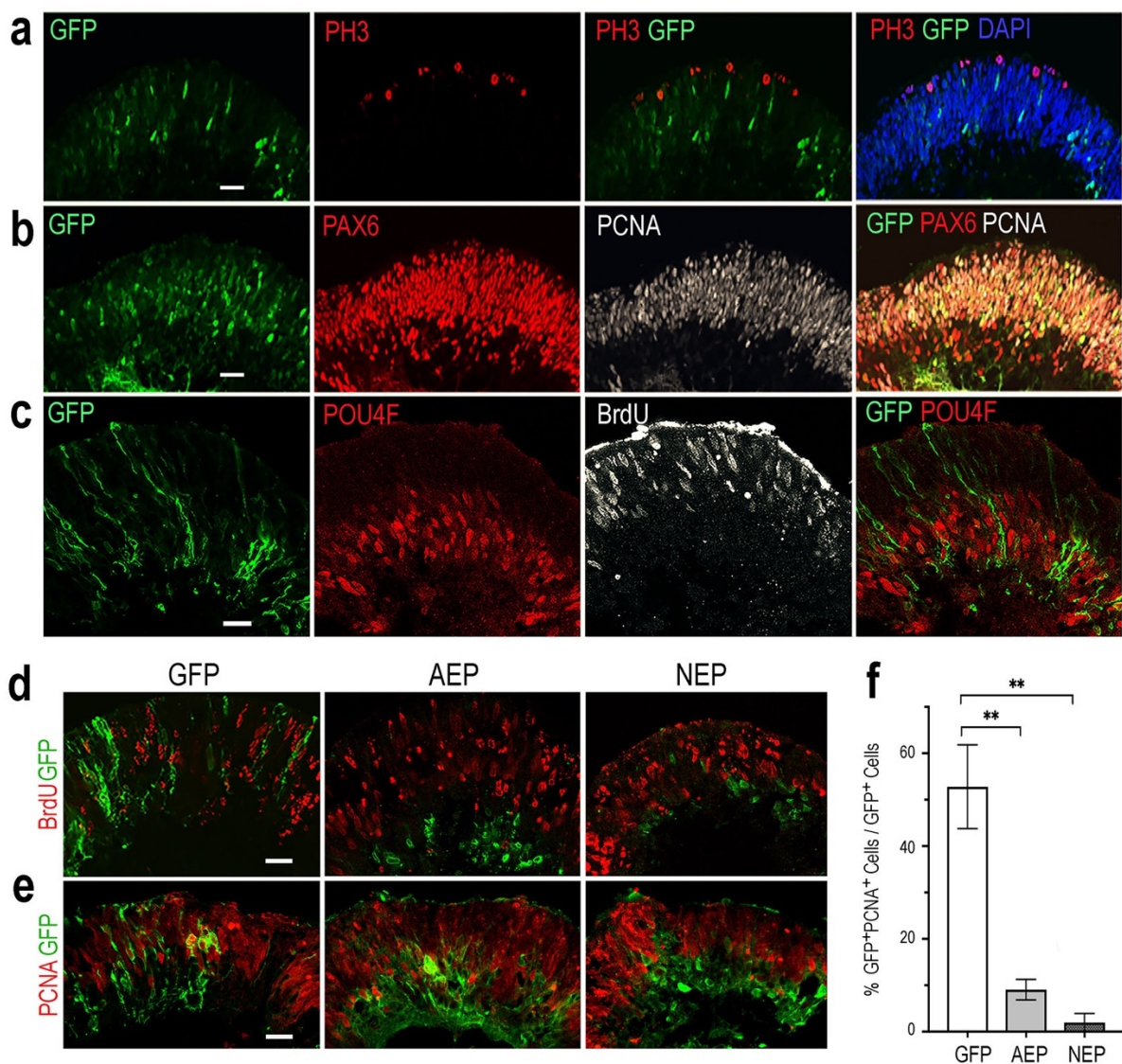


Fig. 2 Influences of viral mediated neurogenic factor expression on cell proliferation.

a-c Immunofluorescence labeling of cross sections from retinal organoids infected with LV-GFP. At Day 34, PH3⁺ dividing cells are located at the ventricular surface (**a**), while PCNA⁺ progenitors occupy the ventricular zone and are co-labeled with PAX6-expressing progenitors (**b**). Note that PAX6⁺PCNA⁻ postmitotic neurons are located to the inner layer of the retinal organoid. At Day 40, proliferating progenitors labeled with BrdU are distributed in the ventricular zone, whereas POU4F⁺ postmitotic retinal ganglion cells (RGCs) reside in the inner layer of the retinal organoid (**c**). Scale bars, 20 μ m. **d, e** Confocal images of cross sections from retinal organoids infected by LV-GFP, LV-AEP, or LV-NEP after 6-day Dox induction. Co-staining of GFP with BrdU at Day 36 (**d**, 3-hour labeling) or PCNA at Day 40 (**e**) shows that most LV-AEP and LV-NEP infected cells are postmitotic. Scale bars, 20 μ m. **f** Quantification of double labeled PCNA⁺GFP⁺ progenitor cells among total viral infected GFP⁺ cells at Day 47. Mean \pm s.e.m. of n= 3 independent samples. One-way ANOVA, ** p < 0.01.

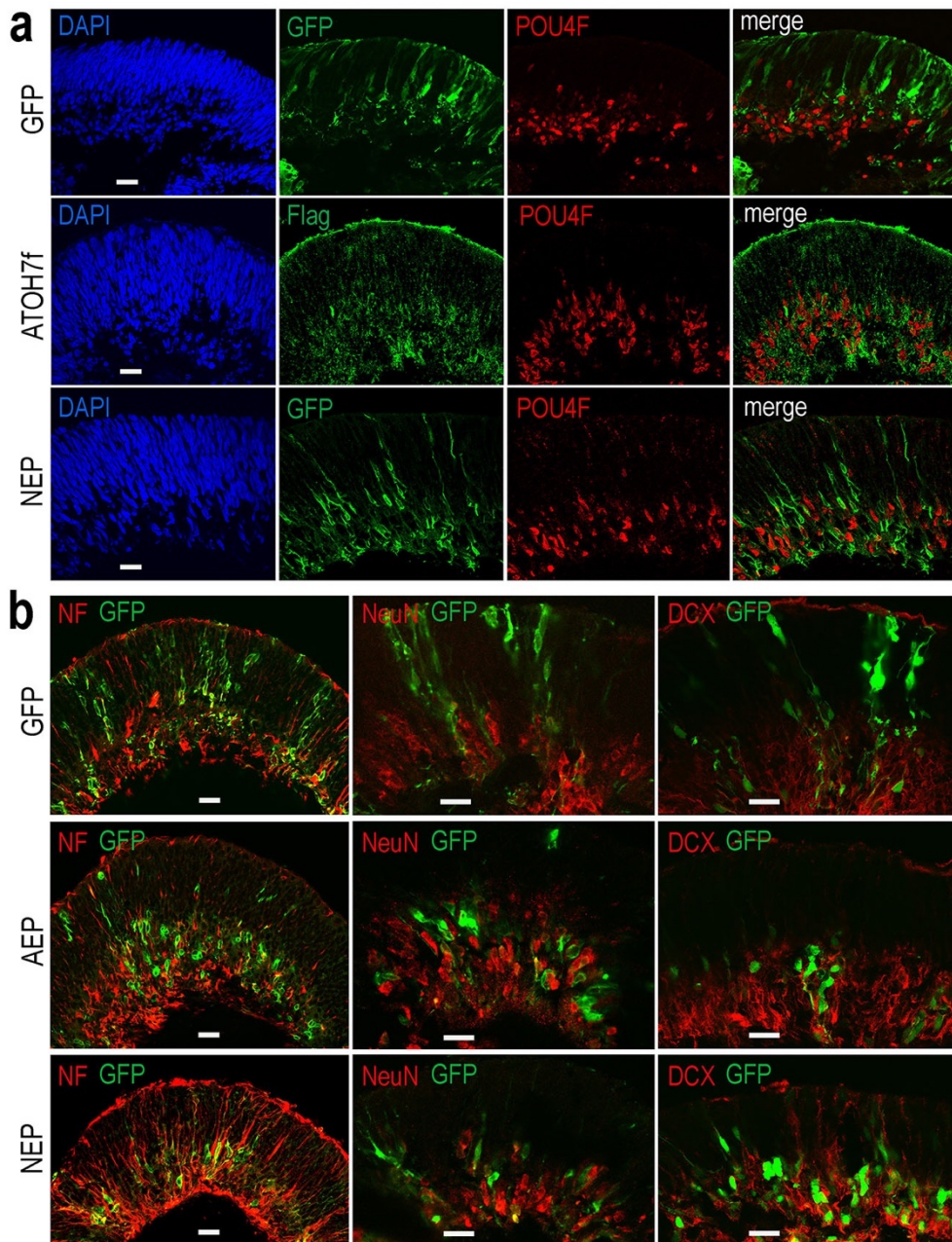


Fig. 3 Effects of viral mediated neurogenic factor expression on retinal ganglion cell genesis.

Confocal images of retinal organoid sections immunolabeled with retinal ganglion cell (RGC) markers. **a** Co-labeling of viral markers with a pan-POU4F antibody in LV-NEP and LV-ATOH7f infected retinal organoids at Day 43. **b** Merged images of viral marker GFP co-labeling with NF145 and NeuN at Day 36, and DCX at Day 46. Scale Bars, 20 μ m.

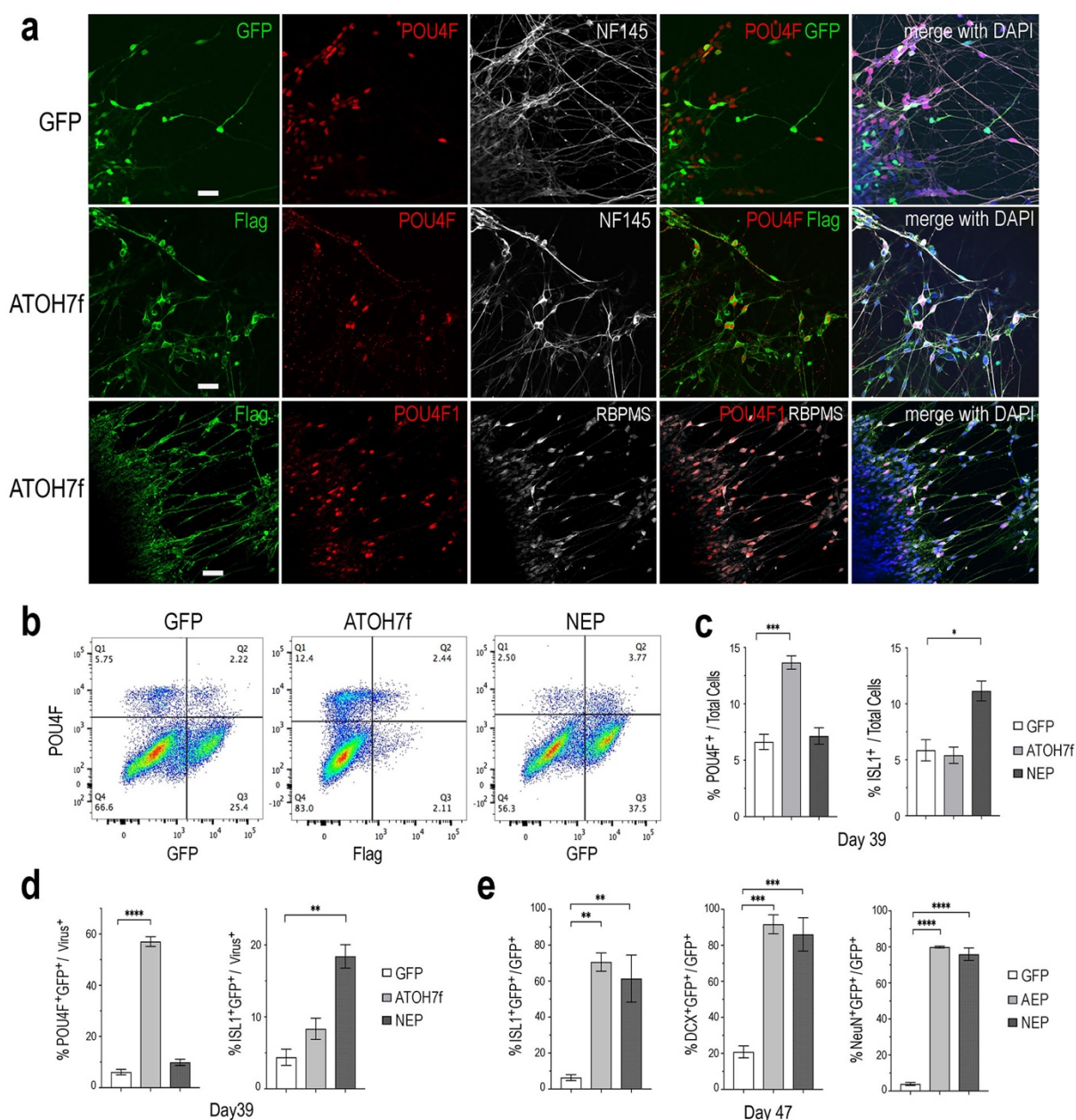


Fig. 4 Impacts of elevating neurogenic factor expression on retinal ganglion cell genesis.

a Immunofluorescent images of attached retinal organoid cultures infected with LV-GFP or LV-ATOH7f after 4-day Dox induction at Day 39. Co-labeling for viral vector markers with POU4F and NF145 at Day 38, or POU4F1 and RBPMS at Day 41 shows high correspondence of LV-ATOH7f infection and RGC marker expression. Scale bars, 20 μ m. **b** Representative flow cytometry profiles of dissociated cells at Day 39 from LV-GFP, LV-ATOH7f, and LV-NEP infected retinal organoids after 4-day Dox induction. Cells were co-labeled for RGC marker POU4F and viral marker Flag for LV-ATOH7f, or GFP for LV-GFP and LV-NEP, respectively. **c, d** Bar graphs show flow cytometry quantification of RGC markers POU4F and ISL1 among total cells (**c**) and viral infected cells (**d**) at Day 39. **e** Quantification of cultured monolayer cells from LV-GFP, LV-AEP, and LV-NEP infected retinal organoids at Day 47 after 7-day Dox induction. Percentages of RGC marker ISL1, DCX, and NeuN positive cells among viral infected GFP⁺ cells are shown. For **c, d, e** Mean \pm s.e.m. of n= 3 independent samples. One-way ANOVA, **** p< 0.0001, *** p< 0.001, ** p< 0.01.

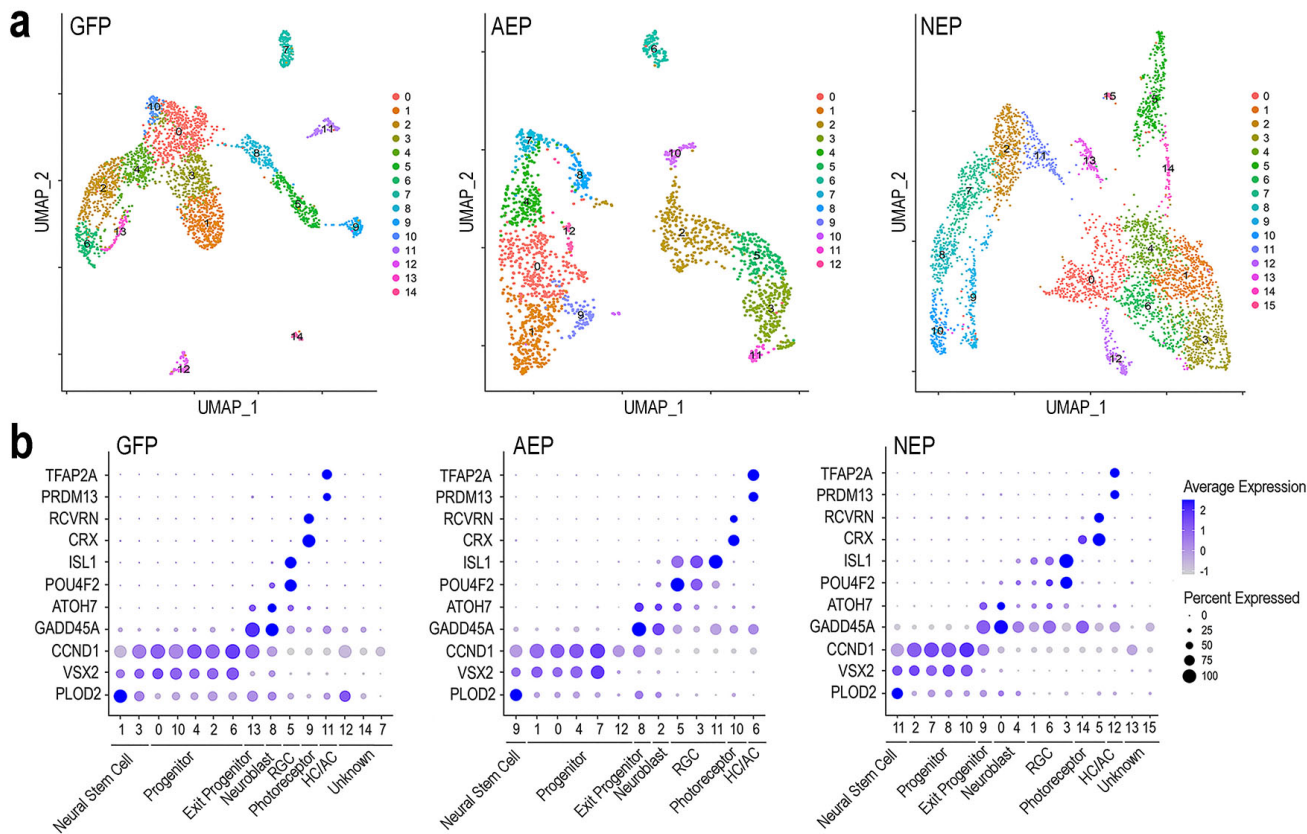


Fig.5 Characterization of lentivirus-infected human retinal organoids by single cell RNA-seq.

a UMAP visualization of cell clustering based on sequencing of single cell cDNA libraries from lentivirus infected retinal organoids between culture Day 45-48 after 8-day Dox induction. The numbers of single cell that passed quality control and used for downstream analysis are 3004 for LV-GFP, 2063 for LV-AEP, and 3909 for LV-NEP samples. **b** Dot plots show assignments of UMAP clusters into seven major cell categories based on expression of known genes for different cell states or types during early retinal development. Minor cell clusters in LV-GFP and LV-NEP infected retinal organoids that do not show characteristic retinal gene expression are designated as “unknown”. The average expression levels are represented by the intensity bar, and the percentages of cells expressing a given gene in a cluster are indicated as the dot size.

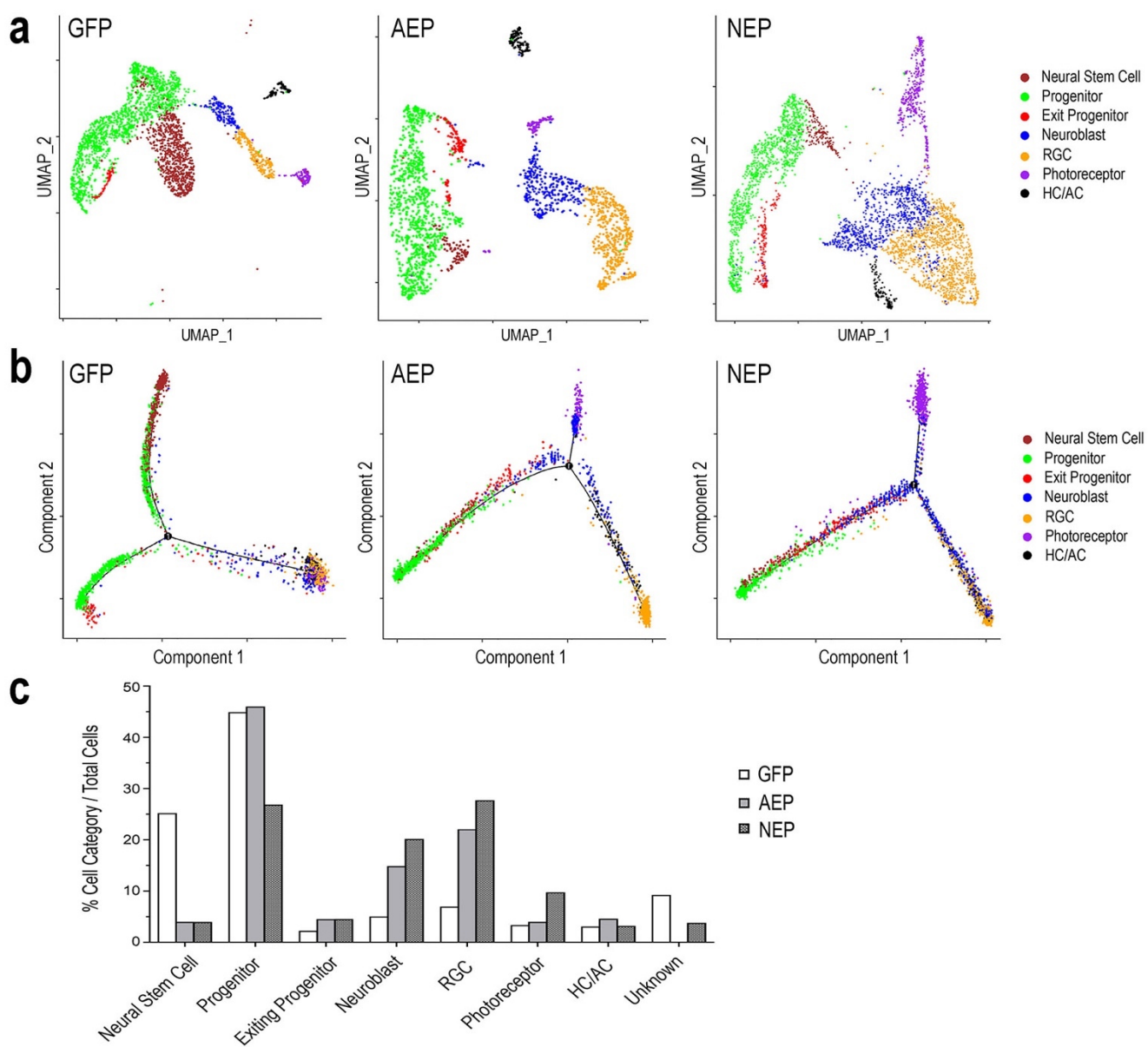


Fig. 6 Distinct cell categories based on single cell RNA-seq profiles and their developmental trajectory.

a UMAP presentations based on cell category assignments for single cell clusters from LV-GFP, LV-AEP, and LV-NEP infected retinal organoids. Each cell category is represented by a single color. The side legend shows the color codes used to represent distinct cell categories. **b** Pseudotime trajectory analysis using Monocle of different cell categories from LV-GFP, LV-AEP, and LV-NEP infected retinal organoid. **c** Bar graph shows the percentages of different cell categories among total cells in LV-GFP, LV-AEP, and LV-NEP infected retinal organoid cells.

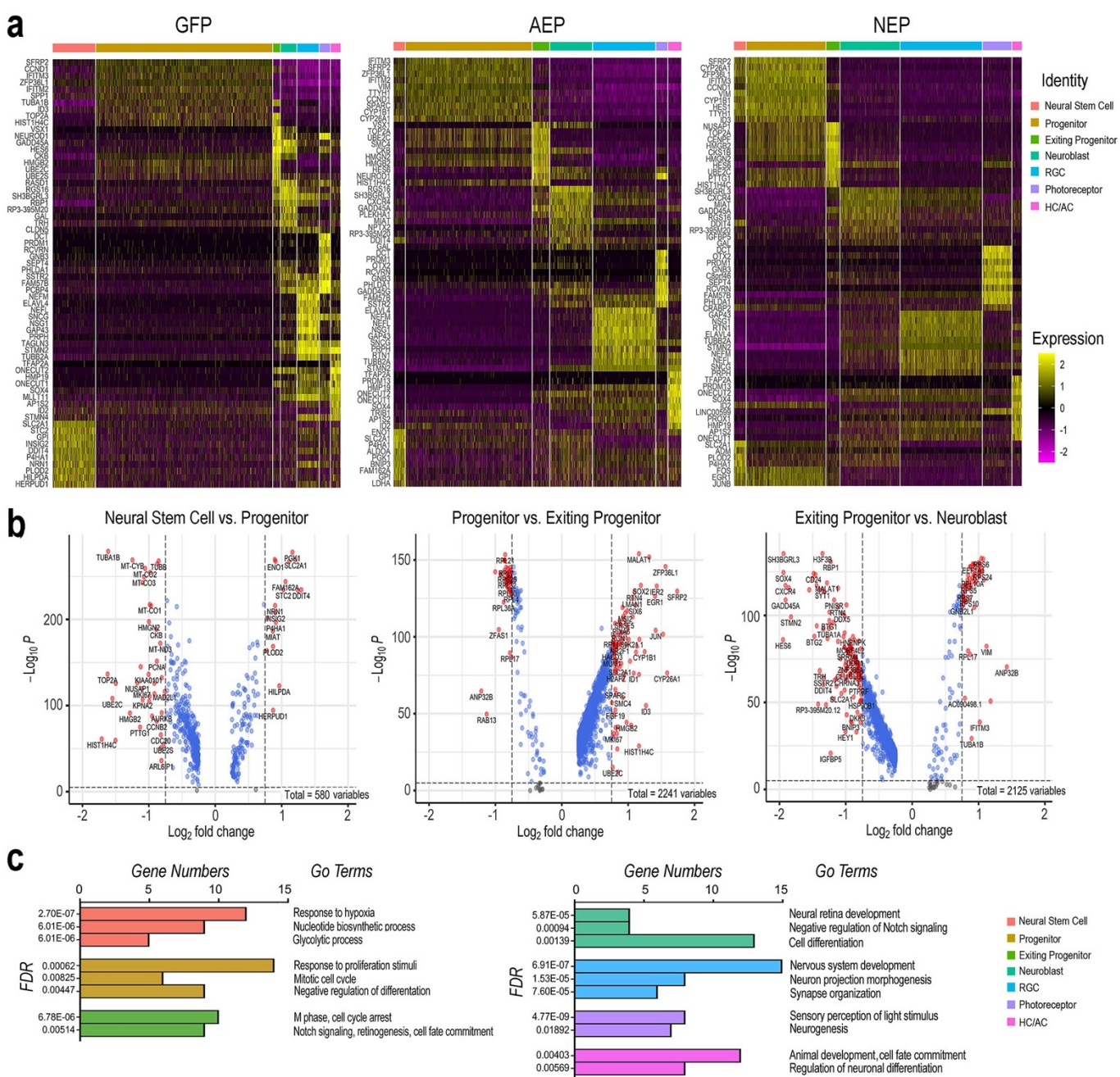


Fig. 7 Effects of elevating neurogenic factor expression on developmental transitions.

a Heatmaps of the top ten DEGs in each cell type category from cells of LV-GFP, LV-AEP, and LV-NEP infected retinal organoids. The side legend indicates the color codes for cell category identities atop the heatmaps. **b** Volcano plots show significant DEGs in LV-GFP infected retinal organoids during the three transitions: from the neural stem cell to the neurogenic progenitor state, from the cycling progenitor to the exiting progenitor state, and from the exiting progenitor to the neuroblast states. Genes with p value < 0.01 and fold change $> \log_2 0.75$ are shown as red dots. **c** Bar graphs show the predominant biological processes using GO pathway analysis for each cell category of LV-GFP infected retinal organoids. The false positive rates (FDR) and the gene numbers among the top 25 DEGs associated with a given GO term are shown. The right-side legend shows the same color codes corresponding to each cell category as in the heatmaps.

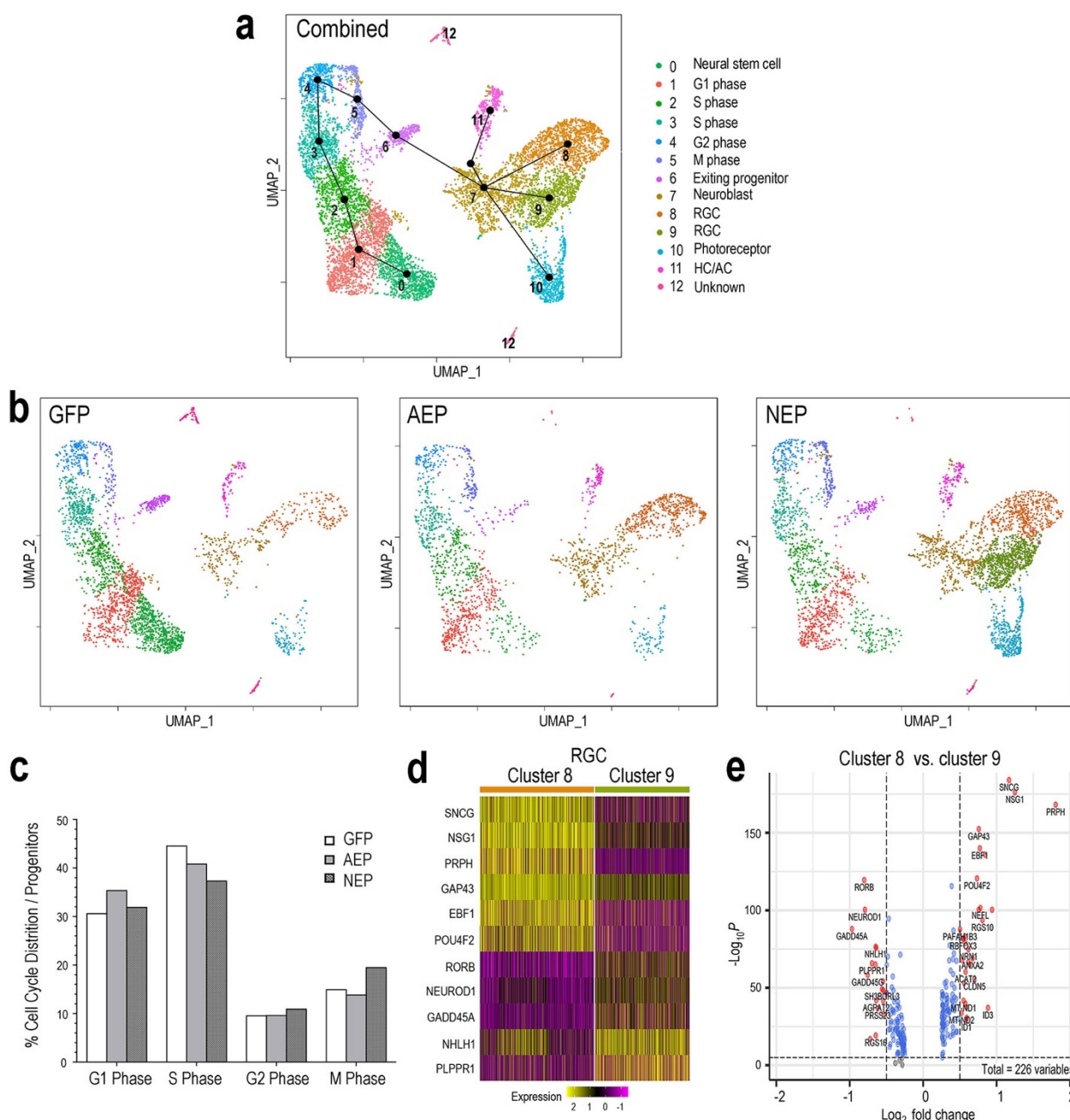


Fig. 8 Influence of neurogenic factors on cell cycle progression and retinal ganglion cell differentiation.

a UMAP of the combined sc RNA-seq dataset from LV-GFP, LV-AEP, and LV-NEP infected retinal organoids. Each cell cluster is assigned to an identity as shown on the side color legend based of feature plots of known genes. Line edges connecting individual clusters are generated by SLINGSHOT analysis to show the predicted developmental trajectory of the entire cell cohort. **b** UMAPs show cell clusters for individual samples from LV-GFP, LV-AEP, and LV-NEP infected retinal organoids with the same cell identity assignments as in the combined UMAP. **c** Distribution of cells in different phases of the cell cycle as percentages of total proliferative progenitor cells. The M phase cells include the exiting progenitors (cluster #6). **d** Heatmap shows differential expression levels of genes in the two RGC clusters 8 and 9. **e** Volcano plot shows DEGs between the two RGC clusters 8 and 9. Genes with p value < 0.01 and fold change $> \log_2 0.5$ are shown as red dots.

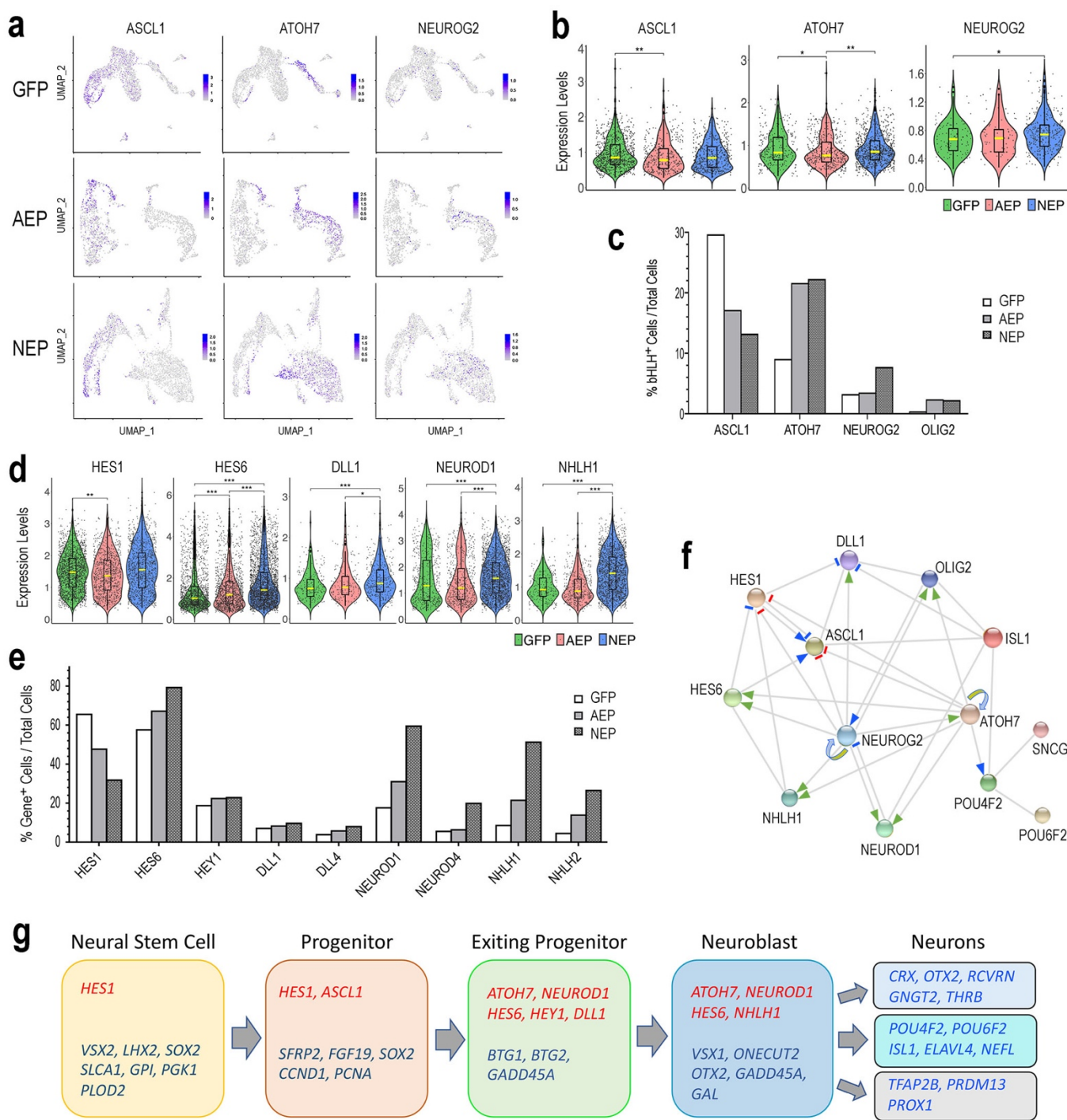


Fig. 9 Regulatory relationship among genes playing roles in early human retinogenesis.

a Feature plots show distribution of ASCL1, ATOH7, and NEUROG2 expressing cells among cell clusters in LV-GFP, LV-AEP, and LV-NEP infected retinal organoids. **b, d** Violin plots show comparisons of LV-GFP (green) versus LV-AEP (red) or LV-NEP (blue) induction on expression levels of endogenous genes in the retinal organoids. The box within the violin represents the middle 50% of the data, and the yellow line within the box indicates the median expression level. Statistical analysis generated P-values were based

Zhang, X. et al

on both the cell counts and expression levels. *** $p<0.001$, ** $p<0.01$, * $p<0.05$. **c, e** Bar graphs show percentages of cells expressing endogenous genes among total viral infected cells in LV-GFP, LV-AEP, and LV-NEP samples. **f** Schematic model based on STRING analysis summarizes a gene network involved in cell cycle exit and early retinogenesis. Grey edges represent protein-protein associations. Positive and negative regulatory relationships are indicated as arrows and short bars, respectively. Previously known molecular interactions from curated databases are shown as blue arrows and short bars. Effects of lentiviral induced ATOH7f and Neurog2 on endogenous human gene expression in retinal organoids are indicated as green arrows and red bars. Looping arrows indicate positive auto-regulation. **g** Summary of sequential expression of bHLH genes (red) and other key genes (blue) during early human retinal organoid development.

Zhang, X. et al

Supplementary Information

Xiangmei Zhang¹, Igor Mandric², Kevin H. Nguyen¹, Thao T. T. Nguyen¹, Matteo Pellegrini², James C. R. Grove¹, Steven Barnes^{1,3}, *Xian-Jie Yang^{1,4}

Description of Additional Supplementary Files

Supplementary Fig. 1 Characterization of human ES cell-derived 3D retinal organoids.

Supplementary Fig. 2 Effect of Dox induction time course on retinal organoid development.

Supplementary Fig. 3 Electrophysiological properties and functionality of Human H9 ES cell-derived retinal neurons.

Supplementary Fig. 4 Fluorescent activated cell sorting of lentivirus infected retinal organoids for single cell RNA-sequencing.

Supplementary Fig. 5 Expression of known genes used to assign cell categories of cell clusters.

Supplementary Fig. 6 Expression of featured known genes in combined sample clusters.

Supplementary Fig. 7 Expression patterns of Notch signaling components and selected bHLH genes in lentiviral infected retinal organoid cells.

Supplementary Fig. 8 Expression patterns of genes involved in cell cycle exit and early retinogenesis.

Supplementary Table 1 DEGs in Different Cell Categories of LV-GFP infected retinal organoids

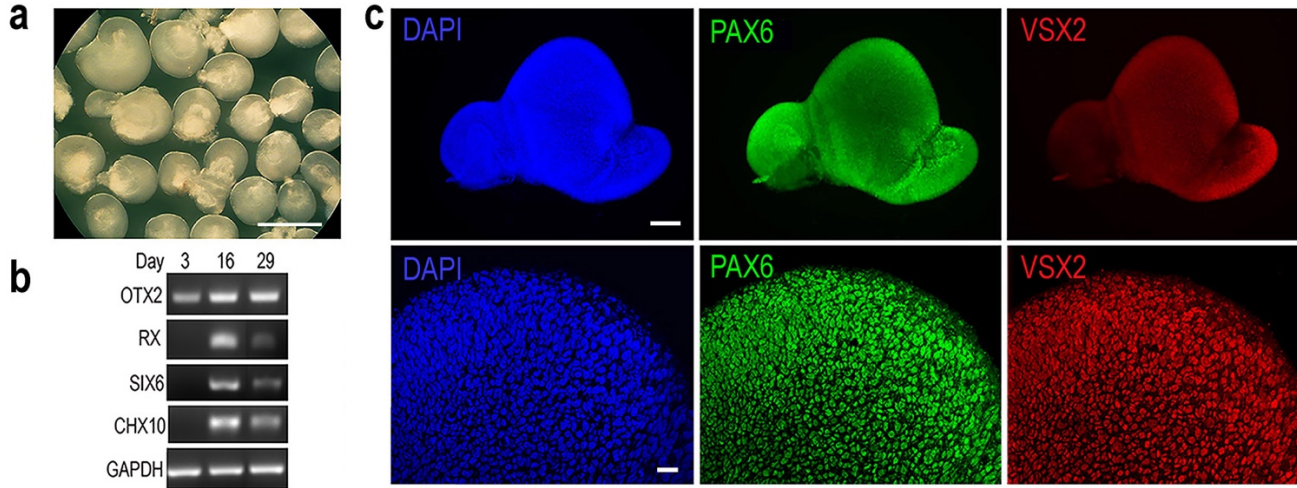
Supplementary Table 2 DEGs in Different Cell Categories of LV-AEP infected retinal organoids

Supplementary Table 3 DEGs in Different Cell Categories of LV-NEP infected retinal organoids

Supplementary Table 4 Top 10 DEGs in LV-GFP infected Different Cell Categories

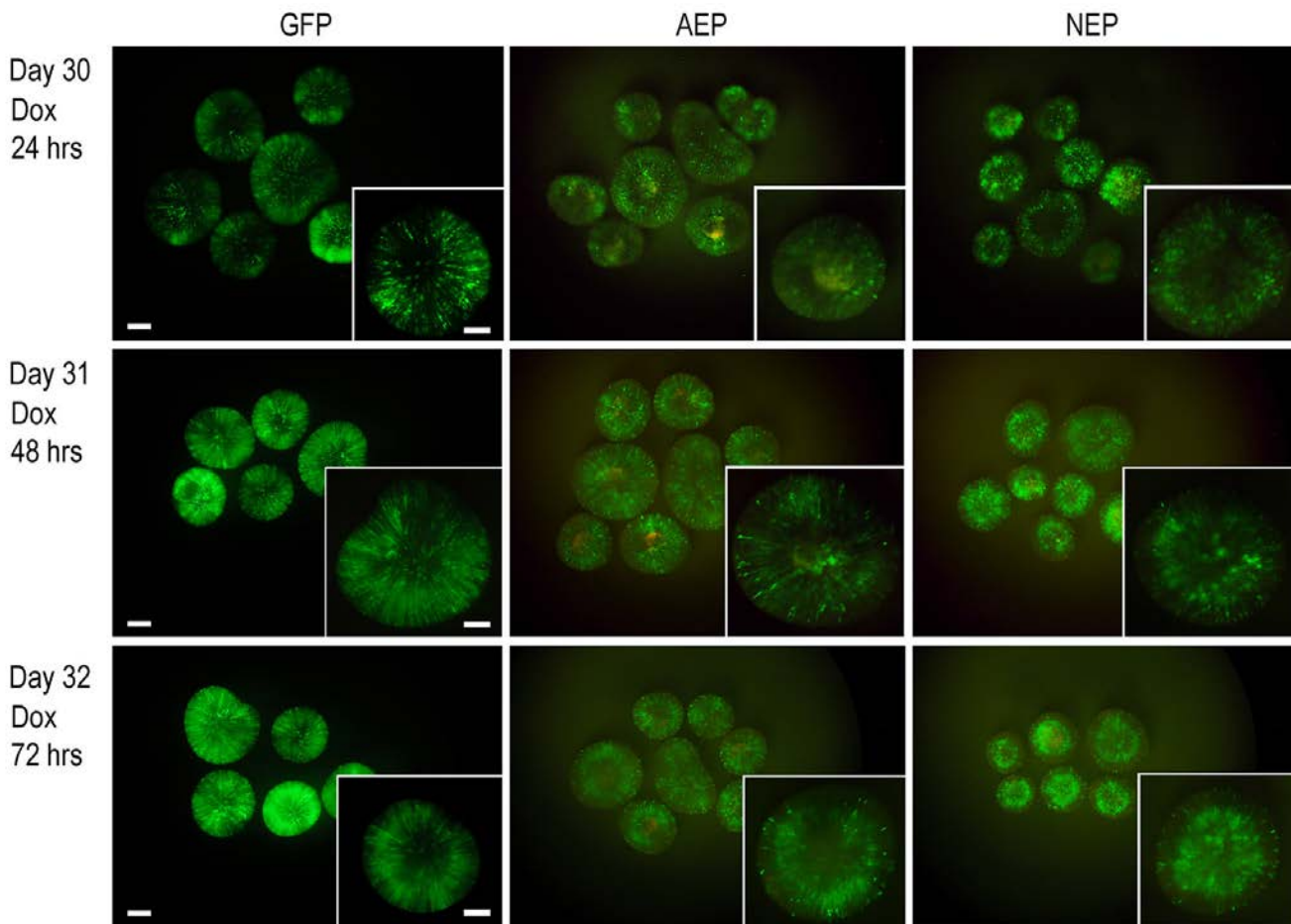
Supplementary Table 5 Top 10 DEGs in LV-AEP infected Different Cell Categories

Supplementary Table 6 Top 10 DEGs in LV-NEP infected Different Cell Categories



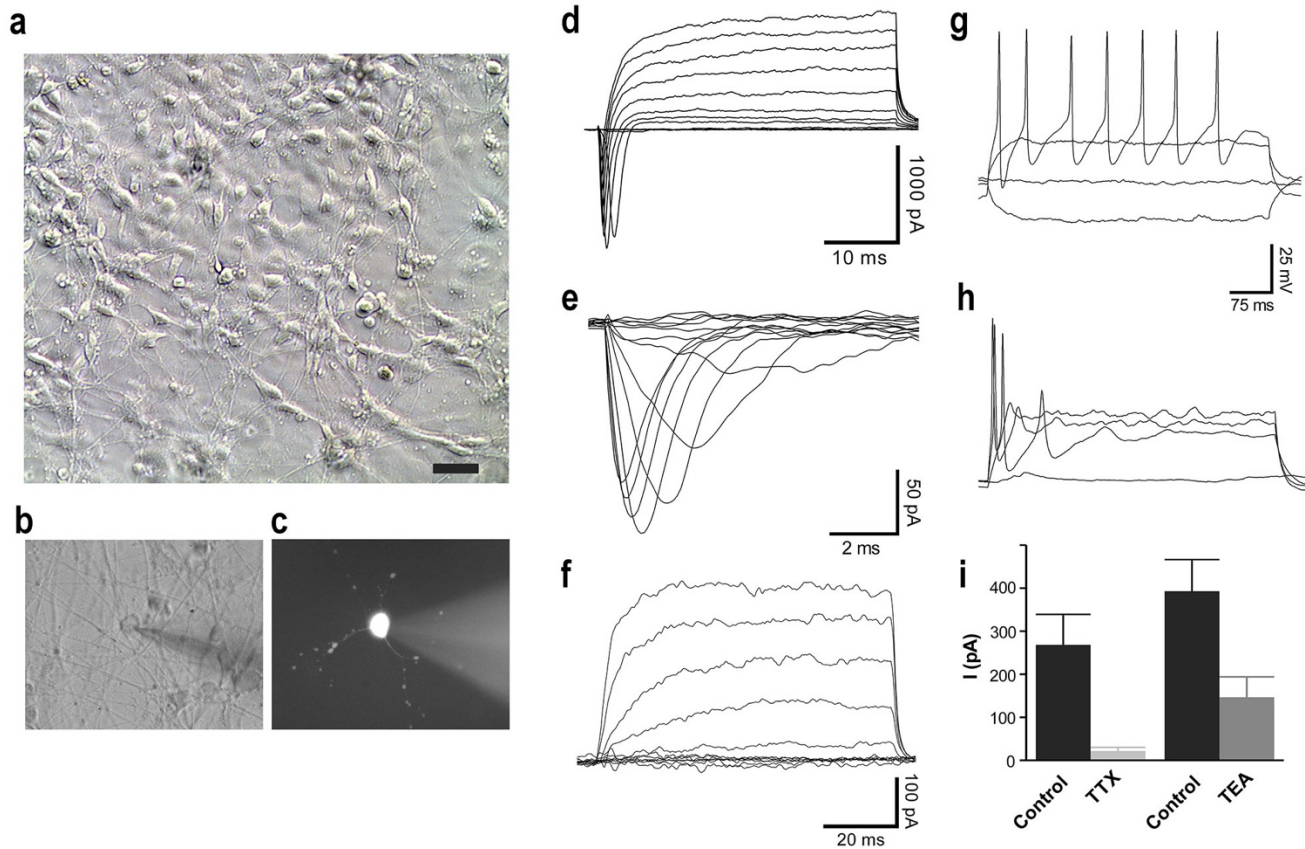
Supplementary Fig 1. Characterization of human ES cell-derived 3D retinal organoids.

a Bright field image shows morphology of a group of H9 ES cell-derived 3D retinal organoid at Day 33. Scale bar, 1 mm. **b** RT-PCR assay detects expression of eye field and neural retina genes at Day 16 and Day 29 in H9 ES cell-derived cultures. **c** Whole mount images show a 3D retinal organoid co-immunolabeled for PAX6 and VSX2 at Day 24. The top panels show low magnification images of the entire retinal organoid (scale bar, 100 μ m), and the bottom panels show confocal images with nuclear labeling of PAX6 and VSX2 in retinal progenitor cells (scale bar, 20 μ m).



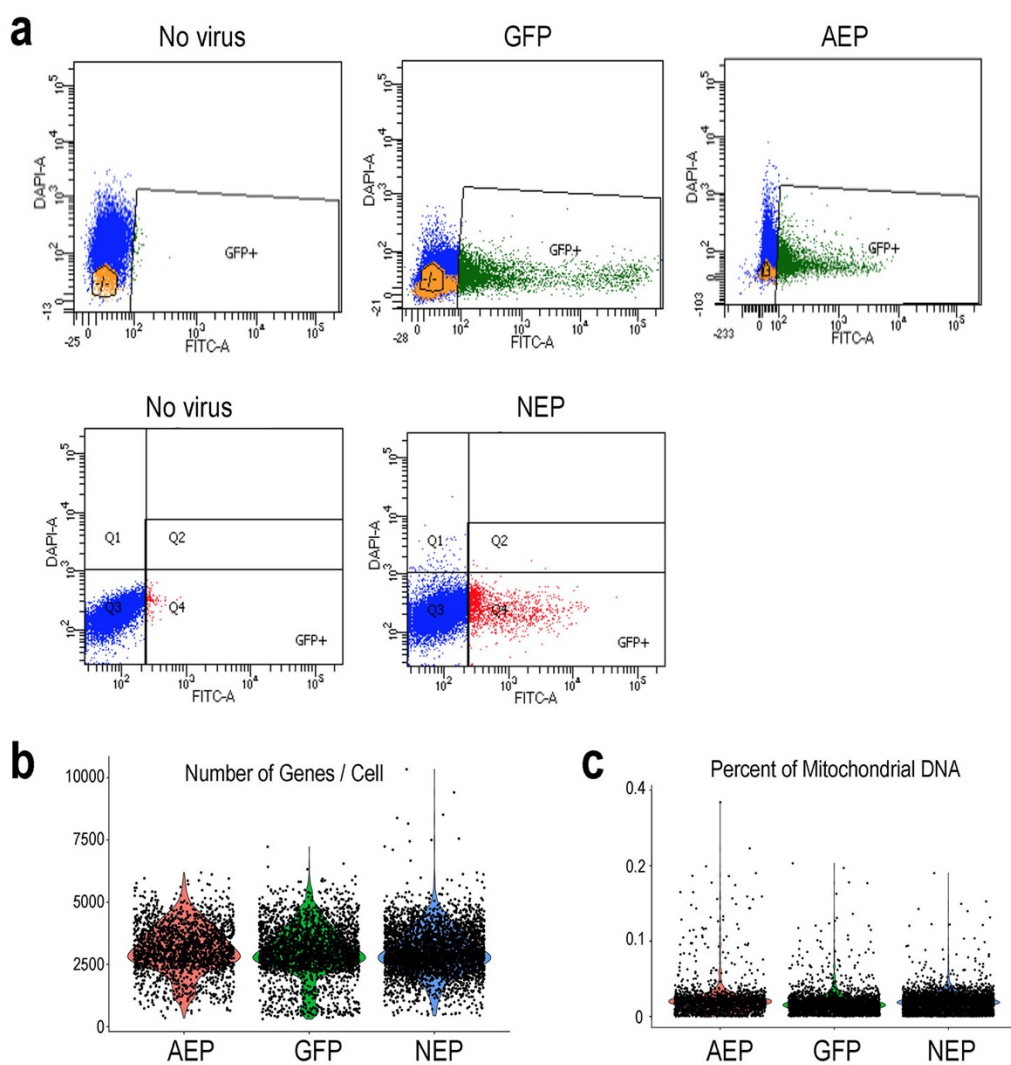
Supplementary Fig 2. Effect of Dox induction time course on retinal organoid development.

Whole mount images show effects of different Dox induction durations on retinal organoid development. After 24-hour of Dox induction, both LV-AEP and LV-NEP infected cells showed a tendency toward localizing to the inner layer, compared to the control LV-GFP virus infected retinal organoids. This trend became more pronounced after 48-hour Dox induction. By 72-hour after the onset of Dox treatments, the majority of GFP⁺ cells were concentrated in the inner layer of the retinal organoids. In contrast, most LV-GFP infected cells remained a ventricular zone distribution pattern after 48- and 72-hour induction. Scale bars, 200 μm for the lower magnification; 100 μm for the insets.



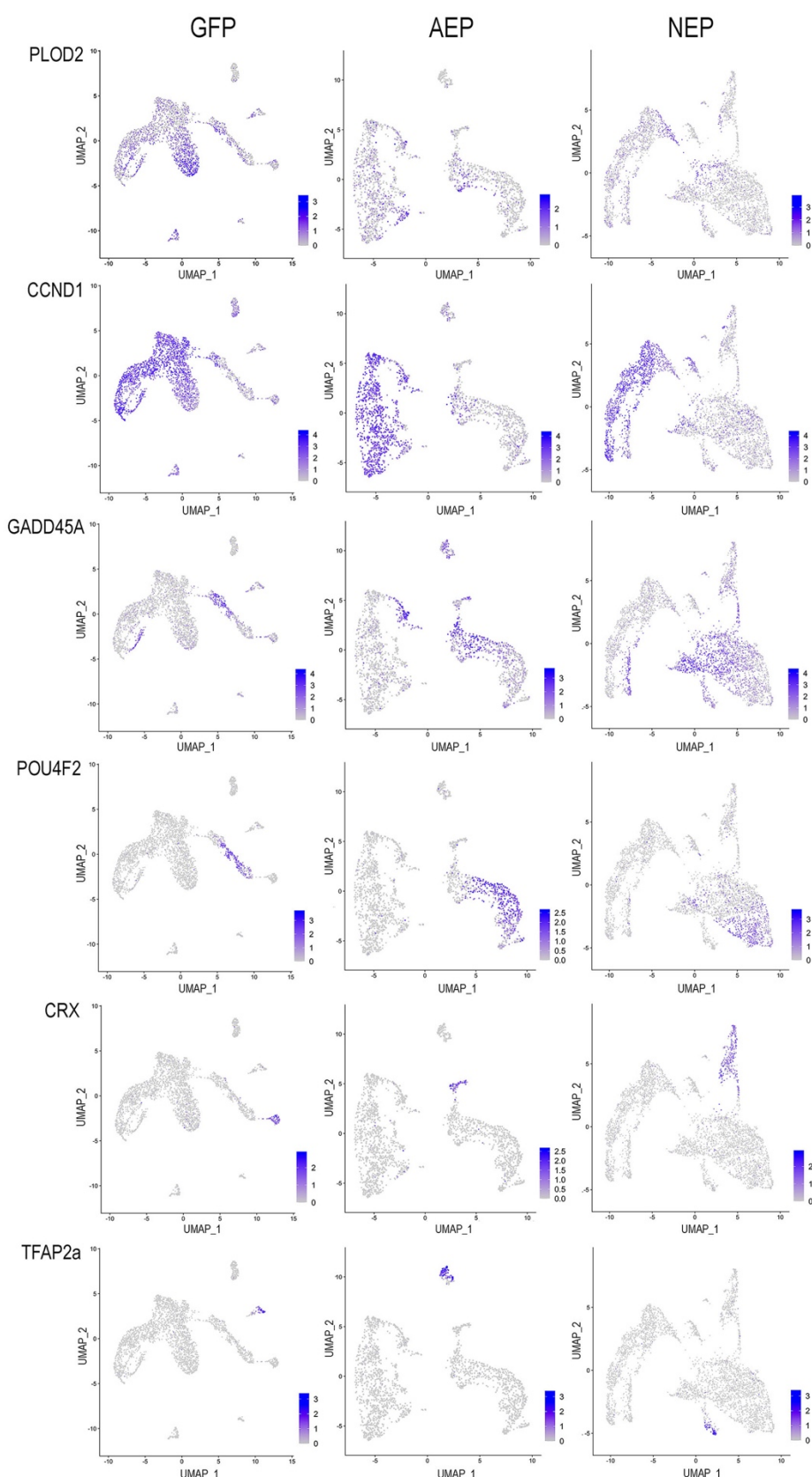
Supplementary Fig 3. Electrophysiological properties and functionality of Human H9 ES cell-derived retinal neurons.

a Bright field view of the dissociated cell culture derived from retinal organoids at Day 40. Scale bar, 20 μ m. **b, c** A neuron being patch recorded is shown in bright field (**b**) and after filling with lucifer yellow dye (**c**). **d - i** Whole cell patch clamp recording of dissociated neurons (Day 37-40) derived from H9 ES retinal organoids cultured as a monolayer. **d** Whole cell voltage clamp of a cell with multipolar neurites stepped from -60 mV to +30 mV in 10 mV steps of 40 ms duration. **e** Example of well-clamped I_{Na} isolated by digital subtraction following block with 100 nM TTX. Steps from -90 to +20 mV are shown. **f** Outward K^{+} currents isolated by digital subtraction following 10 mM TEA application. Steps from -70 to +30 mV are shown. **g** Train of action potentials elicited with depolarizing current in current clamped cells having large I_{Na} . **h** Phasic action potential generation in cells having smaller I_{Na} . **i** Summary of block of peak I_{Na} and I_K at +40 mV by TTX and TEA, respectively. TTX blocked 92% of the transient inward current ($n=7$) and TEA blocked 62% of the sustained outward current at +40 mV ($n=6$).



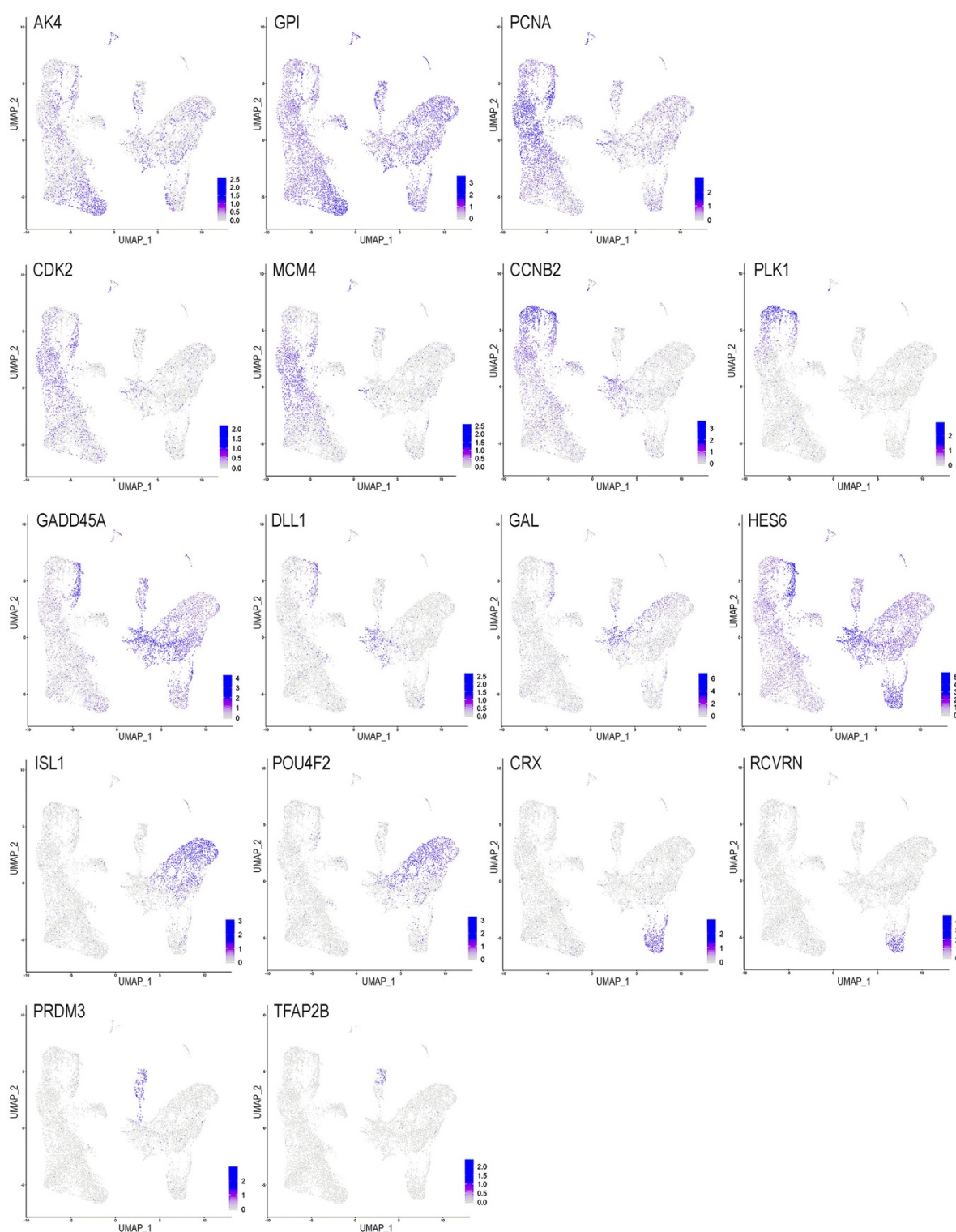
Supplementary Fig 4. Fluorescent activated cell sorting of lentivirus infected retinal organoids for single cell RNA-seq analyses.

a FACS profiles of dissociated retinal organoids infected with LV-GFP, LV-AEP, and LV-NEP between Day 45-48 after 8 day ox treatment. Cells from non-infected retinal organoids were used as negative controls to set the thresholds for GFP⁺ cells. FACS enriched GFP⁺ cells were used for single cell RNA-seq analyses. **b** Violin plots show the numbers of genes detected in single cell RNA-seq analyses using 10X Genomics Chromium and NovaSeq work flow. The cutoff used in this study was 2500 UMI per cell, resulting in mean gene per cell ranging from 2935-3079. For downstream analysis 3004 cells for LV-GFP, 2063 cells for LV-AEP, and 3909 cells for LV-NEP were used. **c** Violin plots show percentage of mitochondrial encoded genes detected in single cell RNA-seq analyses using 10X Genomics Chromium and NovaSeq work flow. The low rates (<0.03%) of transcripts from the mitochondrial genome indicate that the transcripts analyzed in this study are from the nuclear genome.



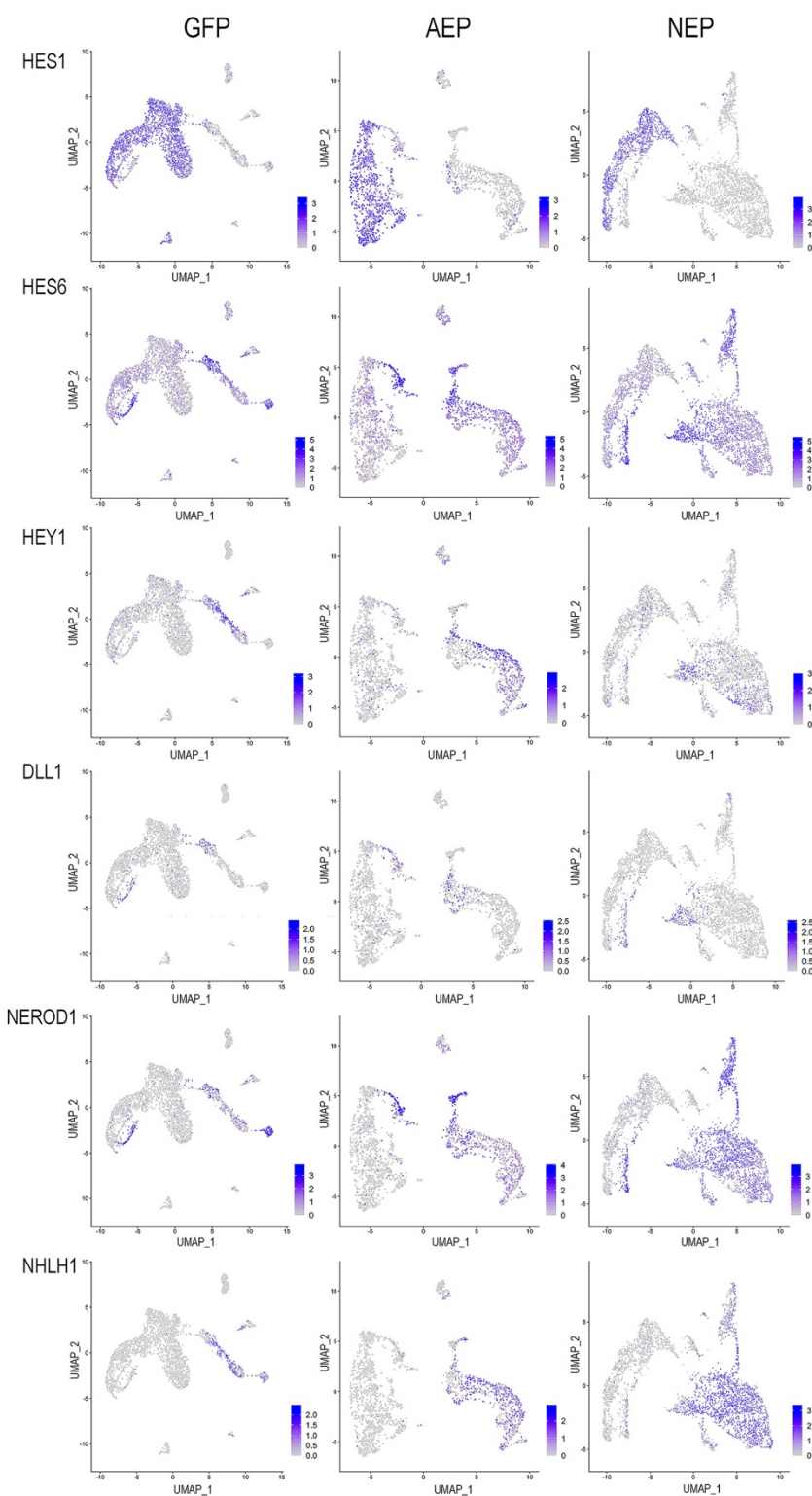
Supplementary Fig 5. Expression of known genes used to assign cell categories of cell clusters.

Feature plots of known genes in LV-GFP, LV-AEP, or LV-NEP infected retinal organoids shown as UMAPs. Genes representing different cell category or states are used to assign cell cluster identities in Figure 5.



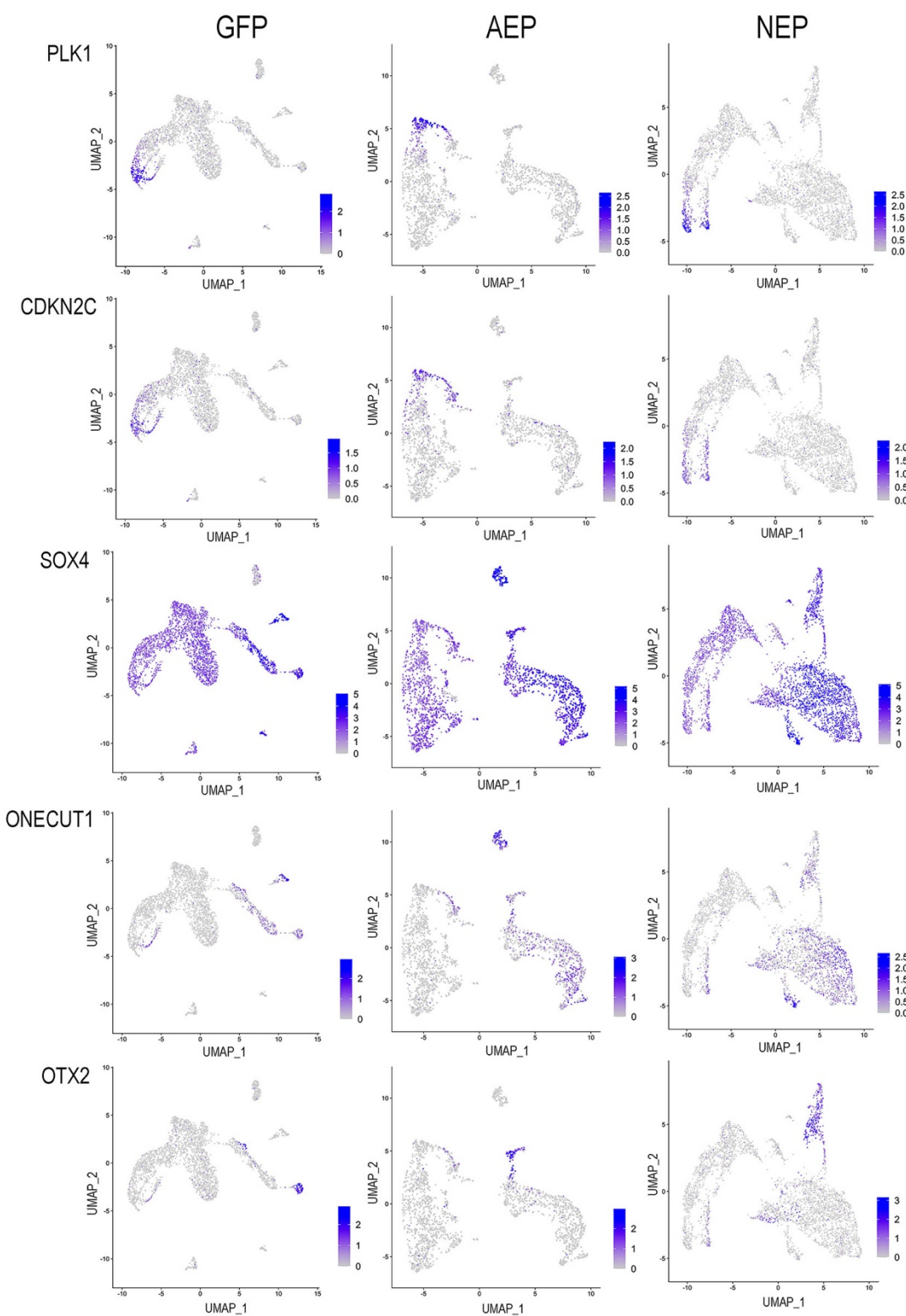
Supplementary Fig 6. Expression of featured known genes in combined sample clusters.

Feature plots of known genes in the combined LV-GFP, LV-AEP, LV-NEP sample clusters shown as UMAPs. Genes representing different cell cycle phases and cell type categories are used to assign cluster identities in Figure 8.



Supplementary Fig 7. Expression patterns of Notch signaling components and selected bHLH genes in lentiviral infected retinal organoid cells.

Feature plots of selected genes quantified in Figure 9 are shown in UMAPs in LV-GFP, LV-AEP, and LV-NEP infected retinal organoid cells. HES1 is predominantly expressed among neural stem cells and progenitors. HES6, DLL1, and NEUROD1 are upregulated in exiting progenitors and neuroblasts. NHLH1 is expressed among postmitotic cells.



Supplementary Fig 8. Expression patterns of genes involved in cell cycle exit and early retinogenesis.

Feature plots of selected genes involved in cell cycle exit (PLK1, CDKN2C) and differentiation of early retinal neurons (SOX4, ONECUT1, OTX2) are shown in UMAPs in LV-GFP, LV-AEP, and LV-NEP infected retinal organoid cells.

SupTable 1 enriched_genes GFP

p_val	avg_logFC	pct.1	pct.2	p_val_adj	cluster	gene
7.9755606001145E-273 bioRxiv preprint doi: https://doi.org/10.1101/2020.10.27.358135 ; this version posted November 9, 2020. The copyright holder for this preprint (which was not certified by peer review) is the author/funder. All rights reserved. No reuse allowed without permission.	1.40687509154545 2.49792717412938E-215 1.10792614355096	0.994 0.979	0.774 0.679	1.52412963068188E-268 4.77353882976125E-211	progenitors	SFRP2
3.43739052011704E-189	0.661234409989596	0.999	0.988	6.56885328394367E-185	progenitors	MDK
1.85787725777464E-183	1.02937240932241	0.917	0.527	3.55040343960734E-179	progenitors	IFITM3
7.4066933197728E-179	0.819761985581814	0.976	0.648	1.41541909340858E-174	progenitors	ZFP36L1
4.51175725400407E-172	0.787631464388297	0.969	0.641	8.62196811240178E-168	progenitors	TTYH1
9.07551000912606E-155	0.881976464884904	0.794	0.328	1.73432996274399E-150	progenitors	IFITM2
5.76141481742139E-154	0.799704968799598	0.94	0.567	1.10100637160923E-149	progenitors	SPP1
6.64350211498513E-148	0.840515644141872	0.996	0.969	1.26957325417366E-143	progenitors	TUBA1B
1.88386152573912E-126	0.621192986811673	0.932	0.727	3.60005937568746E-122	progenitors	DEK
1.18218032574657E-125	0.67921767663654	0.643	0.183	2.2591466025017E-121	progenitors	GINS2
4.57246738821475E-123	0.609213915727916	0.903	0.601	8.73798517887838E-119	progenitors	RP11-89K21.1
4.92471143473067E-116	0.567413808768627	0.896	0.566	9.41112355177032E-112	progenitors	B2M
6.78419789683693E-114	0.643224717975966	0.872	0.408	1.29646021808554E-109	progenitors	HES1
1.25266281234429E-112	0.790896270778651	0.935	0.672	2.39383863438994E-108	progenitors	CYP1B1
3.71157881274742E-110	0.56845054657633	0.965	0.827	7.09282711116033E-106	progenitors	DAPL1
9.47851380992014E-106	0.544128558483986	0.823	0.413	1.81134398907574E-101	progenitors	PLPP3
2.29512269324383E-102	0.538160225222921	0.712	0.303	4.38597946678896E-98	progenitors	TBX2-AS1
2.9634559484066E-100	0.60736485041439	0.932	0.672	5.66316431740501E-96	progenitors	PTH2
4.10383312759495E-100	0.50241902865796	0.943	0.744	7.84242510683395E-96	progenitors	MEST
1.64508262638385E-98	0.621349801715633	0.813	0.418	3.14375289901954E-94	progenitors	SPARC
3.08005162023791E-97	0.513896844518293	0.836	0.404	5.88597864627465E-93	progenitors	COL2A1
6.21477479652623E-95	0.614819187063231	0.591	0.199	1.18764346361616E-90	progenitors	MCM3
8.20939338874565E-90	0.436693803033564	0.985	0.935	1.56881507658929E-85	progenitors	HMGN2
1.03813375597682E-89	0.725014202179418	0.711	0.334	1.98387360767169E-85	progenitors	FGF19
1.1444583992625E-89	0.576919168216335	0.679	0.266	2.18706000099064E-85	progenitors	DIO3
7.43317452505313E-88	0.486400974275083	0.775	0.411	1.42047965173765E-83	progenitors	RARRES2
2.65955593217619E-87	0.503673152067052	0.992	0.872	5.0824113863887E-83	progenitors	MT-ND3
2.9018769860261E-87	0.595989641921429	0.678	0.325	5.54548692029588E-83	progenitors	PCNA
8.78495335048191E-86	0.581726635344588	0.671	0.308	1.67880458527709E-81	progenitors	FGFBP3
9.50542463087766E-85	0.542706182943927	0.597	0.226	1.81648664696072E-80	progenitors	HELLS
7.43147864698818E-84	0.474606936552254	0.998	0.965	1.42015556943944E-79	progenitors	MT-CO2
8.1460831708448E-84	0.621360488583355	0.757	0.474	1.55671649394844E-79	progenitors	TYMS
1.66001317051003E-83	0.465485679411969	0.899	0.728	3.17228516884466E-79	progenitors	ISYNA1
3.2183757795482E-83	0.490762459080629	0.582	0.201	6.15031611471662E-79	progenitors	S1PR3

2.3447809169782E-82	0.442758745237253	0.971	0.81	4.48087633234534E-78	progenitors	DKK 3.00
3.74533094995838E-80	0.700091212262773	0.534	0.185	7.15732744537046E-76	progenitors	KIAA0101
6.4476450063939E-79	0.483141586929653	0.998	0.963	1.23214496072187E-74	progenitors	MT-CO3
bioRxiv preprint doi: https://doi.org/10.1101/2020.10.27.358135 ; this version posted November 9, 2020. The copyright holder for this preprint (which was not certified by peer review) is the author/funder. All rights reserved. No reuse allowed without permission.	0.4236272854560112	0.973	0.744	5.86732794560121E-74	progenitors	SOX2
1.33828391585674E-77	0.603685119175813	0.794	0.495	2.55746056320223E-73	progenitors	ID1
3.44969254424384E-77	0.437593496984861	0.995	0.931	6.59236245204999E-73	progenitors	MT-ND2
3.59026874612646E-76	0.446677955154178	0.579	0.228	6.86100357384766E-72	progenitors	CENPH
4.03455530289855E-76	0.419403791589622	0.421	0.087	7.71003518383913E-72	progenitors	MIR503HG
1.62510926053466E-75	0.435428309792301	0.996	0.979	3.10558379688174E-71	progenitors	HMGB1
4.98192161231705E-75	0.875412079859905	0.733	0.414	9.52045220113788E-71	progenitors	ID3
5.6953711252113E-73	0.479774423345868	0.856	0.633	1.08838542202788E-68	progenitors	NASP
3.53298926407885E-71	0.467483942442178	0.882	0.619	6.75154248365468E-67	progenitors	CYP26A1
1.83072528705826E-70	0.535537424521579	0.741	0.451	3.49851602356834E-66	progenitors	CKS1B
1.24481668509821E-69	0.635295003832914	0.696	0.405	2.37884468522268E-65	progenitors	SMC4
3.7046619019519E-64	0.798452198708058	0.521	0.202	7.07960889463007E-60	progenitors	TOP2A
5.24947467545876E-63	0.425849074858971	0.495	0.177	1.00317461048017E-58	progenitors	FEN1
2.92847307196571E-62	0.445180162747358	0.989	0.908	5.59631204052646E-58	progenitors	MT-CYB
6.54309978667991E-62	0.697204465378261	0.884	0.726	1.25038636923453E-57	progenitors	HMGB2
2.28898711485599E-61	0.765639561374385	0.505	0.196	4.3742543764898E-57	progenitors	CENPF
1.6963439426054E-60	0.420717811566397	0.997	0.967	3.24171327431891E-56	progenitors	MT-CO1
2.06308862397935E-58	0.41501160545408	0.724	0.409	3.94256236042454E-54	progenitors	SEPP1
4.59167516996084E-58	0.425414784252933	0.539	0.237	8.77469124979516E-54	progenitors	DHFR
1.68961814827451E-56	0.525592088713305	0.475	0.172	3.22886028135259E-52	progenitors	NUSAP1
3.01348731706459E-54	0.406246502267912	0.942	0.796	5.75877426291044E-50	progenitors	IER2
2.74138679607937E-53	0.444055898293628	0.55	0.262	5.23879016730768E-49	progenitors	MAD2L1
9.66929493090489E-53	0.471371946233367	0.672	0.416	1.84780226129592E-48	progenitors	MCM7
2.10910537245109E-51	0.54867690882502	0.451	0.175	4.03050036675404E-47	progenitors	BIRC5
5.38642089275047E-51	0.454333561782403	0.451	0.167	1.02934503260462E-46	progenitors	CDK1
2.18359038913561E-49	0.420807851928472	0.518	0.238	4.17284123363815E-45	progenitors	CDH6
3.75865044952468E-49	0.431575939059201	0.704	0.394	7.18278100904166E-45	progenitors	CYR61
1.21272102890455E-47	0.587471409081136	0.385	0.128	2.3175098862366E-43	progenitors	MKI67
6.46889453519932E-43	0.419404262722712	0.839	0.599	1.23620574567659E-38	progenitors	JUNB
4.64085635730905E-41	0.448617273737377	0.362	0.13	8.86867649881759E-37	progenitors	AURKB
6.95174461505258E-39	0.610016279317122	0.497	0.258	1.32847839593655E-34	progenitors	UBE2C
2.46759395815494E-38	0.520143321522578	0.402	0.173	4.7155720540341E-34	progenitors	TPX2
7.61835655943597E-33	0.523314704195058	0.786	0.629	1.45586793850821E-28	progenitors	CKS2
7.36380820794777E-32	0.511591502387503	0.3	0.105	1.40722374853882E-27	progenitors	CDC20

1.85546245477534E-31	0.814642413278677	0.935	0.873	3.54578875107567E-27	progenitors	HIST1H4C
7.2892347948877E-31	0.43184222451599	0.452	0.232	1.39297276930304E-26	progenitors	CCNB2
8.12331374223601E-28	0.59698575183878	0.642	0.469	1.5523652561413E-23	progenitors	PTTG1
bioRxiv preprint doi: https://doi.org/10.1101/2020.10.27.358135 ; this version posted November 9, 2020. The copyright holder for this preprint (which was not certified by peer review) is the author/funder. All rights reserved. No reuse allowed without permission.	0.4287051411923474	0.943	0.167	5.11002958970013E-18	progenitors	CCNB1
7.2954676474322E-155	1.59801553415597	0.866	0.05	1.39416386742429E-150	existing_prog	VSX1
6.60352544408742E-117	0.727883067037444	0.343	0.006	1.26193371236511E-112	existing_prog	RP11-843A23.1
2.5376524724651E-81	1.0560642998102	0.627	0.052	4.84945387488082E-77	existing_prog	MFAP4
1.82812054128679E-71	0.557587653945204	0.493	0.034	3.49353835439905E-67	existing_prog	DLL4
5.31471679219532E-70	0.736852776320794	0.716	0.08	1.01564237898853E-65	existing_prog	BHLHE22
1.03911716785467E-64	2.12932606929404	0.896	0.173	1.98575290777027E-60	existing_prog	NEUROD1
4.76405497382693E-50	0.967624209563029	0.821	0.169	9.10410905498325E-46	existing_prog	SHD
1.54649201390174E-49	0.731412981642897	0.687	0.111	2.95534623856623E-45	existing_prog	CDKN2C
1.24149239692652E-47	1.40548563638122	0.985	0.295	2.37249197052657E-43	existing_prog	GADD45A
2.86340248560657E-46	0.542044286273424	0.552	0.068	5.47196214999416E-42	existing_prog	C8orf46
1.05214282875885E-45	1.00471560669357	0.91	0.234	2.01064494575815E-41	existing_prog	PBK
1.30963881664185E-45	0.749194849063614	0.821	0.163	2.50271977860258E-41	existing_prog	RRM2
1.01620438006571E-43	1.38604262276484	1	0.344	1.94196657030558E-39	existing_prog	NUSAP1
1.46083426287943E-43	2.63111846143287	1	0.588	2.79165427636259E-39	existing_prog	HES6
3.53260657732805E-43	1.14041536306767	0.955	0.271	6.7508111692739E-39	existing_prog	MKI67
4.34505382704302E-43	0.902906248820952	0.791	0.172	8.3033978634792E-39	existing_prog	CDCA3
4.62066640592687E-42	0.594050125177204	0.672	0.115	8.83009350172626E-38	existing_prog	MYBL1
6.74900231902127E-42	0.507400371246714	0.522	0.069	1.28973434316497E-37	existing_prog	DLL1
1.05350474395392E-41	0.998458630196453	0.925	0.278	2.01324756569593E-37	existing_prog	UBE2T
7.10066245155802E-41	0.776982410661886	0.836	0.206	1.35693659449274E-36	existing_prog	SGOL1
8.85734281940211E-40	1.10717671982602	0.97	0.299	1.69263821278774E-35	existing_prog	TPX2
1.58041042184966E-39	0.73287798808578	0.791	0.176	3.02016431615471E-35	existing_prog	CDCA8
1.77055611911868E-39	0.980632863928712	0.806	0.196	3.38353274363579E-35	existing_prog	DOK5
2.79994071784548E-39	1.07253042476517	0.896	0.276	5.35068671180271E-35	existing_prog	PRC1
4.82477763184945E-39	1.56099638527471	1	0.999	9.2201500544643E-35	existing_prog	CKB
6.97183836751321E-39	1.23239848035053	1	0.965	1.33231831203177E-34	existing_prog	HMGN2
1.08268544410143E-38	1.41338645627875	0.985	0.386	2.06901188367782E-34	existing_prog	TOP2A
2.07755422569486E-38	0.923843902999023	0.836	0.211	3.97020612530288E-34	existing_prog	GTSE1
3.92925932111274E-38	0.755438453280477	0.746	0.157	7.50881456264644E-34	existing_prog	RASD1
2.77295413876964E-37	0.527949225101387	0.716	0.155	5.29911535918878E-33	existing_prog	NCAPG
3.44194137894503E-37	0.924203753760683	0.791	0.2	6.57754997516396E-33	existing_prog	NUF2
7.31321183428214E-37	0.980581628275162	1	0.746	1.39755478153132E-32	existing_prog	IDH2
1.52766569132086E-36	1.02382029302317	0.881	0.259	2.91936913611416E-32	existing_prog	AURKB

1.59729578489234E-36	0.721881014185471	0.791	0.19	3.05243224492925E-32	existing_prog	SPC25	
2.51169241501061E-36	0.753274596736131	0.806	0.198	4.79984420508528E-32	existing_prog	SGOL2	
2.59285993689261E-36	0.816670319827165	0.761	0.186	4.95495533940178E-32	existing_prog	CKAP2L	
bioRxiv preprint doi: https://doi.org/10.1101/2020.10.27.358135 ; this version posted November 9, 2020. The copyright holder for this preprint (which was not certified by peer review) is the author/funder. All rights reserved. No reuse allowed without permission.	3.03629292321624E-36	0.497355624466019	0.507	0.075	5.60235577026024E-32	existing_prog	INSM1
7.65469081446276E-36	0.951840337456847	0.836	0.233	1.46281141464383E-31	existing_prog	CCNA2	
1.35978838468871E-35	0.761160428621885	0.91	0.261	2.59855560314013E-31	existing_prog	FBXO5	
3.23633523118906E-35	0.813155405104769	0.776	0.199	6.18463662680229E-31	existing_prog	FAM64A	
3.92165270668022E-35	0.856828517375848	0.881	0.258	7.49427832246591E-31	existing_prog	CDKN2D	
7.12982455184349E-35	0.80385930452932	0.881	0.283	1.36250947185729E-30	existing_prog	ZWINT	
1.02450705570738E-34	0.948922501062978	1	0.985	1.95783298345681E-30	existing_prog	H2AFZ	
1.41196897993069E-34	1.47472975445024	1	0.82	2.69827272064755E-30	existing_prog	HMGB2	
2.86951282578953E-34	0.787073903850393	0.731	0.176	5.48363901008379E-30	existing_prog	PSRC1	
6.04793414891691E-34	1.62890152812534	0.925	0.393	1.15576021585802E-29	existing_prog	UBE2C	
8.23549040130026E-34	0.758637044279571	0.672	0.147	1.57380221568848E-29	existing_prog	AURKA	
9.35928968865454E-34	0.860952879875394	1	0.999	1.78856025950188E-29	existing_prog	PTMA	
3.30532430738971E-33	0.806387285569613	0.881	0.316	6.31647475142173E-29	existing_prog	UCP2	
4.62102669373386E-33	1.13700363673009	1	0.986	8.8307820117254E-29	existing_prog	TUBA1B	
1.14440022447554E-32	1.00429008294443	0.91	0.385	2.18694882897275E-28	existing_prog	H2AFX	
2.31921674074877E-32	0.928571787629098	0.97	0.428	4.4320231915709E-28	existing_prog	MAD2L1	
2.51219741872693E-32	1.13904273631812	0.881	0.331	4.80080926718715E-28	existing_prog	CDK1	
4.2506084272983E-32	1.1474888913394	1	0.622	8.12291270456706E-28	existing_prog	CKS1B	
5.3344428765544E-32	1.1294079923649	0.985	0.576	1.01941203370955E-27	existing_prog	SMC4	
7.85668823783565E-32	0.984786582987625	0.821	0.247	1.50141312225039E-27	existing_prog	CDKN3	
8.02178746056601E-32	0.578592597710502	0.687	0.146	1.53296358371416E-27	existing_prog	ONECUT2	
1.2588052172725E-31	1.47249990993975	0.94	0.46	2.40557677020775E-27	existing_prog	UBE2S	
1.59516973573476E-31	1.33588154265014	0.97	0.374	3.04836936498912E-27	existing_prog	CENPF	
5.14031443825488E-31	0.817606403001444	1	0.989	9.82314089150508E-27	existing_prog	HMGB1	
8.2087487622577E-31	0.598301786668799	0.701	0.166	1.56869188846745E-26	existing_prog	MXD3	
1.3557635702213E-30	0.475357858281166	0.657	0.148	2.59086418269291E-26	existing_prog	KIF15	
1.95706620541264E-30	1.0722482040925	0.881	0.334	3.73995351854356E-26	existing_prog	BIRC5	
7.4217053560326E-30	0.638913982569562	0.731	0.19	1.41828789353783E-25	existing_prog	NDC80	
9.33131488722909E-30	0.666058723520646	0.821	0.248	1.78321427494948E-25	existing_prog	CENPK	
9.90908654614488E-30	0.584211842756503	0.866	0.29	1.89362643896829E-25	existing_prog	ASRGL1	
1.83322285793802E-29	0.613701059785158	0.791	0.225	3.50328888151956E-25	existing_prog	TACC3	
1.9548299228709E-29	0.503775207026738	0.552	0.114	3.7356799826063E-25	existing_prog	ZMYND10	
2.24849728105453E-29	0.483089503081992	0.507	0.095	4.2968783040952E-25	existing_prog	DLEU2	
2.36290431328369E-29	0.627995018553958	0.851	0.26	4.51551014268513E-25	existing_prog	CENPN	

3.7886395640642E-29	0.554625865732959	0.687	0.175	7.24009020692668E-25	existing_prog	RACGAP1
5.65115008315656E-29	0.468574998216204	0.567	0.117	1.07993478089122E-24	existing_prog	CASC5
1.03884387434083E-28	0.515928391805806	0.552	0.106	1.98523064386532E-24	existing_prog	ONECUT1
bioRxiv preprint doi: https://doi.org/10.1101/2020.10.27.358135 ; this version posted November 9, 2020. The copyright holder for this preprint (which was not certified by peer review) is the author/funder. All rights reserved. No reuse allowed without permission.	0.679073335580308	0.791	0.247	1.01489035749471E-23	existing_prog	CENPU
1.25741641292377E-27	0.818581502824748	0.881	0.352	2.40292276509733E-23	existing_prog	CKAP2
2.44522855856349E-27	0.607373934942404	0.776	0.228	4.67283177541482E-23	existing_prog	KIFC1
3.04419149154798E-27	0.62637358685408	1	0.998	5.81744994034819E-23	existing_prog	TUBB
3.05443694817393E-27	1.09596490699613	0.985	0.72	5.83702900796038E-23	existing_prog	CKS2
3.36784990519711E-27	0.42693993637781	0.672	0.164	6.43596116883168E-23	existing_prog	SPC24
3.923708560857E-27	0.690870853343097	0.776	0.243	7.49820705979772E-23	existing_prog	C21orf58
3.94437240827199E-27	0.846042979090783	0.91	0.464	7.53769567220777E-23	existing_prog	USP1
4.34965226823358E-27	0.551268498970132	0.552	0.117	8.31218548459438E-23	existing_prog	BUB1
4.58626210612885E-27	0.78900804776406	0.657	0.174	8.76434688481223E-23	existing_prog	NEK2
1.17593924674731E-26	0.689886435890713	0.955	0.416	2.2472199005341E-22	existing_prog	SMC2
1.19569238641449E-26	0.821281199365484	0.91	0.408	2.28496815043808E-22	existing_prog	EZH2
1.96075667622333E-26	0.562612782563995	0.627	0.149	3.74700600826279E-22	existing_prog	DLGAP5
5.99461693399616E-26	0.712221848205321	0.776	0.283	1.14557129608667E-21	existing_prog	CENPW
8.46745756466602E-26	0.499565187319837	0.612	0.147	1.61813114060768E-21	existing_prog	KIF2C
8.53226925239724E-26	0.790789115618358	0.731	0.231	1.63051665413311E-21	existing_prog	KNSTRN
1.0019510792364E-25	1.21033369267315	0.955	0.567	1.91472851242077E-21	existing_prog	PTTG1
1.13678414260447E-25	1.00757020162547	0.94	0.611	2.17239449651714E-21	existing_prog	CCDC34
3.97063869907024E-25	0.521135420714982	0.597	0.144	7.58789055392323E-21	existing_prog	HJURP
4.08029359587267E-25	0.421260028283671	0.612	0.147	7.79744106171267E-21	existing_prog	APOLD1
6.3013483542176E-25	0.451841086573045	0.612	0.153	1.20418767049098E-20	existing_prog	FOXN4
1.02546496660826E-24	0.727826563894479	0.806	0.263	1.95966355118838E-20	existing_prog	SCG3
1.12870747067033E-24	0.518044050387197	0.612	0.159	2.156959976451E-20	existing_prog	SPAG5
1.38299201032803E-24	0.751008620559249	0.94	0.59	2.64289773173687E-20	existing_prog	MAD2L2
2.02069687795709E-24	0.964805397284007	0.985	0.811	3.86155173377599E-20	existing_prog	SH3BGRL3
3.46183289540347E-24	0.539156297259181	0.448	0.088	6.61556266311602E-20	existing_prog	KIF20A
7.77077128767318E-24	0.800063329819359	0.851	0.375	1.48499439307435E-19	existing_prog	MIS18BP1
8.93729136174812E-24	0.654416196134546	0.836	0.344	1.70791637923007E-19	existing_prog	KIF22
9.79770132878934E-24	0.723128631844356	0.97	0.813	1.87234072393164E-19	existing_prog	H2AFV
1.26972783816991E-23	0.781021710949481	0.97	0.727	2.42644989874269E-19	existing_prog	CARHSP1
1.75915863698097E-23	0.629235926576055	0.687	0.195	3.36175215527064E-19	existing_prog	ASPM
2.80428196517867E-23	0.610516913578043	0.925	0.381	5.35898283545645E-19	existing_prog	IVNS1ABP
3.78796415049074E-23	0.462593667570867	0.597	0.156	7.2387994915878E-19	existing_prog	RTKN2
5.06616039325948E-23	0.5269282774941	0.672	0.206	9.68143251151886E-19	existing_prog	MIR217HG

5.3858508247219E-23	0.70360810529811	0.985	0.825	1.02923609260435E-18	existing_prog	CENPV
1.3157857157885E-22	0.562934242402039	1	0.981	2.51446650287182E-18	existing_prog	HNRNPA0
2.54664090247592E-22	0.531615413236221	0.522	0.126	4.86663076463148E-18	existing_prog	ECT2
bioRxiv preprint doi: https://doi.org/10.1101/2020.10.27.358135 ; this version posted November 9, 2020. The copyright holder for this preprint (which was not certified by peer review) is the author/funder, who has granted bioRxiv a license to display the preprint in perpetuity. It is made available under aCC-BY-NC-ND 4.0 International license.	0.56094552411582108	0.997	0.997	5.1026293529075E-18	existing_prog	H3F3B
2.68276385661043E-22	0.645965482786412	1	0.862	5.12676172998253E-18	existing_prog	HNRNPH3
2.84138156250807E-22	0.643357264441735	0.97	0.531	5.42988016595292E-18	existing_prog	LMNB1
3.63315084798625E-22	0.792885593877269	0.687	0.215	6.94295127050172E-18	existing_prog	CDC20
4.93859274625034E-22	0.861173598435975	0.955	0.671	9.43765073808439E-18	existing_prog	AKR7A2
8.15435031532911E-22	0.841288548585816	0.97	0.75	1.55829634525939E-17	existing_prog	HMGB3
9.8283486415929E-22	0.732244046225503	0.955	0.563	1.8781974254084E-17	existing_prog	TMPO
1.05704903594636E-21	0.468627256642491	0.642	0.183	2.02002070769349E-17	existing_prog	CDCA5
1.19371605230492E-21	0.62837596926876	1	0.975	2.2811913759547E-17	existing_prog	HNRNPA2B1
1.60863278330425E-21	0.73663032910346	0.985	0.643	3.07409724889443E-17	existing_prog	HNRNPAB
1.62403546258723E-21	0.600945241486776	1	0.895	3.10353176900419E-17	existing_prog	COX8A
1.98543475866754E-21	0.708038627882523	0.955	0.53	3.79416582381367E-17	existing_prog	SYNE2
1.99071513297434E-21	1.03881011582548	0.821	0.358	3.80425661911396E-17	existing_prog	CCNB2
3.77405654593291E-21	0.509332080277434	0.657	0.209	7.21222205927779E-17	existing_prog	RAD51AP1
4.91488870599527E-21	0.646060530200647	0.851	0.356	9.39235231715695E-17	existing_prog	ORC6
4.99757252729871E-21	0.946448289360764	1	0.888	9.55036109966783E-17	existing_prog	TUBB4B
1.83884194711725E-20	0.680861118665176	0.955	0.673	3.51402696094107E-16	existing_prog	ANP32E
1.97506787711459E-20	0.510645716922124	0.716	0.247	3.77435471316597E-16	existing_prog	CTPS1
2.11615277381242E-20	0.579214011466861	0.806	0.319	4.04396795075553E-16	existing_prog	CDCA4
3.28049710960312E-20	0.448929296724941	0.776	0.295	6.26902997645157E-16	existing_prog	HIRIP3
3.93439456318215E-20	0.524817608716566	1	0.983	7.51862801024108E-16	existing_prog	RAN
6.40914008625001E-20	0.641335944309705	0.955	0.769	1.22478667048238E-15	existing_prog	CYCS
7.07846415102066E-20	0.43146378705868	0.642	0.199	1.35269449926005E-15	existing_prog	LRR1
9.36679213315851E-20	0.586139549706026	1	0.856	1.78999397664659E-15	existing_prog	SNRPB
1.71435692963519E-19	0.505059736749262	0.612	0.187	3.27613609253284E-15	existing_prog	SGIP1
1.88795042174816E-19	0.667167664019497	0.97	0.944	3.60787325596073E-15	existing_prog	NUCKS1
2.23482668428073E-19	0.495941786854522	1	0.94	4.27075379366048E-15	existing_prog	SRSF3
2.45762647695137E-19	1.52401547361851	1	0.909	4.69652419745406E-15	existing_prog	HIST1H4C
3.11497215209655E-19	0.430910504354717	0.507	0.133	5.9527117826565E-15	existing_prog	PRR11
4.33723760222027E-19	1.12063738142995	0.925	0.623	8.28846105784293E-15	existing_prog	KPNA2
6.45566210546853E-19	0.552595138665424	0.791	0.318	1.23367702835504E-14	existing_prog	ACOT7
8.65356915024466E-19	0.621417544995396	1	0.889	1.65369706461175E-14	existing_prog	SRSF7
1.09788538263019E-18	0.668489554106055	0.896	0.594	2.09805896620629E-14	existing_prog	BUB3
1.24999736620085E-18	0.739022414077329	0.985	0.865	2.38874496680982E-14	existing_prog	CALM3

1.30757640368737E-18	0.500552623105022	1	0.995	2.49877850744656E-14	existing_prog	HSP90AA1
1.43722483088099E-18	0.640386871748233	0.507	0.135	2.74653665181356E-14	existing_prog	PLK1
1.45439361165621E-18	0.540609655547444	1	0.992	2.77934619187502E-14	existing_prog	RBP1
bioRxiv preprint doi: https://doi.org/10.1101/2020.10.27.358135 ; this version posted November 9, 2020. The copyright holder for this preprint (which was not certified by peer review) is the author/funder. All rights reserved. No reuse allowed without permission.	0.53501198099808	0.935	0.942	3.60656771504701E-14	existing_prog	GPX4
2.01955187769093E-18	0.481188722657536	1	0.947	3.85936363826736E-14	existing_prog	PTGES3
2.36019359688321E-18	0.54937292396843	0.985	0.838	4.51032996364381E-14	existing_prog	ANAPC11
3.04292591872982E-18	0.810702014427682	0.716	0.305	5.81503143069269E-14	existing_prog	ASCL1
3.78955338539334E-18	0.593612479445626	0.537	0.155	7.24183651948668E-14	existing_prog	CENPE
4.52092817237355E-18	0.629734261402795	0.493	0.13	8.63949373740586E-14	existing_prog	CENPA
5.28928676337322E-18	0.566246024801876	0.836	0.399	1.01078270048062E-13	existing_prog	RNASEH2A
5.33887516251819E-18	0.50391963766812	0.746	0.289	1.02025904355723E-13	existing_prog	KIF20B
9.9949658977713E-18	1.01948895468172	0.687	0.264	1.9100379830641E-13	existing_prog	CCNB1
1.01985187396183E-17	0.579847899522071	0.985	0.808	1.94893693114105E-13	existing_prog	PFN2
1.14365363204442E-17	0.579784403883895	0.985	0.962	2.18552209083689E-13	existing_prog	DYNLL1
1.22235419140206E-17	0.678509418899904	0.91	0.698	2.33591885976934E-13	existing_prog	TFDP2
1.54168922784746E-17	0.601936939717664	1	0.835	2.9461681144165E-13	existing_prog	SFPQ
2.27297529109121E-17	0.619934344332238	1	0.886	4.3436557812753E-13	existing_prog	PSIP1
3.21249468090969E-17	0.530435261170503	0.985	0.9	6.13907733521842E-13	existing_prog	GNG5
3.25173046059795E-17	0.616523761289199	0.672	0.249	6.21405691020269E-13	existing_prog	CLSPN
4.31278633183837E-17	0.480255305369712	0.687	0.258	8.24173468014313E-13	existing_prog	ATAD5
5.98112408920069E-17	0.679367621256931	0.896	0.59	1.14299281344625E-12	existing_prog	BTG3
7.05784183596672E-17	0.54087315020425	0.97	0.816	1.34875357485324E-12	existing_prog	NDUFA6
1.10669931816531E-16	0.541429756968349	0.761	0.316	2.11490239701391E-12	existing_prog	DBF4
1.34767003235185E-16	0.577645293057622	0.985	0.851	2.57539743182438E-12	existing_prog	DEK
1.78332989971708E-16	0.45206893819097	0.716	0.289	3.40794343835934E-12	existing_prog	EZR
1.7860768166379E-16	0.471787720764954	0.985	0.769	3.41319279659503E-12	existing_prog	CBX5
1.9320496789175E-16	0.524879746440815	0.97	0.889	3.69214693641134E-12	existing_prog	BANF1
2.64059478486281E-16	0.503539419022965	0.761	0.327	5.04617663387283E-12	existing_prog	MBD4
3.07228528331517E-16	0.423672505124707	1	0.999	5.8711371764153E-12	existing_prog	ACTB
3.14665496357511E-16	0.584967298857062	0.985	0.834	6.01325763539204E-12	existing_prog	SNRPD1
3.22083488672693E-16	0.51184697578656	0.836	0.407	6.15501546853517E-12	existing_prog	DDX39A
4.62024796193196E-16	0.414893396203158	0.567	0.175	8.82929385525198E-12	existing_prog	KIF23
7.45534897911763E-16	0.682722745068206	0.657	0.27	1.42471718990938E-11	existing_prog	ATAD2
7.62856337642994E-16	0.536533775981538	0.642	0.226	1.45781846123576E-11	existing_prog	GADD45G
7.83225021558751E-16	0.624496109817043	0.97	0.822	1.49674301619877E-11	existing_prog	DBI
1.470459262346E-15	0.538554991906177	1	0.83	2.81004765034321E-11	existing_prog	TMSB15A
1.64295449789108E-15	0.565173791977879	0.821	0.412	3.13968604546986E-11	existing_prog	TUBG1

1.85820468526203E-15	0.414199159639356	0.731	0.303	3.55102915353574E-11	existing_prog	VRK1	
1.89146614143581E-15	0.628367478748164	0.955	0.848	3.61459179628384E-11	existing_prog	TECR	
3.6832522208033E-15	0.443013134599973	0.821	0.415	7.03869499395511E-11	existing_prog	MRPS11	
bioRxiv preprint doi: https://doi.org/10.1101/2020.10.27.358135 ; this version posted November 9, 2020. The copyright holder for this preprint (which was not certified by peer review) is the author/funder. All rights reserved. No reuse allowed without permission.	4.54181670276641E-15	0.467321002683824	0.776	0.390	8.67941171898601E-08	existing_prog	TMEM237
5.12091774175975E-15	0.584255904088769	0.985	0.883	9.78607380450289E-11	existing_prog	RANBP1	
7.15289795252774E-15	0.622149504087734	0.94	0.643	1.36691879872805E-10	existing_prog	TYMS	
9.62132765162401E-15	0.455562244297669	0.701	0.286	1.83863571422535E-10	existing_prog	TP53I11	
1.16156076257522E-14	0.421957959301112	0.582	0.206	2.21974261728124E-10	existing_prog	MND1	
1.23298749202809E-14	0.586477549656768	0.866	0.571	2.35623909726567E-10	existing_prog	SKA2	
1.6079819155053E-14	0.462555145369162	0.701	0.28	3.07285344053064E-10	existing_prog	TUBB6	
1.70562759619634E-14	0.440179185805063	0.791	0.354	3.25945433633121E-10	existing_prog	RNASEH2B	
3.39812560143503E-14	0.4386447714146	0.657	0.267	6.49381802434235E-10	existing_prog	C12orf75	
3.64011003200618E-14	0.498694342717105	0.761	0.38	6.95625027116382E-10	existing_prog	SPATA33	
5.04313173984207E-14	0.455878858554358	0.985	0.874	9.63742475483819E-10	existing_prog	XRCC5	
6.61133572393447E-14	0.47059274525142	0.761	0.386	1.26342625684388E-09	existing_prog	C3orf14	
6.89707795198377E-14	0.676734320930328	0.955	0.679	1.3180315966241E-09	existing_prog	CXCR4	
7.21508072777141E-14	0.418396065446653	0.955	0.722	1.37880192707712E-09	existing_prog	RALY	
8.76691668115262E-14	0.504542779483222	0.866	0.522	1.6753577776827E-09	existing_prog	DTYMK	
9.69907538921649E-14	0.43183156610555	0.567	0.203	1.85349330687927E-09	existing_prog	ASF1B	
1.04420448225961E-13	0.535489204372765	0.955	0.792	1.99547476559811E-09	existing_prog	RORB	
1.14461520333701E-13	0.460871608471683	0.866	0.6	2.18735965357702E-09	existing_prog	NDUFAF3	
1.29326415975915E-13	0.502207128605265	0.97	0.701	2.47142780929973E-09	existing_prog	PCM1	
1.33307387119196E-13	0.450220007689563	0.836	0.457	2.54750416784783E-09	existing_prog	DNMT1	
1.68341242072585E-13	0.436544767848116	0.776	0.391	3.2170011360071E-09	existing_prog	CMC2	
3.04163241360669E-13	0.464313522430363	1	0.994	5.81255954240239E-09	existing_prog	CALM2	
4.85147824987789E-13	0.598589029973144	0.776	0.472	9.27117493551665E-09	existing_prog	RP11-620J15.3	
5.29017827788993E-13	0.477172946272073	0.94	0.799	1.01095306890477E-08	existing_prog	RHEB	
5.66473481411248E-13	0.585592322040451	0.866	0.61	1.08253082297689E-08	existing_prog	RP11-247C2.2	
8.70779498092252E-13	0.528028710983658	1	0.989	1.66405962085429E-08	existing_prog	UBB	
8.82759128437437E-13	0.459447027380423	0.955	0.82	1.68695269444394E-08	existing_prog	CSRP2	
9.32318785205118E-13	0.421391381895904	0.881	0.45	1.78166119852698E-08	existing_prog	RRM1	
1.07057806062089E-12	0.457336866267186	0.731	0.338	2.04587467384653E-08	existing_prog	RGS16	
1.13648869674787E-12	0.728776575820256	0.761	0.393	2.17182989948518E-08	existing_prog	KIAA0101	
1.370145848536E-12	0.433406983900842	0.985	0.769	2.61834871655229E-08	existing_prog	SRSF10	
1.37651759770544E-12	0.524876795354795	0.821	0.496	2.63052512921509E-08	existing_prog	RUVBL2	
3.17487682194764E-12	0.701594129414413	0.896	0.536	6.06718960674195E-08	existing_prog	PCNA	
3.75692208495467E-12	0.422392076955953	0.97	0.771	7.17947810434837E-08	existing_prog	MINOS1	

4.33463474677906E-12	0.41014221169251	0.94	0.76	8.28348700109479E-08	existing_prog	LSM 3.00	
4.72793711634055E-12	0.468493023969694	1	0.955	9.03508782932679E-08	existing_prog	RBMX	
8.78798355157668E-12	0.595541853250563	0.955	0.806	1.6793836567063E-07	existing_prog	SOX11	
bioRxiv preprint doi: https://doi.org/10.1101/2020.10.27.358135 ; this version posted November 9, 2020. The copyright holder for this preprint (which was not certified by peer review) is the author/funder. All rights reserved. No reuse allowed without permission.	(v1) 13228012970765E-11	0.4601526142701288	0.731	0.999	0.257787027928008E-07	existing_prog	ACYP1
1.63944034373044E-11	0.418109379202562	0.448	0.146	3.13297049686887E-07	existing_prog	SEPT4	
1.7287032700469E-11	0.463560667042139	0.896	0.593	3.30355194905962E-07	existing_prog	RPA3	
1.84067353572295E-11	0.457453250415625	0.955	0.755	3.51752712676657E-07	existing_prog	CXXC5	
2.29402257417861E-11	0.458020177536025	0.925	0.802	4.38387713925533E-07	existing_prog	C12orf57	
4.31468796243351E-11	0.482071918542891	0.97	0.807	8.24536869621044E-07	existing_prog	SMC3	
4.61089843303976E-11	0.509087668284836	0.806	0.475	8.81142690553897E-07	existing_prog	TTC14	
5.63524934865388E-11	0.434435087046771	0.881	0.671	1.07689615052776E-06	existing_prog	PIN1	
9.28792231640838E-11	0.432362773548856	0.448	0.16	1.77492195466564E-06	existing_prog	TRIM59	
1.30560699575696E-10	0.410330215441379	0.925	0.727	2.49501496889155E-06	existing_prog	HNRNPD	
1.62022705770316E-10	0.414695764283488	0.776	0.455	3.09625390727074E-06	existing_prog	HADH	
1.77268587313438E-10	0.466818825289126	0.925	0.772	3.38760270355979E-06	existing_prog	LSM 5.00	
2.05879394686686E-10	0.451072393409713	0.94	0.698	3.93435523246257E-06	existing_prog	SIVA1	
3.7514233330002E-10	0.452014620191996	0.821	0.492	7.16896998936338E-06	existing_prog	HSPB11	
4.31297587004103E-10	0.472503908187023	0.761	0.428	8.24209688764841E-06	existing_prog	DNAJC9	
6.07657902274107E-10	0.413788014084568	0.97	0.868	1.16123425124582E-05	existing_prog	HSPA8	
7.86285799414643E-10	0.740192928976348	0.881	0.808	1.50259216268138E-05	existing_prog	ARL6IP1	
9.256954378403E-10	0.416439647297423	0.97	0.868	1.76900398171281E-05	existing_prog	ILF2	
1.02177217069418E-09	0.514011450189366	0.94	0.845	1.95260661819658E-05	existing_prog	HN1	
1.28196955218856E-09	0.526117700140458	0.627	0.311	2.44984381423234E-05	existing_prog	PMAIP1	
1.40528082216074E-09	0.424530722650161	0.761	0.442	2.68549165114918E-05	existing_prog	FBLN1	
1.62156377275418E-09	0.532350948412918	0.806	0.537	3.09880836973323E-05	existing_prog	RSBN1	
1.90206971751925E-09	0.413083244018549	0.657	0.306	3.63485523017928E-05	existing_prog	ELAVL3	
2.42329444768809E-09	0.465938216410469	0.776	0.503	4.63091568953195E-05	existing_prog	MZT1	
2.58919506711583E-09	0.426405809366869	0.657	0.343	4.94795177325834E-05	existing_prog	RPL39L	
4.9228488664755E-09	0.591911334174737	0.522	0.233	9.40756418383467E-05	existing_prog	CCNA1	
1.29458186808956E-08	0.412652580961797	0.896	0.714	0.000247394594991915	existing_prog	PLEKHA1	
1.50804610281939E-08	0.428720108798211	0.507	0.24	0.000288187610248786	existing_prog	UHRF1	
5.75739279162626E-08	0.430262848852526	0.806	0.577	0.00110023776247978	existing_prog	PNRC2	
7.66395314754871E-08	0.503049287893151	0.731	0.45	0.00146458144649656	existing_prog	HELLS	
1.09523154317262E-07	0.453003554958961	0.701	0.418	0.00209298747900288	existing_prog	DHFR	
1.36034363117301E-07	0.56850798857836	0.866	0.687	0.00259961667917162	existing_prog	MSI1	
4.77304085803537E-07	0.975887054279481	0.761	0.602	0.00912128107970559	existing_prog	TRH	
8.07079066748753E-07	0.493338155022717	0.746	0.553	0.0154232809655687	existing_prog	GYG1	

1.58465566595118E-106	1.23781838970503	0.781	0.136	3.02827697763271E-102	neuroblasts	RASD1
1.6616461240833E-92	0.741685296593291	0.563	0.071	3.17540574312318E-88	neuroblasts	ATOH7
6.36977366660474E-87	0.730510066731239	0.523	0.064	1.21726374768817E-82	neuroblasts	MFNG
bioRxiv preprint doi: https://doi.org/10.1101/2020.10.27.358135 ; this version posted November 9, 2020. The copyright holder for this preprint (which was not certified by peer review) is the author/funder, who has granted bioRxiv a license to display the preprint in perpetuity. It is made available under aCC-BY-NC-ND 4.0 International license.	1e-176935434095007	0.007	0.015	3.97696219241208E-82	neuroblasts	RGS16
5.83735191721759E-83	1.80571880822077	0.861	0.28	1.11551795138028E-78	neuroblasts	GADD45A
7.19447670985993E-82	0.80117347576678	0.649	0.112	1.37486449925423E-77	neuroblasts	SERPINI1
1.90310815081433E-80	0.866161502910653	0.689	0.13	3.63683967620619E-76	neuroblasts	SRRM4
1.04864307441901E-76	0.629884861322005	0.404	0.04	2.00395691521472E-72	neuroblasts	DLX1
1.08573466592505E-76	0.475617981179439	0.344	0.027	2.07483894658276E-72	neuroblasts	INSM2
1.36643906209204E-71	1.45433707165045	0.993	0.805	2.61126504765789E-67	neuroblasts	SH3BGRL3
1.95708713178716E-71	1.03370974860396	1	0.992	3.73999350884525E-67	neuroblasts	RBP1
1.44821355741916E-69	0.644731703802066	0.424	0.05	2.76753610822801E-65	neuroblasts	DLX2
9.30910987572058E-66	1.86753029882987	0.967	0.577	1.7789708972502E-61	neuroblasts	HES6
4.03321739470783E-65	1.6520567018224	0.695	0.195	7.70747844128665E-61	neuroblasts	RP3-395M20.12
5.9775221966911E-60	0.66663269295326	0.457	0.071	1.14230449178767E-55	neuroblasts	EYA2
6.41903252508829E-59	0.57913341409928	0.411	0.059	1.22667711554437E-54	neuroblasts	CPLX2
3.69492704780951E-55	0.765957783999238	0.603	0.134	7.06100558836397E-51	neuroblasts	ONECUT2
3.82064926409705E-54	0.466568044894968	0.384	0.055	7.30126074368947E-50	neuroblasts	KIF19
9.03514813873752E-54	0.819854982841998	0.404	0.061	1.72661680931274E-49	neuroblasts	C8orf46
1.16725065794747E-53	0.714156291268321	0.43	0.071	2.23061600733762E-49	neuroblasts	SLC18A2
6.44534272293777E-53	0.734502846712077	0.616	0.16	1.23170499435341E-48	neuroblasts	SHD
1.00948029377479E-52	2.70905334751122	0.596	0.163	1.92911684140362E-48	neuroblasts	GAL
1.29603131874905E-51	0.408723264442989	0.331	0.041	2.47671585012944E-47	neuroblasts	SLC38A4
2.80502728696237E-49	0.789978667553161	0.364	0.053	5.36040714538508E-45	neuroblasts	VSX1
3.83147868294806E-49	0.832640791560016	0.55	0.128	7.32195576311373E-45	neuroblasts	SSTR2
1.41224222946798E-47	0.972156429632829	0.861	0.467	2.69879490051331E-43	neuroblasts	BCL7A
1.53874975256987E-47	0.477594554244557	1	1	2.94055077716103E-43	neuroblasts	HNRNPA1
8.11593908711094E-47	0.984734364281078	0.596	0.173	1.5509559595469E-42	neuroblasts	HEY1
1.0791334410257E-46	0.79759959633114	1	0.999	2.06222400580011E-42	neuroblasts	TMSB4X
8.11922275965311E-46	1.39163024172413	0.894	0.589	1.55158346936971E-41	neuroblasts	TRH
6.25777181707622E-45	0.905052579186777	0.954	0.804	1.19586019424327E-40	neuroblasts	PFN2
2.43887621759109E-43	0.627845403367391	0.404	0.078	4.66069245181657E-39	neuroblasts	BHLHE22
2.66370156923192E-42	0.768317853681771	0.881	0.507	5.09033369880219E-38	neuroblasts	LIMD2
4.78216209423465E-42	0.426908953139424	0.404	0.08	9.13871176208241E-38	neuroblasts	FAM131C
8.76172732190475E-42	0.706758525458542	0.609	0.188	1.674366091216E-37	neuroblasts	DOK5
2.93330190173303E-41	0.943927653695822	0.927	0.706	5.60553993421182E-37	neuroblasts	PLEKHA1
4.80617199719035E-41	0.977792384426526	0.901	0.534	9.18459468663075E-37	neuroblasts	PCBP4

7.37189400044997E-41	0.679880579959383	0.603	0.195	1.40876894348599E-36	neuroblasts	MIR217HG
3.05543056594878E-40	0.441980543316606	0.358	0.064	5.83892781152812E-36	neuroblasts	DLL1
3.40636087712455E-37	0.798990025767911	0.689	0.252	6.50955563618501E-33	neuroblasts	SCG3
bioRxiv preprint doi: https://doi.org/10.1101/2020.10.27.358135 ; this version posted November 9, 2020. The copyright holder for this preprint (which was not certified by peer review) is the author/funder, who has granted bioRxiv a license to display the preprint in perpetuity. It is made available under aCC-BY-NC-ND 4.0 International license.	0.95287821352907	0.98	0.0	8.58166799921617e-03	neuroblasts	SOX11
4.92535771504197E-37	0.602505877317312	0.98	0.874	9.41235859344521E-33	neuroblasts	MLLT11
6.06442670051336E-37	0.489939627796424	0.444	0.11	1.1589119424681E-32	neuroblasts	MYBL1
5.26444664841311E-35	0.687386741899258	0.755	0.367	1.00603575451174E-30	neuroblasts	CADM3
7.16574383585295E-35	0.756103779328917	0.887	0.652	1.3693736470315E-30	neuroblasts	NOVA1
1.3582387027706E-34	1.21826979255327	0.384	0.089	2.59559416099461E-30	neuroblasts	CLDN5
2.5221865686959E-34	0.539247771136472	0.987	0.969	4.81989853277787E-30	neuroblasts	SLC25A6
2.55254061067758E-33	0.928983285304947	0.921	0.672	4.87790510700485E-29	neuroblasts	CXCR4
4.9699816310975E-33	0.582720104216525	0.728	0.334	9.49763489702733E-29	neuroblasts	GPC2
5.83942725300662E-33	0.867708875368664	0.98	0.882	1.11591454804957E-28	neuroblasts	MIAT
1.18623998550459E-31	0.590771146067792	0.603	0.241	2.26690461229927E-27	neuroblasts	NECAB3
2.91680289099396E-31	0.579704978756405	0.94	0.715	5.57401032468946E-27	neuroblasts	BASP1
8.88478751273591E-31	0.624431421543707	1	0.999	1.69788289368383E-26	neuroblasts	CKB
3.65279098126775E-30	0.561328696393872	0.974	0.885	6.98048356520266E-26	neuroblasts	CD24
1.97588953220589E-28	0.689871187151764	0.278	0.056	3.77592489604546E-24	neuroblasts	GUCA1A
2.03361211721204E-27	0.608223105410011	0.576	0.223	3.8862327559922E-23	neuroblasts	ELAVL2
3.54255037241753E-26	0.538853443433974	0.351	0.086	6.7698137616899E-22	neuroblasts	POU4F2
2.10038658262666E-25	0.566521387646824	0.887	0.693	4.01383875939954E-21	neuroblasts	TFDP2
5.56425524312496E-25	0.608623426473325	0.682	0.369	1.06332917696118E-20	neuroblasts	DST
1.26895193104293E-24	0.656065591120707	0.675	0.378	2.42496714022304E-20	neuroblasts	IVNS1ABP
5.6358887924228E-24	0.5399339912281	0.921	0.782	1.077018348232E-19	neuroblasts	SYT1
4.49367114739375E-23	0.5563949169616	0.702	0.368	8.58740556266946E-19	neuroblasts	TAGLN3
6.74314100663028E-23	0.519242014174363	0.927	0.788	1.28861424636705E-18	neuroblasts	RORB
7.24651302924944E-23	0.730962002934514	0.483	0.173	1.38480863988957E-18	neuroblasts	NEUROD1
5.18274952967147E-22	0.610241861827657	0.53	0.219	9.90423435120217E-18	neuroblasts	GADD45G
3.70301845735884E-21	0.538270865591583	0.715	0.427	7.07646827201275E-17	neuroblasts	LCA5
7.63386878233176E-21	0.430067519949726	0.305	0.083	1.4588323243036E-16	neuroblasts	TMEM176A
1.16068572066148E-20	0.418670041546735	0.305	0.085	2.21807041218409E-16	neuroblasts	TMEM176B
5.43944972497504E-20	0.475291501872421	0.629	0.356	1.03947884244273E-15	neuroblasts	COL13A1
9.46554207190568E-19	0.412263740249802	0.47	0.204	1.80886508994117E-14	neuroblasts	GALNT2
1.27814527279117E-18	0.50241198211324	0.675	0.44	2.44253561630392E-14	neuroblasts	ABRACL
3.95156459647263E-18	0.485750170398956	0.503	0.242	7.55143994385919E-14	neuroblasts	CBFA2T2
1.38614056287302E-17	0.410500098848831	0.596	0.325	2.64891461565034E-13	neuroblasts	RNF165
6.27621824991792E-17	0.442086041174611	0.914	0.863	1.19938530755931E-12	neuroblasts	HNRNPH3

1.32993860668739E-16	0.410721114037269	0.589	0.299	2.54151267737959E-12	neuroblasts	ELAVL3
2.16302941515425E-16	0.451531767198246	0.675	0.442	4.13354921235978E-12	neuroblasts	STRADB
4.07478343482386E-16	0.5090974461781	0.808	0.666	7.78691114394839E-12	neuroblasts	NKAIN4
bioRxiv preprint doi: https://doi.org/10.1101/2020.10.27.358135 ; this version posted November 9, 2020. The copyright holder for this preprint (which was not certified by peer review) is the author/funder, who has granted bioRxiv a license to display the preprint in perpetuity. It is made available under aCC-BY-NC-ND 4.0 International license.	0.693947518010684	0.795	0.694	0.586595123076071	neuroblasts	BTG2
5.57219625033368E-15	0.457120407066497	0.755	0.536	1.06484670343877E-10	neuroblasts	ZNF385A
5.97773159119219E-15	0.412110163888751	0.775	0.59	1.14234450707683E-10	neuroblasts	BAZ1A
1.18888149526372E-14	0.416948788740937	0.947	0.916	2.27195253744896E-10	neuroblasts	BTG1
4.30444330152722E-14	0.455385694115611	0.715	0.544	8.22579114921852E-10	neuroblasts	PTPRF
4.94507652247817E-14	0.629055921272875	0.57	0.376	9.45004123445579E-10	neuroblasts	CYB5A
6.37781590871135E-14	0.410685347116419	0.848	0.755	1.21880062015474E-09	neuroblasts	CXXC5
6.55578148671363E-14	0.408227574801278	0.887	0.81	1.25280984211097E-09	neuroblasts	FSCN1
6.57818844149995E-14	0.491019269965977	0.848	0.746	1.25709181117064E-09	neuroblasts	IDH2
1.25150118727142E-13	0.51557694173143	0.709	0.549	2.39161876887568E-09	neuroblasts	GYG1
3.66074642179876E-13	0.478208602771046	0.775	0.607	6.99568641205743E-09	neuroblasts	RP11-247C2.2
5.73467084938061E-13	0.412005160128412	0.808	0.673	1.09589559931663E-08	neuroblasts	SVBP
1.90921743944868E-11	0.925623267561783	0.43	0.233	3.64851452678643E-07	neuroblasts	IGFBP5
1.21338502700887E-10	0.460899925807656	0.795	0.671	2.31877878661394E-06	neuroblasts	AKR7A2
7.07105802493425E-09	0.461203746181325	0.536	0.393	0.000135127918856494	neuroblasts	ZBTB16
6.45393806674989E-07	0.405659489957649	0.748	0.688	0.012333475645559	neuroblasts	MSI1
0	2.53809497444755	0.891	0.016	0	photorecept	DCT
0	1.79281106208741	0.832	0.018	0	photorecept	PRDM1
7.81670995248656E-261	1.38980833973537	0.861	0.032	1.49377327192018E-256	photorecept	CRX
2.20625823600128E-243	1.17041092787141	0.564	0.008	4.21615948899845E-239	photorecept	PCAT4
6.99993736059569E-240	1.44529657266869	0.574	0.009	1.33768802960984E-235	photorecept	PDC
1.29866380169276E-234	1.3473345445236	0.822	0.034	2.48174652503487E-230	photorecept	NEUROD4
1.40590900713316E-226	0.754386966314286	0.485	0.005	2.68669211263147E-222	photorecept	MRLN
3.88741666209532E-219	0.640983530594756	0.465	0.004	7.42885324126415E-215	photorecept	KCNH6
7.91879893696982E-214	0.591194403975293	0.436	0.003	1.51328247685493E-209	photorecept	RBP3
4.22505299368878E-212	0.776523094785964	0.485	0.006	8.07407627093925E-208	photorecept	AIPL1
1.70753483978972E-210	1.05915492849506	0.584	0.014	3.26309907883816E-206	photorecept	VTN
5.99753656390127E-205	0.678532080848775	0.574	0.014	1.14612923736153E-200	photorecept	MAOA
1.14349557578976E-201	1.60160775348288	0.881	0.055	2.18522004533424E-197	photorecept	OTX2
1.79493797776546E-196	1.98740664572594	0.653	0.024	3.4301264755098E-192	photorecept	RCVRN
9.83210446360317E-195	0.921259129720934	0.733	0.034	1.87891516299457E-190	photorecept	MCC
4.03270980146411E-193	1.18870011798627	0.584	0.017	7.70650843059792E-189	photorecept	SLC38A5
7.65879124566634E-191	0.753154638782466	0.416	0.004	1.46359500704684E-186	photorecept	SERPINI2
6.4160580545524E-183	1.75792736202719	0.792	0.049	1.22610869422496E-178	photorecept	GNB3

1.71561967793E-180	1.18562960051155	0.713	0.035	3.27854920452423E-176	photorecept	MIR7-3HG	
5.07925030854116E-179	0.955079553448176	0.594	0.021	9.70644733962217E-175	photorecept	NXPH4	
6.16890566477342E-165	0.447796643034644	0.376	0.005	1.1788778725382E-160	photorecept	RP11-184I16.4	
bioRxiv preprint doi: https://doi.org/10.1101/2020.10.27.358135 ; this version posted November 9, 2020. The copyright holder for this preprint (which was not certified by peer review) is the author/funder. All rights reserved. No reuse allowed without permission.	1.96230533018969E-160	0.691012876431804	0.525	0.018	3.75002281599120E-156	photorecept	RIMS1
3.6116547514821E-150	0.505776714024995	0.337	0.004	6.90187223008229E-146	photorecept	TJP3	
3.79037577622643E-140	0.671811317586215	0.337	0.005	7.2434081083687E-136	photorecept	RBP4	
6.15065605193973E-140	0.90663191051257	0.545	0.026	1.17539037152568E-135	photorecept	TULP1	
1.74174942247712E-137	0.464526200359118	0.287	0.002	3.32848314635379E-133	photorecept	IMPG2	
7.48766983341795E-137	1.33947344163112	0.881	0.1	1.43089370516617E-132	photorecept	THRB	
4.29654495224848E-136	0.474973147737696	0.376	0.008	8.21069740374685E-132	photorecept	AANAT	
6.15709755759269E-136	0.965265327540207	0.713	0.053	1.17662134325596E-131	photorecept	LINC00599	
9.23156906995129E-130	0.51984448582369	0.287	0.003	1.76415284926769E-125	photorecept	LINC00458	
3.26982573470338E-115	1.6203356690814	0.921	0.134	6.24863697901815E-111	photorecept	SYT4	
1.03472421379948E-112	1.62778005261522	0.871	0.125	1.9773579725708E-108	photorecept	SEPT4	
7.63685788101221E-111	0.454181055741877	0.297	0.006	1.45940354106143E-106	photorecept	CTB-12O2.1	
9.85220748449355E-109	1.98729829403436	0.95	0.161	1.88275685028672E-104	photorecept	NEUROD1	
5.4770830855518E-106	0.549481311115036	0.307	0.008	1.04667057764895E-101	photorecept	GSG1	
1.10235223035941E-105	1.2269576671301	0.921	0.144	2.10659511221683E-101	photorecept	SEZ6L2	
1.48960636176196E-104	0.593993745576755	0.376	0.015	2.8466377573271E-100	photorecept	GUCY1A2	
5.95248470384837E-103	0.935766394346266	0.693	0.075	1.13751982690542E-98	photorecept	SH3BP5	
5.15434428115015E-100	0.466485901193762	0.317	0.01	9.84995192127793E-96	photorecept	FSTL5	
3.67492018197016E-97	0.893417777371866	0.713	0.087	7.02277246774497E-93	photorecept	ROBO2	
7.41486052410519E-97	0.880440150588005	0.644	0.067	1.4169798461565E-92	photorecept	NRXN1	
5.41587624456727E-93	1.97736147740527	0.931	0.216	1.0349739503368E-88	photorecept	PHLDA1	
1.83262632941913E-92	0.961927639467295	0.663	0.075	3.50214891551997E-88	photorecept	SYP	
2.98941308612055E-92	1.66753426505955	0.812	0.126	5.71276840757638E-88	photorecept	SSTR2	
2.79256254814977E-90	2.32822297749944	1	0.301	5.33658702951421E-86	photorecept	FAM57B	
3.51034579390474E-87	1.60897695385476	0.921	0.21	6.70827081215195E-83	photorecept	GADD45G	
5.20952248969202E-85	0.472781773841845	0.376	0.021	9.95539747780144E-81	photorecept	RAB26	
6.74673076491083E-83	1.25157428463035	0.762	0.119	1.28930024917446E-78	photorecept	CHRNA3	
4.92097837224432E-82	0.454046671379419	0.366	0.02	9.4039896693589E-78	photorecept	RAMP1	
5.00814390699263E-80	1.1793122457455	0.881	0.181	9.57056300626291E-76	photorecept	ATP1A3	
2.16181785742552E-78	1.24688104427108	0.564	0.061	4.13123392554016E-74	photorecept	C8orf46	
6.67563831133522E-77	1.08399554173431	0.723	0.121	1.27571448129616E-72	photorecept	AMER2	
6.47365070145123E-69	0.597865264945467	0.515	0.059	1.23711464904733E-64	photorecept	LINC01315	
4.09607273628819E-68	0.42426118166234	0.396	0.032	7.82759499904673E-64	photorecept	GABBR2	
6.70372321835886E-68	0.526947173638723	0.505	0.054	1.28108150702838E-63	photorecept	CHGB	

2.42587043379549E-66	0.851217943622566	0.752	0.139	4.63583839898319E-62	photorecept	SRRM4
5.78558822568288E-66	0.936080473667367	0.812	0.168	1.105625909928E-61	photorecept	INA
2.56871091520144E-65	0.415337381694207	0.287	0.016	4.90880655894994E-61	photorecept	NPFFR2
bioRxiv preprint doi: https://doi.org/10.1101/2020.10.27.358135 ; this version posted November 9, 2020. The copyright holder for this preprint (which was not certified by peer review) is the author/funder, who has granted bioRxiv a license to display the preprint in perpetuity. It is made available under aCC-BY-NC-ND 4.0 International license.	184728491049718	0.597	0.597	5.8441941849014E-61	photorecept	PCBP4
1.46970382667726E-63	0.530051656203523	0.376	0.031	2.80860401278025E-59	photorecept	NRL
5.60695214829989E-59	0.540785750289721	0.366	0.033	1.07148855554011E-54	photorecept	DPP10
1.86930903966515E-58	0.454003415402537	0.376	0.034	3.5722495748001E-54	photorecept	CNTNAP2
3.1432090368236E-57	0.671860138515674	0.604	0.096	6.00667246936991E-53	photorecept	CTC-378H22.2
5.36864676033881E-56	1.16843644529125	0.842	0.212	1.02594839590075E-51	photorecept	SNCG
1.61771752960117E-51	1.08115514327798	0.861	0.254	3.09145819906783E-47	photorecept	SCG3
4.61581163544179E-51	0.516597302058879	0.624	0.112	8.82081603532927E-47	photorecept	SNAP25
9.59994169328827E-51	0.55982123501573	0.465	0.064	1.83454885758739E-46	photorecept	CHGA
5.02871397124126E-47	0.502296108955249	0.267	0.021	9.60987239904204E-43	photorecept	TUBA4A
2.28360099547202E-46	0.798246934009904	0.416	0.058	4.36396150234703E-42	photorecept	RXRG
3.87282477907582E-46	0.634851270653058	0.624	0.141	7.4009681528139E-42	photorecept	PHACTR2
6.46286290260725E-46	1.00718288319611	0.99	0.842	1.23505310068824E-41	photorecept	CPE
1.50855605611218E-45	1.03711528994597	1	0.45	2.88285062323038E-41	photorecept	STMN2
2.01035361980219E-45	0.755850082770525	1	0.997	3.84178576744199E-41	photorecept	H3F3B
4.72996659814913E-44	1.12356561795107	0.851	0.377	9.038966169063E-40	photorecept	PIK3R1
5.34979266234613E-44	1.21873026727069	1	0.999	1.02234537777435E-39	photorecept	TMSB4X
5.76227446654604E-43	0.933712288144509	0.911	0.438	1.10117065055695E-38	photorecept	STRADB
5.18986069794164E-42	0.585709067731851	0.505	0.092	9.91782379376648E-38	photorecept	CADPS
1.58786023918027E-41	1.12462960604805	0.96	0.683	3.0344009170735E-37	photorecept	ENO2
9.41339343570124E-41	0.993110473634667	0.911	0.467	1.79889948556251E-36	photorecept	ATP2B1
1.32114477382076E-40	0.797160020475573	0.931	0.365	2.52470766277147E-36	photorecept	TAGLN3
1.3327077122619E-40	0.408043190011464	0.297	0.032	2.54680443813249E-36	photorecept	KIAA1107
1.59996514673446E-40	1.13749425528039	0.97	0.914	3.05753339540955E-36	photorecept	PRDX1
3.33952267784538E-40	0.578173485151358	0.416	0.068	6.38182783736252E-36	photorecept	STX3
6.05996734658118E-40	1.02901210140098	0.941	0.581	1.15805975993166E-35	photorecept	CADM1
6.97369967266715E-40	0.499793005872298	0.446	0.076	1.33267400744669E-35	photorecept	RPS6KL1
1.87845577279726E-39	1.11088410248872	0.99	0.887	3.58972898181557E-35	photorecept	TUBB4B
4.13196101485067E-39	0.815122006079279	0.743	0.265	7.89617749937962E-35	photorecept	ROGDI
6.68898371824859E-39	1.13560916094749	0.911	0.766	1.27826478855731E-34	photorecept	GUK1
1.52255404642509E-37	0.431601784734685	0.426	0.072	2.90960078271835E-33	photorecept	INSM1
1.678678991013E-36	0.417038581923417	0.455	0.084	3.20795555182585E-32	photorecept	TRIM9
6.36221463085059E-36	0.490432654081843	0.446	0.085	1.21581921595555E-31	photorecept	AFAP1
1.12493939121114E-35	0.697245494686271	0.614	0.154	2.1497591766045E-31	photorecept	RASD1

1.61189428362677E-35	0.652198985535318	0.663	0.196	3.08032997601075E-31	photorecept	SERPINF1
4.14910691969962E-35	1.07654258614017	0.881	0.415	7.92894332354598E-31	photorecept	DCX
6.88329391226035E-33	0.881679112565492	0.941	0.671	1.31539746663295E-28	photorecept	SVBP
bioRxiv preprint doi: https://doi.org/10.1101/2020.10.27.358135 ; this version posted November 9, 2020. The copyright holder for this preprint (which was not certified by peer review) is the author/funder. All rights reserved. No reuse allowed without permission.	0.612737104877615	0.644	0.176	1.86689235746015E-28	photorecept	RTN1
5.80965841702401E-31	0.480792129432683	0.287	0.04	1.11022572349329E-26	photorecept	CHODL
3.11076422522206E-30	0.923649793794301	0.96	0.841	5.94467043439935E-26	photorecept	SPCS1
3.93582058610535E-30	0.745362497345047	0.931	0.732	7.52135314004732E-26	photorecept	ATP6V0B
1.8936606382021E-29	0.739135111515581	0.693	0.284	3.61878547960422E-25	photorecept	REEP6
6.12373462859737E-29	0.649362257997219	0.99	0.997	1.17024568752496E-24	photorecept	TMSB10
2.20459568360253E-28	0.772081717442605	0.941	0.706	4.21298235136443E-24	photorecept	APLP1
3.42445628554665E-28	0.718301598546447	0.891	0.605	6.54413596167965E-24	photorecept	SEPW1
3.72302510255316E-28	0.544883088407391	0.495	0.123	7.11470097097909E-24	photorecept	CELF3
5.61032588512595E-28	0.409514532226284	0.515	0.138	1.07213327664757E-23	photorecept	PCBP3
5.99708141705114E-28	0.695589943082977	0.98	0.974	1.14604225879847E-23	photorecept	GSTP1
6.40908617240405E-28	0.754300435147375	0.624	0.219	1.22477636754641E-23	photorecept	MAP1LC3A
9.88605834859541E-28	0.922468697153884	0.723	0.296	1.88922575041658E-23	photorecept	STC1
1.26809908713367E-27	0.637560571963118	0.891	0.587	2.42333735551244E-23	photorecept	HES6
2.22794999547445E-27	0.845041724347665	0.941	0.752	4.25761244135167E-23	photorecept	GPX1
2.30847030545748E-27	0.417546898292614	0.356	0.067	4.41148675372925E-23	photorecept	SRRM3
2.88609316271297E-27	0.626987149580566	0.921	0.67	5.51532403394449E-23	photorecept	TERF2IP
4.86226324595433E-27	0.69596102592477	0.891	0.535	9.29178506301873E-23	photorecept	ZNF385A
5.18411781135518E-27	0.620042807676196	0.762	0.34	9.90684913749974E-23	photorecept	GPC2
2.96961905655699E-26	0.61801593313051	0.594	0.216	5.67494201708041E-22	photorecept	PTP4A3
3.22264040934773E-26	0.415867832196577	1	1	6.1584658222635E-22	photorecept	ACTG1
3.96749461836641E-26	0.828032757131758	0.822	0.51	7.58188221569821E-22	photorecept	NELL2
5.44941012730271E-26	0.593941174748798	0.96	0.851	1.04138227532755E-21	photorecept	SNRPN
5.68727941724785E-26	0.802982476975534	0.644	0.282	1.08683909663606E-21	photorecept	BCL2L1
1.34044559264023E-25	0.612604854077913	0.97	0.877	2.56159152753547E-21	photorecept	MLLT11
3.89902420824687E-25	0.537309977389277	0.98	0.809	7.45103526195977E-21	photorecept	SH3BGRL3
1.19904178143173E-24	0.621342345792739	0.535	0.177	2.29136884431604E-20	photorecept	SLC16A9
1.27278163505583E-24	0.552842267417041	1	0.989	2.43228570459168E-20	photorecept	STMN1
4.80179480139059E-24	0.415483844664121	0.307	0.057	9.17622986545741E-20	photorecept	MFAP4
1.82197090667193E-23	0.582504807603328	0.584	0.224	3.48178640265006E-19	photorecept	RGS2
1.05963386367532E-22	0.692107098030728	0.871	0.556	2.02496031348354E-18	photorecept	BEX1
1.19881733524208E-22	0.47881448404886	0.307	0.062	2.29093992764761E-18	photorecept	FILIP1L
1.22078966497712E-22	0.594051693731302	0.931	0.872	2.33292904977127E-18	photorecept	GABARAPL2
1.52781513820377E-22	0.483705353565822	0.99	0.996	2.9196547291074E-18	photorecept	TUBB2B

1.52880421040586E-22	1.01061849954637	0.752	0.423	2.92154484608559E-18	photorecept	S100A13
1.78179193291311E-22	0.584917951759041	0.624	0.246	3.40500438379696E-18	photorecept	LBH
2.14827035754251E-22	0.41569028543415	0.347	0.076	4.10534465326373E-18	photorecept	KIRREL2
bioRxiv preprint doi: https://doi.org/10.1101/2020.10.27.358135 ; this version posted November 9, 2020. The copyright holder for this preprint (which was not certified by peer review) is the author/funder. All rights reserved. No reuse allowed without permission.	bioRxiv preprint doi: https://doi.org/10.1101/2020.10.27.358135 ; this version posted November 9, 2020. The copyright holder for this preprint (which was not certified by peer review) is the author/funder. All rights reserved. No reuse allowed without permission.	bioRxiv preprint doi: https://doi.org/10.1101/2020.10.27.358135 ; this version posted November 9, 2020. The copyright holder for this preprint (which was not certified by peer review) is the author/funder. All rights reserved. No reuse allowed without permission.	bioRxiv preprint doi: https://doi.org/10.1101/2020.10.27.358135 ; this version posted November 9, 2020. The copyright holder for this preprint (which was not certified by peer review) is the author/funder. All rights reserved. No reuse allowed without permission.	bioRxiv preprint doi: https://doi.org/10.1101/2020.10.27.358135 ; this version posted November 9, 2020. The copyright holder for this preprint (which was not certified by peer review) is the author/funder. All rights reserved. No reuse allowed without permission.	bioRxiv preprint doi: https://doi.org/10.1101/2020.10.27.358135 ; this version posted November 9, 2020. The copyright holder for this preprint (which was not certified by peer review) is the author/funder. All rights reserved. No reuse allowed without permission.	SOX4
6.05860959249461E-22	0.576020617569594	0.98	0.822	1.15780029312572E-17	photorecept	VAMP2
7.8769964250466E-22	0.666411415647544	0.851	0.559	1.50529401682641E-17	photorecept	CRMP1
1.16674598417198E-21	1.56356144878339	0.297	0.062	2.22965157575266E-17	photorecept	NTS
1.26471945671546E-21	0.716573910401387	0.752	0.422	2.41687888178325E-17	photorecept	ABHD14A
3.00770754413128E-21	0.424235938551121	0.366	0.087	5.74772911683488E-17	photorecept	RBFOX3
9.89888914332991E-21	0.459717023280286	0.96	0.963	1.89167771529035E-16	photorecept	COX7A2
1.19772311858172E-20	0.407288382528001	1	0.999	2.28884887960966E-16	photorecept	ACTB
1.89082636719078E-20	0.519359562881873	0.95	0.85	3.61336918770159E-16	photorecept	GPM6A
3.13714419748025E-20	0.471382191326957	0.535	0.179	5.99508256138475E-16	photorecept	MAPT
4.13589110547006E-20	0.650204301718874	0.921	0.72	7.90368790255328E-16	photorecept	BASP1
5.37007129662098E-20	0.587364058579281	1	0.97	1.02622062478427E-15	photorecept	MORF4L2
6.92580848677639E-20	0.528186739936587	0.851	0.565	1.32352200182297E-15	photorecept	BAD
7.20873862269747E-20	0.595393299141954	0.782	0.451	1.37758995079749E-15	photorecept	PGRMC2
7.94776758630122E-20	0.536069718639997	0.703	0.336	1.51881838574216E-15	photorecept	CCDC181
9.62501652995802E-20	0.473776275312077	0.703	0.301	1.83934065887498E-15	photorecept	RAB3A
1.30615725068293E-19	0.468601153195667	0.535	0.205	2.49606650605508E-15	photorecept	STXBP1
2.03216112933839E-19	0.635843181529088	0.762	0.426	3.88345991816567E-15	photorecept	SCARB2
3.2219335635786E-19	0.461090321677238	0.97	0.944	6.15711503999871E-15	photorecept	COX6A1
3.65487171315241E-19	0.536328715863067	0.822	0.501	6.98445984383426E-15	photorecept	GDI1
6.14546610130115E-19	0.765962141668001	0.723	0.423	1.17439857195865E-14	photorecept	PEG10
1.05631071861236E-18	0.444989489722533	0.337	0.087	2.01860978326822E-14	photorecept	GPC3
3.30631180778086E-18	0.430052629501224	0.416	0.129	6.31836186466922E-14	photorecept	ARHGEF2
3.33206511704746E-18	0.440549100310245	0.96	0.872	6.36757643867769E-14	photorecept	SSR4
4.61640351846176E-18	0.531428162566337	0.931	0.794	8.82194712378043E-14	photorecept	YWHAZ
4.91628729427506E-18	0.546074729582391	0.842	0.607	9.39502501935964E-14	photorecept	WRB
5.00378973947507E-18	0.490993997149205	0.931	0.754	9.56224219213687E-14	photorecept	CXXC5
5.67580976662309E-18	0.567808455733637	0.653	0.319	1.08464724640167E-13	photorecept	MEIS2
7.24775315602514E-18	0.481515533151513	0.574	0.26	1.3850456281164E-13	photorecept	NUDT14
7.43332760601869E-18	0.410620823044454	0.98	0.939	1.42050890551017E-13	photorecept	ATP6V1G1
7.69407808060821E-18	0.563521121579584	0.861	0.675	1.47033832120423E-13	photorecept	UQCC2
1.18543526899172E-17	0.505688485903038	0.762	0.469	2.26536679904317E-13	photorecept	RHOT1
1.2043870922383E-17	0.466369769669917	0.436	0.153	2.30158373326739E-13	photorecept	CLN6
1.37985640631844E-17	0.425758349173637	0.931	0.83	2.63690559247453E-13	photorecept	ATP5C1

2.52027825564705E-17	0.605885860525155	0.762	0.526	4.81625174654152E-13	photorecept	IFT57
4.37304919490607E-17	0.519722821251666	0.812	0.597	8.3568970114655E-13	photorecept	SPTSSA
4.38010412837243E-17	0.434597143973224	0.901	0.791	8.37037898931972E-13	photorecept	DYNLRB1
bioRxiv preprint doi: https://doi.org/10.1101/2020.10.27.358135 ; this version posted November 9, 2020. The copyright holder for this preprint (which was not certified by peer review) is the author/funder, who has granted bioRxiv a license to display the preprint in perpetuity. It is made available under aCC-BY-NC-ND 4.0 International license.	0.564094526745118	0.772	0.484	9.28639889608641E-13	photorecept	PRRT2
6.45003714849528E-17	0.494464285428978	0.941	0.766	1.23260209907745E-12	photorecept	DAAM1
1.33561646101139E-16	0.532386534781716	0.832	0.594	2.55236305699276E-12	photorecept	BEX2
1.40385927942189E-16	0.634169838808684	0.693	0.417	2.68277508297523E-12	photorecept	ZHX1
3.07514796334039E-16	0.416344861822183	0.525	0.209	5.87660775794348E-12	photorecept	PPP2R5B
4.00559536391713E-16	0.478824457669385	0.554	0.243	7.65469274044564E-12	photorecept	SDC2
4.92551382531233E-16	0.505525345774448	0.95	0.784	9.41265692017186E-12	photorecept	SYT1
1.15581623343775E-15	0.511394310098104	0.97	0.977	2.20876482209954E-11	photorecept	BSG
1.20217278020881E-15	0.420903354159442	0.545	0.244	2.29735218297904E-11	photorecept	AKAP13
2.02474826911698E-15	0.465469309778851	0.881	0.753	3.86929394228254E-11	photorecept	PET100
2.51965788792414E-15	0.527178863271759	0.782	0.59	4.81506622382303E-11	photorecept	GRINA
3.40250293167222E-15	0.46101741116887	0.554	0.24	6.50218310242561E-11	photorecept	TSPAN7
3.86243581580489E-15	0.678594256679222	0.782	0.568	7.38111484400314E-11	photorecept	DHRS7
4.11199862656164E-15	0.435409285896491	0.554	0.25	7.85802937535929E-11	photorecept	NECAB3
9.6748165992952E-15	0.660808843076651	0.673	0.408	1.84885745212531E-10	photorecept	UNC119
1.78997379469625E-14	0.40626446013913	0.941	0.911	3.42063992166454E-10	photorecept	NDUFB11
2.00846599683477E-14	0.46269041814804	0.861	0.698	3.83817851995124E-10	photorecept	FAM96B
2.1400626619397E-14	0.499866915367401	0.871	0.685	4.08965974696677E-10	photorecept	MAP1LC3B
6.29934181859537E-14	0.62564570880385	0.733	0.515	1.20380422153358E-09	photorecept	TMX1
8.2501904106754E-14	0.467113341387212	0.673	0.402	1.57661138748007E-09	photorecept	CHCHD10
1.07654096882602E-13	0.463785157025851	0.752	0.501	2.05726979142653E-09	photorecept	TCAF1
1.12902085289365E-13	0.437079824150913	0.644	0.383	2.15755884987977E-09	photorecept	NAPA
1.55158253731609E-13	0.563000391135255	0.832	0.627	2.96507422881104E-09	photorecept	OCIAD2
1.82108617987426E-13	0.450512991265707	0.485	0.22	3.48009568973971E-09	photorecept	PRNP
1.94882458859377E-13	0.407325812609458	0.455	0.19	3.7242037888027E-09	photorecept	FAM221A
2.55333719151734E-13	0.451401928736293	0.782	0.528	4.87942737298964E-09	photorecept	APMAP
3.8229073394453E-13	0.4896941722054	0.822	0.587	7.30557592567997E-09	photorecept	PCSK1N
4.72509850901641E-13	0.492825058792358	0.653	0.413	9.02966325073037E-09	photorecept	TBCC
5.74304434514337E-13	0.4475350092189	0.653	0.376	1.0974957743569E-08	photorecept	DST
6.86823930701919E-13	0.462183046349754	0.564	0.286	1.31252053157137E-08	photorecept	LOXL1
1.02973298465014E-12	0.665641671708439	0.713	0.52	1.96781973366642E-08	photorecept	LIMD2
8.82323066614884E-12	0.458847089546838	0.851	0.686	1.68611938030104E-07	photorecept	AKAP9
9.25605408739087E-12	0.453296118145921	0.881	0.726	1.7688319361004E-07	photorecept	APP
1.10085952734031E-11	0.444946067032474	0.604	0.357	2.10374255674734E-07	photorecept	SLC22A17

1.12653983144512E-11	0.477143379738682	0.782	0.582	2.15281761789162E-07	photorecept	ARMCX3
2.24831497394021E-11	0.421662082571763	0.782	0.638	4.29652991519974E-07	photorecept	CHMP2A
2.2812230782368E-11	0.490750127886315	0.95	0.902	4.35941730251052E-07	photorecept	HMGA1
bioRxiv preprint doi: https://doi.org/10.1101/2020.10.27.358135 ; this version posted November 9, 2020. The copyright holder for this preprint (which was not certified by peer review) is the author/funder. All rights reserved. No reuse allowed without permission.	0.421662082571763	0.95	0.916	9.65634223961699E-07	photorecept	SARAF
7.2136442490745E-11	0.485002524555603	0.564	0.341	1.37852741599814E-06	photorecept	ITSN1
8.05892484764399E-11	0.411302574070103	0.673	0.459	1.54006053838477E-06	photorecept	MARK3
1.80311643682317E-10	0.435392655826665	0.901	0.757	3.44575551076909E-06	photorecept	UCHL1
2.27416938611187E-10	0.485212084735969	0.446	0.219	4.34593769685978E-06	photorecept	PLEKHB1
3.36662069584508E-10	0.430085106470482	0.693	0.514	6.43361214975995E-06	photorecept	COX17
4.0360904577341E-10	0.406763331767565	0.891	0.865	7.71296886472987E-06	photorecept	COX7B
4.64768520258599E-10	0.450161609711423	0.693	0.462	8.88172642214182E-06	photorecept	TXNIP
5.70242393562075E-10	0.522697816052571	0.683	0.489	1.08973321409713E-05	photorecept	CMSS1
9.30596901381941E-10	0.784711102771893	0.812	0.748	1.77837067854089E-05	photorecept	KCNQ1OT1
1.37834382211446E-09	0.433703444516617	1	0.998	2.63401504406074E-05	photorecept	PKM
3.18943656910227E-09	0.408183147460354	0.683	0.474	6.09501328355443E-05	photorecept	IFI27L2
1.72604618773732E-08	0.424464814085325	0.921	0.854	0.000329847426476602	photorecept	GNAS
1.97278946618646E-08	0.455873332671868	0.455	0.245	0.000377000066988232	photorecept	GNG3
5.02041725484834E-08	0.4805188371702	0.545	0.344	0.000959401737401519	photorecept	CDKN1C
5.18562318607406E-08	0.524387895470742	0.545	0.375	0.000990972590858753	photorecept	ARL4D
1.16494635398591E-07	0.433550153679213	1	0.995	0.00222621248246707	photorecept	ALDOA
8.14872554039789E-07	0.409440115171965	0.257	0.11	0.0155722145077004	photorecept	PALMD
1.66316011651183E-06	1.02753882168935	0.436	0.28	0.031782989826541	photorecept	ISOC1
0	1.33365513479041	0.766	0.024	0	rgc	ISL1
6.05856382299077E-292	1.15353668428893	0.761	0.031	1.15779154657354E-287	rgc	EBF1
6.83826479193271E-283	1.74475653920269	0.876	0.063	1.30679240173834E-278	rgc	NEFM
8.93178430434726E-275	1.38654790035087	0.799	0.043	1.70686398056076E-270	rgc	POU4F2
1.21117925290698E-253	1.60314977443565	0.742	0.043	2.31456355230524E-249	rgc	ELAVL4
5.32751985385658E-218	0.893555455948559	0.708	0.047	1.01808904407199E-213	rgc	RBFOX3
1.28811951404136E-217	1.35143029161244	0.718	0.052	2.46159639133304E-213	rgc	CNTN2
5.7859085436687E-217	0.87922073785625	0.603	0.027	1.10568712269509E-212	rgc	PCSK2
1.68783340711472E-215	1.231828823212	0.799	0.075	3.22544964099623E-211	rgc	OLFM1
8.03303157311853E-205	1.21634126560276	0.837	0.097	1.53511233362295E-200	rgc	PPP1R1A
4.21051803814329E-197	1.61871436608795	0.732	0.07	8.04629997089184E-193	rgc	NEFL
4.54528126733512E-169	1.86078476725769	0.919	0.178	8.68603250187741E-165	rgc	SNCG
6.25681677417204E-157	2.39364505699298	0.852	0.171	1.19567768554428E-152	rgc	NSG1
1.98001973578114E-153	0.698967824863108	0.641	0.063	3.78381771507775E-149	rgc	RUNDCC3A
3.24489148845082E-148	0.762729148672185	0.593	0.053	6.20098763442952E-144	rgc	NHLH1

3.59936534527968E-146	0.432190909827262	0.359	0.01	6.87838717482947E-142	rgc	LDB3	
2.95911441452419E-145	0.718075992484285	0.584	0.05	5.65486764615574E-141	rgc	SLC18A2	
7.88674169471337E-143	2.46425886392925	0.952	0.331	1.50715633785973E-138	rgc	GAP43	
bioRxiv preprint doi: https://doi.org/10.1101/2020.10.27.358135 ; this version posted November 9, 2020. The copyright holder for this preprint (which was not certified by peer review) is the author/funder. All rights reserved. No reuse allowed without permission.	1.50566339108605E-142	0.617286269760112	0.579	0.053	1.8776274036544E-138	rgc	STX1A
1.78653806768638E-142	1.05712405856721	0.813	0.14	3.41407424734867E-138	rgc	INA	
2.9006950240863E-142	0.977519309165531	0.722	0.095	5.54322819102892E-138	rgc	CHRNA3	
5.18627711382802E-142	1.94591534625095	0.603	0.068	9.91097556452535E-138	rgc	PRPH	
1.44863040958365E-141	0.816741414259569	0.646	0.071	2.76833271271436E-137	rgc	CTC-378H22.2	
2.14890976794928E-141	0.749783427450784	0.66	0.079	4.10656656655108E-137	rgc	DPYSL3	
2.2881198258703E-141	0.911678791554877	0.799	0.121	4.37259698723814E-137	rgc	SEZ6L2	
4.85248356466687E-140	0.543628257639341	0.507	0.039	9.2730960920784E-136	rgc	SLIT1	
3.10266126617349E-138	0.553738957316047	0.483	0.033	5.92918567965754E-134	rgc	NFASC	
2.65020884634599E-133	0.613315878759181	0.455	0.029	5.06454910536718E-129	rgc	TTC9B	
1.27579741404468E-132	1.6192275686326	0.967	0.338	2.43804885823938E-128	rgc	TAGLN3	
1.25908102607717E-130	0.449814220919476	0.344	0.012	2.40610384083347E-126	rgc	ADAM11	
1.28574486485278E-130	2.21079637469672	0.995	0.426	2.45705843673367E-126	rgc	STMN2	
5.35410609921562E-125	0.880461369705424	0.612	0.081	1.02316967556011E-120	rgc	POU6F2	
6.80359960162265E-125	1.34647175110051	0.904	0.267	1.30016788387009E-120	rgc	RAB3A	
4.06205179164299E-123	0.889525232805156	0.813	0.156	7.76258097382975E-119	rgc	ATP1A3	
7.9366469711695E-122	1.24127954950377	0.823	0.206	1.51669323619049E-117	rgc	GNG3	
1.41330739782442E-118	0.573236557534245	0.555	0.06	2.70083043724247E-114	rgc	HMP19	
1.88489517405326E-117	1.41169046341312	0.957	0.389	3.60203467761578E-113	rgc	DCX	
2.89336209979428E-117	1.57768810928951	1	0.999	5.52921497270687E-113	rgc	TUBA1A	
7.58428121722799E-116	0.56682661272755	0.531	0.059	1.44935614061227E-111	rgc	PBX3	
1.01019360224152E-115	1.04296036432112	0.823	0.195	1.93047997388355E-111	rgc	ELAVL2	
2.99838554836733E-114	0.978941322287585	0.9	0.225	5.72991478292998E-110	rgc	SCG3	
3.32659775134586E-114	0.818654535099913	0.675	0.109	6.35712830282194E-110	rgc	CELF4	
2.41619572171135E-112	0.621803427258908	0.522	0.056	4.6173500241904E-108	rgc	ASIC4	
4.95399741336246E-111	1.22598482929101	1	0.995	9.46708905693566E-107	rgc	TUBB2B	
1.63390559350465E-108	1.25334539357629	1	0.991	3.12239358918739E-104	rgc	MAP1B	
7.58895979355147E-108	0.600985416504806	0.612	0.091	1.45025021654769E-103	rgc	SNAP25	
6.69768791638936E-107	0.524031045063588	0.478	0.049	1.27992816082201E-102	rgc	L1CAM	
6.62904902689299E-106	1.05817744821259	0.871	0.269	1.26681126903925E-101	rgc	ELAVL3	
6.47553600499823E-104	0.733457122728724	0.694	0.119	1.23747493055516E-99	rgc	SYT4	
7.6773411788153E-104	0.965276073877025	0.703	0.15	1.4671398992716E-99	rgc	MAPT	
1.68429277743746E-103	0.556707598651197	0.526	0.066	3.21868349768299E-99	rgc	GDAP1L1	
1.54604562286825E-102	0.483610602000837	0.502	0.058	2.95449318530123E-98	rgc	EPS8L1	

2.56602472713392E-99	0.592395471739664	0.617	0.097	4.90367325355292E-95	rgc	CELF3
4.61190659072856E-99	1.58325292053938	0.976	0.644	8.81335349488229E-95	rgc	TUBB2A
9.40556523653911E-99	1.49601386370778	0.976	0.872	1.79740351670262E-94	rgc	MLLT11
bioRxiv preprint doi: https://doi.org/10.1101/2020.10.27.358135 ; this version posted November 9, 2020. The copyright holder for this preprint (which was not certified by peer review) is the author/funder, who has granted bioRxiv a license to display the preprint in perpetuity. It is made available under aCC-BY-NC-ND 4.0 International license.	0.764926887501405	0.526	0.07	3.74846549499685E-03	rgc	CLDN5
1.68562576889984E-96	0.435855042528343	0.45	0.047	3.2212308443676E-92	rgc	SRRM3
2.26565865051617E-96	1.50260201469032	0.675	0.153	4.3296736811364E-92	rgc	RTN1
8.08385348961173E-96	0.432289454218194	0.44	0.045	1.5448244018648E-91	rgc	PPP1R17
9.54639369055513E-96	0.419021884561086	0.421	0.041	1.82431583426509E-91	rgc	CEND1
8.91278941881823E-94	0.690481302765505	0.287	0.015	1.70323405793616E-89	rgc	CALB2
5.8356453931518E-93	0.538705790869869	0.34	0.025	1.11519183463131E-88	rgc	DCC
1.0197845559893E-92	1.37778389471754	0.995	0.997	1.94880828649555E-88	rgc	TMSB10
5.22048388789722E-92	0.476595450875973	0.512	0.069	9.97634470977158E-88	rgc	ATCAY
7.88645473239036E-91	0.708280085054251	0.876	0.282	1.5071014993598E-86	rgc	FAM57B
2.52041623149689E-89	1.0389991417517	0.986	0.882	4.81651541839055E-85	rgc	CD24
7.61331402554302E-88	0.407471461459979	0.45	0.053	1.45490431028127E-83	rgc	RUNX1T1
3.15700520903996E-87	0.42551497764574	0.435	0.049	6.03303695447537E-83	rgc	CHGA
7.88909362213135E-86	1.23557167700358	0.952	0.708	1.5076057911893E-81	rgc	BASP1
7.89795712269957E-84	1.06785525094418	0.957	0.521	1.50929960614789E-79	rgc	PCBP4
2.36471912508379E-80	0.417385391989486	0.306	0.023	4.51897824803512E-76	rgc	NHLH2
6.80694835361317E-79	0.575513895096963	0.311	0.026	1.30080783037548E-74	rgc	RGS10
2.52979599735531E-78	0.712518272539182	0.565	0.113	4.834440150946E-74	rgc	POU2F2
2.47719171639749E-77	0.859171165505238	0.904	0.481	4.73391337003561E-73	rgc	GDI1
4.49862463403063E-77	0.570798204766427	0.569	0.106	8.59687167563253E-73	rgc	SERPINI1
2.23684877526354E-76	0.786129334273503	0.727	0.212	4.27461800952862E-72	rgc	TSPAN7
9.00015547371981E-75	0.490225626386094	0.579	0.114	1.71992971102786E-70	rgc	IGLON5
1.48649192359273E-74	1.1080562607272	0.933	0.749	2.84068606598571E-70	rgc	UCHL1
1.82791111381188E-74	1.05100999766049	0.914	0.569	3.49313813849451E-70	rgc	PCSK1N
4.01362116899565E-73	0.894763936213589	0.967	0.837	7.67003005395069E-69	rgc	HN1
6.02527163617545E-73	0.972285502934994	0.9	0.543	1.15142940967313E-68	rgc	CRMP1
1.27270267164753E-72	0.902654461776461	1	0.976	2.43213480551842E-68	rgc	SOX4
2.71076286209913E-72	0.982843808566421	0.947	0.696	5.18026782947144E-68	rgc	APLP1
3.67440214963494E-72	0.67454936888361	0.579	0.116	7.02178250795237E-68	rgc	SSTR2
6.19487936546699E-72	0.532197806926964	0.608	0.124	1.18384144674074E-67	rgc	SRRM4
1.47700539870207E-71	0.744473692918963	0.78	0.278	2.82255731691965E-67	rgc	KLF7
1.71547818673311E-70	0.470461829490791	0.44	0.068	3.27827881484698E-66	rgc	TMEM176B
8.62353938221693E-69	0.493715457425519	0.435	0.069	1.64795837594166E-64	rgc	TMEM59L
9.00138821592251E-68	1.39335447997463	0.947	0.664	1.72016528806279E-63	rgc	CXCR4

3.15633262054803E-67	0.470216886644711	0.378	0.051	6.03175163786728E-63	rgc	NTRK1
1.91387716774715E-66	0.661283007553289	0.569	0.131	3.65741926756481E-62	rgc	RAB3B
6.54442335166844E-66	0.784793156286069	0.804	0.348	1.25063930250384E-61	rgc	NAGK
bioRxiv preprint doi: https://doi.org/10.1101/2020.10.27.358135 ; this version posted November 9, 2020. The copyright holder for this preprint (which was not certified by peer review) is the author/funder. All rights reserved. No reuse allowed without permission.	0.6804605030368	0.892	0.999	0.7810767158251E-61	rgc	STMN4
2.91869621499902E-64	0.955989601923514	0.866	0.518	5.57762846686313E-60	rgc	KLC1
3.30309911067413E-64	1.21550265587156	0.938	0.805	6.31222240049825E-60	rgc	SH3BGRL3
3.59261864720733E-64	0.406060060401106	0.397	0.061	6.8654942348132E-60	rgc	REEP1
2.8237401338199E-63	0.507091500028693	0.416	0.068	5.39616739572983E-59	rgc	TMEM176A
7.24031450046331E-63	0.4259433673191	0.359	0.047	1.38362410103854E-58	rgc	DLX2
5.21541246922346E-62	0.79648048197117	0.938	0.803	9.96665322868603E-58	rgc	ETFB
6.48146837926932E-62	0.406290936316917	0.321	0.039	1.23860860727837E-57	rgc	MYC
2.41012073423224E-60	0.707434991877511	0.933	0.659	4.6057407231178E-56	rgc	TERF2IP
1.48975486818735E-59	0.664698262104226	0.531	0.133	2.84692155310602E-55	rgc	MAB21L2
2.1045997394144E-59	0.862366639108281	0.947	0.855	4.02189010202091E-55	rgc	C4orf48
3.19190328054967E-59	0.416884839488213	0.44	0.079	6.09972716913042E-55	rgc	CADPS
9.32199749909239E-59	1.06234410698872	0.589	0.164	1.78143372207656E-54	rgc	HEY1
1.31622272927541E-58	0.721819555075207	1	0.999	2.51530163564531E-54	rgc	TMSB4X
1.31874311860696E-57	0.941591649497639	1	0.994	2.5201180996579E-53	rgc	CALM2
1.44261727814429E-56	0.753829284769034	0.775	0.321	2.75684161853374E-52	rgc	GPC2
3.31227318471144E-56	0.469972141006517	0.555	0.144	6.32975405598357E-52	rgc	TUBB3
8.13868480561345E-56	0.712114050650694	0.56	0.157	1.55530266635273E-51	rgc	SCG5
3.01660182900838E-55	0.554020844304531	0.976	0.962	5.76472609523501E-51	rgc	COX7A2
4.26412028851252E-55	0.68638825543295	0.675	0.24	8.14873387134743E-51	rgc	CDKN2D
5.29981077571973E-55	0.76787366890599	0.909	0.54	1.01279383924004E-50	rgc	BEX1
1.1425651376505E-54	0.665427656327872	0.785	0.35	2.18344197805012E-50	rgc	RBFOX2
1.08586260222726E-53	0.545713364206398	0.708	0.253	2.07508343285629E-49	rgc	STMN3
1.15081774132745E-53	0.46560747581527	0.282	0.035	2.19921270367676E-49	rgc	FABP3
1.19047663588458E-53	0.500739629391955	0.536	0.14	2.27500085117544E-49	rgc	CCDC184
3.00397801280603E-52	1.06948742104217	0.967	0.797	5.74060198247233E-48	rgc	SOX11
1.42863467773053E-51	0.614947305628854	0.627	0.211	2.73012086914305E-47	rgc	PGM2L1
2.90703911979149E-51	0.474767956000412	0.612	0.184	5.55535175792154E-47	rgc	STXBP1
6.35485145414487E-51	0.518938156105276	0.967	0.971	1.21441211288709E-46	rgc	MORF4L2
1.54077393419273E-50	0.515214200171585	1	0.999	2.9444189882423E-46	rgc	ACTB
3.27297331440915E-50	1.09504000683698	0.943	0.882	6.25465200383589E-46	rgc	MIAT
9.12233634806579E-50	0.77797841110578	0.866	0.493	1.74327847611537E-45	rgc	NELL2
1.344332904763E-49	0.644928115557422	0.957	0.846	2.56902018100209E-45	rgc	DYNC1I2
4.16872778083366E-49	0.768907843094068	0.919	0.675	7.96643878917312E-45	rgc	ENO2

6.24697511402738E-49	0.648318738258603	0.876	0.556	1.19379694429063E-44	rgc	DYNC1H1
8.38288740902198E-49	0.578094682955794	0.694	0.265	1.6019697838641E-44	rgc	CD200
1.65385499813672E-48	0.574940339741931	0.995	0.989	3.16051690143926E-44	rgc	STMN1
bioRxiv preprint doi: https://doi.org/10.1101/2020.10.27.358135 ; this version posted November 9, 2020. The copyright holder for this preprint (which was not certified by peer review) is the author/funder, who has granted bioRxiv a license to display the preprint in perpetuity. It is made available under aCC-BY-NC-ND 4.0 International license.	0.62508008546255	0.823	0.458	8.95248390467750E-14	rgc	DYNC1LI1
1.46764204661364E-47	0.543415175812318	0.746	0.315	2.80466395107866E-43	rgc	MAP2
1.84422881366707E-47	0.613749953440657	0.799	0.438	3.52432126291777E-43	rgc	YWHAG
5.28925858027731E-47	0.68671399739046	0.971	0.862	1.01077731469099E-42	rgc	HSPA8
6.04432261128886E-46	0.706970723456807	0.727	0.365	1.1550700510173E-41	rgc	C14orf132
8.13412611384977E-46	0.465063552710212	0.56	0.175	1.55443150035669E-41	rgc	GLRX
1.15621723452839E-45	0.595086259896929	0.833	0.502	2.20953113518376E-41	rgc	RAB6A
1.77102494011534E-45	0.541719069784905	1	0.998	3.38442866056041E-41	rgc	TUBB
2.19306931409487E-45	0.42940399071849	0.603	0.189	4.1909554592353E-41	rgc	PPP2R5B
1.35521235807955E-43	0.574552664144579	0.904	0.747	2.58981081629002E-39	rgc	RAB2A
2.52288140448579E-43	0.458257868709261	0.617	0.222	4.82122636397235E-39	rgc	CACNB3
4.19677700179684E-43	0.56888239165736	0.746	0.381	8.02004085043376E-39	rgc	RUFY3
1.10249112223136E-42	0.449346889179654	0.995	0.99	2.10686053458413E-38	rgc	CFL1
3.43652351700529E-42	0.708868934923536	0.708	0.311	6.56719644099712E-38	rgc	NRN1
7.29190563278538E-42	0.671346681335076	0.766	0.411	1.39348316642529E-37	rgc	KIF5C
8.87422596971037E-42	0.523119093541381	0.679	0.292	1.69586458281165E-37	rgc	CEP170
7.99252610376117E-41	0.753758623575026	0.89	0.735	1.52737173842876E-36	rgc	PAFAH1B3
3.84973834161415E-40	0.474487657200566	0.421	0.109	7.35684997082464E-36	rgc	KIF5A
7.39597859770878E-40	0.536851490567675	0.971	0.943	1.41337151002215E-35	rgc	COX6A1
1.29547637655841E-39	0.570519910547558	0.565	0.207	2.47565535560312E-35	rgc	MAP1LC3A
2.70574153628169E-39	0.536043576140595	0.89	0.754	5.1706720758343E-35	rgc	NREP
3.64931287529899E-39	0.409507480663422	0.512	0.157	6.97383690469636E-35	rgc	RAB33A
5.21028219066426E-38	0.417982686418858	0.531	0.176	9.9568492663594E-34	rgc	ADD2
1.95258645592897E-37	0.500298858660243	0.957	0.876	3.73139271728027E-33	rgc	EIF4A1
2.19002286859039E-37	0.506010687405939	0.651	0.291	4.18513370187625E-33	rgc	CARD19
2.45329990957561E-37	0.540495633328484	0.885	0.727	4.68825612719899E-33	rgc	ATP6V0B
2.85878629977421E-36	0.494085827737173	0.641	0.287	5.46314061886852E-32	rgc	TPD52
3.21834033156431E-36	0.557352813531728	0.809	0.503	6.15024837361939E-32	rgc	KIF1A
1.48899164794912E-35	0.655740359854616	0.9	0.707	2.84546303923077E-31	rgc	FDFT1
2.82869290023834E-35	0.455914027499568	0.617	0.263	5.40563213235546E-31	rgc	TMEM55A
5.68848007950521E-35	0.429986743440481	0.976	0.933	1.08706854319345E-30	rgc	PSMA7
7.08894562578963E-34	0.484389934711612	0.933	0.913	1.3546975090884E-29	rgc	NDUFB8
8.65629664631099E-34	0.523327289428818	0.722	0.336	1.65421828911003E-29	rgc	PFKFB3
9.62897691576309E-34	0.593741070454873	0.933	0.759	1.84009748860233E-29	rgc	DAAM1

1.80072498087638E-33	0.506131204771077	0.837	0.698	3.44118543845477E-29	rgc	PFDN2
3.46660939938129E-33	0.610913558700894	0.99	0.993	6.62469056221764E-29	rgc	RBP1
4.24435569903227E-33	0.478335116535944	0.962	0.86	8.11096374085067E-29	rgc	CALM3
bioRxiv preprint doi: https://doi.org/10.1101/2020.10.27.358135 ; this version posted November 9, 2020. The copyright holder for this preprint (which was not certified by peer review) is the author/funder, who has granted bioRxiv a license to display the preprint in perpetuity. It is made available under aCC-BY-NC-ND 4.0 International license.	0.452694790620026	0.923	0.90	Not yet assigned	rgc	TXN
6.48373288075152E-33	0.44787637772259	0.947	0.894	1.23904135351162E-28	rgc	PRDX5
7.57191265545192E-33	0.42414771059215	0.598	0.246	1.44699250845686E-28	rgc	ACLY
1.01929174080039E-32	0.505796342022941	0.77	0.478	1.94786651666955E-28	rgc	IDH1
1.1879005284783E-32	0.670373030866288	0.866	0.658	2.27007790992204E-28	rgc	NKAIN4
1.19048675365917E-32	0.804075322237765	1	1	2.27502018624267E-28	rgc	CRABP1
2.43140936400749E-32	0.520229397383322	0.962	0.986	4.64642329461831E-28	rgc	CCNI
6.21966015992611E-32	1.02616399501493	0.694	0.426	1.18857705656188E-27	rgc	SAT1
7.62645033891371E-32	0.54726758955761	0.641	0.34	1.45741465976641E-27	rgc	MAP4
9.08370562573758E-32	0.549986448496136	0.842	0.739	1.73589614507845E-27	rgc	TBCB
1.15089239794912E-31	0.477219833748133	0.656	0.338	2.19935537248077E-27	rgc	CCDC112
2.5002483129876E-31	0.549196259181565	0.713	0.359	4.77797452611931E-27	rgc	DST
3.97917188652552E-31	0.432786484964947	0.947	0.921	7.60419747515027E-27	rgc	TTC3
4.71528031761258E-31	0.459357619044709	0.852	0.617	9.01090068695764E-27	rgc	OClAD2
6.73475494396643E-31	0.565731361852537	0.689	0.339	1.28701166979199E-26	rgc	PFKP
7.06938628701771E-31	0.526333534841429	0.847	0.674	1.35095971944908E-26	rgc	PCMT1
7.65719071689374E-31	0.441480742928549	0.766	0.448	1.46328914599839E-26	rgc	ACTR1A
8.88884921086379E-31	0.624813745649442	0.856	0.679	1.69865908419607E-26	rgc	MAP1LC3B
1.79182147654656E-30	0.499288551907143	0.679	0.374	3.42417084168048E-26	rgc	HCFC1R1
1.95350826178169E-30	0.471590188298268	0.923	0.859	3.7331542882648E-26	rgc	MGST3
2.38841961156086E-30	0.4892663866398	0.847	0.66	4.5642698776928E-26	rgc	ARPC5
2.85250252817859E-30	0.675804336797648	0.828	0.575	5.45113233134929E-26	rgc	CADM1
2.88042887565719E-30	0.582777451406447	0.904	0.683	5.50449958138088E-26	rgc	SLC16A3
4.41055176443086E-30	0.523211625020818	0.818	0.594	8.42856442182737E-26	rgc	DPYSL2
4.89597679946044E-30	0.714149763947993	0.856	0.591	9.35621166376891E-26	rgc	HMGCS1
6.71944174037942E-30	0.511821151888191	0.584	0.259	1.28408531658651E-25	rgc	TLE4
7.01204167001813E-30	0.454580577096854	0.871	0.789	1.34000116314047E-25	rgc	DYNLRB1
1.05471094872721E-29	0.436291628776352	0.976	0.931	2.0155526230177E-25	rgc	PAX6
1.21950719462149E-29	0.46346363301991	0.909	0.724	2.33047824892166E-25	rgc	DBN1
1.55825435885661E-29	0.463264691986143	0.914	0.806	2.97782407977499E-25	rgc	FSCN1
2.13828493518493E-29	0.543552133540049	0.56	0.247	4.08626251113841E-25	rgc	DUSP4
2.54162875924858E-29	0.584880738155335	0.718	0.43	4.85705255892404E-25	rgc	MSMO1
7.96276999881893E-29	0.493044343459464	0.67	0.36	1.5216853467743E-24	rgc	PODXL2
9.1282756148785E-29	0.511802565865589	0.833	0.566	1.74441347000328E-24	rgc	DPYSL4

8.46179032383547E-28	0.446509294700988	0.895	0.885	1.61704813088496E-23	rgc	USMG5
5.86918819509958E-27	0.4791285285621	0.737	0.484	1.12160186408353E-22	rgc	FNBP1L
6.05926690900333E-27	0.451731226302912	0.895	0.691	1.15792590631054E-22	rgc	TPPP3
bioRxiv preprint doi: https://doi.org/10.1101/2020.10.27.358135 ; this version posted November 9, 2020. The copyright holder for this preprint (which was not certified by peer review) is the author/funder. All rights reserved. No reuse allowed without permission.	0.4212079416969285	0.598	0.282	2.481062467716071e-23	rgc	SEMA6A
1.32289216237085E-26	0.451165979261851	0.646	0.346	2.5280469222907E-22	rgc	TMEM14A
4.79053655786362E-26	0.446106839057561	0.9	0.749	9.15471536207738E-22	rgc	CXXC5
4.80072665625263E-26	0.466079563336429	0.9	0.794	9.17418864009877E-22	rgc	CALM1
8.41569205573376E-26	0.423435967419762	0.632	0.337	1.60823875185072E-21	rgc	EPB41
1.12658288875449E-25	0.429216685725393	0.651	0.363	2.15289990040983E-21	rgc	ZC2HC1A
3.61853918360269E-25	0.435183102606266	0.608	0.321	6.91502837986474E-21	rgc	VAT1
3.66529239989621E-25	0.68884710727901	0.746	0.533	7.00437377620166E-21	rgc	ACAT2
3.75562073752276E-25	0.70083584604062	0.517	0.25	7.17699122940599E-21	rgc	SNCA
2.65335167271631E-24	0.419100761767618	0.9	0.763	5.07055504656087E-20	rgc	DNAJB6
4.77073549323085E-24	0.500997337535531	0.785	0.533	9.11687552756416E-20	rgc	FAM63B
6.52488600428686E-24	0.510835174571609	0.732	0.468	1.24690571541922E-19	rgc	BCL7A
1.7009720255149E-23	0.429301850775145	0.914	0.779	3.25055754075898E-19	rgc	SYT1
4.80263023446621E-23	0.41767389859747	0.641	0.334	9.17782637806492E-19	rgc	MAP1A
5.54346674327713E-23	0.415435160506479	0.78	0.593	1.05935649464026E-18	rgc	PFDN4
1.64278269578863E-22	0.415102377640312	0.718	0.475	3.13935773165207E-18	rgc	BZW2
2.00575826965724E-22	0.453746351097084	0.699	0.46	3.83300405331498E-18	rgc	ATP6V0E2
4.06583695960505E-22	0.424902359946405	0.699	0.452	7.76981442980525E-18	rgc	STARD3NL
6.1475814099696E-22	0.427847430279775	0.526	0.254	1.17480280744519E-17	rgc	SMAD9
7.97039015205372E-22	0.409222346399232	0.818	0.671	1.52314155805747E-17	rgc	DTD1
1.56300745187304E-21	0.410397225841339	0.435	0.18	2.98690724052939E-17	rgc	MVD
2.63212746901584E-21	0.420032993719752	0.856	0.726	5.02999559328927E-17	rgc	RAB1A
4.82302209241807E-21	0.477729124268798	0.804	0.616	9.21679521861093E-17	rgc	CXADR
5.35871244195606E-21	0.418538236722019	0.569	0.31	1.0240499476578E-16	rgc	ACOT7
1.57612295723043E-20	0.431815168500083	0.66	0.414	3.01197097126735E-16	rgc	CRIP2
2.42022130927659E-19	0.43572869701396	0.895	0.78	4.62504292202756E-15	rgc	CDC42
3.00628043943834E-19	0.427444507230189	0.737	0.506	5.74500191976666E-15	rgc	ALDOC
3.11288018416273E-19	0.441629686077166	0.699	0.449	5.94871403193498E-15	rgc	SCD
4.04418228868722E-19	0.412899287520904	0.679	0.455	7.72843235368127E-15	rgc	TSC22D3
2.11422693841162E-18	0.489560132836363	0.871	0.741	4.04028767930461E-14	rgc	KCNQ1OT1
4.98845127927761E-18	0.437794996453086	0.727	0.49	9.5329303946995E-14	rgc	HK1
2.54155296665125E-17	0.425438155624352	0.612	0.368	4.85690771927055E-13	rgc	INSIG1
4.51506433039351E-17	0.520736926948378	0.895	0.793	8.628287935382E-13	rgc	DDIT4
2.2131434183323E-14	0.487159707034564	0.344	0.157	4.22931707243303E-10	rgc	MAFB

2.66956557478096E-14	0.465982181870024	0.713	0.509	5.10153981340641E-10	rgc	HERPUD1
5.55108109643704E-14	0.426083542016607	0.67	0.49	1.06081159752912E-09	rgc	TAGLN2
2.52151974495831E-13	0.478866590053713	0.794	0.696	4.81862423261533E-09	rgc	SQLE
bioRxiv preprint doi: https://doi.org/10.1101/2020.10.27.358135 ; this version posted November 9, 2020. The copyright holder for this preprint (which was not certified by peer review) is the author/funder. All rights reserved. No reuse allowed without permission.	0.609802854077114	0.531	0.392	5.08274996391748E-07	rgc	RGS16
1.93570942202742E-10	0.437593408576453	0.569	0.397	3.69914070549439E-06	rgc	CASP3
2.34856100902955E-258	1.9415508564384	0.652	0.011	4.48810008825547E-254	hc/ac	TFAP2A
4.28738339216995E-177	1.02503546498328	0.5	0.011	8.19318966243677E-173	hc/ac	PRDM13
1.55302907781835E-162	0.769623926071452	0.478	0.012	2.96783856771086E-158	hc/ac	BARHL2
8.31840108452566E-126	0.814526481397073	0.565	0.031	1.58964644725285E-121	hc/ac	SPATS2L
4.01413646679045E-123	1.76249219831456	0.957	0.132	7.67101478803654E-119	hc/ac	ONECUT2
8.55991666997373E-111	0.871501166719104	0.489	0.025	1.63580007563198E-106	hc/ac	NPPC
2.17247211630203E-107	0.568476029710888	0.326	0.008	4.15159421425317E-103	hc/ac	TFAP2C
2.97990372775993E-102	0.593721307198401	0.315	0.008	5.69459602374923E-98	hc/ac	CLEC4G
3.97561951181722E-99	1.3497925095472	0.707	0.076	7.59740888708271E-95	hc/ac	HMP19
1.2906809217173E-83	0.618700240354591	0.424	0.027	2.46649124140177E-79	hc/ac	ONECUT3
4.9952793241554E-79	0.506654784615845	0.315	0.014	9.54597878846097E-75	hc/ac	NDST3
3.26483224549167E-76	0.826897819621784	0.522	0.051	6.23909442113457E-72	hc/ac	LRRN3
1.02964032892273E-65	1.10282017526688	0.728	0.132	1.96764266857134E-61	hc/ac	CELF4
2.50216838763408E-65	0.892460668074118	0.543	0.067	4.78164378876873E-61	hc/ac	RUNX1T1
8.10839146785995E-64	0.693727926231585	0.533	0.062	1.54951360950804E-59	hc/ac	LINC00599
9.83831533531314E-62	0.455725241021822	0.283	0.015	1.88010206057834E-57	hc/ac	PTGFR
1.20881240855296E-61	1.22079022460648	0.63	0.099	2.31004051274471E-57	hc/ac	ONECUT1
4.59065478460819E-60	2.12190030735959	1	0.451	8.77274129338626E-56	hc/ac	STMN2
6.09078902599377E-60	0.621022851963661	0.489	0.057	1.16394978286741E-55	hc/ac	PLXNA2
7.0718113254791E-60	0.770841567858395	0.793	0.151	1.35142314429906E-55	hc/ac	SEZ6L2
5.93044219657939E-58	0.687686446724049	0.38	0.034	1.13330750376632E-53	hc/ac	PROX1
5.16668657406341E-57	0.916028121905171	0.815	0.185	9.87353804303517E-53	hc/ac	ATP1A3
2.15654880866339E-52	1.73862906000784	1	0.977	4.12116477335574E-48	hc/ac	SOX4
2.30167450275582E-50	0.822897720910597	0.467	0.062	4.39849997476637E-46	hc/ac	NTRK1
5.4980636460876E-50	0.602466044429908	0.424	0.049	1.05067996276734E-45	hc/ac	TTC9B
5.20913158585306E-48	0.969843225277253	0.685	0.145	9.95465046056519E-44	hc/ac	SYT4
1.15482554306622E-47	0.785490098793129	0.75	0.172	2.20687161279955E-43	hc/ac	INA
5.80684656704035E-46	0.460768053309762	0.359	0.038	1.10968837896141E-41	hc/ac	GRIA2
3.08417096870498E-45	1.21129892303644	1	0.876	5.89385072119522E-41	hc/ac	MLLT11
1.87990359857481E-43	1.10526374768156	0.859	0.297	3.59249577687647E-39	hc/ac	RAB3A
6.46566821521944E-43	1.03373578672829	1	0.997	1.23558919592843E-38	hc/ac	TMSB10
7.77916292769687E-43	1.07599262377152	0.761	0.251	1.48659803548287E-38	hc/ac	TRIB1

7.97100623504082E-43	1.02064439742538	0.989	0.808	1.5232592915163E-38	hc/ac	ETFB
5.38218349019485E-41	0.65370374071109	0.587	0.121	1.02853526497624E-36	hc/ac	CELF3
7.41395355304391E-41	0.784775203559515	0.859	0.256	1.41680652398669E-36	hc/ac	SCG3
bioRxiv preprint doi: https://doi.org/10.1101/2020.10.27.358135 ; this version posted November 9, 2020. The copyright holder for this preprint (which was not certified by peer review) is the author/funder, who has granted bioRxiv a license to display the preprint in perpetuity. It is made available under aCC-BY-NC-ND 4.0 International license.	0.691383538990478	0.467	0.084	0.688502420712412E-06	hc/ac	PLPPR1
1.33282491224548E-40	0.803382137882621	0.946	0.367	2.54702840730111E-36	hc/ac	TAGLN3
2.20408634584189E-37	0.42107151252206	0.326	0.04	4.21200900690385E-33	hc/ac	NKD2
4.42459046476641E-37	0.4766639345547	0.337	0.044	8.45539237816862E-33	hc/ac	OLFM3
1.0126107081594E-36	1.22880326073114	0.967	0.848	1.93509906329262E-32	hc/ac	AP1S2
1.40856757517616E-36	0.92930490111728	1	0.886	2.69177263616164E-32	hc/ac	CD24
1.14147174511883E-35	0.558422860357629	0.489	0.094	2.18135250492208E-31	hc/ac	RUND3A
1.5309576830155E-35	0.739317480382274	0.75	0.217	2.92566013224261E-31	hc/ac	SNCG
2.32357465652777E-35	0.973418000642994	0.978	0.718	4.44035116862457E-31	hc/ac	BASP1
4.07311187831937E-35	0.906297921206855	1	0.932	7.78371679946832E-31	hc/ac	PAX6
7.94985477618399E-35	0.877766654010745	0.967	0.757	1.51921724772876E-30	hc/ac	NREP
1.5753579074689E-33	0.923901310095046	0.913	0.558	3.01050896117307E-29	hc/ac	CRMP1
7.51736853006566E-33	0.86166668458545	0.967	0.706	1.43656912609555E-28	hc/ac	APLP1
1.76685055074627E-32	0.929919389604343	0.935	0.754	3.37645140247612E-28	hc/ac	CXXC5
2.44942665928017E-32	0.461284803619925	0.293	0.036	4.68085434588441E-28	hc/ac	NHLH2
2.81432353183936E-32	1.20097554358389	0.924	0.587	5.37817226934501E-28	hc/ac	ID2
3.26982799074903E-32	1.18836703645669	0.609	0.178	6.24864129032139E-28	hc/ac	RTN1
4.6942112596226E-32	1.27061487486526	0.837	0.419	8.9706377171388E-28	hc/ac	STMN4
1.68604826418911E-31	0.735953850741271	0.62	0.177	3.22203823286539E-27	hc/ac	MAPT
1.71346439722762E-31	0.481699775609703	0.391	0.068	3.27443046310199E-27	hc/ac	CHGA
5.31364752483192E-31	0.698203002875973	0.62	0.196	1.01543804199538E-26	hc/ac	MIR124-2HG
1.23021369141634E-30	0.450733471177589	0.38	0.068	2.35093836429663E-26	hc/ac	TACC2
1.1976184887683E-29	0.952644361848335	0.967	0.684	2.28864893203622E-25	hc/ac	ENO2
1.82333668233063E-29	0.759487126082294	0.783	0.298	3.48439639993384E-25	hc/ac	ELAVL3
3.04455747152362E-29	0.76076092593097	0.793	0.358	5.81814932808164E-25	hc/ac	RP11-96L14.7
4.52184743551148E-28	0.452294952848704	0.413	0.086	8.64125044926243E-24	hc/ac	TMEM59L
5.35567810228683E-28	0.789516380925071	0.88	0.536	1.02347008534701E-23	hc/ac	ZNF385A
2.47553247451111E-27	0.723242568925224	0.989	0.842	4.73074255879074E-23	hc/ac	HN1
2.65307873744379E-26	0.473097296834879	0.326	0.057	5.07003346725508E-22	hc/ac	MGLL
2.95586887100153E-26	0.554464313630032	0.478	0.119	5.64866541248393E-22	hc/ac	SNAP25
4.06227519486142E-26	0.596774231867288	0.674	0.238	7.76300789738017E-22	hc/ac	GNG3
6.73487358135772E-26	0.571853742828108	0.5	0.137	1.28703434139746E-21	hc/ac	IGLON5
2.30297784148197E-25	0.423698286137575	0.413	0.09	4.40099065507204E-21	hc/ac	GDAP1L1
3.35274868683971E-25	0.645959550199279	1	0.983	6.40710274055069E-21	hc/ac	CCNI

1.24518671380568E-24	0.480250303706921	0.304	0.053	2.37955181008265E-20	hc/ac	GATM
1.31239335608411E-24	0.81063162263617	1	0.995	2.50798370347674E-20	hc/ac	TUBB2B
1.72854852272203E-24	0.535796817950547	1	1	3.3032562269218E-20	hc/ac	ACTG1
bioRxiv preprint doi: https://doi.org/10.1101/2020.10.27.358135 ; this version posted November 9, 2020. The copyright holder for this preprint (which was not certified by peer review) is the author/funder, who has granted bioRxiv a license to display the preprint in perpetuity. It is made available under aCC-BY-NC-ND 4.0 International license.	0.654436590707272414	0.603	0.221	5.93841827698659E-20	hc/ac	MAP1LC3A
6.28711615550569E-24	0.658705392813199	0.359	0.077	1.20146789731714E-19	hc/ac	KIRREL2
9.75345026180357E-24	0.640261053648882	0.946	0.67	1.86388434503066E-19	hc/ac	TERF2IP
1.48561173380483E-23	0.429239350214634	0.75	0.312	2.83900402330103E-19	hc/ac	FAM57B
2.12300609304285E-23	0.612889411262131	1	0.999	4.05706464380488E-19	hc/ac	TUBA1A
2.89290204674444E-23	0.496081955519569	0.935	0.541	5.52833581132863E-19	hc/ac	PCBP4
6.1206275465589E-23	0.672999781368472	0.5	0.141	1.16965192414741E-18	hc/ac	PPP1R1A
3.16957439581675E-21	0.697983545031838	0.935	0.791	6.0570566704058E-17	hc/ac	RORB
1.62189752095611E-20	0.547045913120384	0.978	0.921	3.09944616254713E-16	hc/ac	TTC3
3.3668034588326E-19	0.640465327476867	0.75	0.427	6.4339614098291E-15	hc/ac	KIF5C
5.10256458752471E-19	0.729447718540697	0.848	0.587	9.75100092675972E-15	hc/ac	PCSK1N
7.69176619995728E-19	0.623329368972088	0.707	0.343	1.46989652081184E-14	hc/ac	GPC2
8.29187071742843E-19	0.530811163874514	0.935	0.81	1.58457649410057E-14	hc/ac	FSCN1
8.76097619638699E-19	0.522331227415157	0.598	0.239	1.67422255112955E-14	hc/ac	TSPAN7
9.62325199032843E-19	0.816407000622824	0.75	0.421	1.83900345535176E-14	hc/ac	DCX
1.29460413776928E-18	0.737346574303219	1	0.999	2.4739885072771E-14	hc/ac	TMSB4X
1.66022370749862E-18	0.86459247127365	0.946	0.805	3.17268750502987E-14	hc/ac	SOX11
2.81471097118166E-18	0.407668775106464	1	0.994	5.37891266592815E-14	hc/ac	MARCKSL1
3.2540854571735E-18	0.452793909243635	1	1	6.21855730865856E-14	hc/ac	GAPDH
5.73796222863896E-18	0.446246649295359	0.413	0.125	1.0965245818929E-13	hc/ac	NOL4
1.37031246237793E-17	0.574827733419059	0.609	0.284	2.61866711560422E-13	hc/ac	NDRG4
2.71754674912681E-16	0.488987129591467	0.511	0.211	5.19323183758133E-12	hc/ac	C12orf49
5.38794995853607E-16	0.460430634471495	0.924	0.733	1.02963723707624E-11	hc/ac	ATP6V0B
1.51804517943855E-15	0.597753273133683	0.913	0.784	2.90098433790706E-11	hc/ac	TSC22D1
2.54355604244998E-15	0.634392686815673	0.913	0.768	4.86073559712192E-11	hc/ac	DAAM1
3.96315654230705E-15	0.620299246422739	0.902	0.756	7.57359215234878E-11	hc/ac	PHYHIPL
3.97640939682809E-15	0.502221382112833	0.978	0.944	7.59891835733848E-11	hc/ac	COX6A1
4.08169438113147E-15	0.553930001354112	0.652	0.375	7.80011796234224E-11	hc/ac	ATAT1
6.29970455949962E-15	0.530028273359261	0.5	0.212	1.20387354132038E-10	hc/ac	SULF2
6.67623338737705E-15	0.618613316912678	0.761	0.461	1.27582820032775E-10	hc/ac	TXNIP
2.9276901750188E-14	0.464539090563415	0.978	0.962	5.59481592446093E-10	hc/ac	COX7A2
5.31855096633495E-14	0.617627997019921	0.728	0.502	1.01637508966661E-09	hc/ac	ZEB2
7.004378852974E-14	0.45654417144587	0.554	0.268	1.33853679880333E-09	hc/ac	CECR1
8.60864473673304E-14	0.47777508639479	0.728	0.471	1.64511200918968E-09	hc/ac	RERE

8.85203955870892E-14	0.844062759652825	0.815	0.664	1.69162475966927E-09	hc/ac	TUBB2A
2.76016956676337E-13	0.489128686357178	0.707	0.449	5.27468404208481E-09	hc/ac	SEPT6
2.87090760087961E-13	0.461585991836346	0.446	0.179	5.48630442528094E-09	hc/ac	SCG5
bioRxiv preprint doi: https://doi.org/10.1101/2020.10.27.358135 ; this version posted November 9, 2020. The copyright holder for this preprint (which was not certified by peer review) is the author/funder. All rights reserved. No reuse allowed without permission.	0.55606274957605	0.717	0.486	0.724550801999003E-08	hc/ac	BZW2
5.00907219958048E-13	0.452451175078047	0.772	0.537	9.5723369733983E-09	hc/ac	KLC1
6.58002109667787E-13	0.466817165298081	0.739	0.505	1.25744203157514E-08	hc/ac	GDI1
7.49388714478371E-13	0.577932099394091	0.75	0.501	1.43208183336817E-08	hc/ac	EFNA5
1.33378831562813E-12	0.581204901748688	0.641	0.401	2.54886947116535E-08	hc/ac	STARD4-AS1
1.47476312955121E-12	0.420649946333808	0.435	0.177	2.81827234057237E-08	hc/ac	SV2A
1.59653762011511E-12	0.467190044074408	0.522	0.226	3.05098339203997E-08	hc/ac	GADD45G
1.99560302750269E-12	0.459279581074976	0.478	0.212	3.81359738555765E-08	hc/ac	PPP2R5B
3.0855863188168E-12	0.469837348376698	0.707	0.468	5.89655545525891E-08	hc/ac	RNF24
4.43667309853472E-12	0.457692181351391	0.359	0.129	8.47848229129986E-08	hc/ac	PCP4L1
9.76208698325219E-12	0.69339153098626	0.62	0.386	1.86553482249949E-07	hc/ac	PDLIM4
1.15733219236899E-11	0.514255022221791	0.739	0.519	2.21166181961714E-07	hc/ac	ISCA1
1.35065024691896E-11	0.453130559390549	1	0.998	2.58109262186213E-07	hc/ac	ENO1
1.59415406223291E-11	0.434908716333093	0.348	0.127	3.04642841292708E-07	hc/ac	ESRRG
2.20463718693916E-11	0.442039917591058	0.5	0.259	4.21306166424074E-07	hc/ac	EVL
2.28517261381974E-11	0.499727101957461	0.62	0.357	4.36696486500953E-07	hc/ac	PFKP
3.15549803217669E-11	0.443495060599106	0.728	0.519	6.03015673948965E-07	hc/ac	KIF1A
4.86111010604526E-11	0.428034912590745	0.424	0.196	9.28958141265248E-07	hc/ac	ADD2
9.74613931666716E-11	0.604344861549835	0.62	0.413	1.86248722341509E-06	hc/ac	MPPED2
2.02402317288325E-10	0.637863302142038	0.717	0.547	3.86790828337989E-06	hc/ac	PTPRF
3.69397421311326E-10	0.670242075769724	0.87	0.869	7.05918472125944E-06	hc/ac	FAM162A
4.7854048262774E-10	0.428006842919984	0.826	0.688	9.14490862301611E-06	hc/ac	SARS
5.60477234300846E-10	0.413333645065802	0.587	0.355	1.07107199474892E-05	hc/ac	CITED2
5.97284940642298E-10	0.497772698812793	1	0.985	1.14141152156743E-05	hc/ac	PGK 1.00
8.18610896452086E-10	0.484272984863689	0.783	0.56	1.56436542311994E-05	hc/ac	BEX1
9.35953071207124E-10	0.515171036680754	0.522	0.299	1.78860631907681E-05	hc/ac	SEMA6A
7.40377691543973E-09	0.518492063081801	0.565	0.355	0.000141486176854053	hc/ac	ZNF385D
3.57917115061438E-08	0.439005526830867	0.815	0.696	0.000683979606882407	hc/ac	SLC16A3
5.12985312746522E-08	0.446068545501988	0.424	0.242	0.000980314932658604	hc/ac	CDC42EP3
1.03625359608347E-06	0.609661929017099	0.533	0.341	0.0198028062211551	hc/ac	RGS16
5.23425939472817E-151	1.14155452016634	0.995	0.915	1.00026697033255E-146	stem_cells	SLC2A1
1.87761454988888E-140	1.08937888613719	0.834	0.299	3.58812140483764E-136	stem_cells	STC2
2.77590027316862E-136	1.18549703280372	0.968	0.789	5.30474542202523E-132	stem_cells	GPI
1.39749757548281E-129	0.956761975856372	0.91	0.461	2.67061786674765E-125	stem_cells	INSIG2

1.21031069880101E-125	0.654305324708193	1	0.999	2.31290374540874E-121	stem_cells	EIF1	
8.21286962102296E-124	1.14328670467328	0.985	0.768	1.56947938457749E-119	stem_cells	DDIT4	
8.63568118614085E-124	0.933003209699659	0.971	0.694	1.65027867467152E-119	stem_cells	P4HA1	
bioRxiv preprint doi: https://doi.org/10.1101/2020.10.27.358135 ; this version posted November 9, 2020. The copyright holder for this preprint (which was not certified by peer review) is the author/funder, who has granted bioRxiv a license to display the preprint in perpetuity. It is made available under aCC-BY-NC-ND 4.0 International license.	1.38799681730411E-120	0.918667871961046	0.787	0.203	2.65246191786805E-116	stem_cells	NRN1
9.30370679019865E-118	0.831829051856233	0.995	0.984	1.77793836760696E-113	stem_cells	PGK 1.00	
6.26081592738986E-116	0.674096668538598	1	0.995	1.1964419237242E-111	stem_cells	ALDOA	
5.60507060033651E-114	0.958886841325971	0.895	0.507	1.07112899172431E-109	stem_cells	PLOD2	
2.44647117333528E-109	0.772781529794244	0.993	0.945	4.67520641224372E-105	stem_cells	BNIP3	
2.94712843743071E-107	0.60668832883626	1	0.998	5.63196244393009E-103	stem_cells	ENO1	
1.20608154194797E-102	0.812700269734533	0.98	0.85	2.30482182666256E-98	stem_cells	FAM162A	
1.43866432066906E-95	1.0879783356735	0.861	0.559	2.74928751679858E-91	stem_cells	HILPDA	
1.80976344600939E-93	0.676049853323226	0.927	0.627	3.45845794532394E-89	stem_cells	EPB41L4A-AS1	
1.59808534952949E-91	0.582830963506685	0.584	0.157	3.05394110295085E-87	stem_cells	PDE4C	
1.35767268502714E-90	0.553624165461258	0.993	0.966	2.59451250108687E-86	stem_cells	ZFAS1	
1.4806845709779E-90	0.636152980054385	0.993	0.946	2.82958821513877E-86	stem_cells	WSB1	
4.52760486265286E-87	0.698118123219599	0.692	0.245	8.65225289252962E-83	stem_cells	STC1	
1.96759310405407E-83	0.749023033630725	0.633	0.213	3.76007042184733E-79	stem_cells	ADM	
4.68280902251893E-83	0.656906186879006	0.677	0.268	8.94884804203368E-79	stem_cells	PFKFB4	
1.14892702959881E-80	0.938827359825493	0.802	0.476	2.19559955356332E-76	stem_cells	HERPUD1	
3.12087460381549E-80	0.707880102787677	0.746	0.381	5.96399136789141E-76	stem_cells	CASP7	
3.350875672392E-78	0.714377789506199	0.704	0.295	6.40352340994112E-74	stem_cells	DDIT3	
7.16690091584174E-78	0.650657309057143	0.707	0.311	1.36959476501736E-73	stem_cells	FUT11	
1.20812131514202E-76	0.682605552393887	0.77	0.403	2.3087198332364E-72	stem_cells	TMEM45A	
4.44878632202066E-72	0.515139039887776	0.988	0.949	8.50163066138147E-68	stem_cells	C4orf3	
1.71548626053585E-71	0.547780868270675	0.572	0.196	3.27829424388401E-67	stem_cells	NOL3	
6.23837360567404E-69	0.603286006631235	0.885	0.65	1.19215319604431E-64	stem_cells	SNHG7	
2.44752941791932E-64	0.53892120378175	0.726	0.36	4.67722871764382E-60	stem_cells	ESPN	
2.39749525519325E-62	0.515096868380666	0.687	0.309	4.58161343267431E-58	stem_cells	PFKP	
3.48912254037813E-62	0.585382856980681	0.824	0.522	6.6677131746626E-58	stem_cells	IGFBP2	
9.80551036249678E-62	0.676588627124918	0.658	0.316	1.87383303027314E-57	stem_cells	MTHFD2	
1.90446717800549E-61	0.635664086138146	0.878	0.662	3.6394367771685E-57	stem_cells	SLC3A2	
1.52199267419952E-59	0.481442608913168	0.435	0.123	2.90852800039529E-55	stem_cells	HIST1H2AC	
1.3119114628763E-58	0.576858167563049	0.77	0.464	2.5070628055566E-54	stem_cells	ARRDC3	
1.43126000080549E-56	0.512847944181705	0.543	0.211	2.73513786153929E-52	stem_cells	VEGFA	
3.68371950582054E-54	0.57538639836757	0.846	0.62	7.03958797562305E-50	stem_cells	CDCA7L	
8.07831946172299E-53	0.558124565795843	0.932	0.77	1.54376684913526E-48	stem_cells	NR2F1	
2.3065012832134E-52	0.462383776770044	0.509	0.195	4.40772395222081E-48	stem_cells	SLC2A3	

4.09725203396316E-51	0.488129593501269	0.298	0.064	7.82984863690359E-47	stem_cells	TRIB3
5.55361473044841E-51	0.515779673931523	0.746	0.436	1.06129577498869E-46	stem_cells	AK4
3.11524827402233E-50	0.546517115828641	0.741	0.46	5.95323945165667E-46	stem_cells	SHMT2
bioRxiv preprint doi: https://doi.org/10.1101/2020.10.27.358135 ; this version posted November 9, 2020. The copyright holder for this preprint (which was not certified by peer review) is the author/funder. All rights reserved. No reuse allowed without permission.	0.496344386378058	0.903	0.94	1.78957676811085E-44	stem_cells	BTG1
7.69395259833877E-48	0.526354253131651	0.606	0.303	1.47031434154254E-43	stem_cells	ASNS
6.41812753143685E-47	0.442384107878632	0.531	0.223	1.22650417125758E-42	stem_cells	ANKRD37
2.3242584858461E-46	0.577878903637537	0.934	0.818	4.44165796645191E-42	stem_cells	NEAT1
1.22527815079817E-45	0.487153230132445	0.614	0.33	2.34150654617531E-41	stem_cells	AARS
1.52300720005503E-45	0.493740265198221	0.902	0.664	2.91046675930516E-41	stem_cells	SLC16A3
1.7110440878082E-45	0.414741033619211	0.88	0.687	3.26980525180147E-41	stem_cells	ATF4
2.9547468647689E-44	0.455857813463666	0.557	0.272	5.64652125857336E-40	stem_cells	FBXO17
5.17312999718432E-44	0.426208337459528	0.636	0.318	9.88585142461923E-40	stem_cells	PFKFB3
2.10160086555675E-41	0.539030166838892	0.819	0.581	4.01615925407896E-37	stem_cells	ZFP36L2
5.66839758120354E-41	0.435246477179325	0.65	0.382	1.083230777768E-36	stem_cells	KDM3A
4.43531477908668E-40	0.424404360649876	1	0.98	8.47588654283464E-36	stem_cells	VIM
2.45481778649851E-39	0.427411805804481	0.667	0.384	4.69115678999865E-35	stem_cells	P4HA2
6.33700090987427E-39	0.40747206661566	0.941	0.827	1.21100087387697E-34	stem_cells	PNRC1
5.29917235188722E-38	0.420549403155229	0.932	0.83	1.01267183644565E-33	stem_cells	RBPJ
3.64902519190336E-37	0.475043728105709	0.797	0.589	6.97328714172731E-33	stem_cells	PHGDH
3.86716360504566E-36	0.450868682868746	0.804	0.673	7.39014964924225E-32	stem_cells	SARS
4.30985204489802E-35	0.474349567123348	0.743	0.551	8.23612725780012E-31	stem_cells	SNHG8
2.42785260668006E-34	0.421827619378489	0.523	0.273	4.6396263313656E-30	stem_cells	CHPF
4.32932378127964E-34	0.447539036652862	0.682	0.476	8.27333774602539E-30	stem_cells	TAF1D
2.27657048921006E-32	0.494278613608413	0.677	0.476	4.35052620488043E-28	stem_cells	XBP1
2.53004229717275E-32	0.43316160218394	0.465	0.231	4.83491082989713E-28	stem_cells	GBE1
5.20198070961671E-32	0.421541283464565	0.778	0.602	9.94098513607753E-28	stem_cells	PLIN2
1.15940233552497E-31	0.437816614256036	0.665	0.448	2.21561786318822E-27	stem_cells	FIGN
1.31870548571796E-29	0.429035033081093	0.961	0.846	2.52004618320702E-25	stem_cells	FOS
3.66326512858574E-28	0.509710266783278	0.653	0.479	7.00049966072735E-24	stem_cells	PSAT1
1.58251296604571E-27	0.422563755213576	0.792	0.636	3.02418227811335E-23	stem_cells	HSPA9
4.19012729389103E-21	0.460796934158202	0.689	0.579	8.00733325862576E-17	stem_cells	EIF4EBP1
8.60241184335559E-21	0.439380333490938	0.474	0.281	1.64392090326525E-16	stem_cells	ATF3
8.51154423781783E-11	0.504231910901186	0.866	0.768	1.62655610384699E-06	stem_cells	CYP26A1

SupTable 2 enriched_genes AEP

p_val	avg_logFC	pct.1	pct.2	p_val_adj	cluster	gene
bioRxiv preprint doi: https://doi.org/10.1101/2020.10.27.358135 ; this version posted November 9, 2020. The copyright holder for this preprint (which was not certified by peer review) is the author/funder. All rights reserved. No reuse allowed without permission.						
6.39573942155995E-271	1.80017474019716	0.953	0.315	1.17182737681821E-266	progenitors	IFITM3
2.77180252852078E-262	1.95164088218322	0.984	0.575	5.0784965927557E-258	progenitors	SFRP2
2.73807012392059E-253	1.44337180480181	0.96	0.328	5.0166920810473E-249	progenitors	ZFP36L1
9.51532528948643E-242	1.43313963944759	0.885	0.206	1.7433978995397E-237	progenitors	IFITM2
9.48862977211164E-238	1.27200932559519	0.999	0.866	1.7385067468463E-233	progenitors	VIM
1.79464429574571E-226	1.17531169252608	0.965	0.36	3.28814727866529E-222	progenitors	TTYH1
4.16180920452147E-224	1.41824425120026	0.972	0.448	7.62526682452424E-220	progenitors	CCND1
1.58397835401464E-215	1.21337205474433	0.862	0.205	2.90216514022563E-211	progenitors	SPARC
1.36481719445221E-210	1.12955800366686	0.863	0.172	2.50061806367534E-206	progenitors	HES1
5.61711941352772E-196	0.871355283551297	0.846	0.18	1.02916861894655E-191	progenitors	COL2A1
9.14441681819035E-193	1.1078561843259	0.901	0.292	1.67544004942884E-188	progenitors	SPP1
3.38423673173026E-192	1.09285311013656	0.874	0.244	6.20059853987618E-188	progenitors	PTH2
5.96497905353651E-190	1.35613068953389	0.938	0.485	1.09290346218896E-185	progenitors	CYP1B1
9.2058347267253E-189	0.992153652694508	0.758	0.115	1.68669303863061E-184	progenitors	DIO3
1.55509396178448E-188	0.502148650119497	0.999	0.995	2.84924315678153E-184	progenitors	RPLP1
6.33585475307241E-185	0.96930413469545	0.805	0.182	1.16085530785793E-180	progenitors	SEPP1
9.4948331636421E-185	0.888691675924667	0.932	0.435	1.7396433322425E-180	progenitors	B2M
1.5960352862935E-182	0.899023828807152	0.999	0.941	2.92425585154695E-178	progenitors	MDK
2.12247629726536E-177	0.502602025414512	0.999	0.997	3.88880107184959E-173	progenitors	RPL41
1.55181299509014E-174	0.590666455356784	0.999	0.994	2.84323176960415E-170	progenitors	RPS6
1.27171155538868E-166	0.932462948630414	0.954	0.664	2.33002991178314E-162	progenitors	DAPL1
1.38220334962372E-166	0.764220907037175	0.81	0.212	2.53247297718058E-162	progenitors	PLPP3
3.85262260187086E-164	1.30534936143499	0.8	0.222	7.05877513114779E-160	progenitors	CYP26A1
2.15149782010797E-160	0.637463313440224	0.734	0.139	3.94197430600183E-156	progenitors	VSX2
7.21890244914507E-156	1.06842815169855	0.712	0.147	1.32264730673236E-151	progenitors	CYR61
1.00709380535929E-153	0.451841628765609	1	0.99	1.8451972701793E-149	progenitors	RPS27A
1.07664037406773E-153	0.622603629889368	0.987	0.909	1.97262049336689E-149	progenitors	EEF1D
3.42229250005221E-153	0.476361041854261	1	0.997	6.27032431859565E-149	progenitors	RPS4X
8.8329187817478E-151	0.46120398759269	1	0.994	1.61836737919183E-146	progenitors	RPL7
1.40393448653563E-150	0.438781273948661	1	1	2.57228876623058E-146	progenitors	EEF1A1
1.84954225323841E-150	0.742858471326186	0.961	0.778	3.38873131638342E-146	progenitors	SIX6
1.61460855901773E-148	0.431051117301695	1	0.997	2.95828580183228E-144	progenitors	RPS15
1.69781729004095E-148	0.449300619606865	1	0.997	3.11074083881303E-144	progenitors	RPS2
5.61184381461745E-148	0.723211771037213	0.914	0.486	1.02820202371421E-143	progenitors	NPC2
3.89445232522395E-144	0.457142886313588	1	0.992	7.13541555027533E-140	progenitors	RPLP0

1.04245185745496E-140	0.8642418177764	0.653	0.117	1.90998029322898E-136	progenitors	CDH6
1.78751422041562E-138	0.426075197258907	0.998	0.992	3.2750835546455E-134	progenitors	RPS17
1.21066181943235E-137	0.439988116184301	1	0.988	2.21817458556395E-133	progenitors	RPS12
bioRxiv preprint doi: https://doi.org/10.1101/2020.10.27.358135 ; this version posted November 9, 2020. The copyright holder for this preprint (which was not certified by peer review) is the author/funder. All rights reserved. No reuse allowed without permission.	0.607028870990866	0.563	0.06	2.92626502242083E-135	progenitors	IFITM1
8.46748600421716E-133	0.709167595282924	0.924	0.566	1.55141278569267E-128	progenitors	MEST
1.27409155971975E-132	0.614678229323999	0.775	0.255	2.33439055571853E-128	progenitors	NPM3
6.69560825814795E-132	0.732109134659585	0.925	0.601	1.22676934505787E-127	progenitors	RP11-89K21.1
2.03572107602894E-129	0.411914704486038	1	0.997	3.72984815550022E-125	progenitors	RPS3
5.21481609396763E-129	0.617057971628948	0.953	0.745	9.55458604736749E-125	progenitors	PRDX6
3.67681034338536E-125	0.416390864891039	0.999	0.992	6.73665191115066E-121	progenitors	RPS24
7.50609807269964E-125	0.587090942886193	0.718	0.182	1.37526728888003E-120	progenitors	ZFP36L2
2.78775163534922E-124	0.647626186886121	0.721	0.207	5.10771854628684E-120	progenitors	TIMP1
1.28538284373606E-123	0.662631407736138	0.726	0.223	2.3550784462932E-119	progenitors	S1PR3
1.30552254047892E-122	0.50261806967557	0.651	0.136	2.39197839866548E-118	progenitors	FZD5
2.50362462365036E-122	0.62128747009105	0.767	0.279	4.58714103545218E-118	progenitors	RHOC
9.56210448371281E-121	0.585922572523067	0.696	0.201	1.75196878350586E-116	progenitors	TBX2-AS1
2.94673949137587E-119	0.504553587390239	0.685	0.161	5.39901609609887E-115	progenitors	FKBP10
2.29719721100082E-118	0.609685745814902	0.679	0.176	4.2089247299957E-114	progenitors	RARRES2
8.76327429584956E-117	0.437876113839407	0.998	0.985	1.60560711648556E-112	progenitors	RPL12
6.71152937506225E-116	0.71954416092147	0.673	0.184	1.22968641209891E-111	progenitors	GINS2
6.9007642810851E-116	0.646431597734649	0.948	0.479	1.26435803158041E-111	progenitors	SOX2
1.19044316434885E-114	0.539725357935225	0.555	0.092	2.18112996571996E-110	progenitors	SPHK1
1.51895500831729E-114	0.796066079914921	0.864	0.433	2.78302936623894E-110	progenitors	EGR1
7.34862708578662E-112	0.644233208759359	0.49	0.055	1.34641545465782E-107	progenitors	PAX2
1.20063668771052E-111	0.756805453711716	0.564	0.103	2.19980653922321E-107	progenitors	FGF19
1.66214230317833E-111	0.570429742822345	0.746	0.25	3.04537712788334E-107	progenitors	LHX2
1.23806629342201E-110	0.586453781682541	0.953	0.836	2.26838506280781E-106	progenitors	CNN3
3.15357347957224E-110	0.494638405781524	0.649	0.162	5.77797732927226E-106	progenitors	EMP3
3.35307091925872E-110	0.548591486043476	0.967	0.836	6.14349653826582E-106	progenitors	HMGN3
9.67004124266848E-109	0.735734104814773	0.545	0.095	1.77174495648172E-104	progenitors	LAMP5
8.82187402796818E-108	0.644793790838203	0.942	0.719	1.61634375940433E-103	progenitors	DEK
2.50668826725127E-106	0.425288628942032	0.999	0.973	4.59275424325778E-102	progenitors	NAP1L1
8.92994554912001E-104	0.977637142005964	0.874	0.472	1.63614462350977E-99	progenitors	FOS
1.33245962985034E-102	0.494459413714167	0.648	0.184	2.4413325338118E-98	progenitors	CYBA
1.13405929006998E-101	0.903643544739252	0.51	0.094	2.07782343126622E-97	progenitors	PLP1
9.72564879407866E-101	0.545870042686504	0.733	0.282	1.78193337205109E-96	progenitors	RPL22L1
1.99290147969752E-100	0.412531754758534	0.498	0.079	3.65139409110179E-96	progenitors	NR2E1

1.41703183873654E-98	0.847083246277834	0.757	0.317	2.59628573493308E-94	progenitors	ID1
2.15656165850744E-96	0.491554645773554	0.389	0.025	3.95125227071733E-92	progenitors	LIX1
9.38817852042885E-96	0.84195036633133	0.598	0.166	1.72010206851297E-91	progenitors	KIAA0101
bioRxiv preprint doi: https://doi.org/10.1101/2020.10.27.358135 ; this version posted November 9, 2020. The copyright holder for this preprint (which was not certified by peer review) is the author/funder, who has granted bioRxiv a license to display the preprint in perpetuity. It is made available under aCC-BY-NC-ND 4.0 International license.	0.624675000926917	0.758	0.942	0.75894772919450E-91	progenitors	TMEM106C
5.85178834970706E-95	0.540627821490698	0.957	0.752	1.07216466143333E-90	progenitors	DKK 3.00
9.90673678048087E-95	0.580177646787293	0.515	0.105	1.81511231291971E-90	progenitors	FABP7
2.01804785810519E-94	0.551984512977796	0.979	0.896	3.69746728562033E-90	progenitors	HMGN2
2.79918475879047E-94	0.724864513669461	0.755	0.337	5.12866631505591E-90	progenitors	TYMS
5.82932396660203E-94	0.501526949652847	0.886	0.495	1.06804873716082E-89	progenitors	CD99
2.53884375957638E-93	0.483175917719731	0.703	0.267	4.65166953629584E-89	progenitors	HOMER2
3.80560646291023E-92	0.470185138513248	0.74	0.314	6.97263216134413E-88	progenitors	DNPH1
4.8685483791184E-91	0.771870761410883	0.997	0.977	8.92015434022074E-87	progenitors	TUBA1B
9.95114249560968E-88	0.561600483102065	0.804	0.425	1.8232483280456E-83	progenitors	NUDT4
1.7646337577608E-87	0.499900223032965	0.758	0.357	3.23316197096934E-83	progenitors	DNAJC1
1.00737835606075E-86	0.51200368866597	0.83	0.487	1.8457186239745E-82	progenitors	SIVA1
2.17704982711022E-86	1.01363137209528	0.724	0.291	3.98879069323134E-82	progenitors	ID3
1.06158657163944E-85	0.493937281374717	0.726	0.33	1.94503891655778E-81	progenitors	DCBL2
8.65113651208167E-85	0.574014964154954	0.596	0.188	1.5850612317436E-80	progenitors	HLA-DRB1
7.70735524042249E-83	0.500328750292882	0.798	0.418	1.41214162715021E-78	progenitors	CALD1
1.36719052455371E-79	0.556044770473071	0.965	0.894	2.50496647908732E-75	progenitors	NUCKS1
2.65084832152635E-78	0.46378154508918	0.942	0.737	4.85688429470059E-74	progenitors	CLIC1
2.90459013034951E-75	0.511064417083809	0.635	0.244	5.32179003682638E-71	progenitors	HELLS
4.76501397805828E-75	0.409705301038187	0.625	0.216	8.73045861059837E-71	progenitors	RAX
1.81119665051745E-74	0.619703212507674	0.8	0.434	3.31847450307807E-70	progenitors	JUNB
2.80984318495437E-73	0.482174614853019	0.872	0.605	5.1481946834734E-69	progenitors	ISYNA1
9.47059749868389E-73	0.79048007405773	0.842	0.57	1.73520287370886E-68	progenitors	HMGB2
1.81562917507304E-71	0.648775314598702	0.913	0.714	3.32659577456883E-67	progenitors	IER2
2.36498847129972E-71	0.452938574025794	0.787	0.449	4.33313187711535E-67	progenitors	GGH
7.21244783653589E-71	0.484795175597538	0.53	0.16	1.32146469261011E-66	progenitors	PTN
8.42491671052318E-69	0.568563335747259	0.758	0.41	1.54361323970206E-64	progenitors	CKS1B
5.82943149732246E-68	0.422619078384004	0.713	0.353	1.06806843893942E-63	progenitors	PXMP2
4.19674504549025E-67	0.489776606195466	0.624	0.255	7.68927627234724E-63	progenitors	MCM3
7.95115660939312E-67	0.522385911904125	0.798	0.506	1.45681091397301E-62	progenitors	ITM2C
4.6640556232898E-65	0.491184216426527	0.568	0.21	8.54548271299157E-61	progenitors	MAD2L1
2.14935490251364E-64	0.57161849355019	0.482	0.136	3.93804805238549E-60	progenitors	CDK1
3.97803924854653E-64	0.558895200338958	0.695	0.363	7.28856351118694E-60	progenitors	PCNA
7.85095908362885E-64	0.445842335181791	0.573	0.221	1.43845272330248E-59	progenitors	CENPH

1.94002136956555E-63	0.432446867296665	0.877	0.661	3.55450715331801E-59	progenitors	NASP
7.00017991314918E-62	0.45818725689876	0.314	0.041	1.28257296368719E-57	progenitors	CTGF
1.00241597211133E-60	0.646161587624423	0.488	0.154	1.83662654410237E-56	progenitors	BIRC5
bioRxiv preprint doi: https://doi.org/10.1101/2020.10.27.358135 ; this version posted November 9, 2020. The copyright holder for this preprint (which was not certified by peer review) is the author/funder, who has granted bioRxiv a license to display the preprint in perpetuity. It is made available under a CC-BY-ND 4.0 International license .	0.462638567493862	0.795	0.40	6.52891715471762E-56	progenitors	GPM6B
2.7537153916273E-57	0.878790459382209	0.518	0.192	5.04535734053954E-53	progenitors	CENPF
4.60976308641156E-57	0.610473101184958	0.708	0.408	8.44600792692327E-53	progenitors	SMC4
6.45512654891852E-57	0.459200725341429	0.577	0.254	1.18270828629285E-52	progenitors	DHFR
7.22730099071838E-56	0.410706206586003	0.287	0.039	1.32418608751942E-51	progenitors	RGS5
4.11723746372932E-55	0.407908310179099	0.761	0.42	7.54360248104487E-51	progenitors	ANP32E
6.44088266739508E-54	0.607141149982925	0.505	0.182	1.18009852232013E-49	progenitors	NUSAP1
1.03834328433134E-52	0.424956101060721	0.715	0.404	1.90245256555187E-48	progenitors	SPINT2
8.05904026327339E-50	0.681285682114313	0.417	0.131	1.47657735703695E-45	progenitors	MKI67
8.78591605249311E-48	0.466977498043043	0.514	0.215	1.60975553913779E-43	progenitors	H2AFX
1.05272459039088E-46	0.818607485869565	0.51	0.222	1.92880199451417E-42	progenitors	TOP2A
1.51101717886682E-46	0.415053365346429	0.977	0.947	2.76848567511978E-42	progenitors	CLU
2.4262923778481E-45	0.434738306072159	0.352	0.099	4.44545289469328E-41	progenitors	FOSB
4.64327795688836E-45	0.806074380368831	0.474	0.185	8.50741387261086E-41	progenitors	UBE2C
5.17860161958421E-44	0.42478650232818	0.324	0.083	9.48823388740218E-40	progenitors	ASPM
1.03777979534598E-43	0.688957361148325	0.646	0.359	1.90142014103291E-39	progenitors	PTTG1
2.34463105814324E-42	0.473068495838724	0.374	0.117	4.29583302473004E-38	progenitors	AURKB
7.22414435376919E-42	0.616326018634183	0.784	0.545	1.32360772849759E-37	progenitors	CKS2
2.69022812132081E-39	0.405505603344405	0.986	0.98	4.92903596388398E-35	progenitors	H2AFZ
3.90031376067727E-39	0.433898955788973	0.337	0.103	7.14615487231289E-35	progenitors	CCNA2
1.47898143682347E-38	0.484693368925437	0.458	0.185	2.70978978854797E-34	progenitors	CCNB2
2.63059298249787E-37	0.409733409130101	0.877	0.731	4.8197724625326E-33	progenitors	DUT
6.80924804533022E-37	0.56476252665312	0.365	0.126	1.2475904268654E-32	progenitors	CCNB1
9.9989307738371E-36	0.559725162340537	0.418	0.177	1.83200409638243E-31	progenitors	TPX2
2.83617203217341E-34	0.454580052880396	0.867	0.671	5.19643439734813E-30	progenitors	JUN
8.61049865539059E-32	0.504193264891657	0.321	0.113	1.57761556364066E-27	progenitors	CDC20
2.60261631817133E-26	0.685054679017001	0.941	0.875	4.76851361815351E-22	progenitors	HIST1H4C
4.42805413677031E-81	0.64266613403417	0.287	0.009	8.11308078939056E-77	existing_prog	RP11-843A23.1
3.24944976314277E-76	1.20598430460788	0.59	0.075	5.95364185603018E-72	existing_prog	VSX1
4.4045382135748E-73	0.761810490371143	0.385	0.027	8.06999491491175E-69	existing_prog	MFAP4
1.4633970439065E-63	1.17077229349151	0.918	0.289	2.68123606384548E-59	existing_prog	NUSAP1
7.6895577374573E-59	0.948232262892269	0.852	0.222	1.40888076865693E-54	existing_prog	MKI67
4.65636371203299E-58	0.867492662946866	0.762	0.179	8.53138959318685E-54	existing_prog	GTSE1
7.1348673247806E-57	1.29987975957748	0.902	0.316	1.3072503912463E-52	existing_prog	TOP2A

8.87665322226976E-56	0.939988115611692	0.779	0.197	1.62638040338427E-51	existing_prog	AURKB
1.07542437130816E-55	1.22589353178636	0.861	0.28	1.97039253311082E-51	existing_prog	UBE2C
2.08819795546601E-52	0.830634273923243	0.705	0.18	3.82599629400482E-48	existing_prog	SPC25
bioRxiv preprint doi: https://doi.org/10.1101/2020.10.27.358135 ; this version posted November 9, 2020. The copyright holder for this preprint (which was not certified by peer review) is the author/funder, who has granted bioRxiv a license to display the preprint in perpetuity. It is made available under aCC-BY-NC-ND 4.0 International license.	0.71356431542058	0.697	0.159	5.41665492757027E-48	existing_prog	CKAP2L
7.9181733171021E-51	0.916466645084957	0.828	0.25	1.45076771515945E-46	existing_prog	TPX2
1.86172486697596E-49	0.699908676801261	0.746	0.192	3.41105230127335E-45	existing_prog	KIFC1
6.48330311191483E-49	1.1991704912128	0.934	0.517	1.18787079616503E-44	existing_prog	SMC4
3.60804442597192E-48	0.920009945599518	0.77	0.244	6.61065899726575E-44	existing_prog	PRC1
1.08810794931923E-47	0.856565141275213	0.664	0.17	1.99363138474269E-43	existing_prog	RRM2
1.21431921707625E-47	0.72765317692361	0.713	0.176	2.2248756695271E-43	existing_prog	CCNA2
2.04267743353065E-47	0.81049355348626	0.721	0.198	3.74259359371486E-43	existing_prog	PBK
2.55670871375579E-45	0.7523314861242	0.656	0.164	4.68440170534337E-41	existing_prog	NUF2
1.41403476009927E-43	0.637316426293331	0.607	0.144	2.59079448745388E-39	existing_prog	MXD3
3.71704333678363E-43	0.699065129224374	0.648	0.167	6.81036680165497E-39	existing_prog	FAM64A
4.20441488419837E-43	1.38336128533363	1	0.997	7.70332895082825E-39	existing_prog	CKB
1.4217078801883E-42	0.62466089119329	0.639	0.159	2.60485317808101E-38	existing_prog	CDCA3
1.84623651301491E-42	0.681031848983399	0.664	0.179	3.38267453914592E-38	existing_prog	SGOL1
2.04891166895415E-41	1.21864140609545	0.967	0.931	3.7540159598578E-37	existing_prog	HMGN2
2.09284747656753E-41	1.11506070144048	0.82	0.307	3.83451514656702E-37	existing_prog	CENPF
3.08755826812554E-41	0.469773641764119	0.484	0.093	5.65702425885962E-37	existing_prog	ESCO2
3.71834359751627E-41	0.536008754593753	0.533	0.116	6.81274913936931E-37	existing_prog	SPAG5
4.59461439012068E-41	0.474357713235901	0.451	0.081	8.41825248557911E-37	existing_prog	ZMYND10
1.16260164382321E-40	1.39816044459392	0.91	0.677	2.13011873181288E-36	existing_prog	HMGB2
3.51809044657167E-40	0.981533936559921	0.992	0.986	6.44584531620861E-36	existing_prog	TUBA1B
5.49215858117061E-40	0.54245276245428	0.582	0.142	1.00627329524208E-35	existing_prog	NCAPG
1.27435767074656E-39	0.830771344322784	0.762	0.26	2.33487812434185E-35	existing_prog	CDK1
1.85519822724442E-38	0.521752852050806	0.508	0.11	3.39909419195723E-34	existing_prog	CDKN2C
5.21586823515221E-38	0.632153772275555	0.705	0.234	9.55651378044588E-34	existing_prog	CENPU
2.9320110818604E-37	0.727817115954867	0.672	0.208	5.37203070418463E-33	existing_prog	ATAD2
3.72191299394516E-37	0.468874013442293	0.484	0.103	6.81928898750633E-33	existing_prog	APOLD1
1.46740736262052E-36	0.82077136199665	0.779	0.321	2.68858376979332E-32	existing_prog	H2AFX
5.52196770934954E-36	0.868428412627099	0.754	0.275	1.01173492370702E-31	existing_prog	BIRC5
1.12278064821554E-35	2.31057854494181	0.836	0.665	2.05715870366051E-31	existing_prog	HES6
1.40353735647241E-35	0.787236911298309	0.697	0.235	2.57156114452875E-31	existing_prog	CLSPN
1.48631095347828E-35	0.78111827389401	0.82	0.407	2.7232189289629E-31	existing_prog	EZH2
2.35484872867286E-35	0.546153041936482	0.549	0.133	4.31455384067442E-31	existing_prog	NEK2
2.87559672535867E-35	0.718974785600076	0.689	0.227	5.26866832020215E-31	existing_prog	C21orf58

4.26554455217065E-35	0.47595773147457	0.32	0.045	7.81533072848707E-31	existing_prog	DLL4
6.90294608887592E-35	0.712649633912278	0.77	0.311	1.26475778240385E-30	existing_prog	KIF22
9.31904083467461E-35	0.719784525519047	0.705	0.258	1.70743466172908E-30	existing_prog	ZWINT
bioRxiv preprint doi: https://doi.org/10.1101/2020.10.27.358135 ; this version posted November 9, 2020. The copyright holder for this preprint (which was not certified by peer review) is the author/funder. All rights reserved. No reuse allowed without permission.	bioRxiv preprint doi: https://doi.org/10.1101/2020.10.27.358135 ; this version posted November 9, 2020. The copyright holder for this preprint (which was not certified by peer review) is the author/funder. All rights reserved. No reuse allowed without permission.	bioRxiv preprint doi: https://doi.org/10.1101/2020.10.27.358135 ; this version posted November 9, 2020. The copyright holder for this preprint (which was not certified by peer review) is the author/funder. All rights reserved. No reuse allowed without permission.	bioRxiv preprint doi: https://doi.org/10.1101/2020.10.27.358135 ; this version posted November 9, 2020. The copyright holder for this preprint (which was not certified by peer review) is the author/funder. All rights reserved. No reuse allowed without permission.	bioRxiv preprint doi: https://doi.org/10.1101/2020.10.27.358135 ; this version posted November 9, 2020. The copyright holder for this preprint (which was not certified by peer review) is the author/funder. All rights reserved. No reuse allowed without permission.	bioRxiv preprint doi: https://doi.org/10.1101/2020.10.27.358135 ; this version posted November 9, 2020. The copyright holder for this preprint (which was not certified by peer review) is the author/funder. All rights reserved. No reuse allowed without permission.	TACC3
1.23786137855436E-34	0.531769344520315	0.557	0.144	2.2680096177873E-30	existing_prog	MCM10
2.2942087455237E-34	1.03132142361579	0.828	0.518	4.20344926354852E-30	existing_prog	CCDC34
2.67428028323938E-34	0.714180330468456	0.984	0.992	4.89981633495119E-30	existing_prog	HMGB1
2.71499500670384E-34	1.02028024565844	0.844	0.548	4.97441385128278E-30	existing_prog	CKS1B
6.75931478678871E-34	0.582634112580753	0.656	0.218	1.23844165523543E-29	existing_prog	FBXO5
2.01203296668221E-33	0.868734677688423	0.877	0.501	3.68644680155515E-29	existing_prog	TYMS
2.08340172231595E-33	1.02014180752337	0.844	0.464	3.81720863562729E-29	existing_prog	PTTG1
2.44743552165881E-32	0.749197672549171	0.656	0.215	4.48419136278328E-28	existing_prog	CDKN3
2.80404356692415E-32	0.729203729520664	0.697	0.278	5.13756862331842E-28	existing_prog	UBE2T
9.07678369416114E-32	0.576877755474043	0.615	0.184	1.6630483084442E-27	existing_prog	SGOL2
9.12274574297757E-32	0.793298532014985	0.754	0.346	1.67146947502835E-27	existing_prog	MAD2L1
1.12404055825525E-31	0.479123806335649	0.475	0.115	2.05946711083527E-27	existing_prog	FANCI
1.26619083552312E-31	0.843427855974749	0.861	0.773	2.31991484884545E-27	existing_prog	IDH2
1.31666368057358E-31	0.682517450755399	0.615	0.18	2.41239119554692E-27	existing_prog	CDC20
2.32188225488446E-31	0.445357461388481	0.582	0.161	4.25415266739931E-27	existing_prog	NDC80
2.44168838712243E-31	0.524078099404067	0.598	0.183	4.47366146288572E-27	existing_prog	RAD51AP1
2.81703680906141E-31	0.548649566786824	0.607	0.187	5.16137484156232E-27	existing_prog	ASF1B
3.54030170163514E-31	0.831132955907002	0.73	0.28	6.4865407777359E-27	existing_prog	CCNB2
3.87023621418907E-31	0.783543436988433	0.967	0.871	7.09104679163722E-27	existing_prog	TUBB4B
4.56107296802125E-31	0.80529444122009	0.811	0.456	8.35679789200853E-27	existing_prog	USP1
8.10954135582279E-31	0.48479839868396	0.516	0.137	1.48583016721385E-26	existing_prog	HJURP
8.595194241308E-31	0.496860236037717	0.541	0.15	1.57481148889245E-26	existing_prog	CDCA5
2.06336366457826E-30	0.724332766376646	0.738	0.306	3.78049490624029E-26	existing_prog	MIS18BP1
2.26018319623132E-30	0.625146097410941	0.746	0.316	4.14110765213502E-26	existing_prog	ORC6
4.99624138192224E-30	0.729967752883365	0.738	0.372	9.15411345995793E-26	existing_prog	RNASEH2A
1.1377464616429E-29	0.410009799687805	0.369	0.07	2.08457906702212E-25	existing_prog	C8orf46
6.20041520861325E-29	1.65828612519295	0.656	0.293	1.13604007452212E-24	existing_prog	NEUROD1
1.67624175419659E-28	0.756453369036249	0.984	0.982	3.07121014203899E-24	existing_prog	H2AFZ
2.92375445530603E-28	0.684779223577374	0.861	0.5	5.3569029130117E-24	existing_prog	LMNB1
4.32180124012827E-28	0.79656853456098	0.861	0.489	7.91840423216301E-24	existing_prog	PCNA
4.85895644892816E-28	0.430265769670974	0.377	0.081	8.90258000572617E-24	existing_prog	ARHGAP11B
2.30508272107849E-27	0.466875984175721	0.5	0.143	4.22337256156E-23	existing_prog	MYBL2
5.09752281784441E-27	0.409350612726814	0.385	0.083	9.33968130685453E-23	existing_prog	KIF20A

5.15204109315026E-27	0.547024817874911	0.615	0.227	9.4395696908699E-23	existing_prog	CENPK
5.24244157478403E-27	0.661450334538314	0.738	0.353	9.60520145331929E-23	existing_prog	FEN1
6.50968125043036E-27	0.825136142016455	0.844	0.639	1.19270379870385E-22	existing_prog	CKS2
bioRxiv preprint doi: https://doi.org/10.1101/2020.10.27.358135 ; this version posted November 9, 2020. The copyright holder for this preprint (which was not certified by peer review) is the author/funder. All rights reserved. No reuse allowed without permission.	0.67560118716404	0.938	0.274	1.28824691466981E-22	existing_prog	SHD
8.63561955318153E-27	0.622232927563976	0.934	0.843	1.58221821453392E-22	existing_prog	SRSF2
1.28832348780998E-26	0.482203614034711	0.959	0.971	2.36046629436545E-22	existing_prog	HNRNPA0
1.54420451479533E-26	0.667422292366548	0.869	0.812	2.82929151200801E-22	existing_prog	H2AFV
6.12534337070208E-26	0.618423510314417	0.664	0.276	1.12228541238004E-21	existing_prog	CENPW
9.39627318383742E-26	0.605680023385544	0.689	0.298	1.72158517274269E-21	existing_prog	MFGE8
1.12731453038447E-25	0.542196922793562	0.631	0.245	2.06546568257043E-21	existing_prog	CENPN
1.15767442574638E-25	0.664238338342988	0.779	0.332	2.12109108285251E-21	existing_prog	KIAA0101
1.16699283779072E-25	0.671671938558126	0.754	0.373	2.13816427740016E-21	existing_prog	SMC2
2.45834177947094E-25	0.654642008961729	0.803	0.534	4.50417380834667E-21	existing_prog	SYNE2
2.52253905585802E-25	0.415841073865744	0.516	0.159	4.62179605814306E-21	existing_prog	SPC24
2.71168046945668E-25	0.69679093344608	0.811	0.577	4.96834095613852E-21	existing_prog	TMPO
2.89363233236102E-25	0.486275904274949	0.975	0.98	5.30171315935186E-21	existing_prog	HNRNPA2B1
4.33559862742685E-25	0.43291654540455	0.508	0.154	7.94368380517148E-21	existing_prog	MYBL1
4.90825008538755E-25	1.61095769030704	0.91	0.904	8.99289580644707E-21	existing_prog	HIST1H4C
7.21355639288538E-25	0.460543305785755	0.549	0.168	1.32166780230446E-20	existing_prog	ASPM
8.87874442886569E-25	0.62644702784991	0.705	0.323	1.62676355425677E-20	existing_prog	CKAP2
1.16940026694088E-24	0.709381461332097	0.59	0.21	2.14257516908908E-20	existing_prog	CCNB1
2.12572120781245E-24	0.467590400617049	0.607	0.219	3.89474639695398E-20	existing_prog	CENPM
2.15842813471748E-24	0.692916362811874	0.77	0.496	3.95467202842937E-20	existing_prog	BTG3
4.21168691387062E-24	0.689520007461044	0.861	0.806	7.71665276359374E-20	existing_prog	CARHSP1
9.06528432046205E-24	0.634443448389865	0.902	0.876	1.66094139319506E-19	existing_prog	PSIP1
1.34748153283793E-23	0.444079841701774	0.508	0.156	2.46885566446565E-19	existing_prog	CDCA8
1.4503875608814E-23	1.07552388354366	0.738	0.415	2.6574000890469E-19	existing_prog	GADD45A
2.62980016951033E-23	0.590637668780847	0.639	0.253	4.81831987057682E-19	existing_prog	KIF20B
2.97821212691239E-23	0.650333512834999	0.984	0.924	5.45668025892887E-19	existing_prog	FUS
5.37240563825817E-23	0.515915365168009	0.459	0.135	9.84332161041661E-19	existing_prog	DLGAP5
1.24592427226639E-22	0.718565972374421	0.557	0.232	2.28278245164648E-18	existing_prog	PMAIP1
7.98446188674077E-22	0.424678652480759	0.467	0.145	1.46291310688864E-17	existing_prog	KIF23
8.63977624969442E-22	0.551849012294027	0.639	0.299	1.58297980446901E-17	existing_prog	CDCA4
1.79642818198085E-21	0.563289865752971	0.746	0.376	3.29141571502531E-17	existing_prog	DHFR
1.88365250158575E-21	0.588678587444153	0.926	0.926	3.45122811340541E-17	existing_prog	NUCKS1
2.0460642328769E-21	0.613711858816312	0.746	0.405	3.74879888747705E-17	existing_prog	FBLN1
2.49058432704092E-21	0.669443173330478	0.836	0.838	4.56324860400437E-17	existing_prog	CENPV

2.61698030112986E-20	0.597327878282037	0.885	0.815	4.79483130773014E-16	existing_prog	DEK
2.91733327840973E-20	0.423547239509437	0.5	0.192	5.3451380327023E-16	existing_prog	LRRK1
3.7037132238108E-20	0.632776555595873	0.77	0.56	6.78594336866615E-16	existing_prog	ANP32E
bioRxiv preprint doi: https://doi.org/10.1101/2020.10.27.358135 ; this version posted November 9, 2020. The copyright holder for this preprint (which was not certified by peer review) is the author/funder. All rights reserved. No reuse allowed without permission.	4.44434679269375E-20	0.574	0.293	8.14293219357048E-16	existing_prog	HIST1H1C
1.08930221190058E-19	0.589485715393164	0.754	0.397	1.99581951264424E-15	existing_prog	HELLS
1.63879426429464E-19	0.630282786165865	0.803	0.502	3.00259885104063E-15	existing_prog	DNMT1
1.69967022783735E-19	0.433478699332	0.475	0.158	3.11413579144359E-15	existing_prog	PSRC1
2.62792901033136E-19	0.522471679089018	0.852	0.86	4.81489153272911E-15	existing_prog	SNRPB
3.47971138492401E-19	0.484460284118453	0.902	0.879	6.37552719945777E-15	existing_prog	SRSF7
1.16936642826151E-18	0.562726483912662	0.852	0.779	2.14251316986074E-14	existing_prog	TECR
1.36810240979921E-18	0.515657339913692	0.549	0.224	2.50663723523412E-14	existing_prog	UHRF1
2.35508016135173E-18	0.538300916574704	0.639	0.333	4.31497787162864E-14	existing_prog	RFC4
2.42966576987826E-18	0.408766810004577	0.934	0.905	4.45163362357095E-14	existing_prog	HNRNPU
3.88593994633601E-18	0.52450785034827	0.73	0.465	7.11981916967684E-14	existing_prog	DDX39A
4.23811102379544E-18	0.657932865452504	0.779	0.664	7.76506701779801E-14	existing_prog	AKR7A2
8.48418464268893E-18	0.577171633811192	0.959	0.671	1.55447231023347E-13	existing_prog	SOX2
9.79772193888076E-18	0.496749486606715	0.877	0.875	1.79513861364173E-13	existing_prog	HNRNPH3
1.25962216055076E-17	0.606534423804309	0.738	0.625	2.3078797225611E-13	existing_prog	MAD2L2
1.4197112032164E-17	1.19632448661223	0.705	0.577	2.6011948665331E-13	existing_prog	UBE2S
2.44687017142004E-17	0.647086372672556	0.885	0.738	4.48315552807579E-13	existing_prog	KPNA2
3.25318647170153E-17	0.45431050374514	0.631	0.313	5.96048825345154E-13	existing_prog	HIRIP3
4.84103233406269E-17	0.504905002920475	0.689	0.405	8.86973944246965E-13	existing_prog	ASRGL1
7.04294985116185E-17	0.53193299661946	0.697	0.428	1.29040927172987E-12	existing_prog	DNAJC9
8.02435845596678E-17	0.467564928625368	0.689	0.374	1.47022295630223E-12	existing_prog	GMNN
1.10173027102746E-16	0.466589038158633	0.877	0.754	2.01859020257652E-12	existing_prog	SRSF10
1.69224880918731E-16	0.487848120598253	0.902	0.767	3.100538268193E-12	existing_prog	HNRNPf
1.7340617258883E-16	0.619420975591563	0.893	0.749	3.17714789417254E-12	existing_prog	NASP
2.04984623476296E-16	0.489305538540709	0.885	0.815	3.75572827133269E-12	existing_prog	SMC3
2.12839118797021E-16	0.552332323147155	0.811	0.618	3.89963833459902E-12	existing_prog	BUB3
2.37120284695638E-16	0.423858357790909	0.934	0.895	4.34451785619348E-12	existing_prog	XRCC5
4.15777202584889E-16	0.521081837303562	0.803	0.645	7.61786990576034E-12	existing_prog	TFDP2
4.41484195597927E-16	0.536822922511004	0.984	0.999	8.08887343174522E-12	existing_prog	PTMA
4.57957958939428E-16	0.497132121318554	0.803	0.751	8.39070572368819E-12	existing_prog	HNRNPAB
6.69888173839969E-16	0.599469429618125	0.77	0.632	1.22736911210959E-11	existing_prog	SIVA1
7.20088256755751E-16	0.424992928115643	0.557	0.262	1.31934570402789E-11	existing_prog	EZR
7.97190223931203E-16	0.447775549398156	0.762	0.55	1.46061192828675E-11	existing_prog	DTYMK
1.41309093684613E-15	0.605349804469405	0.836	0.832	2.58906521448948E-11	existing_prog	HMGB3

4.61592546035944E-15	0.432944345125405	0.926	0.884	8.45729862847056E-11	existing_prog	PDIA6
5.54609184058852E-15	0.406389611508635	0.549	0.244	1.01615494703263E-10	existing_prog	CHAF1A
5.82606136711014E-15	0.46182133624544	0.844	0.776	1.06745096368192E-10	existing_prog	CSRP2
5.84304843716806E-15	0.5419516278628112	0.697	0.440	1.07056303465793E-10	existing_prog	RRM1
7.19905692384292E-15	0.428623426853069	0.336	0.103	1.3190112095865E-10	existing_prog	PLK1
7.65757528133974E-15	0.467378414766062	0.516	0.243	1.40302094304707E-10	existing_prog	CCP110
7.9468415936761E-15	0.616413299903691	0.77	0.548	1.45602031679333E-10	existing_prog	MCM7
8.58713633539769E-15	0.588093942910959	0.811	0.908	1.57333511937156E-10	existing_prog	RANBP1
1.43255948976998E-14	0.48461575713923	0.713	0.518	2.62473549715656E-10	existing_prog	TUBG1
1.61424273943259E-14	0.442447122918969	0.852	0.795	2.95761554718838E-10	existing_prog	CBX5
5.09612889638028E-14	0.499035706239358	0.59	0.337	9.33712736394796E-10	existing_prog	UCP2
6.62811619290626E-14	0.470311327337576	0.664	0.413	1.21440344886428E-09	existing_prog	CDKN2D
8.96958488556113E-14	0.4383422770159	0.795	0.857	1.64340734273251E-09	existing_prog	NDUFA6
1.26286708895124E-13	0.436344751702188	0.795	0.658	2.31382508037647E-09	existing_prog	EIF4A3
1.6225720163926E-13	0.509717438356444	0.697	0.402	2.97287644843453E-09	existing_prog	MCM3
1.81984019898409E-13	0.415277764343778	0.598	0.341	3.33431121257865E-09	existing_prog	RNASEH2B
1.8987520614377E-13	0.466045100103919	0.836	0.884	3.47889352696616E-09	existing_prog	GNG5
1.97501551793619E-13	0.471842117071717	0.779	0.645	3.61862343196268E-09	existing_prog	BAZ1A
2.41653839736366E-13	0.464176011828487	0.754	0.537	4.42758165164969E-09	existing_prog	EXOSC8
3.18920000019795E-13	0.63868488604916	0.738	0.485	5.84325224036268E-09	existing_prog	AHI1
3.37924326818627E-13	0.471962265705871	0.574	0.275	6.19144951597088E-09	existing_prog	RASD1
8.66011584111962E-13	0.431468059944565	0.811	0.692	1.58670642440994E-08	existing_prog	PCM1
1.0158982088724E-12	0.430936337821673	0.73	0.527	1.86132869829602E-08	existing_prog	SAE1
1.07475746061661E-12	0.439511741102705	0.639	0.397	1.96917061934175E-08	existing_prog	IVNS1ABP
1.22340126185023E-12	0.44398997434816	0.869	0.921	2.24151579196199E-08	existing_prog	CALM3
1.2292353242255E-12	0.441178147625038	0.803	0.773	2.25220496104597E-08	existing_prog	ANP32B
2.58773837226475E-12	0.413996950966318	0.672	0.448	4.74125424566347E-08	existing_prog	ACYP1
4.34870069701102E-12	0.42225250844432	0.467	0.217	7.9676894170636E-08	existing_prog	LIG1
7.92206764504071E-12	0.45969765530725	0.73	0.541	1.45148123392436E-07	existing_prog	PTBP1
1.19333239608988E-11	0.417516193477604	0.721	0.535	2.18642361611588E-07	existing_prog	SMC1A
1.41966938329913E-11	0.421911075201295	0.754	0.588	2.60111824408066E-07	existing_prog	NUCB2
1.57937296308047E-11	0.436140032798239	0.656	0.425	2.89372714295604E-07	existing_prog	CD47
1.61386934532931E-11	0.43069997253334	0.893	0.809	2.95693141451236E-07	existing_prog	SRRM1
1.63574229120269E-11	0.53445434819434	0.697	0.475	2.99700702594158E-07	existing_prog	TTC14
2.35598044240097E-11	0.456341822865932	0.713	0.491	4.31662736656706E-07	existing_prog	SLF1
5.90483485564865E-11	0.409905316865182	0.787	0.684	1.08188384225195E-06	existing_prog	PLEKHA1
2.72314540830078E-10	0.627492082646325	0.762	0.667	4.98934701708868E-06	existing_prog	TRH

3.46745638355089E-10	0.405567536164549	0.795	0.828	6.35307358594194E-06	existing_prog	RHEB
3.84391908869079E-10	0.441690684547178	0.803	0.875	7.04282855429926E-06	existing_prog	DBI
6.08806933916079E-10	0.432365704006837	0.754	0.657	1.11545606432104E-05	existing_prog	RAD21
bioRxiv preprint doi: https://doi.org/10.1101/2020.10.27.358135 ; this version posted November 9, 2020. The copyright holder for this preprint (which was not certified by peer review) is the author/funder. All rights reserved. No reuse allowed without permission.	0.427398527510519	0.918	0.970	0.670030061166021e-05	existing_prog	DYNLL1
1.17441615619086E-08	0.539443115258417	0.648	0.463	0.00021517652813729	existing_prog	RP11-620J15.3
1.56534624646036E-08	0.497180119137831	0.418	0.214	0.000286802739276468	existing_prog	DOK5
2.28850370354718E-08	0.43831953841518	0.492	0.274	0.000419299648563915	existing_prog	KNSTRN
2.71063789649745E-08	0.453912751795063	0.336	0.161	0.000496643075396263	existing_prog	ASCL1
4.03346410576603E-08	0.405705279749923	0.672	0.511	0.000739011293458452	existing_prog	MZT1
6.0675858013404E-08	0.41494794639119	0.607	0.396	0.00111170307052159	existing_prog	WHSC1
7.66332071589974E-08	0.49526640748948	1	1	0.00140407362156715	existing_prog	MALAT1
3.80238631583176E-148	1.92035935445039	0.938	0.367	6.96673220786695E-144	neuroblasts	RGS16
2.02572660026704E-105	0.85900268313353	1	0.995	3.71153627700927E-101	neuroblasts	RBP1
3.74870399622489E-101	0.755480420337904	0.599	0.116	6.86837546188325E-97	neuroblasts	MFNG
7.52013513064403E-101	1.2576381383528	0.984	0.886	1.3778391586366E-96	neuroblasts	SH3BGRL3
2.11331468448761E-93	1.24191233140106	0.954	0.603	3.87201516491819E-89	neuroblasts	CXCR4
2.56560011041505E-83	0.576515598985461	0.508	0.097	4.70069252230246E-79	neuroblasts	SLC38A4
2.00740780047695E-77	1.16832909368441	0.801	0.37	3.67797257203388E-73	neuroblasts	GADD45A
1.34643387705273E-72	0.731595762098747	0.521	0.122	2.46693614953602E-68	neuroblasts	FAM131C
2.6701594327663E-72	0.985456908782068	0.889	0.655	4.89226611271441E-68	neuroblasts	PLEKHA1
2.47904382237406E-69	0.743580965504135	0.664	0.216	4.54210409135375E-65	neuroblasts	SLC18A2
6.9502029373399E-69	0.726812293001565	0.717	0.265	1.27341618217942E-64	neuroblasts	SERPINI1
2.72740805013327E-68	1.03216913098815	0.961	0.72	4.99715702945417E-64	neuroblasts	MIAT
1.54763247240593E-65	0.780464939906733	0.971	0.672	2.83557221594214E-61	neuroblasts	PCBP4
3.19375709677407E-65	0.646071304512208	0.694	0.254	5.85160175270946E-61	neuroblasts	SRRM4
5.04671644188818E-65	0.669727501611013	0.518	0.138	9.24659386482751E-61	neuroblasts	TMEM176B
9.92038997381218E-65	0.514263242684127	0.997	0.972	1.81761385100187E-60	neuroblasts	SLC25A6
1.03892019308211E-64	0.716736904530433	0.355	0.054	1.90350957776505E-60	neuroblasts	LINC01551
1.60147553306834E-61	0.734806206185849	0.505	0.137	2.9342234716878E-57	neuroblasts	TMEM176A
2.39716675218779E-61	0.953813717715007	0.404	0.081	4.39208892335848E-57	neuroblasts	NPTX2
6.91304814656842E-61	0.435418262604391	1	0.998	1.26660868141427E-56	neuroblasts	HNRNPA1
7.84918896379659E-61	0.697489401066472	0.958	0.757	1.43812840194681E-56	neuroblasts	RORB
1.42316491199058E-59	0.805217845617764	0.756	0.413	2.60752275174915E-55	neuroblasts	LCA5
1.01826703524858E-56	0.715413282012765	0.857	0.576	1.86566886198246E-52	neuroblasts	BCL7A
5.785581439653E-55	0.604643055009035	0.358	0.062	1.06003423137322E-50	neuroblasts	VSX1
1.95700808470239E-54	0.574820944604027	0.638	0.238	3.58563021279172E-50	neuroblasts	SHD
3.95513814238366E-50	0.46852901706645	0.99	0.955	7.24660410447535E-46	neuroblasts	EIF3E

6.14396514381198E-48	0.792085854998001	0.596	0.239	1.12569729364923E-43	neuroblasts	RASD1
7.17348557059775E-47	1.123359176442	0.485	0.165	1.31432602624492E-42	neuroblasts	RP3-395M20.12
2.8244893779434E-44	0.578990759439862	0.873	0.641	5.17502943826789E-40	neuroblasts	HES6
bioRxiv preprint doi: https://doi.org/10.1101/2020.10.27.358135 ; this version posted November 9, 2020. The copyright holder for this preprint (which was not certified by peer review) is the author/funder. All rights reserved. No reuse allowed without permission.	0.6773810241896515E-43	0.977	0.694	5.658546041121094E-08	neuroblasts	ZNF385A
3.5336065160948E-42	0.640082651551314	0.814	0.577	6.47427385878889E-38	neuroblasts	LIMD2
9.29343716665382E-42	0.59222875032636	0.586	0.248	1.70274355767431E-37	neuroblasts	GADD45G
2.27349730570959E-41	0.63792135052316	0.837	0.688	4.16550176352111E-37	neuroblasts	NOVA1
5.64641336136136E-40	0.461650560492292	0.704	0.3	1.03453585606863E-35	neuroblasts	CHRNA3
1.22869004959224E-39	0.454420530694637	1	0.999	2.25120590886291E-35	neuroblasts	TMSB4X
4.28016805139417E-39	0.618572988726848	0.736	0.431	7.8421239037644E-35	neuroblasts	TXNIP
3.89130138221403E-38	0.464733990975009	0.342	0.089	7.12964239249255E-34	neuroblasts	DLX1
3.79289068870292E-37	0.551033975751958	0.599	0.264	6.94933431984149E-33	neuroblasts	ONECUT2
4.67636385820417E-36	0.552939372799447	0.717	0.454	8.56803386100168E-32	neuroblasts	DST
7.0881509334532E-36	0.444340738275223	0.401	0.136	1.2986910140273E-31	neuroblasts	MYBL1
6.10561121788245E-35	0.58655738312496	0.997	0.998	1.11867008734042E-30	neuroblasts	CKB
2.54285303037617E-33	0.447036103443962	0.528	0.251	4.65901532225522E-29	neuroblasts	NECAB3
5.71905669120376E-33	0.912768028476612	0.811	0.644	1.04784556696235E-28	neuroblasts	DDIT4
2.1562466039526E-31	0.504811120488397	0.453	0.177	3.95067502776195E-27	neuroblasts	NHLH1
2.50404795777593E-31	0.510346832793373	0.375	0.126	4.58791666823707E-27	neuroblasts	DLX2
1.19703604892264E-30	0.418682768708012	0.479	0.219	2.19320944883605E-26	neuroblasts	ME3
1.60929759289665E-30	0.416974478066255	0.971	0.905	2.94855504970524E-26	neuroblasts	SSR4
2.09500671021304E-30	0.459742237214789	0.73	0.466	3.83847129445233E-26	neuroblasts	CADM3
2.15164765038055E-29	0.41494713103073	0.436	0.178	3.94224882502724E-25	neuroblasts	ATOH7
2.39727792452181E-28	0.420968528618996	0.883	0.776	4.39229261330885E-24	neuroblasts	SVBP
2.45603541545048E-28	0.462636552793122	0.837	0.696	4.49994808818837E-24	neuroblasts	RHOBTB3
4.66425570515144E-27	0.434380708567444	0.521	0.274	8.54584930297847E-23	neuroblasts	MIR217HG
5.35147775933605E-26	0.452107781390414	0.919	0.85	9.80497755065551E-22	neuroblasts	PFN2
5.35348872567894E-26	0.513159671612502	0.759	0.603	9.80866204318896E-22	neuroblasts	GYG1
1.06674578166114E-25	0.446688773657181	0.349	0.131	1.95449162115955E-21	neuroblasts	CPLX2
1.85219428508282E-25	0.477209255249673	0.443	0.193	3.39359036912875E-21	neuroblasts	CTC-378H22.2
3.40275277091317E-25	0.417272814368399	0.697	0.518	6.2345236268671E-21	neuroblasts	ABRACL
8.2805283848121E-24	0.615035436524387	0.489	0.228	1.51715841066527E-19	neuroblasts	CLDN5
1.08096741962456E-23	0.490304788603546	0.622	0.417	1.98054850623612E-19	neuroblasts	IGFBP2
2.47706266699306E-23	0.452682265531214	0.772	0.633	4.53847421846468E-19	neuroblasts	TFDP2
1.25340623846546E-22	0.441140193960156	0.798	0.577	2.29649091011642E-18	neuroblasts	PRSS23
1.37280680449703E-22	0.413401520719856	0.564	0.355	2.51525662719945E-18	neuroblasts	ZBTB16
3.28647137113426E-22	0.430628585593396	0.257	0.083	6.02147284619219E-18	neuroblasts	ASS1

3.17749994628376E-21	0.501434146828147	0.388	0.177	5.82181540158111E-17	neuroblasts	STC2
4.51769911970773E-19	0.427864695143776	0.912	0.875	8.27732832712849E-15	neuroblasts	BTG1
1.98554092459001E-16	0.509718014127686	0.818	0.716	3.63790808203382E-12	neuroblasts	SLC2A1
bioRxiv preprint doi: https://doi.org/10.1101/2020.10.27.358135 ; this version posted November 9, 2020. The copyright holder for this preprint (which was not certified by peer review) is the author/funder, who has granted bioRxiv a license to display the preprint in perpetuity. It is made available under aCC-BY-NC-ND 4.0 International license.	2.18878439106377	0.892	0.189	4.17693243169542E-15	neuroblasts	GAL
2.4949833364345E-15	0.411669028018731	0.58	0.437	4.5713084690153E-11	neuroblasts	PDLIM4
2.90777306980679E-15	0.485978379307679	0.459	0.261	5.3276218185E-11	neuroblasts	SSTR2
3.87383503954299E-11	0.687358851145344	0.723	0.664	7.09764055945067E-07	neuroblasts	TRH
9.65701865162901E-11	0.412984596863738	0.853	0.831	1.76935895735147E-06	neuroblasts	BNIP3
1.32281477626319E-238	2.24286358839265	0.768	0.014	2.42366123306941E-234	photorecept	DCT
5.61478754150251E-220	1.06987332094168	0.561	0.003	1.02874137335409E-215	photorecept	PCAT4
7.27689077219759E-211	1.22878532042018	0.744	0.018	1.33327192728204E-206	photorecept	CRX
6.86769652936541E-207	1.13651466603401	0.683	0.013	1.25829935811033E-202	photorecept	NXPH4
1.29626112107639E-192	1.05092250974927	0.634	0.012	2.37500962603616E-188	photorecept	VTN
1.9255751452955E-164	1.75679765800481	0.695	0.025	3.52803878121042E-160	photorecept	PRDM1
1.16341626805247E-161	0.769768407626434	0.439	0.004	2.13161128632574E-157	photorecept	MRLN
3.83865615277828E-151	1.45688916442888	0.817	0.046	7.03318580312036E-147	photorecept	OTX2
3.31466830977718E-149	1.14526576233302	0.756	0.038	6.07313527717375E-145	photorecept	NEUROD4
8.06584154276311E-141	1.05382507343093	0.451	0.008	1.47782348746506E-136	photorecept	SERPINI2
1.18522550433467E-140	0.553901217011478	0.39	0.004	2.17157016904198E-136	photorecept	AIPL1
6.20711003228119E-138	1.74044750000154	0.476	0.01	1.13726670011456E-133	photorecept	RCVRN
2.47863740556338E-130	0.929268179321381	0.39	0.005	4.54135945447323E-126	photorecept	PDC
1.51552411619195E-129	0.550926266782263	0.305	0.001	2.77674328568688E-125	photorecept	CABP5
6.77264936052829E-127	0.765079088871651	0.549	0.02	1.24088481583599E-122	photorecept	MCC
1.26527890982901E-118	0.497275771594635	0.39	0.007	2.3182440185887E-114	photorecept	AANAT
2.81610154722921E-118	1.06276170583385	0.476	0.015	5.15966125483336E-114	photorecept	SLC38A5
1.6655468543144E-110	0.536454697421984	0.5	0.02	3.05161494647484E-106	photorecept	MAOA
2.7800971429975E-104	1.45588816611958	0.707	0.059	5.09369398540002E-100	photorecept	GNB3
4.20402156134127E-104	0.662967956869152	0.427	0.014	7.70260830468948E-100	photorecept	TULP1
2.55926937378718E-96	0.406866427147698	0.354	0.009	4.68909334665287E-92	photorecept	AQP3
2.00593992659935E-93	0.433760090139577	0.341	0.008	3.67528313351533E-89	photorecept	KCNH6
1.35003100736953E-91	0.537052175715088	0.317	0.007	2.47352681170246E-87	photorecept	HOTAIRM1
7.35449793209437E-84	0.481578949406499	0.427	0.02	1.34749111111833E-79	photorecept	MVP
4.94596508578299E-83	0.472608114088242	0.317	0.009	9.0619972301716E-79	photorecept	DPP10-AS1
2.10280320845106E-75	1.25845911016383	0.78	0.121	3.85275603852403E-71	photorecept	THRB
2.9586221051355E-73	0.658481104185214	0.28	0.008	5.42078742102926E-69	photorecept	RBP4
1.19981388090468E-72	0.453997019277054	0.341	0.014	2.19829899259355E-68	photorecept	FSTL5
1.00597507140801E-60	1.82815049566438	0.878	0.218	1.84314752583376E-56	photorecept	PHLDA1

1.29917966874025E-59	1.06987538493004	0.659	0.101	2.38035698906589E-55	photorecept	MIR7-3HG
2.97837902702056E-59	0.45169727141517	0.402	0.03	5.45698605330707E-55	photorecept	RIMS1
2.88033389114746E-56	1.48515343225882	0.939	0.272	5.27734775536037E-52	photorecept	GADD45G
bioRxiv preprint doi: https://doi.org/10.1101/2020.10.27.358135 ; this version posted November 9, 2020. The copyright holder for this preprint (which was not certified by peer review) is the author/funder. All rights reserved. No reuse allowed without permission.	1.067103816530643E-54	0.537	0.009	1.9628469854739E-41	photorecept	C8orf46
1.81538136733053E-50	1.98287380925581	0.963	0.432	3.32614174122299E-46	photorecept	FAM57B
4.1995810729425E-47	0.593225649422027	0.5	0.069	7.69447244184525E-43	photorecept	STX3
5.6333511734969E-47	1.66329792428303	0.878	0.291	1.0321426020081E-42	photorecept	NEUROD1
1.00589615250844E-46	0.48958821548219	0.317	0.024	1.84300293062596E-42	photorecept	DPP10
1.18098448573458E-45	0.69279715352606	0.61	0.102	2.16379977476289E-41	photorecept	LINC00599
7.08804285432245E-43	0.421064138747937	0.329	0.028	1.29867121176896E-38	photorecept	KCNK3
8.33793037533453E-43	0.432180322367311	0.28	0.02	1.52767560336879E-38	photorecept	SLC40A1
1.19280130927581E-41	0.738252185978414	0.695	0.16	2.18545055885514E-37	photorecept	ROBO2
3.2626646322653E-41	0.795268988972914	0.707	0.168	5.97785413923648E-37	photorecept	SYP
1.51221103528758E-40	0.849356043507306	0.549	0.093	2.7706730588539E-36	photorecept	STC1
1.05009886319939E-38	0.58534450488583	0.598	0.121	1.92399113715393E-34	photorecept	NRXN1
1.81991301707216E-38	0.725702294216615	0.585	0.117	3.3344446298796E-34	photorecept	SH3BP5
1.68450714178623E-37	0.882423385110521	0.634	0.158	3.08635398518073E-33	photorecept	AMER2
2.91722340275673E-37	1.25948258186172	0.732	0.218	5.34493671853088E-33	photorecept	SEPT4
5.12509161024223E-37	0.854078060001808	0.768	0.241	9.39019284828581E-33	photorecept	MEIS2
6.67364050599618E-37	1.32535107851136	0.805	0.27	1.22274441350862E-32	photorecept	SSTR2
9.52498060034193E-37	0.989279387342336	0.963	0.547	1.74516694559465E-32	photorecept	ATP2B1
1.06587728859886E-36	0.44956783375851	0.341	0.038	1.95290036817082E-32	photorecept	KIAA1107
3.43577363099601E-34	0.427481756181904	0.439	0.069	6.29502444671088E-30	photorecept	CNTNAP2
5.82242618537286E-34	0.43083705117957	0.256	0.022	1.06678492568401E-29	photorecept	TUBA4A
1.014068341604E-33	0.646807137941415	0.561	0.127	1.85797601548685E-29	photorecept	PHACTR2
1.06469535744194E-31	1.09546269761097	0.841	0.319	1.95073483390513E-27	photorecept	SYT4
1.23718802372177E-31	1.02190856253709	0.988	0.663	2.26677589706303E-27	photorecept	ENO2
1.39489223153211E-31	1.12979602344953	0.976	0.931	2.55572154661314E-27	photorecept	PRDX1
1.51891183170736E-31	0.770173199167454	1	0.993	2.78295025805422E-27	photorecept	H3F3B
2.06921027826802E-31	0.864080743892854	1	0.999	3.79120707184267E-27	photorecept	TMSB4X
4.78722346937168E-31	1.24846553999345	0.927	0.708	8.7711508405828E-27	photorecept	PCBP4
4.14850642314878E-30	0.912935119010439	0.963	0.809	7.60089346849319E-26	photorecept	GUK1
3.81044124807606E-29	0.882276031674965	0.671	0.241	6.98149045472496E-25	photorecept	REEP6
4.20133779208133E-29	0.786984175117667	0.854	0.332	7.69769110265142E-25	photorecept	SEZ6L2
6.78322560781642E-29	0.476117567468043	0.305	0.038	1.24282259586412E-24	photorecept	SGK1
7.51634381529779E-29	0.913299559851525	0.829	0.363	1.37714451383886E-24	photorecept	ATP1A3
1.53680153973766E-28	0.932901305628296	0.951	0.826	2.81572778110734E-24	photorecept	CPE

2.62569576553634E-28	0.804185672577034	0.817	0.371	4.81079978161568E-24	photorecept	PIK3R1	
1.59268877944821E-27	0.789052131634197	0.756	0.339	2.91812438170502E-23	photorecept	BCL2L1	
1.21913953387586E-26	0.571044121088066	0.598	0.17	2.23370745396736E-22	photorecept	CADPS	
bioRxiv preprint doi: https://doi.org/10.1101/2020.10.27.358135 ; this version posted November 9, 2020. The copyright holder for this preprint (which was not certified by peer review) is the author/funder. All rights reserved. No reuse allowed without permission.	bioRxiv preprint doi: https://doi.org/10.1101/2020.10.27.358135 ; this version posted November 9, 2020. The copyright holder for this preprint (which was not certified by peer review) is the author/funder. All rights reserved. No reuse allowed without permission.	0.641306352242048	0.861	0.510	0.57753011410081E-21	photorecept	STRADB
1.24303019025255E-25	0.460532424267266	0.463	0.105	2.27747991458072E-21	photorecept	LINC01315	
1.68434339733186E-24	0.778844945804404	1	0.981	3.08605397259143E-20	photorecept	GSTP1	
3.58540117163227E-24	0.846910367466967	0.756	0.361	6.56917202666465E-20	photorecept	ROGDI	
4.2796371075861E-24	0.469923071575685	0.366	0.069	7.84115110851924E-20	photorecept	CHODL	
4.41880756940878E-24	0.49795325925379	0.415	0.089	8.09613922867076E-20	photorecept	PTPRN	
1.11906748347298E-22	0.699933262853713	0.89	0.39	2.05035544321919E-18	photorecept	INA	
2.70480402450257E-22	0.55532409134929	0.683	0.274	4.95574193369362E-18	photorecept	NUDT14	
3.63669357509726E-22	0.724601845711727	0.976	0.852	6.6631499682932E-18	photorecept	SPCS1	
4.2703104132131E-21	0.56438616591493	0.988	0.897	7.82406273908904E-17	photorecept	GABARAPL2	
1.5442041904539E-20	0.695619752667892	0.805	0.446	2.82929091774963E-16	photorecept	SCARB2	
1.5495015794119E-20	0.722575380848917	0.744	0.343	2.83899679379849E-16	photorecept	MAP1LC3A	
1.61450060525505E-20	0.66417817899428	0.732	0.302	2.95808800894829E-16	photorecept	SRRM4	
3.07862760616431E-20	0.577249667521895	0.951	0.752	5.64066150001425E-16	photorecept	SEPW1	
5.433619979097E-20	0.471114181871079	0.585	0.192	9.95547852570152E-16	photorecept	CHGB	
1.58236539147524E-19	0.50894191821585	0.378	0.089	2.89920987026093E-15	photorecept	RXRG	
1.61007286877861E-19	0.648425653628174	0.927	0.666	2.94997551017616E-15	photorecept	CADM1	
3.96529650436061E-19	0.500431236065256	0.476	0.15	7.26521625528951E-15	photorecept	CLN6	
6.03608169540646E-19	0.662868462515277	0.902	0.505	1.10593088823237E-14	photorecept	SCG3	
7.19520418152116E-19	0.5702850117599	0.427	0.118	1.31830531013831E-14	photorecept	CHRNA5	
2.9958461511642E-18	0.580753452850379	0.598	0.215	5.48898931816304E-14	photorecept	CTC-378H22.2	
1.15684279874964E-17	0.773979991757644	0.768	0.473	2.11956737586909E-13	photorecept	PEG10	
1.18847270818816E-17	0.591440302069482	0.939	0.786	2.17751969594235E-13	photorecept	SVBP	
2.15031514006232E-17	0.679824270196546	0.927	0.699	3.93980739962219E-13	photorecept	OCIAD2	
2.55259933892646E-17	0.515566345775635	0.683	0.283	4.67687250878106E-13	photorecept	CELF3	
3.95145254871639E-17	0.490151277494196	0.927	0.643	7.23985135975817E-13	photorecept	WRB	
4.44019718693121E-17	1.09618708304872	0.744	0.445	8.13532928589536E-13	photorecept	S100A13	
4.66000725089474E-17	1.01920746089202	0.976	0.872	8.53806528508934E-13	photorecept	TUBB4B	
7.81386205366729E-17	0.674150525521097	0.793	0.493	1.43165580547292E-12	photorecept	ABHD14A	
8.54123304785249E-17	0.689033468662025	0.841	0.591	1.56492471902753E-12	photorecept	DHRS7	
1.35888907704487E-16	0.579352373149559	0.671	0.277	2.48975656696161E-12	photorecept	RASD1	
1.68740557487284E-16	0.582039334802641	0.878	0.614	3.09166449428201E-12	photorecept	GRINA	
1.78391665682464E-16	0.744633706932963	0.793	0.531	3.26849209863411E-12	photorecept	IFT57	
2.00000992731331E-16	0.519565616570435	0.951	0.852	3.66441818882344E-12	photorecept	SNRPN	

2.91390448219605E-16	0.535853358363991	0.963	0.814	5.3388557922796E-12	photorecept	ATP6V0B
3.47618279500155E-16	0.65328516192399	0.854	0.638	6.36906211700184E-12	photorecept	BAD
5.17529283836461E-16	0.463792030016815	0.902	0.666	9.48217153845164E-12	photorecept	HES6
bioRxiv preprint doi: https://doi.org/10.1101/2020.10.27.358135 ; this version posted November 9, 2020. The copyright holder for this preprint (which was not certified by peer review) is the author/funder. All rights reserved. No reuse allowed without permission.	0.693397698486242	0.476	0.474	8.51919398159203E-12	photorecept	PLEKHB1
2.25178092010093E-15	0.408357352777647	0.537	0.221	4.12571300180893E-11	photorecept	PRNP
3.87609493653089E-15	0.663402723480999	0.902	0.516	7.1017811427119E-11	photorecept	DCX
7.30264280274924E-15	0.46595676985935	0.524	0.197	1.33799021431972E-10	photorecept	SERPINF1
7.64056800936612E-15	0.514699267458944	0.963	0.768	1.39990487067606E-10	photorecept	APLP1
9.01140804177333E-15	0.431037702236904	0.5	0.175	1.65107018141371E-10	photorecept	CHGA
1.31009259747972E-14	0.649404223835341	0.549	0.235	2.40035165710235E-10	photorecept	ARL4D
1.32440377332928E-14	0.555982658281273	0.902	0.718	2.4265725934939E-10	photorecept	TERF2IP
2.0113828055861E-14	0.481039881180237	0.354	0.102	3.68525557639485E-10	photorecept	ALCAM
2.01276761479677E-14	0.471816246904756	0.72	0.418	3.68779282383064E-10	photorecept	TBCC
2.21439109006061E-14	0.539435085370661	0.951	0.827	4.05720735520905E-10	photorecept	VAMP2
3.13249786616764E-14	0.745522996318966	0.561	0.246	5.73936259039235E-10	photorecept	DDIT3
7.09350975944171E-14	0.524867616092248	0.524	0.223	1.29967285812491E-09	photorecept	RGS2
7.33172351017634E-14	0.707800422700063	0.646	0.39	1.34331838153451E-09	photorecept	UNC119
2.0490016030837E-13	0.491942762950017	0.793	0.515	3.75418073716995E-09	photorecept	PAPSS1
3.21641363148031E-13	0.540667354860102	0.927	0.747	5.89311305559822E-09	photorecept	MAP1LC3B
4.40773478356279E-13	0.496016576219411	0.744	0.476	8.07585167044374E-09	photorecept	PRRT2
8.00581327457298E-13	0.654653778622717	0.756	0.464	1.46682510816726E-08	photorecept	TXNIP
1.01355211912323E-12	0.525745710792951	0.707	0.346	1.85703019265759E-08	photorecept	CHRNA3
1.06562142313998E-12	0.489236309590034	0.951	0.902	1.95243157147707E-08	photorecept	SARAF
1.12866679812662E-12	0.634715495787235	0.89	0.827	2.06794330752759E-08	photorecept	GPX1
1.269259926518E-12	0.583023664532388	0.707	0.469	2.32553803736629E-08	photorecept	TMX1
1.96857645444029E-12	0.528822891368708	0.805	0.419	3.60682577982549E-08	photorecept	SNCG
2.26496073752414E-12	0.423032598851327	0.744	0.464	4.14986106329173E-08	photorecept	RHOT1
2.42607436311163E-12	0.477690466923086	0.707	0.415	4.44505344809313E-08	photorecept	CHCHD10
2.5044104198598E-12	0.559773200340184	0.866	0.707	4.58858077126712E-08	photorecept	NLRP1
3.35932033238014E-12	0.453265767848997	1	0.97	6.1549467129869E-08	photorecept	SOX4
4.23569631316821E-12	0.455206211737369	0.585	0.269	7.7606427849868E-08	photorecept	SNAP25
5.67910816490408E-12	0.448193500635786	0.866	0.632	1.04052619797373E-07	photorecept	BEX2
5.74755410029053E-12	0.421445192964839	0.72	0.449	1.05306686225523E-07	photorecept	MARK3
6.78744306945778E-12	0.438635326728064	0.951	0.824	1.24359531918605E-07	photorecept	BEX4
1.0466132278158E-11	0.479138532526476	0.902	0.82	1.91760475600411E-07	photorecept	GPM6A
1.2601904929107E-11	0.455185368409941	0.841	0.552	2.30892102111099E-07	photorecept	NELL2
1.97802628402412E-11	0.5068454220228	0.963	0.862	3.62413975758898E-07	photorecept	HMGA1

2.15985869353823E-11	0.412904780051993	0.744	0.485	3.95729309830075E-07	photorecept	REEP5
3.52636620080298E-11	0.486203150450258	0.707	0.433	6.46100815311121E-07	photorecept	PGRMC2
3.91213557859312E-11	0.510533072833261	0.902	0.69	7.16781480709832E-07	photorecept	BEX1
bioRxiv preprint doi: https://doi.org/10.1101/2020.10.27.358135 ; this version posted November 9, 2020. The copyright holder for this preprint (which was not certified by peer review) is the author/funder. All rights reserved. No reuse allowed without permission.	0.4516911481018805	0.939	0.872	2.42620704866472E-06	photorecept	PLD3
1.65087944392445E-10	0.420225309716721	0.866	0.711	3.02474131715839E-06	photorecept	AKAP9
1.71876961512885E-10	0.520927757513761	0.634	0.408	3.14912968883908E-06	photorecept	ZHX1
1.99826890218819E-10	0.411654519782417	0.902	0.571	3.6612282825892E-06	photorecept	TAGLN3
7.43263086123709E-10	0.456622429017584	0.988	0.964	1.36180662639586E-05	photorecept	MORF4L2
3.73104889217243E-09	0.416526130709231	0.89	0.701	6.83602778023832E-05	photorecept	UQCC2
7.73989326359876E-09	0.628390853649543	0.756	0.496	0.000141810324375657	photorecept	STMN4
8.79905205879396E-09	0.421908185416458	0.707	0.459	0.000161216231821223	photorecept	TLE1
1.00759239418096E-08	0.836325913667296	0.476	0.279	0.000184611078461835	photorecept	ISOC1
2.41585147194473E-08	0.415393772889832	0.756	0.585	0.000442632306689714	photorecept	SPTSSA
3.04031920702872E-08	0.568764504271918	1	0.973	0.000557047285111803	photorecept	ALDOA
4.61755072872958E-08	0.5725611294198	0.951	0.876	0.000846027644517833	photorecept	GNAS
6.95542729949893E-08	0.42701763742294	0.585	0.39	0.00127437338981419	photorecept	SLC22A17
9.17733953181798E-08	0.565645629300957	0.646	0.45	0.00168147214901969	photorecept	S100A6
1.10739590980087E-07	0.407917846168003	1	0.987	0.00202897078593715	photorecept	TPI1
1.3186669923144E-07	0.441399389997017	0.402	0.195	0.00241606166331844	photorecept	ARHGEF2
1.05381939657002E-06	0.489043506322252	0.817	0.753	0.0193080789839559	photorecept	NEAT1
4.12885434629089E-294	1.74139838543831	0.892	0.081	7.56488693327417E-290	rgc	ELAVL4
7.36627409341882E-278	1.71048945121131	0.949	0.136	1.3496487393962E-273	rgc	NEFM
6.67339091049203E-271	1.40615680633365	0.846	0.072	1.22269868262035E-266	rgc	ISL1
1.34088353486753E-257	1.67410573149885	0.875	0.118	2.45676681258428E-253	rgc	NEFL
4.79957329257803E-256	1.14978404234964	0.824	0.072	8.79377818666147E-252	rgc	EBF1
6.14578460448607E-253	2.39383643489055	0.974	0.277	1.12603065523394E-248	rgc	NSG1
1.41670908233324E-236	2.31226238061525	0.993	0.489	2.59569438065097E-232	rgc	GAP43
3.23325966951756E-226	1.17194414912514	0.831	0.116	5.92397836649008E-222	rgc	OLFM1
1.35781657799554E-215	0.942472043308463	0.765	0.081	2.48779153420342E-211	rgc	RBFOX3
2.18222751118301E-215	1.70725969084125	0.963	0.285	3.99827724598952E-211	rgc	SNCG
4.31768818247487E-213	1.0500650402601	0.804	0.091	7.91086828793046E-209	rgc	POU4F2
5.70669595896323E-213	2.0146760642284	0.719	0.075	1.04558083360124E-208	rgc	PRPH
1.33208048521058E-209	0.947611113113253	0.721	0.065	2.44063786500283E-205	rgc	PCSK2
9.08280794619406E-202	1.39459307352519	0.927	0.295	1.66415207190168E-197	rgc	GNG3
1.16240486759746E-196	1.32546874198298	1	0.998	2.12975819841206E-192	rgc	TUBA1A
9.17746278554224E-195	1.07990820204009	0.866	0.172	1.68149473156705E-190	rgc	PPP1R1A
1.03206708508868E-194	1.56429345706391	0.881	0.221	1.89095331329947E-190	rgc	RTN1

2.32959685186912E-193	1.19653989147956	0.996	0.988	4.2682873519946E-189	rgc	MAP1B	
6.95585847837954E-191	0.930738114643387	0.73	0.099	1.2744523904087E-186	rgc	POU6F2	
2.88594093298044E-189	1.38213325162072	1	0.888	5.28762097740677E-185	rgc	MLLT11	
bioRxiv preprint doi: https://doi.org/10.1101/2020.10.27.358135 ; this version posted November 9, 2020. The copyright holder for this preprint (which was not certified by peer review) is the author/funder. All rights reserved. No reuse allowed without permission.	3.29587390252419E-187	1.539286542061	0.932	0.404	6.03870016420481E-183	rgc	DCX
8.30031088456194E-184	1.47628228700844	0.982	0.667	1.52078296026944E-179	rgc	TUBB2A	
6.27056278195291E-180	1.2448289413368	0.998	0.998	1.14889251290941E-175	rgc	TMSB10	
6.3076623804346E-178	0.811674761251817	0.778	0.129	1.15568990134323E-173	rgc	RUND3A	
7.7158900020107E-177	1.51416014880798	1	0.618	1.4137053661684E-172	rgc	STMN2	
1.22482885607572E-175	0.92498196466174	0.826	0.164	2.24413143010194E-171	rgc	MAPT	
3.00533438879438E-172	1.01830864060153	0.925	0.264	5.50637366714906E-168	rgc	INA	
5.12079008563861E-170	1.08392778210676	0.892	0.254	9.38231159490706E-166	rgc	RAB3A	
4.75927235727686E-169	1.13588025949762	0.989	0.814	8.71993881300265E-165	rgc	BASP1	
4.23246420727882E-166	1.02332542393902	1	0.992	7.75472092057626E-162	rgc	TUBB2B	
2.89114321402881E-163	0.990242626589847	1	0.994	5.29715259674358E-159	rgc	CALM2	
1.50442628804625E-162	0.785296202685684	0.767	0.14	2.75640984495834E-158	rgc	DPYSL3	
3.7630324456163E-160	1.24355399085955	0.974	0.475	6.89462804685819E-156	rgc	TAGLN3	
1.11768055551666E-158	1.34419477269971	0.936	0.384	2.04781431381762E-154	rgc	STMN4	
6.04063303437872E-158	1.12932554438556	0.976	0.808	1.10676478455887E-153	rgc	UCHL1	
5.51983622942862E-157	0.761364136223641	0.618	0.068	1.01134439395591E-152	rgc	TTC9B	
3.05019161751677E-156	1.01575479558086	0.987	0.716	5.58856108161422E-152	rgc	APLP1	
3.70239416527123E-153	0.59551908283357	0.629	0.074	6.78352658960995E-149	rgc	STX1A	
3.01863824895184E-151	1.00524206116507	0.945	0.577	5.53074899972956E-147	rgc	KLC1	
3.90934029124049E-148	0.804112647272506	0.829	0.229	7.16269328161083E-144	rgc	TSPAN7	
1.44553111574644E-147	0.982456931501196	0.969	0.644	2.64850211027063E-143	rgc	CRMP1	
2.8185766443616E-147	1.04895995995764	0.969	0.652	5.16419612779932E-143	rgc	PCSK1N	
6.25712055250115E-147	0.881485775530192	0.978	0.819	1.14642962762926E-142	rgc	PAFAH1B3	
2.00672444098608E-146	0.962682199740585	0.985	0.886	3.6767205207747E-142	rgc	CD24	
9.10708772428932E-144	0.556126741642391	0.607	0.073	1.66860061284429E-139	rgc	L1CAM	
1.08355204765365E-143	0.467513943939864	0.457	0.022	1.98528406171101E-139	rgc	NRG1	
3.91470140041519E-140	0.88572534674955	0.818	0.214	7.17251590584071E-136	rgc	CELF4	
2.95245567146934E-139	0.489661951333758	0.44	0.02	5.40948928126613E-135	rgc	ADAM11	
3.83986111346666E-138	0.470467854365821	0.505	0.039	7.03539353209362E-134	rgc	HSPA12A	
1.3583974040531E-137	0.855394846152596	0.923	0.332	2.48885572370608E-133	rgc	ELAVL3	
1.81635286768544E-137	0.893353821716333	0.971	0.917	3.32792172417326E-133	rgc	C4orf48	
1.13257629666284E-136	0.831182841345955	0.837	0.308	2.07510629074566E-132	rgc	KLF7	
1.41104537448011E-135	0.857180138308023	0.987	0.872	2.58531733512246E-131	rgc	HN1	
4.99141845077152E-132	0.502215691140479	0.552	0.065	9.14527688550359E-128	rgc	REEP1	

1.42975369072576E-130	1.20853504319499	0.857	0.386	2.61959471214774E-126	rgc	SAT1
9.10669026814255E-128	0.548005314463879	0.501	0.052	1.66852779092908E-123	rgc	PPP2R2B
2.77444988112392E-127	0.684084715155839	0.756	0.215	5.08334707219524E-123	rgc	GLRX
bioRxiv preprint doi: https://doi.org/10.1101/2020.10.27.358135 ; this version posted November 9, 2020. The copyright holder for this preprint (which was not certified by peer review) is the author/funder, who has granted bioRxiv a license to display the preprint in perpetuity. It is made available under aCC-BY-NC-ND 4.0 International license.						
4.83921968044565E-126	0.895271633375106	0.848	0.37	8.86641829851251E-122	rgc	C14orf132
7.76313377058183E-126	0.912927270900317	0.815	0.231	1.422361369446E-121	rgc	CHRNA3
1.25146953223876E-125	0.776650783894721	0.662	0.144	2.29294247696786E-121	rgc	RAB3B
1.17992471110083E-124	0.838169018088775	0.686	0.155	2.16185805567893E-120	rgc	SCG5
6.72801331379931E-121	0.82191588110875	0.576	0.094	1.23270659935431E-116	rgc	CNTN2
8.13706270907195E-121	0.69723070170103	0.837	0.253	1.49087262955616E-116	rgc	ATP1A3
1.98826091077695E-118	0.45089441272832	0.486	0.049	3.64289164072553E-114	rgc	ZNF804A
2.01807928971846E-118	0.895479226853411	0.91	0.465	3.69752487462217E-114	rgc	NELL2
4.28529705587378E-118	0.777506560700588	0.629	0.137	7.85152126577194E-114	rgc	MAB21L2
6.99511098758653E-118	0.553981169812244	0.47	0.048	1.2816442351456E-113	rgc	MYC
1.01287684077604E-117	0.787624353076225	0.912	0.463	1.85579294766987E-113	rgc	KIF5C
1.00756126758084E-115	0.747573525662131	0.422	0.035	1.84605375446162E-111	rgc	RGS10
1.11303943700533E-115	0.539928008834857	0.598	0.105	2.03931085648116E-111	rgc	EPS8L1
1.1385487523292E-115	0.806390103382054	0.848	0.294	2.08604902401755E-111	rgc	ELAVL2
1.23411369520548E-115	0.625546577196461	0.626	0.141	2.26114311235547E-111	rgc	CCDC184
2.9244593454761E-115	0.649923861717785	0.804	0.225	5.3581944127813E-111	rgc	SEZ6L2
1.027255200089E-112	0.636478689762834	0.466	0.05	1.88213697760307E-108	rgc	NHLH2
5.03268921309648E-112	0.688521475894939	0.782	0.215	9.22089317623536E-108	rgc	SYT4
7.2751089900999E-111	0.720072293684404	0.945	0.664	1.3329454691661E-106	rgc	TERF2IP
2.3212189059686E-110	0.409997213607274	0.47	0.052	4.25293727951567E-106	rgc	AKAP6
2.08776880376001E-109	0.61170237027612	0.971	0.931	3.82521000224909E-105	rgc	TXN
1.74442057933279E-107	0.562544745564655	0.998	0.963	3.19612738545353E-103	rgc	COX6A1
1.63244328023133E-106	0.43408784193912	0.444	0.047	2.99096257803985E-102	rgc	SLIT1
1.80659788930477E-104	0.660761207427474	0.987	0.986	3.31004865278421E-100	rgc	CCNI
3.33709605436047E-104	0.719328434833301	0.916	0.562	6.11422739079925E-100	rgc	GDI1
1.3064709547764E-103	0.494754852155391	0.868	0.336	2.39371608334131E-99	rgc	FAM57B
1.89093461953832E-103	0.865908065424126	0.673	0.195	3.46457040991812E-99	rgc	NRN1
8.68583535001427E-103	0.694125298535895	0.877	0.487	1.59141875282962E-98	rgc	NAGK
1.12732348078541E-101	0.697323971593736	0.956	0.802	2.06548208149503E-97	rgc	ETFB
1.23187395428027E-100	0.443161648043537	0.998	0.989	2.25703945903232E-96	rgc	CFL1
1.41298250510188E-100	0.513066775847989	0.681	0.168	2.58886654584766E-96	rgc	SNAP25
1.61547527062075E-99	0.650643686527975	0.82	0.372	2.95987379083134E-95	rgc	PODXL2
5.20240955729372E-99	0.432435044593764	0.512	0.088	9.53185479087356E-95	rgc	PBX3

2.74387035180954E-98	0.658906733902441	0.837	0.405	5.02731925858544E-94	rgc	RBFOX2	
6.66575836673971E-98	0.668606822936448	0.923	0.407	1.22130024795405E-93	rgc	SCG3	
1.52651729223875E-97	0.747855320661304	0.747	0.294	2.79688498283983E-93	rgc	DUSP4	
bioRxiv preprint doi: https://doi.org/10.1101/2020.10.27.358135 ; this version posted November 9, 2020. The copyright holder for this preprint (which was not certified by peer review) is the author/funder, who has granted bioRxiv a license to display the preprint in perpetuity. It is made available under aCC-BY-NC-ND 4.0 International license.	1.67090306415697E-97	0.674420568250504	0.843	0.020	0.06112059414841E-93	rgc	CALB2
3.00635143839943E-97	0.891504691714855	0.64	0.162	5.50823710543543E-93	rgc	CLDN5	
5.186932802122E-97	0.697960044885914	0.949	0.785	9.50349828004792E-93	rgc	YWHAH	
5.86027671677897E-97	0.433033013613079	0.587	0.117	1.07371990004824E-92	rgc	IGLON5	
2.6197010183676E-96	0.592231668930167	0.949	0.809	4.79981620585311E-92	rgc	TBCB	
1.1605505161459E-94	0.630988416373291	0.888	0.513	2.12636065568251E-90	rgc	RAB6A	
1.45323359435652E-94	0.515445087963921	0.989	0.958	2.66261459158001E-90	rgc	MORF4L2	
1.46983786001806E-94	0.425619510740466	0.479	0.073	2.69303692712508E-90	rgc	NFASC	
9.75708211909468E-94	0.625475022081543	0.996	0.964	1.78769258586053E-89	rgc	SOX4	
1.43580043833584E-93	0.579043763119576	0.714	0.236	2.63067356311892E-89	rgc	PGM2L1	
2.30880702211744E-93	0.70503311868274	0.969	0.645	4.23019622592358E-89	rgc	PCBP4	
2.41410046027548E-93	0.504552388587299	0.697	0.186	4.42311486331673E-89	rgc	CELF3	
2.51913771613146E-93	0.510453909638443	0.609	0.139	4.61556412349606E-89	rgc	GDAP1L1	
6.42590627372325E-93	0.620097257700688	0.793	0.324	1.17735454747157E-88	rgc	CDKN2D	
8.06837422020271E-91	0.592976123461542	0.818	0.357	1.47828752462554E-86	rgc	STMN3	
3.27067600299953E-90	0.579039859303446	0.846	0.433	5.99253257269574E-86	rgc	YWHAG	
5.86229772037263E-90	0.512337971531459	0.969	0.965	1.07409018832667E-85	rgc	COX7A2	
1.56646297040349E-89	0.502772447965775	0.993	0.992	2.87007345437327E-85	rgc	STMN1	
1.62118571627323E-88	0.526980148885523	0.534	0.107	2.97033646935581E-84	rgc	ASIC4	
5.66852576699155E-88	0.571188462972606	0.941	0.799	1.03858729102819E-83	rgc	RAB2A	
9.35432148756384E-88	0.683836743652614	0.578	0.152	1.71389878295145E-83	rgc	POU2F2	
5.84899197760417E-87	0.464321850507716	0.626	0.169	1.07165231013664E-82	rgc	PCBP3	
2.26603757365677E-86	0.683691477136346	0.925	0.634	4.15183404245394E-82	rgc	BEX1	
3.29463732981373E-86	0.451571160099484	0.462	0.076	6.03643451568472E-82	rgc	TMEM59L	
3.96414808586284E-86	0.509376498574769	0.982	0.943	7.2631121229179E-82	rgc	EIF4G2	
4.05244450637634E-86	0.54289377784214	0.974	0.87	7.42488882458274E-82	rgc	DYNC1I2	
1.02949799845084E-85	0.581149805130244	0.84	0.432	1.88624623276163E-81	rgc	RUFY3	
1.69570479612608E-85	0.605363378261287	0.769	0.357	3.10687032746221E-81	rgc	TMEM14A	
1.34367870042896E-83	0.409111238267894	0.442	0.073	2.46188811492594E-79	rgc	ADCY1	
2.40486190271591E-83	0.541676652609848	0.741	0.283	4.40618797815608E-79	rgc	CD200	
7.57311888048045E-83	0.460833830870502	0.556	0.123	1.38754684128163E-78	rgc	NHLH1	
7.65282596081655E-83	0.521391963556916	0.686	0.258	1.40215077254081E-78	rgc	TMEM55A	
2.5751819675031E-80	0.52111164467085	1	0.999	4.71824840085919E-76	rgc	TMSB4X	
3.7332998792561E-80	0.467317386294559	0.98	0.951	6.84015203877303E-76	rgc	YWHAQ	

7.78338304029502E-80	0.616560369532356	0.888	0.657	1.42607144064285E-75	rgc	OCIAD2
2.12234132932384E-79	0.629199482046399	0.723	0.336	3.88855378358714E-75	rgc	MAP4
4.31965606661749E-79	0.464673749686776	0.69	0.246	7.91447384525656E-75	rgc	OPTN
bioRxiv preprint doi: https://doi.org/10.1101/2020.10.27.358135 ; this version posted November 9, 2020. The copyright holder for this preprint (which was not certified by peer review) is the author/funder. All rights reserved. No reuse allowed without permission.	0.597702639704774	0.921	0.007	0.919763872460717E-74	rgc	ENO2
3.00898929214867E-78	0.614650677847063	0.826	0.378	5.51307018107479E-74	rgc	GPC2
3.96162406359675E-78	0.459477004869948	0.991	0.948	7.25848760932197E-74	rgc	PSMA7
1.08163547978039E-77	0.456101896435866	0.651	0.213	1.98177252605363E-73	rgc	TRIM36
1.4362494610122E-77	0.475978440277239	0.648	0.18	2.63149626246656E-73	rgc	SLC18A2
4.56374575418028E-77	0.576702944970692	0.941	0.785	8.36169497080911E-73	rgc	ATP6V0B
6.13880563062619E-77	0.485690572273759	0.956	0.915	1.12475196764333E-72	rgc	USMG5
1.06568452890177E-76	0.460608955043864	0.519	0.119	1.95254719385382E-72	rgc	PPP1R17
1.97570020213019E-76	0.799460403161583	0.985	0.833	3.61987791034294E-72	rgc	SOX11
1.52380586118491E-75	0.618089497953616	0.69	0.265	2.79191709886299E-71	rgc	MAP1LC3A
1.7858952019951E-75	0.552938685546649	0.991	0.952	3.27211718909543E-71	rgc	HSPA8
4.67309356171899E-75	0.532655389488811	0.873	0.521	8.56204202378154E-71	rgc	DYNC1LI1
5.09505542847331E-75	0.515638518014245	0.952	0.876	9.33516055604881E-71	rgc	DYNLT1
5.53838724820895E-75	0.545732063374844	0.76	0.391	1.01474331161684E-70	rgc	HCFC1R1
1.14284579087582E-74	0.428119111176889	0.407	0.071	2.09392205804268E-70	rgc	ZNF503
3.6537589458338E-74	0.571883709677937	0.868	0.579	6.6944171405567E-70	rgc	CXADR
8.60693599634418E-74	0.557046321352991	0.782	0.403	1.57696281325018E-69	rgc	ACOT7
1.99739583056071E-73	0.463691974602043	0.675	0.25	3.65962864075333E-69	rgc	TPD52
4.79215094015323E-73	0.527940097901761	0.763	0.345	8.78017895254874E-69	rgc	CEP170
5.91334809395628E-73	0.47334499436541	0.495	0.118	1.08344363777467E-68	rgc	KIF5A
7.15289927539346E-73	0.523401598408129	0.912	0.704	1.31055420523759E-68	rgc	PCMT1
1.44688503042924E-72	0.514844841160654	0.905	0.739	2.65098275275245E-68	rgc	PFDN2
1.75512568583877E-72	0.516477479027181	0.987	0.886	3.21574128159379E-68	rgc	PAX6
1.8842944888781E-71	0.558698637539577	0.769	0.396	3.45240436252245E-67	rgc	CRIP2
5.24908888973084E-71	0.422936672747567	0.598	0.191	9.61738066376485E-67	rgc	RUFY2
9.44613104340504E-71	0.490603389162866	0.965	0.874	1.73072012977267E-66	rgc	EIF4A1
2.2881869155538E-70	0.54745857854927	0.637	0.193	4.19241606667768E-66	rgc	SSTR2
3.07416457153755E-70	0.542188157353054	0.93	0.804	5.63248432797109E-66	rgc	VAMP2
4.24026008140724E-70	0.435286038442855	0.582	0.18	7.76900452115434E-66	rgc	PPP2R5B
7.91561186266533E-70	0.468640626944103	0.976	0.916	1.45029840547754E-65	rgc	TTC3
1.61823677675578E-69	0.498456401313893	0.723	0.323	2.96493342237194E-65	rgc	VAT1
3.37445787424198E-69	0.545217231499907	0.752	0.385	6.18268171718616E-65	rgc	CCDC112
4.22097504712336E-69	0.529029276720958	0.776	0.376	7.73367048133942E-65	rgc	TUBA1C
6.86138005896114E-68	0.421010710558112	1	1	1.25714205440286E-63	rgc	TUBB

1.6695131279467E-67	0.481036703983678	0.958	0.915	3.05888195302394E-63	rgc	NDUFB8
4.51561111573255E-67	0.558476684499741	0.771	0.407	8.27350268624518E-63	rgc	TSC22D3
2.29760637601972E-66	0.542918040568909	0.963	0.797	4.20967440214334E-62	rgc	DAAM1
bioRxiv preprint doi: https://doi.org/10.1101/2020.10.27.358135 ; this version posted November 9, 2020. The copyright holder for this preprint (which was not certified by peer review) is the author/funder, who has granted bioRxiv a license to display the preprint in perpetuity. It is made available under aCC-BY-NC-ND 4.0 International license.	0.654043262742862	0.945	0.703	6.55041369014609E-62	rgc	MIAT
5.00306635461218E-66	0.43861109706274	0.963	0.918	9.16661817492044E-62	rgc	PRDX5
5.00823555228673E-66	0.432950363452869	0.629	0.228	9.17608917889974E-62	rgc	EFNA3
5.23084202598234E-66	0.437692635588864	0.967	0.902	9.58394876000484E-62	rgc	VDAC2
5.63122766075674E-66	0.625831156447266	0.905	0.695	1.03175353200385E-61	rgc	NKAIN4
7.11188907751946E-66	0.466342851937105	0.934	0.826	1.30304031678312E-61	rgc	DYNLRB1
1.64219403278665E-65	0.678113583663412	0.888	0.716	3.0088279068717E-61	rgc	MAP1LC3B
6.74800773921508E-65	0.566119103735224	0.855	0.516	1.23636997797899E-60	rgc	KIF1A
7.7200473697213E-65	0.602473324934083	0.886	0.618	1.41446707908034E-60	rgc	CADM1
1.55705560346029E-64	0.656110768205143	0.596	0.243	2.85283727665994E-60	rgc	NKAIN3
2.70768632183044E-64	0.854255499006478	0.578	0.234	4.96102287885773E-60	rgc	SNCA
3.52838314477347E-64	0.497849863442421	0.963	0.787	6.46470359785395E-60	rgc	SYT1
6.55227354542061E-64	0.477676975331265	0.705	0.338	1.20050755899196E-59	rgc	CARD19
2.17975163420981E-63	0.690704816709283	0.837	0.507	3.99374094419922E-59	rgc	HMGCS1
8.36144903636468E-63	0.496314840007528	0.785	0.427	1.53198469244274E-58	rgc	MAP2
1.25207054248241E-62	0.417848459279709	0.637	0.243	2.29404364793627E-58	rgc	KIFAP3
2.35425275785137E-62	0.451738295286036	0.648	0.266	4.31346190293527E-58	rgc	CACNB3
3.04635754611165E-62	0.431418633117329	0.637	0.254	5.58153629598576E-58	rgc	FSD1
3.94319918900536E-62	0.54130813858443	0.938	0.82	7.22472955409563E-58	rgc	CDC42
5.63360754830516E-62	0.508365710803338	0.516	0.146	1.03218957500047E-57	rgc	HEY1
1.45367601162577E-61	0.461434991550713	0.958	0.815	2.66342518850074E-57	rgc	FSCN1
2.95197120050925E-61	0.433859852834725	0.662	0.277	5.40860163357305E-57	rgc	NDRG4
3.89546222257375E-61	0.508167375788281	0.745	0.412	7.13726588419963E-57	rgc	FEZ1
5.30954903459906E-61	0.457843910905633	0.916	0.789	9.7281557411924E-57	rgc	DNAJB6
9.35278236249233E-61	0.471560862972372	0.934	0.814	1.71361678445585E-56	rgc	CYCS
3.4746198925863E-60	0.480945717962866	0.943	0.799	6.36619856719662E-56	rgc	FABP5
3.62509298105255E-60	0.496635976155188	0.815	0.5	6.64189535988449E-56	rgc	FNBP1L
5.15631474389315E-60	0.445256675567284	0.938	0.832	9.44739987376103E-56	rgc	SNRPN
6.32235555013274E-60	0.433174680412123	0.708	0.286	1.15838198389532E-55	rgc	RP11-96L14.7
7.54653838981593E-60	0.495788054290821	0.787	0.448	1.38267676378207E-55	rgc	KIF3A
2.2314897891057E-59	0.509412477642736	0.609	0.248	4.08853559159946E-55	rgc	SMAD9
3.08470079078308E-59	0.530047857940371	0.864	0.613	5.65178878887276E-55	rgc	DYNC1H1
5.2356587286299E-59	0.467459318042535	0.895	0.74	9.5927739225957E-55	rgc	ARPC5
1.28141451067931E-58	0.467153951393379	0.745	0.393	2.34780766646663E-54	rgc	ZC2HC1A

1.90006428305232E-58	0.522313906679223	0.844	0.635	3.48129777940847E-54	rgc	DPYSL2
1.268030112892E-57	0.494768423411387	0.956	0.845	2.32328477284073E-53	rgc	CALM1
1.44947903686894E-57	0.413683036962665	0.596	0.233	2.65573549135127E-53	rgc	HRAS
bioRxiv preprint doi: https://doi.org/10.1101/2020.10.27.358135 ; this version posted November 9, 2020. The copyright holder for this preprint (which was not certified by peer review) is the author/funder. All rights reserved. No reuse allowed without permission.	0.408299038544304	0.963	0.874	2.77633093520678E-53	rgc	MGST3
2.39129259497574E-57	0.429643183846087	0.765	0.427	4.38132629251455E-53	rgc	GRB2
2.59446391198708E-57	0.49298883292783	0.727	0.4	4.75357677954272E-53	rgc	ATAT1
3.08572310591885E-57	0.528659982621973	0.811	0.568	5.65366187466452E-53	rgc	ATP6V0E2
4.87455796852465E-57	0.474668897444841	0.919	0.769	8.93116510993086E-53	rgc	NME1
2.38250433358664E-56	0.419700817262351	0.941	0.849	4.36522443999744E-52	rgc	YWHAB
2.42487899720035E-56	0.481155911249948	0.714	0.371	4.44286329867048E-52	rgc	EPB41
1.07607582720355E-55	0.700935177541595	0.793	0.54	1.97158613060235E-51	rgc	ACAT2
1.64446249958468E-55	0.478741007604624	0.787	0.47	3.01298419173905E-51	rgc	FHL1
3.22906681556455E-55	0.464053597029642	0.622	0.276	5.91629621947737E-51	rgc	PKIB
4.11431509837341E-55	0.448699662208957	0.923	0.794	7.53824812323976E-51	rgc	YWHAZ
6.38520143313387E-54	0.417615111917749	0.941	0.848	1.16989660657879E-49	rgc	NDUFB7
9.51082757200674E-54	0.530787861260716	0.699	0.359	1.74257382774308E-49	rgc	MSMO1
1.8509914008472E-53	0.576595091886423	0.886	0.674	3.39138644463224E-49	rgc	FDFT1
3.77001921034522E-53	0.455964241250492	0.84	0.602	6.90742919719452E-49	rgc	WRB
7.71712794546434E-53	0.450820473571626	0.807	0.502	1.41393218216798E-48	rgc	IDH1
7.80900338884854E-50	0.527913000527845	0.798	0.512	1.43076560090483E-45	rgc	IFRD1
8.49787271463074E-50	0.578503980469958	0.767	0.445	1.55698023877464E-45	rgc	HERPUD1
1.19467718546249E-49	0.423778250272332	0.807	0.558	2.18888753920437E-45	rgc	SLC25A4
1.34817198921186E-49	0.418648813420682	0.901	0.739	2.47012071863397E-45	rgc	NREP
1.40701141273906E-49	0.479198922755872	0.78	0.501	2.57792631042051E-45	rgc	FAM63B
2.12255197577103E-49	0.414246159946021	0.802	0.499	3.88893973000768E-45	rgc	STARD3NL
2.21763694867252E-49	0.455159033499935	0.743	0.428	4.0631544173578E-45	rgc	KIF21A
2.95612648376533E-49	0.444124158992195	0.633	0.298	5.41621494355484E-45	rgc	KIDINS220
1.00847746047576E-48	0.418609250156644	0.703	0.374	1.84773240308368E-44	rgc	DYNLT3
1.83894063235512E-48	0.412160282299552	0.877	0.652	3.36930702660104E-44	rgc	DTD1
1.47206154214699E-47	0.406527932531181	0.512	0.195	2.69711115752171E-43	rgc	MVD
3.59046335291656E-47	0.492132759390138	0.829	0.588	6.57844695521373E-43	rgc	BEX2
2.22563599445124E-46	0.547913680337346	0.877	0.637	4.07781026903356E-42	rgc	SQLE
1.12492019711697E-44	0.480428580214646	0.598	0.261	2.06107878515771E-40	rgc	ASNS
1.16015831524062E-44	0.40848814039453	0.8	0.525	2.12564206518386E-40	rgc	ARHGDIA
1.36053192785199E-44	0.413663478651875	0.602	0.298	2.49276659821041E-40	rgc	EPB41L3
1.74016775481385E-44	0.415552470889448	0.87	0.653	3.18833536036993E-40	rgc	SIX3
2.69316037119302E-41	0.521643941088454	0.277	0.059	4.93440843209985E-37	rgc	PCP4

3.15583652052936E-39	0.48207510445856	0.853	0.599	5.78212367291389E-35	rgc	CXCR4
4.86162966303498E-39	0.406991713244434	0.818	0.555	8.90747786861268E-35	rgc	DPYSL4
7.14224960007327E-38	0.408804245947629	0.859	0.683	1.30860297172542E-33	rgc	VPS35
bioRxiv preprint doi: https://doi.org/10.1101/2020.10.27.358135 ; this version posted November 9, 2020. The copyright holder for this preprint (which was not certified by peer review) is the author/funder. All rights reserved. No reuse allowed without permission.	0.614843980461769	0.659	0.994	1.0876584246054E-01	rgc	MPPED2
8.63364598481747E-33	0.596600929335693	0.646	0.408	1.58185661733826E-28	rgc	CASP3
3.46669727333226E-32	0.406076722643132	0.877	0.684	6.35168274419936E-28	rgc	SARS
1.48291163159534E-27	0.493863958199496	1	0.999	2.71699069140899E-23	rgc	CRABP1
1.64573128630501E-27	0.55664611795514	0.857	0.743	3.01530886276805E-23	rgc	TSC22D1
2.21050252751246E-22	0.467065189195997	0.626	0.438	4.05008273090833E-18	rgc	TAGLN2
1.0627823901897E-21	0.46817729326957	0.525	0.308	1.94722989530557E-17	rgc	MTHFD2
1.1103731610065E-251	2.12263183380489	0.768	0.014	2.03442570559611E-247	hc/ac	TFAP2A
4.54344425863255E-198	1.09574466629866	0.632	0.012	8.32449857066657E-194	hc/ac	PRDM13
1.21101536918587E-146	0.665697765592853	0.389	0.003	2.21882235942235E-142	hc/ac	TFAP2B
2.4084838393134E-112	0.794270374042992	0.558	0.031	4.41282409039001E-108	hc/ac	NDST3
5.13156184722427E-108	0.816859008703915	0.537	0.029	9.40204761648431E-104	hc/ac	SPATS2L
5.13187294689624E-76	1.62828437612529	0.884	0.205	9.4026176133033E-72	hc/ac	HMP19
6.30875998265711E-75	1.02498380827955	0.579	0.065	1.15589100402244E-70	hc/ac	PROX1
9.04150578804771E-74	1.54629631306233	0.979	0.282	1.6565846904861E-69	hc/ac	ONECUT2
1.01425515580165E-72	0.861544427495706	0.589	0.068	1.85831829645978E-68	hc/ac	BARHL2
8.08904393668218E-71	0.813107945721212	0.389	0.024	1.48207463007891E-66	hc/ac	NPPC
3.33603230400502E-65	0.964173597268338	0.642	0.095	6.11227838739799E-61	hc/ac	ONECUT3
1.39108178050353E-63	1.45040152226063	0.863	0.229	2.54874003823858E-59	hc/ac	ONECUT1
4.06450194187189E-61	0.909523634632826	0.632	0.098	7.44698045789768E-57	hc/ac	LINC00599
4.26516611959661E-56	1.57486074155381	1	0.97	7.8146373643249E-52	hc/ac	SOX4
1.98117270771394E-52	1.21846345379997	0.874	0.332	3.62990463507348E-48	hc/ac	TRIB1
5.73623597848123E-48	1.49272513533908	0.968	0.86	1.05099315597733E-43	hc/ac	AP1S2
4.46012231278163E-46	1.31429875353724	1	0.688	8.1718361014785E-42	hc/ac	STMN2
1.52741930721007E-42	0.726009670454814	0.537	0.102	2.79853765467029E-38	hc/ac	PLXNA2
1.07810951104725E-41	0.945903585531158	0.989	0.904	1.97531224614077E-37	hc/ac	PAX6
2.23702840004878E-41	0.437870024470562	0.337	0.037	4.09868343456938E-37	hc/ac	WDR7
1.05670246841988E-39	1.23876554334889	0.947	0.459	1.9360902626389E-35	hc/ac	ID2
2.00533842099179E-38	0.913729042333477	0.989	0.829	3.67418105494116E-34	hc/ac	ETFB
1.09802253390459E-37	0.82938646613161	0.663	0.199	2.01179688661998E-33	hc/ac	SULF2
1.75301995977208E-36	1.00805571610234	0.821	0.324	3.2118831702944E-32	hc/ac	CELF4
1.26028839320839E-35	0.674653785461897	0.589	0.145	2.30910039403642E-31	hc/ac	RUNX1T1
1.88521389778598E-35	0.89367350361542	0.989	0.847	3.45408890352348E-31	hc/ac	CXXC5
4.41281094121139E-34	0.929022493342771	0.968	0.484	8.0851522064875E-30	hc/ac	STMN4

1.16288287040378E-33	0.756888783586806	0.568	0.15	2.1306339951538E-29	hc/ac	PLPPR1
1.321753411285E-31	0.855080439395744	0.979	0.766	2.42171660015638E-27	hc/ac	APLP1
2.28970679966089E-31	0.850613863436192	0.821	0.317	4.19520079833868E-27	hc/ac	SYT4
bioRxiv preprint doi: https://doi.org/10.1101/2020.10.27.358135 ; this version posted November 9, 2020. The copyright holder for this preprint (which was not certified by peer review) is the author/funder, who has granted bioRxiv a license to display the preprint in perpetuity. It is made available under aCC-BY-NC-ND 4.0 International license.	0.646901238808449	0.783	0.359	0.661147612428E-27	hc/ac	RP11-96L14.7
5.72194806241825E-31	0.789565333549811	0.895	0.386	1.04837532399627E-26	hc/ac	INA
1.07694364367595E-30	0.737269778474283	0.684	0.25	1.97317614394307E-26	hc/ac	MIR124-2HG
7.21194049220743E-30	0.832172404447895	1	0.846	1.32137173698225E-25	hc/ac	BASP1
1.38338383312044E-29	0.643225526327909	0.674	0.217	2.53463585904328E-25	hc/ac	SEPT4
1.07336333263609E-28	0.497667969422201	1	0.994	1.96661629805584E-24	hc/ac	MARCKSL1
5.73644785929016E-28	0.964007845532261	0.811	0.346	1.05103197677914E-23	hc/ac	RTN1
8.68964216312076E-28	0.814665358953785	0.937	0.767	1.59211623712699E-23	hc/ac	NREP
1.19208057888438E-27	0.694331425360365	1	0.993	2.18413003663197E-23	hc/ac	TUBB2B
2.95297488779075E-27	0.717414885144629	0.758	0.289	5.41044058941021E-23	hc/ac	MAPT
5.93487745326567E-27	0.50627423370468	0.263	0.035	1.08738824698734E-22	hc/ac	CPNE4
5.96518690150805E-26	0.728800381101465	0.853	0.372	1.0929415440943E-21	hc/ac	RAB3A
1.65464692938187E-25	0.773607713356478	1	0.909	3.03164410401345E-21	hc/ac	MLLT11
2.60263768103958E-25	0.615607021398163	0.579	0.17	4.76855275920072E-21	hc/ac	TTC9B
3.64512601060162E-25	0.677294738377006	0.453	0.118	6.67859987662429E-21	hc/ac	LRRN3
4.11606632403905E-25	0.478050341847485	1	1	7.54145671890434E-21	hc/ac	MALAT1
1.05956446251127E-24	0.666471228352712	1	0.998	1.94133400821316E-20	hc/ac	TMSB10
3.82830890400531E-24	0.675921435419658	0.968	0.703	7.01422757391853E-20	hc/ac	CRMP1
3.98017177177509E-24	0.862088847049112	0.821	0.534	7.29247072024632E-20	hc/ac	EFNA5
1.43520133678757E-23	0.447581851881842	0.368	0.08	2.62957588926218E-19	hc/ac	NTRK2
1.92247524195388E-23	0.804470088876521	0.874	0.657	3.5223591383079E-19	hc/ac	ZNF385A
4.44265325882762E-23	0.643548226506505	0.568	0.204	8.13982930082397E-19	hc/ac	IGLON5
2.13424505983347E-22	0.614282321450433	1	0.903	3.91036379862688E-18	hc/ac	CD24
3.21183510186937E-22	0.583361053222163	0.684	0.28	5.88472427364506E-18	hc/ac	CELF3
8.46864878758777E-22	0.643774574309854	0.958	0.827	1.55162583086183E-17	hc/ac	DAAM1
1.27078710967465E-21	0.599638523006006	0.989	0.893	2.3283361423459E-17	hc/ac	HN1
1.61892686984073E-21	0.541479276459746	1	0.998	2.96619781092219E-17	hc/ac	TUBA1A
1.84204397371695E-21	0.722650150089631	0.895	0.766	3.3749929686442E-17	hc/ac	PHYIPL
2.08195034710658E-21	0.559243843023036	0.937	0.818	3.81454942596868E-17	hc/ac	GPM6A
5.67121593379424E-21	0.491282634213607	0.421	0.12	1.03908018338978E-16	hc/ac	MIR181A1HG
2.93274589765288E-20	0.498370792631087	0.895	0.413	5.3733770336796E-16	hc/ac	SNCG
3.51000488979315E-20	0.541655321099234	0.411	0.113	6.431030959079E-16	hc/ac	NTRK1
6.26856634126068E-20	0.480965136035681	0.989	0.97	1.14852672504578E-15	hc/ac	COX6A1
8.64562955868943E-20	0.559180223383519	0.905	0.503	1.58405224774308E-15	hc/ac	SCG3

9.56025845982761E-20	0.529542294885375	0.484	0.175	1.75163055500961E-15	hc/ac	PELI1
1.00910078397105E-19	0.64882772936228	0.916	0.665	1.84887445639176E-15	hc/ac	ENO2
1.50820217837592E-19	0.664418491187415	0.947	0.711	2.76332803122036E-15	hc/ac	PCSK1N
bioRxiv preprint doi: https://doi.org/10.1101/2020.10.27.358135 ; this version posted November 9, 2020. The copyright holder for this preprint (which was not certified by peer review) is the author/funder. All rights reserved. No reuse allowed without permission.	0.642497102820977	0.992	0.992	0.427368693214041E-14	hc/ac	STMN1
1.09833201370862E-18	0.594256117903859	0.421	0.136	2.01236391551694E-14	hc/ac	ARHGAP29
1.45527187257787E-18	0.555751647768011	0.758	0.364	2.66634912493717E-14	hc/ac	ATP1A3
2.97780565315374E-18	0.670303885955351	0.905	0.728	5.45593551770827E-14	hc/ac	TUBB2A
3.15518772754137E-18	0.66545887490536	0.695	0.307	5.78093495440129E-14	hc/ac	PPP1R1A
3.58004726951749E-18	0.549766905495032	0.695	0.342	6.55936260720994E-14	hc/ac	MAP1LC3A
6.28602638496259E-18	0.414744065913206	0.358	0.097	1.15172575425284E-13	hc/ac	GRIA2
7.86783982455432E-18	0.463816561049175	0.368	0.105	1.44154561265484E-13	hc/ac	SYBU
9.37186903635973E-18	0.570355971925951	0.474	0.179	1.71711384484183E-13	hc/ac	NOL4
1.10453175406018E-17	0.790649257338089	0.947	0.863	2.02372307978906E-13	hc/ac	SOX11
2.57069630278578E-17	0.450197848865726	0.305	0.073	4.71002976596411E-13	hc/ac	CNTNAP2
3.31982903163396E-17	0.466050907321627	0.853	0.414	6.08259075175974E-13	hc/ac	GNG3
4.28376287979366E-17	0.485215695257106	0.968	0.566	7.84871034835794E-13	hc/ac	TAGLN3
6.1192734918282E-17	0.485225564254118	0.958	0.813	1.12117328917276E-12	hc/ac	ATP6V0B
1.15498536457272E-16	0.59764514506918	0.947	0.779	2.11616418497013E-12	hc/ac	RORB
3.77104125400762E-16	0.693103920792276	1	0.994	6.90930178559277E-12	hc/ac	ENO1
3.8653744857748E-16	0.426866377791661	0.421	0.129	7.08213913283659E-12	hc/ac	NHLH2
5.79346363404753E-16	0.547641343169471	0.526	0.237	1.06147840703019E-11	hc/ac	SV2A
7.50880675212657E-16	0.5971436520908	0.453	0.174	1.37576357312463E-11	hc/ac	THSD7A
8.45293760191096E-16	0.436560351888931	0.453	0.165	1.54874722742213E-11	hc/ac	RPS6KL1
9.12970447501928E-16	0.4759742031965	0.695	0.336	1.67274445391303E-11	hc/ac	SEZ6L2
9.17701796141797E-16	0.552988047324923	0.411	0.142	1.681413230891E-11	hc/ac	ESRRG
1.08308807279602E-15	0.547651762703018	0.779	0.552	1.98443396697686E-11	hc/ac	BZW2
1.17118318725385E-15	0.44605362319806	0.432	0.159	2.14584183568651E-11	hc/ac	RGS17
2.20715908918656E-15	0.685372217016099	0.705	0.473	4.04395688320761E-11	hc/ac	ZEB2
3.03508400165749E-15	0.49581136941969	0.968	0.927	5.56088090783684E-11	hc/ac	C4orf48
3.65618633130204E-15	0.433518879253497	0.568	0.27	6.6988645962116E-11	hc/ac	SERP2
4.87321811578802E-15	0.529563504599678	0.821	0.549	8.92871023174681E-11	hc/ac	KIF5C
5.81342963769563E-15	0.613589587656508	0.832	0.721	1.06513657821859E-10	hc/ac	TPM3
6.9837390597214E-15	0.429025532643905	0.326	0.093	1.27956067052215E-10	hc/ac	PPP1R14A
1.97413709656597E-14	0.484268623099149	0.768	0.463	3.61701398832816E-10	hc/ac	GPC2
2.17416177213781E-14	0.492156643589321	0.884	0.515	3.98349919891089E-10	hc/ac	DCX
2.36063692539922E-14	0.446470992166401	0.916	0.828	4.32515897471645E-10	hc/ac	VAMP2
3.10820358358346E-14	0.474978010255391	0.905	0.717	5.69485060584162E-10	hc/ac	TERF2IP

4.86071609296889E-14	0.553107753886003	0.474	0.217	8.9058040255376E-10	hc/ac	CDC42EP3
1.17628824479243E-13	0.483858078254215	0.789	0.581	2.15519532210869E-09	hc/ac	KIF1A
1.27538258949471E-13	0.534357388734161	0.863	0.714	2.3367559804722E-09	hc/ac	FDFT1
bioRxiv preprint doi: https://doi.org/10.1101/2020.10.27.358135 ; this version posted November 9, 2020. The copyright holder for this preprint (which was not certified by peer review) is the author/funder. All rights reserved. No reuse allowed without permission.	0.629379504101508	0.695	0.424	0.872181254607305E-08	hc/ac	CEP170
6.84198278764468E-13	0.487363996772456	0.4	0.165	1.25358808635226E-08	hc/ac	TBC1D16
7.11965216203823E-13	0.52848045401146	0.516	0.273	1.30446266912864E-08	hc/ac	C12orf49
7.78133175242275E-13	0.463204804620969	0.768	0.552	1.4256956036789E-08	hc/ac	FAM63B
9.62748349487342E-13	0.461437346529577	0.611	0.35	1.76394752593071E-08	hc/ac	NDRG4
1.42022834806837E-12	0.504623864857507	0.758	0.448	2.60214237933087E-08	hc/ac	ELAVL3
1.5777055230723E-12	0.447566170615042	0.537	0.285	2.89067205937306E-08	hc/ac	ADD2
1.6466389514901E-12	0.458988261562538	0.547	0.259	3.01697188692016E-08	hc/ac	SCG5
1.77074682983197E-12	0.488389067791367	0.905	0.689	3.24436234161814E-08	hc/ac	BEX1
2.35152133497629E-12	0.556954464830718	0.726	0.464	4.30845738994356E-08	hc/ac	TXNIP
2.67861813420934E-12	0.542876519553071	0.663	0.44	4.90776414549835E-08	hc/ac	MPPED2
2.92153745958867E-12	0.434053585193696	0.737	0.541	5.35284093345836E-08	hc/ac	TDG
1.00652265686352E-11	0.458092776929095	0.516	0.284	1.84415081190533E-07	hc/ac	EVL
1.28359012063794E-11	0.416170782773424	0.368	0.142	2.35179381903283E-07	hc/ac	ACTL6B
2.41894758653179E-11	0.416621444299726	0.495	0.23	4.43199576804355E-07	hc/ac	GDAP1L1
2.96040230326555E-11	0.505357791983839	0.579	0.362	5.42404910004314E-07	hc/ac	STARD4-AS1
3.16943337279355E-11	0.407845042576651	0.842	0.632	5.80703582563234E-07	hc/ac	BEX2
4.08047005511959E-11	0.422080659843384	0.632	0.349	7.47623723499011E-07	hc/ac	TSPAN7
4.2437192413111E-11	0.433089202177911	0.968	0.941	7.7753423939302E-07	hc/ac	MARCKS
7.64734461789459E-11	0.453366665468398	0.389	0.17	1.40114648089065E-06	hc/ac	PVRL3
8.33378513344068E-11	0.464287449839076	0.937	0.847	1.526916112149E-06	hc/ac	MAB21L1
2.05238606794519E-10	0.452832034700687	0.979	0.927	3.76038175368918E-06	hc/ac	TTC3
2.08627100315221E-10	0.410819739312718	0.768	0.644	3.82246573197548E-06	hc/ac	CCDC90B
2.44397585088782E-10	0.412914726398136	0.842	0.739	4.47785255399667E-06	hc/ac	RPAIN
4.46615214932053E-10	0.438337905094319	0.432	0.224	8.18288396798508E-06	hc/ac	PARD6A
4.78117487880492E-10	0.517652918444165	0.632	0.465	8.76006861294638E-06	hc/ac	ATAT1
5.54667507214568E-10	0.477519523929332	0.653	0.486	1.01626180671853E-05	hc/ac	RNF24
6.36966815821497E-10	0.46876964837726	0.663	0.519	1.16705059994815E-05	hc/ac	CCDC88A
8.05366002590292E-10	0.487284723737913	0.453	0.24	1.47559158994593E-05	hc/ac	BCL11A
9.7851147313707E-10	0.429441042492679	0.874	0.845	1.79282872108174E-05	hc/ac	CDC42
1.1627470813401E-08	0.424519236967475	0.495	0.301	0.000213038520243133	hc/ac	ZNF385D
5.77952733099636E-08	0.43756619478199	0.674	0.575	0.00105892499758515	hc/ac	NT5C3B
8.82732576696906E-08	0.468175436103193	0.526	0.37	0.00161734262702407	hc/ac	GPR162
2.89049151449671E-07	0.412083106724679	0.695	0.569	0.00529595855286088	hc/ac	IFRD1

1.74616404257391E-06	0.430342877564755	0.495	0.343	0.0319932175880392	hc/ac	ALDOC
4.32921057014761E-39	1.09116962446826	1	0.994	7.93197960662446E-35	stem_cells	ENO1
5.49339183605781E-34	1.2821501454216	0.988	0.721	1.00649925220251E-29	stem_cells	SLC2A1
bioRxiv preprint doi: https://doi.org/10.1101/2020.10.27.358135 ; this version posted November 9, 2020. The copyright holder for this preprint (which was not certified by peer review) is the author/funder. All rights reserved. No reuse allowed without permission.						
1.39434675614325E-32	0.897913705579275	1	0.973	2.55472212660566E-28	stem_cells	ALDOA
1.45940201401651E-32	0.833264094409777	0.805	0.295	2.67391637008105E-28	stem_cells	PLOD2
1.80588390681896E-32	0.629265435004812	0.72	0.207	3.3087404940737E-28	stem_cells	SPAG4
7.89616689927275E-32	0.525656807020405	0.476	0.086	1.44673569928475E-27	stem_cells	PDE4C
5.34358631991486E-30	1.01166162914946	1	0.93	9.790518855348E-26	stem_cells	PGK 1.00
2.24724302531134E-29	1.02904775671633	1	0.827	4.11739867097544E-25	stem_cells	BNIP3
2.55877799433127E-29	0.995095245716952	0.976	0.67	4.68819304121375E-25	stem_cells	FAM162A
5.68503236876911E-28	1.10359464079105	0.976	0.619	1.04161163060588E-23	stem_cells	GPI
4.34157075592127E-27	0.599067953538017	0.61	0.178	7.95462593899894E-23	stem_cells	ESPN
5.80816013154025E-27	0.406513172105257	1	0.995	1.0641710993008E-22	stem_cells	RPS8
9.30023408122353E-27	0.577725247074021	0.707	0.234	1.7039888836177E-22	stem_cells	CASP7
1.66855781488651E-26	0.67662009931182	0.646	0.19	3.05713162843507E-22	stem_cells	STC2
1.13509312468489E-25	0.488416409445213	0.463	0.096	2.07971762304766E-21	stem_cells	STC1
1.39685913484514E-24	0.835097818201533	0.817	0.405	2.55932530686327E-20	stem_cells	ZFP36L2
1.50895862399518E-24	0.617697198145528	0.646	0.218	2.76471399088397E-20	stem_cells	AK4
6.42282505910581E-24	0.788948663926038	0.976	0.506	1.17679000732937E-19	stem_cells	PTH2
7.16404527908153E-24	0.5197168516702	1	1	1.31259637603332E-19	stem_cells	GAPDH
1.15729301321879E-23	0.70017134881897	0.988	0.903	2.12039225881947E-19	stem_cells	WSB1
1.18003203472596E-22	0.437841874885706	1	0.986	2.1620546940249E-18	stem_cells	NPM1
1.37240429235406E-22	0.81579693241571	0.78	0.397	2.5145191444511E-18	stem_cells	CDCA7L
1.05495624130083E-21	0.529546084137555	1	0.954	1.93289082531138E-17	stem_cells	MIF
4.61819355763715E-21	0.666854245216729	1	0.91	8.46145423630278E-17	stem_cells	C4orf3
3.07966851091129E-20	0.856933901835392	0.768	0.43	5.64256864569167E-16	stem_cells	HILPDA
1.2094080938547E-19	0.430658952178823	0.476	0.133	2.21587750956058E-15	stem_cells	PFKFB4
1.86042469873209E-19	0.67208003375461	0.695	0.315	3.40867013301693E-15	stem_cells	INSIG2
2.20317281993999E-19	0.513217184009918	1	0.987	4.03665324069406E-15	stem_cells	TPI1
2.71935953120242E-18	0.692300355826827	1	0.922	4.98241053306908E-14	stem_cells	VIM
2.74756761571608E-18	0.655506878723102	0.939	0.657	5.03409338551501E-14	stem_cells	DDIT4
6.52920234152297E-18	0.45773101953944	0.622	0.249	1.19628045301384E-13	stem_cells	P4HA2
8.80169056439683E-18	0.486857509414349	1	0.989	1.61264574520879E-13	stem_cells	PKM
3.40488461128533E-17	0.473435832321538	1	0.959	6.23842958479698E-13	stem_cells	EIF3E
8.62009948780322E-17	0.51099465643109	0.89	0.643	1.57937462815531E-12	stem_cells	SNHG7
9.22730499884842E-15	0.470100245888426	0.988	0.866	1.69062682188901E-10	stem_cells	BNIP3L

1.72312723412624E-14	0.547055650819365	0.634	0.306	3.1571137183661E-10	stem_cells	TMEM45A
6.45659477557639E-14	0.455992807551283	0.78	0.422	1.18297729478111E-09	stem_cells	TIMP1
6.57006102448288E-14	0.615890020104074	0.902	0.55	1.20376658090575E-09	stem_cells	SPP1
bioRxiv preprint doi: https://doi.org/10.1101/2020.10.27.358135 ; this version posted November 9, 2020. The copyright holder for this preprint (which was not certified by peer review) is the author/funder. All rights reserved. No reuse allowed without permission.	0.450534081807488	0.633	0.383	1.44520448471769E-08	stem_cells	ARRDC3
1.53297276619437E-12	0.505444735065962	0.707	0.415	2.80871270222133E-08	stem_cells	FGF9
2.63056763749205E-12	0.442571472234247	0.817	0.453	4.81972602541293E-08	stem_cells	SLC16A3
2.6449535093699E-12	0.52819350127987	0.878	0.665	4.84608381986753E-08	stem_cells	NR2F1
5.34288920088659E-12	0.465603960804191	0.805	0.515	9.78924159386442E-08	stem_cells	LTA4H
8.00907778582754E-12	0.411767844664544	0.988	0.767	1.46742323191932E-07	stem_cells	LMAN1
8.87670337910913E-12	0.450026738699241	0.634	0.287	1.62638959312038E-07	stem_cells	NRN1
1.16464178439927E-11	0.452124151010562	0.634	0.315	2.13385667737634E-07	stem_cells	IGF2
4.7025008989883E-11	0.932198958555707	0.756	0.468	8.61592214712636E-07	stem_cells	CYP26A1
4.70335823954498E-11	0.476304880369461	0.463	0.205	8.61749296649432E-07	stem_cells	FUT11
5.05768234710921E-11	0.445797250042803	0.817	0.601	9.26668559637349E-07	stem_cells	EPB41L4A-AS1
6.04579783571096E-11	0.448077814074914	0.976	0.595	1.10771107945896E-06	stem_cells	ZFP36L1
8.45587695196095E-11	0.449421757050093	0.939	0.677	1.54928577513829E-06	stem_cells	SOX2
2.60429113395465E-10	0.409270588084847	0.951	0.616	4.7715822156317E-06	stem_cells	TTYH1
2.77283825332965E-10	0.555634437665896	0.878	0.642	5.08039424775058E-06	stem_cells	FOS
3.78145639821663E-10	0.406640746701272	0.817	0.463	6.92838441281252E-06	stem_cells	COL2A1
4.16098479991514E-10	0.456574429784865	0.622	0.339	7.62375635040452E-06	stem_cells	ALDOC
6.12133792825982E-10	1.07289940316878	0.805	0.655	1.12155153521576E-05	stem_cells	LDHA
1.28505249072398E-09	0.415821638097638	0.902	0.723	2.35447317350447E-05	stem_cells	WDR54
1.80795618048771E-09	0.421831266152089	0.793	0.467	3.31253731388959E-05	stem_cells	HES1
1.95130959731126E-09	0.408323810311751	0.39	0.163	3.5751894441937E-05	stem_cells	SHISA2
2.34489525140674E-09	0.434753644717505	0.683	0.412	4.29631707962743E-05	stem_cells	CDH11
1.29572466251907E-06	0.436965304690629	0.866	0.754	0.0237402672666744	stem_cells	JUN

SupTable 3 enriched_genes NEP

pval	neg_log10_pval	neg_log10_pval2	pval2	cluster	gene
0	2.15040505118418	0.999	0.526	0	progenitors SFRP2
0	1.84620823017618	0.853	0.252	0	progenitors CYP26A1
0	1.7779501569875	0.996	0.312	0	progenitors ZFP36L1
0	1.69432772775035	0.962	0.278	0	progenitors IFITM3
0	1.58805350397233	0.991	0.412	0	progenitors CCND1
0	1.5118992094342	1	0.769	0	progenitors VIM
0	1.51158747141804	0.95	0.478	0	progenitors CYP1B1
0	1.50081898363016	0.886	0.111	0	progenitors HES1
0	1.43894021706406	0.987	0.366	0	progenitors TTYH1
0	1.41658802756201	0.967	0.336	0	progenitors SPP1
0	1.36233899346843	0.89	0.167	0	progenitors IFITM2
0	1.19038378143608	0.949	0.384	0	progenitors PTH2
0	1.13959166958294	0.753	0.068	0	progenitors IFITM1
0	1.10272592225554	0.976	0.394	0	progenitors B2M
0	1.07258690507434	0.708	0.072	0	progenitors DIO3
0	1.06064854984826	1	0.946	0	progenitors MDK
0	0.998562811126669	0.99	0.388	0	progenitors SOX2
0	0.982144843698158	0.835	0.194	0	progenitors SPARC
0	0.940469155316309	0.952	0.445	0	progenitors NPC2
0	0.924835620594991	0.8	0.115	0	progenitors COL2A1
0	0.891965322538018	0.853	0.182	0	progenitors PLPP3
0	0.858223139553094	0.823	0.193	0	progenitors RARRES2
0	0.829239017675723	0.774	0.138	0	progenitors SEPP1
0	0.611513462513307	1	0.997	0	progenitors RPL41
0	0.607867011145783	1	0.999	0	progenitors RPLP1
4.5565809296804E-306	1.25465556113166	0.724	0.125	8.98010969621414E-302	progenitors CYR61
7.01747328804271E-298	0.648746970281072	1	0.998	1.38300363560746E-293	progenitors RPS6
1.04873209981533E-291	0.529887256136855	1	0.999	2.06684122231604E-287	progenitors RPS15
1.54275789435023E-291	0.5564828974854	0.602	0.058	3.04046725818543E-287	progenitors NR2E1
1.85149631563151E-286	0.623171648126435	0.681	0.106	3.64892893884659E-282	progenitors FZD5
2.83420823904368E-285	0.644308798138501	0.725	0.127	5.58565759750729E-281	progenitors VSX2
1.07566682533779E-278	0.726544571918545	0.761	0.178	2.11992417937571E-274	progenitors TBX2-AS1
8.14018412000608E-278	1.01968624867888	0.687	0.127	1.6042674863708E-273	progenitors FGF19
1.03987150368727E-272	0.506985107386541	1	0.999	2.04937875946688E-268	progenitors RPL7

1.58215494469246E-271	0.557264134430693	0.999	0.996	3.11811096499989E-267	progenitors	RPS12
1.9046169276379E-270	1.05144269717324	0.938	0.422	3.75361904098878E-266	progenitors	EGR1
8.35783148439857E-265	0.667245369960028	0.989	0.897	1.64716142894527E-260	progenitors	EEF1D
1.86590968583823E-255	0.726085010108623	0.521	0.047	3.67733480884998E-251	progenitors	PAX2
8.54983978960253E-255	0.463171612235164	1	1	1.68500242573487E-250	progenitors	RPL13
5.94111854900557E-253	0.720672532677586	0.714	0.158	1.17087564363802E-248	progenitors	S1PR3
6.08760845613205E-252	0.475769643533867	1	0.999	1.1997458745345E-247	progenitors	RPS18
1.4552044742305E-250	0.825064164623589	0.599	0.087	2.86791697781348E-246	progenitors	LAMP5
1.15740345698241E-248	0.494024081926888	0.999	0.996	2.28101073302093E-244	progenitors	RPS17
3.85782772727678E-248	1.02847546402989	0.976	0.68	7.60300688491708E-244	progenitors	IER2
3.39190911710649E-245	0.4883334965077	1	0.996	6.68477448799347E-241	progenitors	RPS27A
4.15405733323629E-242	1.05750319145763	0.889	0.426	8.18681619234207E-238	progenitors	JUNB
7.31512196118627E-241	0.429689060603398	1	1	1.44166423611059E-236	progenitors	RPS23
2.26416146045891E-238	1.22461940862618	0.95	0.546	4.46220940627242E-234	progenitors	FOS
6.46829571679791E-237	0.464847632372436	0.999	0.997	1.27477171986653E-232	progenitors	RPS4X
5.13100653399235E-236	0.58466767159198	0.553	0.072	1.01121876771921E-231	progenitors	SPHK1
8.45611716498731E-236	0.481963295278201	0.999	0.997	1.6665315708757E-231	progenitors	RPS24
2.29948464262219E-235	0.503503382028323	1	0.996	4.53182433367982E-231	progenitors	RPLP0
2.83847284239452E-231	0.461168230860425	1	0.996	5.59406227779111E-227	progenitors	RPS8
8.11378951261563E-231	0.527575096829775	0.645	0.119	1.59906563714629E-226	progenitors	FKBP10
1.11416643679946E-229	0.689821874670287	0.58	0.091	2.19579921364438E-225	progenitors	CDH6
7.89990460958792E-229	0.462343408276226	1	1	1.55691320045759E-224	progenitors	RPS2
8.13853226605996E-229	0.425433734087254	1	0.999	1.6039419389951E-224	progenitors	RPS3A
9.37113660230277E-228	0.667537437232447	0.931	0.448	1.84686360158183E-223	progenitors	CD99
2.44434338204269E-227	0.495359164622597	0.579	0.085	4.81731193732974E-223	progenitors	ZFP36L2
5.11555755656643E-226	0.497488648135855	0.999	0.992	1.00817408324811E-221	progenitors	RPL12
2.71599833412094E-225	0.431094428300721	1	0.998	5.35268951688556E-221	progenitors	RPS15A
7.42425352579234E-225	0.651663300475304	0.801	0.269	1.46317188486315E-220	progenitors	RHOC
5.24958638200182E-223	0.759082507319616	0.991	0.678	1.03458848416492E-218	progenitors	DKK 3.00
2.72649484573062E-222	0.745126895393068	0.948	0.53	5.3733760419659E-218	progenitors	MEST
2.69536525455495E-220	0.760665550803343	0.633	0.139	5.31202584367689E-216	progenitors	GINS2
1.03084171383134E-218	0.845458285086427	0.624	0.13	2.03158284961881E-214	progenitors	KIAA0101
6.14113377862115E-216	0.441861150683239	1	0.997	1.21029464509066E-211	progenitors	RPS7
3.95110548276282E-214	0.863295849210544	0.527	0.075	7.78683868542897E-210	progenitors	PLP1
5.54342352645723E-213	0.541793553332015	0.683	0.16	1.09249790859419E-208	progenitors	EMP3
1.04402474684944E-210	0.557704628654513	0.675	0.16	2.05756397109087E-206	progenitors	CDH11

3.38966906875755E-210	0.484549513712367	0.423	0.032	6.68035980070737E-206	progenitors	MIR503HG
1.0584002645718E-208	1.47309084340855	0.776	0.286	2.08589524141811E-204	progenitors	ID3
3.44869062332934E-208	0.444375200078535	0.455	0.044	6.79667948045745E-204	progenitors	PRSS35
1.28747658466765E-207	0.474695639057121	0.437	0.038	2.537358853063E-203	progenitors	PREL P
1.45985095206567E-202	0.431691444544447	0.5	0.068	2.87707425633101E-198	progenitors	ETV5
9.79229570759391E-202	0.502072109466633	0.617	0.128	1.92986563805261E-197	progenitors	LINC01508
5.98568695628132E-201	0.708226460560816	0.939	0.525	1.17965918534392E-196	progenitors	RP11-89K2
7.13969468480387E-201	0.709375605778812	0.944	0.627	1.40709102848115E-196	progenitors	DEK
9.12110521616475E-200	0.416636966854981	1	0.997	1.79758741600175E-195	progenitors	RPL10A
1.94303879372938E-197	0.70512950883938	0.978	0.699	3.82934085468187E-193	progenitors	DAPL1
2.36036337708525E-197	0.596461957784727	0.692	0.196	4.6518041435596E-193	progenitors	TIMP1
3.88959074782277E-197	0.606973261319248	0.988	0.794	7.66560544580911E-193	progenitors	HMGN3
8.54500374497677E-196	0.881610683224293	0.81	0.317	1.68404933806002E-191	progenitors	ID1
7.43620624702996E-193	0.789548717289947	0.762	0.282	1.46552752716466E-188	progenitors	TYMS
1.96984930328418E-186	0.532793694811181	0.669	0.182	3.88217900691246E-182	progenitors	HOMER2
2.75467127248655E-185	0.437681412865897	0.999	0.977	5.4289061438165E-181	progenitors	RPS10
3.23387515326861E-185	0.609806007743117	0.638	0.169	6.37332115206178E-181	progenitors	HELLS
1.38122541321473E-184	0.420039136558848	0.5	0.081	2.72211904436358E-180	progenitors	MOB3B
2.33198396061786E-184	0.590828208221481	0.991	0.819	4.59587398958568E-180	progenitors	SIX6
6.78134123393227E-183	0.562806665693119	0.966	0.698	1.33646673038337E-178	progenitors	PRDX6
6.23133700110186E-180	0.422085586670628	0.999	0.993	1.22807189617716E-175	progenitors	RPS20
1.24952697023467E-174	0.40738901791358	0.999	0.993	2.46256775293848E-170	progenitors	RPSA
8.96754394349379E-174	0.925119848751912	0.896	0.541	1.76732356038376E-169	progenitors	HMGB2
2.42585282381135E-170	0.629018894750313	0.988	0.876	4.78087074516741E-166	progenitors	HMGN2
2.46007544668514E-169	0.452223924853336	0.515	0.096	4.84831669032708E-165	progenitors	ZWINT
3.48505172472822E-168	0.461652683635937	0.566	0.129	6.86833993909438E-164	progenitors	PCDH11X
2.60428129916815E-167	0.460886629792215	0.616	0.159	5.13251758440059E-163	progenitors	LHX2
1.74711926311189E-166	0.619268427314819	0.929	0.583	3.44322264374091E-162	progenitors	ISYNA1
2.78867301788225E-166	0.43400576202701	0.482	0.083	5.49591678364234E-162	progenitors	IGF2
1.99695173105959E-165	0.443740000514142	0.479	0.084	3.93559247157225E-161	progenitors	MCM5
4.65366528356967E-165	0.549913414119216	0.45	0.069	9.17144354085911E-161	progenitors	ZFP36
1.76869573751937E-162	0.619277252039849	0.629	0.198	3.48574555950318E-158	progenitors	MCM3
6.63044407403802E-161	0.485191844352536	0.638	0.192	1.30672791811141E-156	progenitors	NPM3
6.34122389858948E-160	0.780277742950926	1	0.982	1.24972840593402E-155	progenitors	TUBA1B
5.17672996915231E-156	0.536366931081705	0.955	0.666	1.02022994232054E-151	progenitors	CLIC1
2.60496545279018E-155	0.521501539090796	0.72	0.266	5.13386591435889E-151	progenitors	RPL22L1

1.82752955345995E-154	0.544321282287025	0.697	0.245	3.60169524395888E-150	progenitors	STR6
1.69214246964537E-152	0.489822135077869	0.61	0.18	3.33487437917709E-148	progenitors	CENPH
1.21148753693839E-151	0.668646151393418	0.752	0.329	2.38759963779818E-147	progenitors	CKS1B
1.46389445459581E-151	0.464577606213431	0.68	0.226	2.88504319111743E-147	progenitors	CYBA
1.59619019814329E-151	0.66630508087723	0.547	0.136	3.14577164250079E-147	progenitors	CDK1
1.9991722115486E-150	0.495276391693545	0.627	0.188	3.93996859451998E-146	progenitors	PLA2G16
3.11317132980118E-149	0.542986788987709	0.825	0.425	6.13543805677218E-145	progenitors	SIVA1
6.78200863664974E-148	0.460288627565188	0.597	0.173	1.33659826211093E-143	progenitors	COL18A1
9.3459378342738E-148	0.706891577523547	0.551	0.151	1.84189742837868E-143	progenitors	FOSB
8.42235880186396E-147	0.502278126572407	0.73	0.279	1.65987847267135E-142	progenitors	NUDT4
8.29049590232825E-145	0.449259082746273	0.361	0.045	1.63389093243085E-140	progenitors	COL1A2
9.46175068289337E-143	0.47153924723958	0.76	0.325	1.86472182458463E-138	progenitors	DNPH1
3.18056600689875E-141	0.497209052212188	0.948	0.654	6.26825948639605E-137	progenitors	OSTC
1.22196478779648E-138	0.442753983577262	0.63	0.199	2.4082482037893E-134	progenitors	CDCA7L
3.17651193434005E-138	0.783938665841716	0.713	0.323	6.26026972019737E-134	progenitors	SMC4
9.56118852754561E-134	0.44966879215667	0.73	0.295	1.88431903500869E-129	progenitors	DNAJC1
2.3631024644484E-133	0.751848692037366	0.469	0.108	4.65720233693491E-129	progenitors	MKI67
6.9377776571229E-133	0.544623940918142	0.624	0.214	1.36729722066578E-128	progenitors	MAD2L1
2.84586989251484E-132	0.996650594700696	0.579	0.192	5.60864038416825E-128	progenitors	TOP2A
7.40711505854529E-132	0.519005248575616	0.755	0.33	1.45979423573811E-127	progenitors	DCBL2
6.7012257927382E-131	0.467514830215978	0.54	0.155	1.32067757923284E-126	progenitors	DHFR
1.06912285100712E-130	0.718259241079908	0.541	0.158	2.10702731476484E-126	progenitors	NUSAP1
3.49476035561271E-127	0.596900544623302	0.522	0.155	6.88747370884152E-123	progenitors	ATP6V1B1
6.6197829254232E-127	0.481171855614184	0.999	0.934	1.3046268189424E-122	progenitors	CLU
3.72848951564238E-126	0.952197004060949	0.573	0.194	7.348107137428E-122	progenitors	CENPF
2.22289121698759E-125	0.443280898921937	0.956	0.762	4.38087401043915E-121	progenitors	AC090498.
5.44476707943671E-125	0.478798198322899	0.738	0.342	1.07305469601539E-120	progenitors	TMEM106C
2.75846716041847E-124	0.422467472725933	0.973	0.745	5.43638707975273E-120	progenitors	SEC11A
1.46632650172944E-122	0.406768989126067	0.661	0.256	2.88983626960838E-118	progenitors	GPX7
2.10289238868643E-121	0.497082438310558	0.427	0.092	4.14438031962321E-117	progenitors	PBK
2.19763545546435E-120	0.523111932653521	0.547	0.177	4.33109995562914E-116	progenitors	HLA-DRB1
2.40642391839199E-119	0.459273096182137	0.775	0.377	4.74258025836694E-115	progenitors	CALD1
2.56983392386029E-119	0.45194442679346	0.879	0.551	5.06462869714386E-115	progenitors	GLO1
7.77333889336279E-119	0.617191822121801	0.704	0.345	1.53196962910394E-114	progenitors	PCNA
4.4109191334914E-118	0.521042858521778	0.901	0.605	8.69303942828485E-114	progenitors	MUM1
3.97945367768617E-115	0.406797504996382	0.705	0.296	7.8427073079839E-111	progenitors	TSPAN6

2.04715615197448E-113	0.817081027041132	0.83	0.524	4.0345353443113E-109	progenitors	CKS2
1.6742130441657E-112	1.2044479952532	0.904	0.683	3.29953906744177E-108	progenitors	HIST1H4C
2.0838431812512E-112	0.4229954811784	0.542	0.169	4.10683814160987E-108	progenitors	MIS18BP1
1.9482881014543E-111	0.412555395860981	0.702	0.29	3.83968619034614E-107	progenitors	ID2
9.0233431062401E-108	0.665378842516656	0.519	0.174	1.7783204593778E-103	progenitors	BIRC5
2.13962744300684E-106	0.484562537609016	0.403	0.094	4.21677776467789E-102	progenitors	CCNA2
3.63809365870995E-106	0.572625937069071	0.427	0.113	7.16995498258558E-102	progenitors	AURKB
6.17518949007665E-106	0.447102234434463	0.756	0.391	1.21700634470431E-101	progenitors	RPA3
1.31189794362135E-105	0.410453632884263	0.592	0.221	2.58548846728897E-101	progenitors	CRB1
8.50347466761307E-105	0.419000948744495	0.392	0.09	1.67586478749318E-100	progenitors	KIFC1
1.37375534219405E-102	0.428078624914188	0.981	0.874	2.70739702839604E-98	progenitors	CNN3
4.80536994513009E-102	0.746780405844476	0.699	0.343	9.47042308786237E-98	progenitors	PTTG1
7.70946094977608E-102	0.436143019713762	0.374	0.083	1.51938056398187E-97	progenitors	GTSE1
1.47875227592335E-101	0.658506946610159	0.479	0.155	2.91432498538975E-97	progenitors	TPX2
9.02151256130728E-101	0.416993029930025	0.947	0.685	1.77795969558244E-96	progenitors	LMAN1
6.11640531699555E-100	0.445316056128903	0.916	0.696	1.20542115987348E-95	progenitors	H2AFV
5.62989443127496E-99	0.422815731706129	0.729	0.359	1.10953959451567E-94	progenitors	CCDC34
2.04218025861793E-98	0.407605906699309	0.725	0.358	4.02472885368422E-94	progenitors	FOXP1
1.67653646769194E-97	0.426518809278348	0.83	0.506	3.30411807052727E-93	progenitors	CDK4
8.84056976370459E-97	0.440377541938533	0.606	0.262	1.7422994890309E-92	progenitors	DNAJC9
2.64678577045114E-96	0.811950705691701	0.61	0.275	5.21628539640511E-92	progenitors	UBE2C
4.94399773343369E-95	0.428594540905955	0.41	0.11	9.74363073305111E-91	progenitors	CDKN3
5.11969901965996E-95	0.450090884224192	0.996	0.988	1.00899028279458E-90	progenitors	H2AFZ
3.15849628632203E-92	0.409829653113198	0.854	0.522	6.22476448108346E-88	progenitors	ITM2C
1.53355737602474E-90	0.464503842998076	0.849	0.555	3.02233487666956E-86	progenitors	GPM6B
9.64980668076151E-90	0.640637851485515	0.402	0.114	1.90178390064448E-85	progenitors	CDC20
4.35799647565777E-88	0.434651407601529	0.524	0.201	8.58873945422633E-84	progenitors	FGFBP3
6.08505694317111E-88	0.41273997728971	0.519	0.202	1.19924302236016E-83	progenitors	FEN1
5.92399633379978E-86	0.463730660108884	0.507	0.196	1.16750119746526E-81	progenitors	H2AFX
6.23123486940603E-86	0.542792801104527	0.518	0.191	1.22805176806254E-81	progenitors	CCNB2
3.23296997637366E-84	0.474676187227268	0.346	0.088	6.37153722943721E-80	progenitors	ASPM
2.73225229607898E-82	0.643268248722417	0.431	0.144	5.38472282511246E-78	progenitors	CCNB1
4.92406973131467E-81	0.407411388333705	0.67	0.352	9.70435662647496E-77	progenitors	DTYMK
7.60009429867636E-81	0.457200369249005	0.968	0.859	1.49782658438314E-76	progenitors	NUCKS1
6.97455969729792E-74	0.41460563718661	0.861	0.627	1.37454622514347E-69	progenitors	NASP
1.2126670133732E-73	0.437902328729029	0.724	0.447	2.38992414995591E-69	progenitors	MCM7

4.07490406829252E-66	0.412511109453606	0.887	0.7	8.0308209377909E-62	progenitors	DUT
1.29060905398246E-63	0.530431632416825	0.783	0.489	2.54353232358862E-59	progenitors	PRSS23
1.95181232632104E-61	0.580023176103614	0.92	0.753	3.84663173271351E-57	progenitors	JUN
1.97679919792457E-53	0.511814606185033	0.275	0.085	3.89587585926975E-49	progenitors	GPX3
9.78296259273259E-142	1.00806646503772	0.746	0.107	1.92802626777574E-137	existing_prog	RRM2
2.45908256222127E-139	0.989123794897765	0.633	0.072	4.84635991362568E-135	existing_prog	MFAP4
1.10555993172024E-133	1.06315409177626	0.78	0.123	2.17883751343424E-129	existing_prog	NUF2
1.67070256396834E-133	1.17906911727233	0.746	0.109	3.29262061306881E-129	existing_prog	VSX1
9.46604069556985E-133	0.995658296124311	0.802	0.133	1.86556730028291E-128	existing_prog	GTSE1
6.41520556006799E-132	0.861764828251533	0.825	0.143	1.2643087117782E-127	existing_prog	KIFC1
3.45395564443587E-131	0.9810336112462	0.763	0.124	6.80705578405421E-127	existing_prog	FAM64A
3.28705984419491E-127	0.569512091408498	0.61	0.072	6.47813754093932E-123	existing_prog	CDKN2C
4.63416075000379E-126	0.585752117834348	0.277	0.009	9.13300400610748E-122	existing_prog	RP11-843A
4.73742537717864E-124	1.19016775184641	0.802	0.15	9.33651793334365E-120	existing_prog	CCNA2
2.170971625302E-122	0.880578965381398	0.729	0.114	4.27855087914518E-118	existing_prog	CKAP2L
7.19119665240812E-122	1.17029274581552	0.808	0.155	1.41724103625659E-117	existing_prog	PBK
9.39016262972125E-122	1.5665779818246	0.91	0.233	1.85061325106546E-117	existing_prog	NUSAP1
1.32798740317432E-121	0.89090955539655	0.757	0.13	2.61719757417595E-117	existing_prog	SPC25
3.86628478524458E-121	1.26617100726619	0.859	0.176	7.61967405476002E-117	existing_prog	MKI67
4.16829231115411E-121	0.575773357509693	0.548	0.06	8.21487048682252E-117	existing_prog	CEP55
4.26844247354534E-121	0.634834030553662	0.678	0.098	8.41224642686316E-117	existing_prog	RTKN2
4.47598905334451E-119	0.612504152883437	0.667	0.096	8.82127922633137E-115	existing_prog	SPAG5
1.17077471880848E-114	0.825028458958611	0.684	0.104	2.30736281582775E-110	existing_prog	DLGAP5
1.46061918309493E-113	0.754405352200697	0.797	0.153	2.8785882860435E-109	existing_prog	CENPU
5.89479884790682E-113	1.66641195406698	0.938	0.268	1.16174695694548E-108	existing_prog	TOP2A
8.53962652717362E-111	1.16917819309251	0.831	0.198	1.68298959597538E-106	existing_prog	PRC1
1.60956616038668E-108	1.29796802448667	0.876	0.214	3.17213298889008E-104	existing_prog	TPX2
7.40203771970024E-107	0.823966034194658	0.831	0.182	1.45879359379852E-102	existing_prog	ZWINT
7.56365131315715E-106	0.685394568399064	0.678	0.112	1.49064440079701E-101	existing_prog	NDC80
1.07105765171743E-105	1.0587551561342	0.853	0.231	2.11084042000471E-101	existing_prog	UBE2T
1.25696740572894E-105	0.653137805420613	0.588	0.082	2.47723136321059E-101	existing_prog	BUB1
1.42420851133106E-105	1.35131246829526	0.864	0.221	2.80683013413125E-101	existing_prog	CDK1
4.26196227104595E-105	0.667069937475393	0.638	0.099	8.39947524377736E-101	existing_prog	KIF23
1.39509102730858E-104	0.455187294654011	0.48	0.052	2.74944539661975E-100	existing_prog	CDC25C
2.94740744568244E-104	0.925777194185158	0.701	0.128	5.80875059395096E-100	existing_prog	CDCA3
2.58118069852668E-103	0.567768377316802	0.605	0.088	5.08699092065638E-99	existing_prog	HJURP

1.03367730894225E-102	1.174822131225	0.768	0.165	2.03717124046339E-98	existing_prog	CDKN3
3.35715793611157E-102	0.821968763650528	0.718	0.137	6.61628686048868E-98	existing_prog	SGOL1
8.07106082168513E-102	0.790919213420977	0.672	0.116	1.59064466673771E-97	existing_prog	CDCA8
8.35775204582763E-102	0.534699955679976	0.588	0.085	1.64714577319171E-97	existing_prog	CASC5
1.40780164288421E-101	0.653992623196828	0.791	0.162	2.7744954777962E-97	existing_prog	CENPN
2.14971696018152E-101	0.470111876484793	0.593	0.087	4.23666218512574E-97	existing_prog	POC1A
5.49770278273825E-101	1.07754074082199	0.78	0.172	1.08348726442205E-96	existing_prog	AURKB
1.53908226348524E-100	0.678794093864835	0.763	0.149	3.03322332487671E-96	existing_prog	C21orf58
6.20697903196291E-100	1.14931707376786	0.927	0.299	1.22327142761925E-95	existing_prog	MAD2L1
1.80470058932671E-99	1.25051336453338	0.876	0.241	3.55670392144507E-95	existing_prog	BIRC5
1.29350913432114E-98	1.67066088043172	0.91	0.27	2.5492478019201E-94	existing_prog	CENPF
3.92446644386748E-97	0.48128974539536	0.593	0.09	7.73433846757403E-93	existing_prog	KIF15
2.67999799890103E-96	0.661712789063409	0.672	0.12	5.28174005623416E-92	existing_prog	MXD3
8.52335095558875E-94	0.555490692030685	0.684	0.126	1.67978200632743E-89	existing_prog	RAD51AP1
1.086617967745E-93	1.89557367559608	0.994	0.623	2.14150669083185E-89	existing_prog	HMGB2
3.81791660976481E-92	1.35045892438503	0.96	0.406	7.52435005452448E-88	existing_prog	SMC4
5.00362590068373E-92	0.838937409462381	0.678	0.132	9.86114592506749E-88	existing_prog	SGOL2
1.65867025469401E-91	1.34545562323224	1	0.986	3.26890733795095E-87	existing_prog	TUBA1B
2.50334683364065E-91	1.405817569228	0.96	0.422	4.93359593973899E-87	existing_prog	CKS1B
1.80685316554711E-90	1.14159070456454	0.983	0.436	3.56094621866024E-86	existing_prog	CCDC34
1.83229007897052E-90	0.83589275289571	0.825	0.225	3.61107728763509E-86	existing_prog	CENPW
3.90149312366487E-90	0.958460026819192	0.627	0.112	7.68906264811872E-86	existing_prog	NEK2
3.91477015644521E-90	0.580099334797121	0.588	0.095	7.71522902432223E-86	existing_prog	KIF2C
4.48746356186626E-90	0.647579422577605	0.503	0.069	8.84389318772602E-86	existing_prog	KIF20A
2.01132037055839E-89	0.597729135940204	0.559	0.085	3.96391018629648E-85	existing_prog	TROAP
2.26566738600831E-89	0.711104812949586	0.757	0.166	4.46517728434517E-85	existing_prog	FBXO5
1.38952887466771E-88	1.39020620894491	0.994	0.903	2.73848350619513E-84	existing_prog	HMGN2
2.79969141319241E-88	0.510871255032856	0.588	0.098	5.5176318371196E-84	existing_prog	CDCA5
3.53730875218861E-87	0.997274494596279	1	0.99	6.97132808881331E-83	existing_prog	H2AFZ
4.32006107482677E-86	0.591989183316456	0.621	0.114	8.5139763662686E-82	existing_prog	NCAPG
3.93071268797733E-85	0.864726462276089	0.842	0.245	7.74664856546572E-81	existing_prog	MIS18BP1
5.26708461090518E-85	0.422561419680751	0.514	0.075	1.03803703511719E-80	existing_prog	FOXN4
6.06845338013958E-85	0.482389030230378	0.537	0.083	1.19597079215791E-80	existing_prog	ARHGAP11
8.54682960344488E-85	0.597843474777176	0.723	0.155	1.68440917824692E-80	existing_prog	CENPK
1.70337875718876E-84	0.816205262512284	0.898	0.287	3.3570188546676E-80	existing_prog	SMC2
2.34020876500761E-84	1.24932680574919	1	1	4.612083434077E-80	existing_prog	CKB

3.22300395018262E-84	0.901289232860215	0.599	0.113	6.3518961850199E-80	existing_prog	AURKA
7.22854279008206E-83	0.891300301785784	0.847	0.255	1.42460121306937E-78	existing_prog	H2AFX
7.82767250167975E-83	1.85265267079734	1	0.794	1.54267769663105E-78	existing_prog	HES6
8.04941743125568E-83	0.866796042726614	1	0.993	1.58637918735187E-78	existing_prog	HMGB1
9.66644152436992E-82	0.704801757086453	0.842	0.237	1.90506229562282E-77	existing_prog	ORC6
2.00287774986469E-81	1.1130087882453	0.718	0.169	3.94727146943332E-77	existing_prog	CDC20
2.63247308773326E-81	0.545273382052501	0.616	0.113	5.18807796130471E-77	existing_prog	MYBL1
2.727204989931E-81	0.455193524949636	0.565	0.096	5.37477559415601E-77	existing_prog	MELK
3.41802100877732E-81	0.824711602807656	0.571	0.101	6.73623580409834E-77	existing_prog	CENPA
4.1741409717303E-81	0.910258692925409	0.554	0.095	8.22639702708608E-77	existing_prog	PLK1
1.97289656102834E-79	1.85868819317848	0.876	0.344	3.88818454247465E-75	existing_prog	UBE2C
2.52997298678501E-79	0.674005324024921	0.554	0.095	4.98607076235589E-75	existing_prog	CENPE
4.46427847796062E-79	0.855341599346649	0.65	0.136	8.79820002436479E-75	existing_prog	ASPM
1.17595852176015E-78	1.04258910171645	0.864	0.299	2.3175790546849E-74	existing_prog	CKAP2
2.58575418410828E-78	0.455544139705426	0.508	0.079	5.09600434604061E-74	existing_prog	TTK
7.30060797051741E-78	0.474174614030244	0.435	0.059	1.43880381882957E-73	existing_prog	ZMYND10
7.07525058074481E-77	0.420290302386737	0.452	0.064	1.39439038445319E-72	existing_prog	FAM83D
3.4226528189701E-76	0.76161936806298	0.65	0.143	6.74536417562627E-72	existing_prog	PSRC1
4.23151140536731E-75	0.507402550051183	0.497	0.078	8.3394626776979E-71	existing_prog	HMMR
1.50340794589156E-74	0.671288018024771	0.706	0.177	2.96291637976309E-70	existing_prog	TACC3
1.71787755066228E-74	0.509786119440735	0.655	0.145	3.38559307684523E-70	existing_prog	LRR1
2.03371459409402E-74	0.49179230828697	0.475	0.073	4.00804472204049E-70	existing_prog	APOLD1
3.7443045579389E-74	0.897628141924737	0.989	0.788	7.37927542278598E-70	existing_prog	IDH2
5.87357800682883E-73	0.748447510528848	0.74	0.196	1.15756475358583E-68	existing_prog	KIF20B
6.42150718139983E-73	1.02843572933786	0.932	0.391	1.26555063531028E-68	existing_prog	TYMS
2.5657495980799E-72	0.966930626336587	0.819	0.241	5.05657930789586E-68	existing_prog	KIAA0101
1.94190699551427E-71	0.487772315591603	0.503	0.086	3.82711030675952E-67	existing_prog	PRR11
3.81252477950681E-70	1.29178479738947	0.797	0.257	7.51372383545202E-66	existing_prog	CCNB2
2.01269676074537E-69	0.433401019233152	0.452	0.07	3.96662277607697E-65	existing_prog	DEPDC1
7.0043335639928E-69	1.48098372730913	0.904	0.419	1.3804140587917E-64	existing_prog	PTTG1
3.72575218773825E-68	0.420038434578498	0.537	0.102	7.34271241159454E-64	existing_prog	SPC24
8.70039032209819E-68	0.455985717553871	0.605	0.129	1.71467292467911E-63	existing_prog	MND1
2.56481597426351E-67	0.796674471684897	0.831	0.304	5.05473932207853E-63	existing_prog	KIF22
5.24580449915733E-67	0.538816614163287	0.52	0.102	1.03384315069393E-62	existing_prog	ECT2
2.81750811464345E-66	0.897657440109799	0.91	0.462	5.5527449923393E-62	existing_prog	ANP32E
9.79178615237431E-66	0.818180571451788	0.893	0.39	1.92976521490993E-61	existing_prog	USP1

9.93504548089555E-66	0.737794001142456	0.932	0.415	1.95799876337489E-61	existing_prog	LMNB1
1.27583155922524E-65	0.448413131507791	0.497	0.09	2.5144088369211E-61	existing_prog	MCM10
1.65153895218423E-65	0.502687517279772	0.582	0.122	3.25485296696468E-61	existing_prog	ASF1B
2.31498751216334E-65	0.588365864147076	0.633	0.156	4.56237738897151E-61	existing_prog	RACGAP1
8.50261188558655E-65	1.22860303732218	0.944	0.593	1.6756947504114E-60	existing_prog	CKS2
1.95606740751467E-64	0.864626749689703	0.989	0.702	3.85501764672992E-60	existing_prog	DEK
2.60066359008539E-63	0.837997185188659	0.966	0.747	5.12538780334029E-59	existing_prog	H2AFV
1.46248722056402E-62	0.407581741750791	0.497	0.093	2.88226981428756E-58	existing_prog	CCDC18
4.59755798935861E-62	0.422842431585979	0.463	0.083	9.06086728542796E-58	existing_prog	KIF4A
1.10304169520909E-61	0.600226742426714	0.763	0.248	2.17387457291808E-57	existing_prog	CDCA4
2.38464892531946E-61	0.697106110643131	0.853	0.353	4.6996661020196E-57	existing_prog	EZH2
8.27590298921946E-61	1.23065609748907	0.689	0.201	1.63101496111537E-56	existing_prog	CCNB1
1.08451906086297E-60	0.67305447501417	0.853	0.318	2.13737016514874E-56	existing_prog	UCP2
1.1186531744269E-60	0.725871362299526	0.797	0.287	2.20464167616054E-56	existing_prog	RNASEH2A
1.75933844343441E-60	0.753886071720536	0.932	0.475	3.46730420432053E-56	existing_prog	BTG3
4.85475477712817E-60	0.613932746061378	0.814	0.275	9.56775071476419E-56	existing_prog	CENPH
6.08920962421141E-60	0.74818433156371	0.932	0.504	1.20006143273959E-55	existing_prog	TMPO
1.94517864281097E-59	0.451960962880871	0.599	0.142	3.83355806925186E-55	existing_prog	CENPM
7.8925846669526E-58	0.528997491702145	0.559	0.134	1.55547058616302E-53	existing_prog	DEPDC1B
1.86937605231777E-56	0.6084268597402	0.599	0.155	3.68416632390786E-52	existing_prog	CLSPN
8.86276566888066E-56	0.624544484604792	0.616	0.167	1.746673858023E-51	existing_prog	ATAD2
3.34949051435114E-55	0.787915419612049	1	0.884	6.60117590568323E-51	existing_prog	NUCKS1
2.26865260598881E-54	1.38392772109004	0.904	0.604	4.47106055588274E-50	existing_prog	UBE2S
3.77148906476272E-53	0.471122481785246	0.638	0.179	7.43285064883437E-49	existing_prog	CRNDE
2.18546718572024E-52	0.623682207126468	0.718	0.24	4.30711872961745E-48	existing_prog	DHFR
3.72605644419581E-52	0.629578221067851	0.78	0.297	7.34331204022111E-48	existing_prog	GMNN
5.98842957445726E-52	0.564948413856855	1	0.999	1.18019970053404E-47	existing_prog	PTMA
6.70759982158703E-52	0.567216583484465	0.734	0.256	1.32193377283837E-47	existing_prog	DBF4
3.45816550088976E-51	0.548563783714363	1	0.98	6.81535256915354E-47	existing_prog	HNRNPA2B
3.83108043228536E-51	0.548654784923356	0.638	0.189	7.55029331594799E-47	existing_prog	TUBB6
4.8624362453213E-51	0.881695548420565	0.977	0.795	9.58288935227922E-47	existing_prog	HMGB3
4.95935428514767E-51	0.581035980377263	0.554	0.145	9.77389542516902E-47	existing_prog	UHRF1
8.20374593879231E-51	0.712754286029747	0.989	0.897	1.61679424961719E-46	existing_prog	RANBP1
8.90278590013222E-51	0.740677407262719	0.927	0.59	1.75456104519806E-46	existing_prog	MAD2L2
4.10170928883299E-50	0.481650961811979	0.65	0.187	8.08364866643205E-46	existing_prog	PDLIM1
4.19349521936583E-50	0.856109571037723	0.881	0.423	8.26454037832618E-46	existing_prog	PCNA

1.98116518176859E-49	0.515498580412286	0.757	0.283	3.90448034022954E-45	existing_prog	VRK1
5.30053853542092E-49	0.619999962478016	0.994	0.803	1.04463013456076E-44	existing_prog	SNRPB
(which was not certified by peer review) is the author/funder. All rights reserved. No reuse allowed without permission.	0.6781976439925	0.96	0.779	5.00697033272506E-44	existing_prog	CARHSP1
2.54057759931249E-48						
6.07074077319765E-48	0.718795699593204	0.96	0.696	1.19642159158179E-43	existing_prog	TFDP2
1.19126633465106E-47	0.501412631427991	0.994	0.984	2.34774769233032E-43	existing_prog	RAN
5.87408481976091E-47	0.5418091270333	0.989	0.857	1.15766463627848E-42	existing_prog	SRSF7
1.35689746567041E-46	0.465870910306019	0.424	0.09	2.67417352534325E-42	existing_prog	FAM111B
1.61156822864872E-46	0.559402049728481	0.463	0.11	3.1760786650209E-42	existing_prog	HIST1H1D
3.65200182092742E-46	0.490350566665152	0.701	0.24	7.19736518868375E-42	existing_prog	EZR
4.82472918625797E-46	0.498190150399323	0.701	0.25	9.5085762802772E-42	existing_prog	C12orf75
8.26155467708208E-46	0.796654380187221	0.915	0.583	1.62818719575934E-41	existing_prog	AKR7A2
1.42838067018276E-45	0.766035908106085	0.87	0.501	2.81505262479619E-41	existing_prog	MZT1
4.11166786132697E-45	0.537907506342717	0.763	0.286	8.1032750211032E-41	existing_prog	MFGE8
5.45291508730029E-45	0.621556417728169	0.836	0.38	1.07466050540514E-40	existing_prog	RRM1
1.12446441095305E-44	0.781312375279044	0.893	0.501	2.21609446110628E-40	existing_prog	GYG1
2.95280067279388E-44	0.569435837005456	1	0.891	5.81937956594219E-40	existing_prog	PDIA6
3.00103397031426E-44	0.619161003714139	0.989	0.723	5.91443774869534E-40	existing_prog	CENPV
4.69949722402859E-44	0.897593487490285	0.689	0.271	9.26176912911555E-40	existing_prog	KNSTRN
5.00712167034435E-44	0.473181500825733	0.994	0.984	9.86803538791464E-40	existing_prog	HNRNPA0
1.42033825890129E-43	0.609861151992497	0.847	0.42	2.79920264064267E-39	existing_prog	DTYMK
2.43164210604972E-43	0.628644733881976	0.842	0.454	4.79228026260279E-39	existing_prog	DDX39A
9.02214706997938E-43	0.506202386826034	0.989	0.917	1.77808474455154E-38	existing_prog	SRSF3
1.09268088845408E-42	0.755749029275194	0.921	0.637	2.15345549496529E-38	existing_prog	BUB3
2.61075781083971E-42	0.585494704971045	0.989	0.829	5.1452814936029E-38	existing_prog	DBI
2.90199222244024E-42	0.564318165679303	0.797	0.336	5.71924627198523E-38	existing_prog	DNAJC9
4.073276574237E-42	0.490838736058353	0.797	0.339	8.02761347250627E-38	existing_prog	HADH
4.51703340107638E-42	0.690820953674053	0.966	0.712	8.90216942684134E-38	existing_prog	PSIP1
4.55228788129763E-42	0.424315714901858	0.588	0.18	8.97164895646136E-38	existing_prog	JADE1
4.84999865374688E-42	1.78719991772938	0.944	0.735	9.55837734680436E-38	existing_prog	HIST1H4C
1.02944056684045E-41	0.41935954666089	1	0.946	2.02882146912915E-37	existing_prog	ERH
1.64886433996809E-41	0.483276144609987	0.362	0.073	3.24958184120911E-37	existing_prog	DLL4
3.00548679605295E-41	0.60374991535789	0.605	0.206	5.92321337766115E-37	existing_prog	PMAIP1
1.24705109288385E-40	0.551158606229329	0.989	0.833	2.45768829385549E-36	existing_prog	SNRPD1
2.67456467821183E-40	0.585381382084877	0.96	0.691	5.27103206781987E-36	existing_prog	ANP32B
1.13024333559782E-39	0.581914430276756	0.966	0.788	2.22748356579618E-35	existing_prog	TECR
3.46771680491631E-39	0.488215628435611	0.791	0.358	6.83417627912907E-35	existing_prog	ASRGL1

4.09128526848327E-39	0.439283789203002	0.695	0.265	8.06310500712683E-35	existing_prog	RNASEH2B
4.12145659871778E-39	0.572719193669813	0.893	0.507	8.122566664753E-35	existing_prog	SYNE2
5.63257333968628E-39	0.48811236196904	0.983	0.875	1.11006755378537E-34	existing_prog	BANF1
2.36394032170298E-38	0.539004928210256	0.904	0.473	4.65885358601224E-34	existing_prog	RPA3
3.13018532230494E-38	0.498055864135593	0.706	0.256	6.16896923319858E-34	existing_prog	GINS2
3.24514522149949E-38	0.523919201728144	0.785	0.357	6.39553220253119E-34	existing_prog	CTNNAL1
3.31302809035373E-38	0.471085572908277	0.718	0.284	6.52931576046913E-34	existing_prog	RFC4
2.94127830540808E-37	0.59737138026894	0.898	0.518	5.79667128429824E-33	existing_prog	SIVA1
3.61982440301051E-37	0.66215821682425	0.644	0.245	7.13394993345312E-33	existing_prog	DOK5
5.79923996622777E-37	0.632879935743865	0.893	0.506	1.14291421254417E-32	existing_prog	MCM7
8.11333657161096E-37	0.5406593520124	0.684	0.271	1.59897637153309E-32	existing_prog	FEN1
6.58531370063383E-36	0.494483339369225	1	0.991	1.29783362412091E-31	existing_prog	UBB
8.26588804817868E-36	0.576117749680227	0.819	0.378	1.62904121653505E-31	existing_prog	SHD
8.68559258835634E-36	0.411283045810462	0.723	0.297	1.71175658731327E-31	existing_prog	ITGB3BP
1.88490550957592E-35	0.536079828621773	0.977	0.741	3.71477177827223E-31	existing_prog	CSRP2
1.97697840571522E-35	0.532457413543292	0.808	0.399	3.89622904198356E-31	existing_prog	DNMT1
2.71619455828213E-35	1.1533645893571	0.927	0.788	5.35307623546242E-31	existing_prog	KPNA2
8.28900349406814E-35	0.892419562897125	0.989	0.871	1.63359680861095E-30	existing_prog	TUBB4B
8.74369629134982E-35	0.556419757546561	0.684	0.281	1.72320766509922E-30	existing_prog	HELLS
1.18189127197573E-34	0.518763893131513	0.96	0.716	2.32927131880977E-30	existing_prog	CBX5
1.41222155605735E-34	0.50413729996811	0.904	0.54	2.78320624267782E-30	existing_prog	ANXA5
3.20821724517544E-34	0.440928018365813	0.751	0.329	6.32275454679176E-30	existing_prog	NUDT1
4.27304960245336E-34	0.600592308155804	0.966	0.914	8.42132615651507E-30	existing_prog	CALM3
1.35038572142726E-33	0.530380821304621	0.424	0.121	2.66134017978885E-29	existing_prog	ASCL1
3.0095395579442E-33	0.419758748324203	0.52	0.173	5.93120056079644E-29	existing_prog	GPSM2
3.73116575940131E-33	0.568347244472275	0.966	0.679	7.35338147862811E-29	existing_prog	NASP
4.56714014941493E-33	0.41831221266986	0.989	0.902	9.00091980646695E-29	existing_prog	HNRNPU
1.01039006047933E-32	0.470675717651842	0.87	0.482	1.99127673119266E-28	existing_prog	EXOSC8
1.21039704279601E-32	0.425885537547607	0.593	0.215	2.38545049194238E-28	existing_prog	HMGN5
2.70408861499341E-32	0.425136600121727	0.548	0.194	5.32921784242902E-28	existing_prog	SMCO4
4.84782789356195E-32	0.527989812466509	0.983	0.936	9.55409921263189E-28	existing_prog	RBMX
8.25813304643837E-32	0.516769730895201	0.955	0.807	1.62751286079207E-27	existing_prog	RHEB
1.34430658307203E-31	0.564443589543552	0.955	0.718	2.64935941391836E-27	existing_prog	LSM 5.00
1.98463371306193E-31	0.496651463342136	0.989	0.796	3.91131612170246E-27	existing_prog	SRSF2
3.43209733594179E-31	0.480282868137175	0.802	0.409	6.76397742967409E-27	existing_prog	SAE1
4.47184811348766E-31	0.418890810602563	0.61	0.233	8.81311826206149E-27	existing_prog	TP53I13

6.46207467253753E-31	0.466671691676473	0.977	0.84	1.2735456764637E-26	existing_prog	NDUFA6
1.16468709326409E-30	0.482284260302243	0.763	0.39	2.29536532340486E-26	existing_prog	TMEM237
1.62083759929024E-30	0.510866334319127	0.825	0.496	3.1943467406812E-26	existing_prog	TUBG1
3.08858789571486E-30	0.444303537180196	0.972	0.881	6.08698902487486E-26	existing_prog	TMSB15A
4.3645147871486E-30	0.603892036953742	0.927	0.585	8.60158574251247E-26	existing_prog	GADD45A
1.07770874880601E-29	0.425786812531858	0.695	0.305	2.12394840214688E-25	existing_prog	TGIF1
1.44535382052557E-29	0.466165702181996	0.972	0.736	2.84850330949179E-25	existing_prog	SRSF10
2.06967221337849E-29	0.523583376309644	0.904	0.709	4.07890999812633E-25	existing_prog	HNRNPD
2.15546596858761E-29	0.43140895782785	0.96	0.769	4.24799233089246E-25	existing_prog	RBBP7
2.40835223501657E-29	0.429783395990611	0.994	0.951	4.74638058477065E-25	existing_prog	GPX4
4.15861772342804E-29	0.433728448597805	0.983	0.888	8.19580380933198E-25	existing_prog	ILF2
7.64836829433617E-29	1.11423761895894	0.825	0.605	1.50734042344777E-24	existing_prog	NEUROD1
1.17148061545043E-28	0.465846340939341	0.977	0.857	2.30875399692972E-24	existing_prog	ANAPC11
1.53439758716608E-28	0.420208109674026	0.842	0.461	3.02399076478691E-24	existing_prog	PNRC2
2.55711196912337E-28	0.437468427567218	0.972	0.794	5.03955626874833E-24	existing_prog	C12orf57
2.61093348663434E-28	0.628778810400089	0.763	0.441	5.14562771545895E-24	existing_prog	CDKN2D
2.73176043232638E-28	0.421781082786216	0.774	0.394	5.38375346002883E-24	existing_prog	CMC2
7.23754029725594E-28	0.446010581003151	0.904	0.67	1.4263744417832E-23	existing_prog	HNRNPUL1
7.24723912907194E-28	0.441697305771704	0.836	0.453	1.4282858875575E-23	existing_prog	SMC1A
1.69544160683815E-27	0.411689141563438	0.966	0.867	3.34137631875663E-23	existing_prog	ENY2
2.95443909132085E-27	0.611983375668379	0.763	0.418	5.82260856117512E-23	existing_prog	RP11-620J
3.1842950107753E-27	0.439992627835555	0.966	0.809	6.27560860723596E-23	existing_prog	SMC3
6.8052994104654E-27	0.442445941045074	0.921	0.711	1.34118840781452E-22	existing_prog	LSM 3.00
7.56620391744036E-27	0.409905719939674	0.627	0.27	1.49114746804915E-22	existing_prog	PTPRZ1
1.24871117469162E-26	0.530773372243146	0.983	0.814	2.46095998308225E-22	existing_prog	PFN2
1.35694165140748E-26	0.509863576521012	0.486	0.18	2.67426060659386E-22	existing_prog	HIST2H2AC
3.52340564665716E-26	0.417556642766604	1	0.884	6.94392784843193E-22	existing_prog	FUS
5.01127393223694E-26	0.423624516449622	0.983	0.923	9.87621866565256E-22	existing_prog	COX8A
2.16935800689019E-25	0.418488968651791	0.972	0.795	4.27537075997919E-21	existing_prog	LSM 4.00
6.44140225252086E-25	0.45243827191054	0.797	0.473	1.26947155592681E-20	existing_prog	TTC14
2.55079899707683E-24	0.424282884711062	0.65	0.302	5.02711466343901E-20	existing_prog	MCM3
2.75406068361851E-24	0.472357794887207	0.554	0.236	5.42770279527537E-20	existing_prog	HIST1H1C
5.07409037805493E-24	0.68453798158393	0.446	0.167	1.00000173170707E-19	existing_prog	CCNA1
8.51292946971568E-24	0.420249672527316	0.791	0.457	1.67772813989157E-19	existing_prog	ACYP1
1.01973413392193E-23	0.535476492176534	0.904	0.651	2.00969203113334E-19	existing_prog	RAD21
1.15905918401365E-23	0.471730532622159	0.989	0.837	2.28427383985411E-19	existing_prog	SFPQ

1.45158977968703E-23	0.444099461634136	0.915	0.715	2.8607931378072E-19	existing_prog	PSMC3
1.59288106366085E-23	0.433451129906197	0.91	0.662	3.13925090026281E-19	existing_prog	HNRNPAB
6.76330756658921E-23	0.435315472843012	0.881	0.597	1.3329126552234E-18	existing_prog	SKA2
1.24853889956209E-21	0.443766506334089	0.797	0.523	2.46062046325696E-17	existing_prog	ARL6IP6
5.37892492054482E-21	0.409689477674505	0.74	0.419	1.06007852334097E-16	existing_prog	IVNS1ABP
2.9570731301346E-20	0.443286107466947	0.893	0.66	5.82779972486927E-16	existing_prog	PLEKHA1
4.36198407286684E-20	0.406233067528145	0.78	0.459	8.59659821080597E-16	existing_prog	SLF1
8.87495879125556E-20	0.42573968960857	1	0.959	1.74907687858065E-15	existing_prog	MDK
1.42846313264737E-19	0.4560674455929	0.989	0.971	2.81521514182144E-15	existing_prog	DYNLL1
4.65884893535375E-19	0.424723206980361	0.644	0.348	9.18165948179517E-15	existing_prog	RNF26
9.12789286513247E-18	0.449347833440591	0.78	0.501	1.79892512586031E-13	existing_prog	RUVBL2
4.67456398103796E-17	0.481811236751145	0.938	0.743	9.21263069382962E-13	existing_prog	DUT
2.63361150516711E-10	0.62209598558691	0.876	0.756	5.19032155438333E-06	existing_prog	TRH
3.76075754648137E-10	0.754424582636319	0.938	0.9	7.41170097260549E-06	existing_prog	ARL6IP1
7.28565069991054E-09	0.492143155509343	0.785	0.563	0.000143585603993837	existing_prog	CCND1
6.35405707411928E-08	0.425556839840184	0.638	0.462	0.00125225756816743	existing_prog	TUBA1C
1.16930187145625E-188	0.966624036001392	0.985	0.957	2.30446012826598E-184	neuroblasts	SH3BGRL3
2.30946768397378E-182	1.15929408515216	0.956	0.733	4.55149891157552E-178	neuroblasts	CXCR4
7.04199761050279E-179	0.955966843545263	0.984	0.837	1.38783688907789E-174	neuroblasts	MIAT
1.44450092859416E-135	1.01847166776057	0.849	0.536	2.84682243007337E-131	neuroblasts	GADD45A
8.31289721060183E-103	0.637450009842725	0.645	0.296	1.63830578226541E-98	neuroblasts	MFNG
9.45647113032676E-101	1.06573669165747	0.765	0.507	1.8636813303648E-96	neuroblasts	RGS16
4.98175197196807E-87	0.445342174556293	1	0.999	9.81803678635468E-83	neuroblasts	RBP1
5.1950409656072E-84	0.641098507784459	0.788	0.457	1.02383867350187E-79	neuroblasts	NHLH1
1.70931757053462E-74	0.813698539051603	0.852	0.734	3.36872306800962E-70	neuroblasts	DDIT4
1.15314863707817E-69	0.481945230592964	0.911	0.835	2.27262533395366E-65	neuroblasts	RORB
2.64098666125146E-68	0.482960110198964	0.857	0.716	5.20485651199438E-64	neuroblasts	NOVA1
2.78312308195942E-67	0.646010018455799	0.966	0.966	5.48497896992563E-63	neuroblasts	PGK 1.00
4.32600777642648E-65	0.659544673411374	0.919	0.887	8.52569612578132E-61	neuroblasts	BNIP3
3.7776116415275E-64	0.56036210049032	0.602	0.345	7.4449170231224E-60	neuroblasts	SHD
4.89795774625378E-61	0.946739111301297	0.864	0.788	9.65289512631695E-57	neuroblasts	HES6
2.78709604661635E-58	0.65792598258931	0.426	0.189	5.49280888867151E-54	neuroblasts	STC2
2.25451191664475E-54	0.426243084272642	0.788	0.66	4.44319208532346E-50	neuroblasts	DDR1
3.91029045482908E-54	0.443691053852448	0.654	0.42	7.70640042837715E-50	neuroblasts	SRRM4
9.56353453053372E-53	0.535031156572454	0.934	0.844	1.88478138527759E-48	neuroblasts	SOX11
8.13773484167147E-52	0.532926500351926	0.607	0.363	1.60378478259661E-47	neuroblasts	SLC18A2

4.03038962910287E-51	0.578592690404592	0.792	0.688	7.94309188103594E-47	neuroblasts	FAM162A
5.61322293866983E-51	0.582225903491161	0.735	0.576	1.10625397675305E-46	neuroblasts	SLC16A3
2.74919459532063E-50	0.509132508329174	0.992	0.993	5.4181127084579E-46	neuroblasts	ENO1
1.90613922781007E-48	0.537136512513696	0.582	0.396	3.75661919016808E-44	neuroblasts	IGFBP2
2.45235535717173E-48	0.405896621152859	0.99	0.993	4.83310193791404E-44	neuroblasts	TPI1
1.8149080821709E-47	0.449085314485473	0.319	0.121	3.57682084834241E-43	neuroblasts	LINC01551
6.21541293076044E-43	0.49966053979879	0.74	0.666	1.22493358039427E-38	neuroblasts	LIMD2
1.01352023848792E-42	0.426980320326025	0.725	0.514	1.99744568601199E-38	neuroblasts	ELAVL2
9.47295610908539E-37	0.516038515577907	0.27	0.104	1.86693018997855E-32	neuroblasts	VSX1
1.12755056010244E-33	1.00097391371338	0.405	0.254	2.22217664384989E-29	neuroblasts	RP3-395M2
2.4327308722505E-31	0.445584825263411	0.642	0.534	4.79442600303128E-27	neuroblasts	PDLIM4
9.36962688404133E-30	0.42350069785589	0.603	0.496	1.84656606630687E-25	neuroblasts	LCA5
8.81109422886579E-27	0.405648813524155	0.666	0.51	1.73649045062487E-22	neuroblasts	GADD45G
3.23873258669861E-25	0.697910308353762	0.411	0.263	6.38289418186562E-21	neuroblasts	CLDN5
1.60224839279087E-24	0.454140753957491	0.703	0.663	3.15771113251224E-20	neuroblasts	PLEKHA1
4.27031283708973E-24	0.439667376151727	0.497	0.393	8.41593253933644E-20	neuroblasts	AGPAT2
8.99044134867294E-24	0.430436486361912	0.793	0.753	1.77183618099646E-19	neuroblasts	TRH
6.52772963567797E-22	0.485274289493003	0.425	0.296	1.28648495659941E-17	neuroblasts	RASD1
2.11577992763031E-21	0.700450123851411	0.391	0.252	4.16977908137382E-17	neuroblasts	IGFBP5
1.69586796608113E-08	0.450341334703824	0.286	0.224	0.00033422165875527	neuroblasts	HEY1
1.02459238475717E-07	1.5069924112315	0.287	0.233	0.00201926667187942	neuroblasts	GAL
0	2.42896721596791	0.832	0.041		photoreceptor	DCT
0	1.42077576520909	0.864	0.096		photoreceptor	OTX2
0	1.39708500678511	0.586	0.026		photoreceptor	PRDM1
0	1.2190249150615	0.801	0.044		photoreceptor	CRX
0	1.05168869368146	0.581	0.018		photoreceptor	VTN
1.34403972612283E-302	1.36481170725785	0.683	0.056	2.64883349224286E-298	photoreceptor	SLC38A5
2.16123033047187E-295	0.657276660040997	0.534	0.022	4.25935273529397E-291	photoreceptor	MAOA
2.27127159864859E-285	1.72244069569183	0.801	0.115	4.47622206661664E-281	photoreceptor	GNB3
3.84145088370199E-282	0.939445064510722	0.547	0.028	7.57073140159988E-278	photoreceptor	TULP1
5.32487538999291E-278	1.26278812853488	0.859	0.133	1.0494264418598E-273	photoreceptor	NEUROD4
9.32573179643385E-276	0.666615565205017	0.476	0.016	1.83791522244118E-271	photoreceptor	NXPH4
7.01702246202384E-275	1.22412235602923	0.777	0.107	1.38291478681566E-270	photoreceptor	THR-B
4.47846069943545E-267	0.872225655077788	0.445	0.013	8.82615034644739E-263	photoreceptor	PCAT4
3.93267577436375E-261	0.533089163491024	0.387	0.005	7.75051741611609E-257	photoreceptor	RBP3
7.42168410066655E-257	1.20641311315787	0.492	0.024	1.46266550255936E-252	photoreceptor	PDC

1.99202430743815E-253	0.679203660882694	0.542	0.035	3.9258815050991E-249	photorecepto	MCC
2.41556931898305E-253	0.5685180612382	0.421	0.012	4.76060401385179E-249	photorecepto	KCNH6
1.73605338036364E-235	1.09732569606517	0.448	0.021	3.42141400202067E-231	photorecepto	KCNV2
4.70279551048249E-234	0.679628962097016	0.401	0.012	9.26826939205889E-230	photorecepto	AIPL1
2.97480628134758E-227	0.447798530092378	0.377	0.01	5.86274821927982E-223	photorecepto	RD3
2.86525320976623E-222	0.502376804182764	0.359	0.008	5.64684102580728E-218	photorecepto	IMPG2
3.77263875085534E-218	0.60928026763762	0.476	0.03	7.43511645018571E-214	photorecepto	FSTL5
4.08309335937793E-217	1.7301652160062	0.72	0.117	8.04696039266203E-213	photorecepto	C8orf46
8.37752023354786E-212	1.48042568102138	0.895	0.271	1.65104168762761E-207	photorecepto	SEPT4
1.23490054596383E-201	0.413937535652825	0.309	0.005	2.43374199598552E-197	photorecepto	SLC1A7
2.05610336536132E-199	0.479750597162318	0.395	0.019	4.05216851245408E-195	photorecepto	AANAT
7.21606404542176E-198	1.82800223735372	0.552	0.065	1.42214190207172E-193	photorecepto	RCVRN
1.66553223779897E-196	0.678196350399422	0.374	0.017	3.28243093425421E-192	photorecepto	RBP4
3.77906501604816E-187	1.58681037681391	0.987	0.673	7.44778133362771E-183	photorecepto	FAM57B
1.734737071937E-180	0.920548960583384	0.736	0.16	3.41881982137345E-176	photorecepto	AMER2
2.02609359018831E-179	0.483108106222039	0.288	0.006	3.99302524754313E-175	photorecepto	CABP5
1.57294965357472E-176	1.51786999689233	0.869	0.296	3.09996917726505E-172	photorecepto	PHLDA1
5.22719887257352E-174	1.06608189044534	0.793	0.203	1.03017635380679E-169	photorecepto	MIR7-3HG
4.22309345192598E-171	1.01683006652431	0.576	0.088	8.32287257505573E-167	photorecepto	RXRG
1.61719489534906E-165	0.462139337146842	0.288	0.009	3.18716769975394E-161	photorecepto	MRLN
6.3542533786032E-159	1.12402280355331	0.901	0.382	1.25229625585512E-154	photorecepto	PIK3R1
7.23832054572368E-155	1.00847251610629	1	0.828	1.42652821315122E-150	photorecepto	PCBP4
5.01119921378171E-149	0.522962511955102	0.38	0.032	9.876071410521E-145	photorecepto	RAMP1
1.84080746373481E-146	1.12085903831212	0.969	0.495	3.62786334952857E-142	photorecepto	GADD45G
2.37175318773131E-141	0.855990374568552	0.704	0.185	4.67425118238087E-137	photorecepto	MEIS2
7.23545609169174E-140	0.589749428451951	0.513	0.078	1.42596368655061E-135	photorecepto	CNTNAP2
6.1966524182483E-131	0.987401242495081	0.971	0.807	1.22123625858838E-126	photorecepto	GUK1
6.75741315171146E-131	1.05515185707919	0.984	0.573	1.3317509839393E-126	photorecepto	NEUROD1
2.30366056861721E-122	0.432557382862474	0.322	0.028	4.54005424863079E-118	photorecepto	RIMS1
4.68505262613987E-118	0.462856589577707	0.301	0.024	9.23330171559646E-114	photorecepto	GJD2
9.83547638490418E-118	0.783555101459745	0.717	0.244	1.93837568593692E-113	photorecepto	REEP6
2.52633604331431E-117	0.924703774404037	0.99	0.951	4.97890307416384E-113	photorecepto	PRDX1
2.97567590497303E-116	0.766579710231665	0.652	0.182	5.86446207352085E-112	photorecepto	ROBO2
5.63001887124974E-116	0.524385499310805	0.482	0.086	1.1095641191459E-111	photorecepto	STX3
1.67316889589327E-110	0.54230536461212	1	0.999	3.29748126002645E-106	photorecepto	H3F3B
1.66131396929553E-109	0.743620912079306	0.683	0.214	3.27411757068762E-105	photorecepto	SERPINF1

8.2949224251269E-108	0.954234146620651	0.982	0.865	1.63476331154401E-103	photorecept	TUBB4B
1.20123007874061E-107	0.810335303874486	0.882	0.502	2.36738423918199E-103	photorecept	STRADB
2.16528874874214E-104	0.733662252549863	0.738	0.256	4.26735106602101E-100	photorecept	LINC00599
6.35265513053765E-104	0.430227938073906	0.327	0.038	1.25198127312636E-99	photorecept	DPP10
5.96985677186696E-100	0.721047234080159	0.743	0.266	1.17653937259954E-95	photorecept	SYP
2.03816517684256E-99	0.801885673886812	0.974	0.807	4.01681593052131E-95	photorecept	CPE
1.28086613421994E-98	0.917967090957715	0.798	0.412	2.52433097732067E-94	photorecept	UNC119
2.47040159165222E-97	0.430588358635445	0.429	0.078	4.8686674568282E-93	photorecept	PRCD
3.2581109893249E-97	0.829953419454847	0.929	0.631	6.42108513776152E-93	photorecept	ATP2B1
2.25477421466736E-96	0.559766997965455	0.581	0.156	4.44370902226643E-92	photorecept	LINC01315
4.90486886985664E-95	0.578831955058295	0.382	0.064	9.66651556871346E-91	photorecept	FILIP1L
1.48778149868404E-93	0.673022013869583	0.788	0.366	2.93211977760651E-89	photorecept	BCL2L1
2.26688911364338E-93	0.526857926916012	0.429	0.085	4.46758506516837E-89	photorecept	PHACTR2
1.33997423845772E-91	0.671142086869695	0.987	0.885	2.64082122915247E-87	photorecept	HMGA1
2.85853575119465E-91	0.868082447760535	0.877	0.436	5.63360225845442E-87	photorecept	SYT4
3.32273141140307E-91	0.745205179923788	0.979	0.948	6.54843906559316E-87	photorecept	GSTP1
2.92864279454203E-89	0.748929369814485	0.971	0.764	5.77176921948344E-85	photorecept	ENO2
2.19113294797022E-86	0.727895480305762	0.518	0.147	4.31828481385971E-82	photorecept	PLEKHB1
3.27008410694289E-84	0.611683878863763	1	1	6.44468175796305E-80	photorecept	TMSB4X
6.69984572897633E-83	0.515177602193993	0.518	0.138	1.32040559626666E-78	photorecept	NRXN1
2.44815725376642E-80	0.658143460573962	0.746	0.366	4.82482831572285E-76	photorecept	ROGDI
5.33881632689254E-76	0.826512063071199	0.513	0.153	1.05217392170398E-71	photorecept	TUBA4A
1.81803345104949E-75	0.578941715508807	0.924	0.493	3.58298032532834E-71	photorecept	SEZ6L2
3.51088616976447E-75	0.652557222920258	0.958	0.616	6.91925446337183E-71	photorecept	ATP1A3
2.77359544929611E-74	0.694248380732045	0.927	0.837	5.46620191147278E-70	photorecept	SPCS1
9.90818980447847E-72	0.542048967282718	0.56	0.195	1.95270604666662E-67	photorecept	SDC2
4.41213563808498E-71	0.426400318857647	0.471	0.133	8.69543691553788E-67	photorecept	CLN6
3.21839843737215E-69	0.685166848980461	0.83	0.49	6.34281964037303E-65	photorecept	MAP1LC3A
1.65408162396227E-68	0.523132600625648	0.563	0.194	3.25986406450484E-64	photorecept	SH3BP5
2.8001761198414E-65	0.631608385585601	0.806	0.504	5.51858709698343E-61	photorecept	ABHD14A
5.21495285482252E-63	0.472651297427698	0.99	0.977	1.02776290862842E-58	photorecept	BSG
1.13946470523856E-61	0.536589764546009	0.874	0.589	2.24565704108416E-57	photorecept	SCARB2
1.83849135259837E-60	0.656469959955554	0.683	0.33	3.62329875770087E-56	photorecept	ARL4D
4.31620899021808E-58	0.500418829403497	0.636	0.266	8.50638467792179E-54	photorecept	CHGA
1.54583820213128E-57	0.500880168144076	0.94	0.803	3.04653792876033E-53	photorecept	SVBP
1.46153565980496E-53	0.517344082146663	0.88	0.711	2.88039447834362E-49	photorecept	UQCC2

2.65519894536223E-53	0.515277430882505	0.45	0.143	5.23286608151989E-49	photorecept	STC1
2.69387751688956E-53	0.507375266013551	0.861	0.642	5.30909381028594E-49	photorecept	GRINA
1.43821903582843E-51	0.487248558077403	0.866	0.468	2.83444207581067E-47	photorecept	CHRNA3
4.7669248397809E-51	0.464589676892237	0.565	0.235	9.39465547424019E-47	photorecept	CADPS
1.95187366416048E-50	0.45556997004696	0.699	0.384	3.84675261732747E-46	photorecept	NUDT14
4.1663828579095E-49	0.543716581201815	0.916	0.695	8.21110733636804E-45	photorecept	CADM1
4.87022874066107E-48	0.551364151262023	0.94	0.648	9.59824680209484E-44	photorecept	SCG3
2.18108962811757E-47	0.504205132661147	0.887	0.708	4.29849143909411E-43	photorecept	SEPW1
6.75806321843446E-47	0.49636016500645	0.927	0.827	1.33187909908906E-42	photorecept	GPX1
3.04435287580168E-46	0.421092455464825	0.565	0.256	5.99981064762996E-42	photorecept	CCDC181
3.38440018995476E-46	0.571131960996887	0.848	0.613	6.66997589436283E-42	photorecept	TMX1
1.22161969352506E-45	0.74003204243442	0.573	0.268	2.40756809199918E-41	photorecept	DDIT3
1.61822745307509E-45	0.40866166620975	0.953	0.879	3.18920266452038E-41	photorecept	VAMP2
4.61413738590138E-45	0.59312523848252	0.738	0.487	9.09354196013443E-41	photorecept	IFT57
6.21146989103258E-44	0.539204351420212	0.872	0.7	1.2241564861247E-39	photorecept	AKAP9
1.42114041646721E-43	0.467043507947304	0.827	0.616	2.80078353277358E-39	photorecept	BAD
9.73042104318065E-40	0.452258620641506	0.696	0.437	1.91767137919004E-35	photorecept	ITSN1
1.26161753973219E-38	0.485526934015009	0.652	0.404	2.4863958473042E-34	photorecept	PGRMC2
1.75956887642971E-38	0.515796953428023	0.846	0.545	3.46775834166768E-34	photorecept	SSTR2
2.56324844299665E-38	0.420242692470312	0.911	0.772	5.05165003145781E-34	photorecept	NDUFB1
3.11875776816899E-38	0.447998098155421	0.712	0.448	6.14644780950745E-34	photorecept	ZHX1
3.18843101535058E-38	0.410574009940421	0.602	0.322	6.28375984505293E-34	photorecept	CHCHD10
3.32798142343467E-37	0.520702834614603	0.681	0.427	6.55878578930505E-33	photorecept	PEG10
5.45172658608466E-37	0.437794688331359	0.702	0.46	1.07442627558557E-32	photorecept	RHOT1
1.23344345081287E-36	0.42150669931931	0.791	0.578	2.43087035286201E-32	photorecept	APMAP
2.12118818641702E-36	0.437650975155357	0.597	0.292	4.18043767779066E-32	photorecept	RASD1
1.9501096673652E-35	0.479582805180299	0.895	0.776	3.84327613244334E-31	photorecept	OCIAD2
2.47676295165025E-34	1.06052121155518	0.461	0.234	4.88120442511232E-30	photorecept	ISOC1
8.01284558020149E-33	0.445967187215086	0.649	0.375	1.57917160694611E-28	photorecept	TXNIP
2.04598618321165E-31	0.544969708866865	0.785	0.627	4.03222956987353E-27	photorecept	DHRS7
2.8439505239027E-31	0.590322127446267	0.579	0.347	5.60485769250743E-27	photorecept	S100A13
8.34137162662243E-31	0.409838974629865	0.751	0.526	1.64391752017475E-26	photorecept	CADM2
6.28359841951678E-29	0.45357303562891	0.736	0.526	1.23837157651837E-24	photorecept	CLTB
9.65568284672801E-29	0.412206882293057	0.783	0.661	1.90294197543316E-24	photorecept	SCP2
5.11191889245379E-26	0.420595652368648	0.99	0.986	1.00745697532479E-21	photorecept	ALDOA
9.21728351610386E-25	1.48935056516302	0.545	0.347	1.81654223535375E-20	photorecept	CRABP2

9.995743767765E-23	0.450657970500609	0.27	0.11	1.96996118175113E-18	photorecept	SLC1A5	
2.03295747415172E-21	0.415312973547615	0.267	0.103	4.0065525900582E-17	photorecept	SCG2	
<small>bioRxiv preprint doi: https://doi.org/10.1101/2020.10.27.356135; this version posted November 9, 2020. The copyright holder for this preprint (which was not certified by peer review) is the author/funder. All rights reserved. No reuse allowed without permission.</small>	3.99176256775893E-19	0.515175888212881	0.809	0.648	7.86696566853931E-15	photorecept	KCNQ1OT1
1.97639760235368E-13	0.455306454482603	0.584	0.442	3.89508439471863E-09	photorecept	S100A6	
0	1.67866507543497	0.985	0.59		0	rgc	GAP43
0	1.62664244202391	0.915	0.36		0	rgc	NSG1
0	1.40049703856269	0.937	0.429		0	rgc	RTN1
0	1.17520642487855	0.907	0.292		0	rgc	ELAVL4
0	1.14672627900499	0.989	0.791		0	rgc	TUBB2A
0	1.11760455903467	0.998	0.827		0	rgc	STMN2
0	1.07117627142803	1	1		0	rgc	TUBA1A
0	0.991303434423997	0.998	0.962		0	rgc	MLLT11
0	0.965279326825758	0.999	1		0	rgc	CALM2
0	0.842744764155321	1	0.998		0	rgc	TUBB2B
0	0.812725520670789	1	0.999		0	rgc	TMSB10
8.68960380178683E-295	1.09379052044953	0.645	0.095	1.71254711725615E-290	rgc	ISL1	
3.78162253546257E-291	0.748091365431985	1	0.996	7.45282169288963E-287	rgc	MAP1B	
7.95686439327425E-288	1.04332589759387	0.923	0.45	1.56813883462649E-283	rgc	GNG3	
6.0083713972685E-255	0.83635723882651	0.996	0.727	1.18412983497368E-250	rgc	TAGLN3	
6.38743718994921E-253	0.709638336538498	0.988	0.937	1.25883612139519E-248	rgc	C4orf48	
9.27297395789068E-252	0.85178319339057	0.982	0.581	1.82751770762109E-247	rgc	DCX	
1.11413679880853E-248	0.83049451178865	0.983	0.837	2.19574080309184E-244	rgc	UCHL1	
1.87768401855086E-243	1.12692275958606	0.743	0.214	3.70053966376003E-239	rgc	NEFM	
3.54371986992525E-240	0.852051717013663	0.965	0.713	6.98396311964868E-236	rgc	PCSK1N	
6.07280709821819E-239	0.93264195349365	0.979	0.583	1.19682882291684E-234	rgc	STMN4	
1.30313699795126E-232	1.1381549245492	0.711	0.208	2.56822239556234E-228	rgc	NEFL	
3.53495163067627E-223	0.634316370274441	0.993	0.926	6.9666826737368E-219	rgc	HN1	
7.38981402546041E-223	0.742436445240983	0.898	0.391	1.45638454813774E-218	rgc	INA	
7.59248522111202E-223	0.450822175173964	1	1	1.49632698737676E-218	rgc	ACTB	
6.26722677348952E-220	0.72868844365317	0.958	0.686	1.23514505251931E-215	rgc	KLC1	
9.37110565085139E-219	0.683859859093506	0.984	0.779	1.84685750166979E-214	rgc	CRMP1	
3.42488837259694E-218	0.665075540381014	0.646	0.146	6.74977000471406E-214	rgc	TTC9B	
8.52153982504189E-218	0.700888523898399	0.988	0.809	1.67942506871926E-213	rgc	BASP1	
9.28338265482956E-213	0.469475692197182	0.999	0.999	1.82956905361381E-208	rgc	STMN1	
1.37071866368886E-211	0.636507077971733	0.997	0.935	2.70141234239801E-207	rgc	CD24	
6.58424081163453E-208	0.415038601382757	0.998	0.999	1.29762217915693E-203	rgc	MARCKSL1	

9.84820729405495E-202	0.778382827675226	0.789	0.293	1.94088469351235E-197	rgc	OLFM1
1.11683555681864E-194	1.2404999457904	0.788	0.385	2.20105951537818E-190	rgc	SNCG
1.75123484816245E-194	0.688100917853104	0.566	0.121	3.45133363875855E-190	rgc	EBF1
2.81473320678218E-193	0.6814472080049	0.775	0.291	5.54727620392632E-189	rgc	MAPT
8.74683299670284E-193	0.45646817568293	1	1	1.72382584699019E-188	rgc	TUBB
2.6922060846582E-191	0.574346044710723	0.737	0.238	5.30579975164438E-187	rgc	RUNDCA
3.40238467295977E-188	0.51125544306736	0.996	0.992	6.70541971346912E-184	rgc	CCNI
7.81294492964966E-186	0.761819005019456	0.788	0.323	1.53977518673536E-181	rgc	PPP1R1A
3.18586318517654E-185	0.834657571996366	0.908	0.594	6.27869916534592E-181	rgc	NELL2
9.61179373800558E-184	0.591490773586576	0.958	0.713	1.89429230988614E-179	rgc	GDI1
4.45601495383047E-175	0.722078002092483	0.85	0.37	8.78191427100908E-171	rgc	CELF4
8.26716639300143E-173	0.590597031571899	0.751	0.278	1.62929315273272E-168	rgc	DPYSL3
7.46961384583546E-171	0.765038889018578	0.729	0.301	1.47211149673725E-166	rgc	DUSP4
8.65659420079065E-171	0.628831327835264	0.905	0.544	1.70604158509182E-166	rgc	KIF5C
2.13598784516246E-168	0.5858827107244	0.587	0.146	4.20960484524618E-164	rgc	NHLH2
5.00471129350837E-166	0.629214106187362	0.553	0.132	9.86328501724629E-162	rgc	PCSK2
9.95151510912576E-166	0.600548309924888	0.97	0.799	1.9612445977065E-161	rgc	APLP1
4.62936159265013E-164	0.719183446937811	0.697	0.251	9.12354582679488E-160	rgc	PPP1R17
9.05755822527387E-164	0.596852358250638	0.901	0.469	1.78506357503697E-159	rgc	ELAVL3
4.86037304598942E-161	0.592717958478034	0.854	0.47	9.57882319903594E-157	rgc	RBFOX2
2.46291524402819E-160	0.600086303028742	0.513	0.121	4.85391336293076E-156	rgc	POU6F2
2.51407455382867E-160	0.62952155772288	0.896	0.503	4.95473813068555E-156	rgc	RAB3A
6.85762625991067E-160	0.675975087828757	0.715	0.287	1.35150098330319E-155	rgc	SCG5
8.01456842898563E-160	0.578860883992856	0.768	0.27	1.57951114598449E-155	rgc	SLC18A2
3.62644527877778E-158	0.418577588147371	0.994	0.969	7.14699835541525E-154	rgc	YWHAQ
3.96862725553503E-157	0.683434431583539	0.864	0.435	7.82137059520844E-153	rgc	ELAVL2
9.10166372250914E-156	0.787830517783604	0.646	0.233	1.7937558864321E-151	rgc	MAB21L2
3.72592632845383E-154	0.585213127030433	0.873	0.387	7.34305560811681E-150	rgc	NHLH1
1.23477840149574E-152	0.599382778103856	0.831	0.423	2.43350127366781E-148	rgc	TSPAN7
4.95026788865551E-152	0.55777453325623	0.998	0.984	9.75598795496228E-148	rgc	SOX4
2.22068153491637E-150	0.636652532384057	0.783	0.412	4.37651916901318E-146	rgc	KLF7
9.14294405334802E-150	0.413336445250291	1	1	1.80189141403383E-145	rgc	TMSB4X
9.85381826563759E-145	0.587055152691392	0.924	0.772	1.94199050379186E-140	rgc	PAFAH1B3
2.60949765313853E-144	0.542695849837609	0.94	0.534	5.14279797480542E-140	rgc	ATP1A3
3.43590201109186E-144	0.519658840344247	0.971	0.788	6.77147568345985E-140	rgc	TERF2IP
1.21993853261193E-143	0.53384705856224	0.751	0.294	2.40425486007159E-139	rgc	HMP19

4.75069191502181E-142	0.518783437246009	0.96	0.71	9.36266362612498E-138	rgc	BEX1
1.29310403449337E-141	0.410486546804932	0.481	0.107	2.54844943117954E-137	rgc	AKAP6
2.31447534098241E-141	0.60114819056215	0.572	0.186	4.56136800200813E-137	rgc	RAB3B
9.51910863330698E-140	0.61657466759154	0.765	0.331	1.87602592945214E-135	rgc	SERPINI1
2.16620330274188E-139	1.36607779037133	0.461	0.122	4.2691534690437E-135	rgc	PRPH
2.19549265827703E-137	0.611357000771956	0.488	0.118	4.32687693093238E-133	rgc	POU4F2
7.4088792487642E-137	0.537928198038542	0.966	0.56	1.46014192234645E-132	rgc	SCG3
6.16289709531948E-135	0.531802438099188	0.894	0.548	1.21458375954556E-130	rgc	MAP2
1.90757031154121E-134	0.520638325117409	0.531	0.154	3.75943956998541E-130	rgc	RBFOX3
2.62887705814709E-132	0.499372960209979	0.87	0.403	5.18099090619629E-128	rgc	SEZ6L2
4.48128100336417E-132	0.472201982910314	0.94	0.802	8.83170860143012E-128	rgc	TBCB
1.66920263596285E-126	0.436924881913328	0.567	0.176	3.28966455495558E-122	rgc	L1CAM
2.90115867859113E-124	0.474585064585435	0.975	0.886	5.7176035237674E-120	rgc	PAX6
3.22581720167126E-124	0.455986591771656	0.404	0.083	6.35744054105372E-120	rgc	PPP2R2B
5.29363348522611E-124	0.426952474761686	0.975	0.938	1.04326928726836E-119	rgc	TXN
7.64155196480955E-124	0.430720058579168	0.563	0.183	1.50599706122467E-119	rgc	EPS8L1
7.87033587647843E-124	0.480554011897828	0.93	0.621	1.55108579453637E-119	rgc	GPC2
3.40996699358929E-123	0.441641096345982	0.539	0.171	6.72036295096577E-119	rgc	CCDC184
4.68186669238958E-122	0.684702061106183	0.999	0.999	9.22702287736138E-118	rgc	CRABP1
2.57063831462661E-118	0.455528915872065	0.978	0.938	5.06621399046613E-114	rgc	HSPA8
3.81158354703032E-117	0.464164598263478	0.635	0.233	7.51186885448736E-113	rgc	RUNX1T1
4.58148947356418E-116	0.463624717183134	0.952	0.86	9.02919945450029E-112	rgc	ETFB
8.04608843619363E-115	0.414240553114019	0.766	0.341	1.58572310900504E-110	rgc	CELF3
1.26742380668116E-114	0.488057223736344	0.716	0.394	2.49783883820723E-110	rgc	TMEM14A
2.1802921668625E-114	0.647320696561858	0.846	0.466	4.29691980245261E-110	rgc	SSTR2
1.09285246054864E-113	0.476851747313834	0.729	0.369	2.15379362924927E-109	rgc	PGM2L1
4.91046104443911E-112	0.481288564957699	0.804	0.479	9.6775366263806E-108	rgc	PODXL2
9.42525473300851E-112	0.493068178840526	0.729	0.414	1.85752920278132E-107	rgc	MAP4
1.79354649860353E-111	0.487269322120956	0.755	0.437	3.53472143944784E-107	rgc	ACOT7
2.5548285181826E-109	0.5287394513487	0.624	0.252	5.03505604363426E-105	rgc	ASIC4
4.89670863037467E-109	0.417058517133333	0.673	0.277	9.65043336874239E-105	rgc	GDAP1L1
3.93791028669706E-106	0.570779718176021	0.765	0.405	7.76083359302257E-102	rgc	CHRNA3
1.81018165992609E-105	0.484324578917414	0.764	0.471	3.56750601538233E-101	rgc	NAGK
2.52531515576706E-105	0.407029052251709	0.94	0.829	4.97689110898573E-101	rgc	RAB2A
1.33741058666656E-104	0.406912156092088	0.674	0.293	2.63576878420246E-100	rgc	SNAP25
5.08050263812259E-103	0.447202305903839	0.956	0.83	1.0012654599212E-98	rgc	DAAM1

9.96097331555281E-103	0.634366035791829	0.499	0.177	1.96310862102915E-98	rgc	CNTN2
3.42722677203542E-101	0.451345661927569	0.772	0.488	6.75437852232741E-97	rgc	ATAT1
2.14300982639999E-100	0.456572553378042	0.866	0.649	4.2234437658691E-96	rgc	CXADR
6.03509534770619E-99	0.445357750724954	0.772	0.466	1.18939659112594E-94	rgc	CEP170
1.06061589642765E-97	0.427417773593241	0.886	0.741	2.0902618086796E-93	rgc	ARPC5
2.4027247689917E-97	0.441532552288276	0.837	0.584	4.73528997472884E-93	rgc	FNBP1L
5.43676474954459E-97	0.419316467462847	0.645	0.311	1.07147759684025E-92	rgc	GLRX
1.42455353324536E-93	0.458164660790092	0.748	0.373	2.80751010331996E-89	rgc	SYT4
6.83229379009397E-91	0.405475408937135	0.688	0.363	1.34650846015172E-86	rgc	CDKN2D
1.89236490230936E-90	0.56116024283304	0.285	0.056	3.72947274947128E-86	rgc	RGS10
9.99180309139389E-89	0.431590216681417	0.712	0.435	1.96918455325191E-84	rgc	FEZ1
1.38891032380312E-88	0.439341073818975	0.778	0.544	2.73726446615118E-84	rgc	ATP6V0E2
1.77651615267042E-88	0.475084335932465	0.804	0.571	3.50115803368286E-84	rgc	FAM63B
4.65867041523221E-88	0.411210444761726	0.814	0.557	9.18130765433965E-84	rgc	RAB6A
1.45690620198575E-87	0.421382599818148	0.853	0.647	2.87127074287352E-83	rgc	YWHAH
3.89186713575783E-86	0.41928558337789	0.855	0.664	7.67009175115152E-82	rgc	DYNC1H1
5.22277819268115E-82	0.415700088119859	0.812	0.602	1.0293051262136E-77	rgc	DPYSL2
2.13346312013378E-81	0.548857396834949	0.581	0.275	4.20462911715966E-77	rgc	POU2F2
3.48071375674097E-81	0.406430187022874	0.722	0.441	6.85979067178511E-77	rgc	CCDC112
2.35700459388922E-79	0.425842335827216	0.645	0.363	4.64518465363687E-75	rgc	EPB41L3
2.44458047705307E-77	0.525540410200951	0.965	0.822	4.81777920417619E-73	rgc	SOX11
1.17749666721228E-76	0.531715472953067	0.714	0.479	2.32061043174196E-72	rgc	ACAT2
7.57371860503306E-74	0.442204091001972	0.656	0.404	1.49262846267992E-69	rgc	C14orf132
5.43070092959065E-73	0.447181078534062	0.835	0.652	1.07028253920372E-68	rgc	FDFT1
1.14646247506119E-72	0.42669287339928	0.666	0.4	2.25944824585059E-68	rgc	TSPAN13
3.29842207559256E-63	0.440091947713462	0.513	0.268	6.50053022657781E-59	rgc	NKAIN3
2.369828872281E-62	0.410678437190895	0.728	0.484	4.6704587414914E-58	rgc	EFNA5
2.36879939210611E-58	0.426088830835962	0.899	0.816	4.66842984196273E-54	rgc	PHYHIPL
4.32718108745711E-57	0.473192143516053	0.466	0.237	8.52800848716046E-53	rgc	SNCA
6.68575030027434E-57	0.513515799688636	0.633	0.41	1.31762766917807E-52	rgc	MPPED2
3.73648286614935E-54	0.424808563377473	0.659	0.445	7.36386043260714E-50	rgc	HMGCS1
3.43855633517617E-53	0.664099029926933	0.637	0.462	6.7767068253652E-49	rgc	SAT1
1.43951936272422E-250	1.78941831362287	0.619	0.021	2.83700476005688E-246	hc/ac	TFAP2A
1.07916254507875E-179	1.16821826326153	0.571	0.03	2.1268135438412E-175	hc/ac	PRDM13
6.36670897473882E-89	0.803338097968129	0.484	0.051	1.25475100474153E-84	hc/ac	BARHL2
1.61070590492872E-80	0.439611847910829	0.286	0.017	3.17437919743353E-76	hc/ac	PTGFR

2.8293086949641E-61	1.16167923360779	0.944	0.44	5.57600157603524E-57	hc/ac	ONECUT2
1.16228379969261E-60	1.07143760136788	1	0.988	2.2906289124342E-56	hc/ac	SOX4
1.23456472986471E-60	0.65834441893736	0.325	0.033	2.43308016961736E-56	hc/ac	SPATS2L
1.56164803033879E-54	0.662264321778215	0.389	0.054	3.07769593819169E-50	hc/ac	NDST3
1.24336512000459E-52	0.653353192499799	0.397	0.059	2.45042397850504E-48	hc/ac	ONECUT3
1.28930410157304E-47	0.674475005247918	0.27	0.029	2.54096052338015E-43	hc/ac	NPPC
1.57431637321431E-47	1.43905447292851	0.841	0.39	3.10266270833077E-43	hc/ac	ID2
1.21972883458479E-46	0.971662459931208	0.778	0.289	2.40384158719971E-42	hc/ac	LINC00599
1.65626261443858E-46	0.930895015971393	0.468	0.098	3.26416236053555E-42	hc/ac	PROX1
7.29033246405269E-46	1.03334028832232	0.873	0.41	1.4367787220155E-41	hc/ac	HMP19
9.2672618918328E-46	1.14788890128705	0.968	0.874	1.82639197364241E-41	hc/ac	AP1S2
5.34370025613442E-43	0.710524814741188	0.532	0.131	1.05313644647897E-38	hc/ac	PLXNA2
8.08584746974596E-42	0.907570527345245	0.786	0.364	1.59355881933753E-37	hc/ac	TRIB1
1.73920613616476E-38	0.70595091138935	1	0.909	3.42762745315351E-34	hc/ac	PAX6
9.68404134892103E-35	0.984539251362921	0.667	0.272	1.90853086904536E-30	hc/ac	ONECUT1
3.7731686906161E-30	0.770625020416335	0.738	0.336	7.43616085546621E-26	hc/ac	RUNX1T1
5.81081708746575E-30	0.45231552926271	1	1	1.14519583159775E-25	hc/ac	MALAT1
7.35289990638764E-29	0.766865791920874	0.873	0.496	1.44910951355088E-24	hc/ac	CELF4
1.34046247551194E-28	0.617603951910548	0.254	0.042	2.64178344673893E-24	hc/ac	RP11-834C
7.59046978821108E-28	0.635824012554019	0.96	0.844	1.49592978586064E-23	hc/ac	APLP1
3.21370056035187E-27	0.754858206657841	0.73	0.401	6.33356106434146E-23	hc/ac	RP11-96L1
5.27922947089868E-27	0.685117826714794	1	0.872	1.04043054412471E-22	hc/ac	STMN2
8.92703574379214E-26	0.582160705017501	0.984	0.883	1.75934020438656E-21	hc/ac	ETFB
2.25864219433296E-25	0.595325983565537	0.714	0.381	4.45133203659139E-21	hc/ac	MIR124-2H
1.84354522978167E-23	0.588302052683208	0.929	0.886	3.63325893885371E-19	hc/ac	CXXC5
7.6301784496031E-23	0.622888964543399	0.524	0.215	1.50375556884778E-18	hc/ac	SULF2
1.42005162089178E-22	0.57802375304264	0.881	0.839	2.79863773445352E-18	hc/ac	NREP
2.33240164773208E-20	0.46887281541186	0.341	0.104	4.59669716735039E-16	hc/ac	MIR181A1
1.56405312515074E-18	0.424044017139088	0.302	0.086	3.08243589904709E-14	hc/ac	KIRREL2
1.86896984460395E-17	0.542777984515686	0.254	0.066	3.68336576974547E-13	hc/ac	GATM
4.32955127406391E-17	0.634496318403704	0.468	0.204	8.53267965092515E-13	hc/ac	NTRK1
2.22027439372869E-16	0.442930833940306	0.944	0.848	4.37571677516051E-12	hc/ac	RORB
4.75544626095882E-16	0.436000304389033	0.27	0.078	9.37203349109764E-12	hc/ac	GFRA2
9.88997599075114E-16	0.505966058459649	0.921	0.689	1.94911646825724E-11	hc/ac	STMN4
1.37721946373384E-15	0.472354008262461	0.921	0.837	2.71422411912665E-11	hc/ac	PHYHIPL
4.18924154121727E-15	0.590379660459171	0.81	0.567	8.25615722943099E-11	hc/ac	RTN1

1.18247344566339E-14	0.467363889038992	0.373	0.148	2.3304186667134E-10	hc/ac	GRIA2
1.59487854782199E-14	0.501457718474291	0.849	0.608	3.14318664204758E-10	hc/ac	RAB3A
2.22540609278369E-14	0.432681096220697	0.96	0.857	4.38583032765809E-10	hc/ac	BASP1
2.45850564357973E-14	0.476440697961974	0.556	0.287	4.84522292236692E-10	hc/ac	PLPPR1
8.32410759149105E-14	0.503405140519656	0.683	0.519	1.64051512413106E-09	hc/ac	CCDC88A
2.17194824482379E-13	0.467592416338307	0.937	0.882	4.28047560089872E-09	hc/ac	MAB21L1
2.172922737047E-13	0.461086293846521	0.373	0.161	4.28239613017224E-09	hc/ac	SYBU
2.23402080894794E-13	0.457457212161397	0.738	0.589	4.40280821027459E-09	hc/ac	KIF3A
5.64556816452575E-13	0.511171248513328	0.73	0.548	1.11262857386473E-08	hc/ac	EFNA5
1.3244941145329E-12	0.525280453987737	0.714	0.473	2.61031300092145E-08	hc/ac	SYT4
1.87194847328506E-12	0.435365964447171	0.524	0.265	3.68923605115021E-08	hc/ac	NHLH2
7.45471256648686E-12	0.440967719323541	0.841	0.735	1.46917475260323E-07	hc/ac	ZNF385A
2.27138899977092E-11	0.494729949512903	0.54	0.341	4.47645344074853E-07	hc/ac	ZNF385D
8.61157774625013E-11	0.582086096178076	0.619	0.469	1.69716974223097E-06	hc/ac	MPPED2
1.05516004076964E-10	0.426740946359195	0.595	0.395	2.0795094083488E-06	hc/ac	ALDOC
1.12109288389327E-10	0.476593387843725	0.579	0.405	2.20944985557685E-06	hc/ac	STARD4-AS
1.17968780799667E-10	0.52515853039489	0.595	0.475	2.32492873199984E-06	hc/ac	ZEB2
3.45446802528039E-09	0.491278589806603	0.437	0.261	6.80806558422258E-05	hc/ac	ESRRG
5.78728428899831E-09	0.454149890038537	0.992	0.993	0.000114055798767579	hc/ac	ENO1
9.89350807203226E-09	0.429864219642505	0.675	0.585	0.000194981257083612	hc/ac	FAM215B
1.89743336030902E-08	0.493550502122391	0.286	0.134	0.000373946166649702	hc/ac	LRRN3
4.52915120833721E-08	0.598354360147042	0.627	0.587	0.000892605120139098	hc/ac	HIF1A
2.0161737778086E-07	0.413861453004126	0.373	0.228	0.00397347528130519	hc/ac	CTD-2008L
2.06404879350472E-07	0.415052321722004	0.722	0.722	0.00406782736223911	hc/ac	TPM3
3.83747496262694E-07	0.538433527699976	0.778	0.708	0.00756289565634518	hc/ac	FAM162A
8.088053121027E-07	0.447019071808157	0.635	0.554	0.01593993509092	hc/ac	PDLIM4
1.68248737987099E-66	1.39239449977265	0.981	0.754	3.31584612824975E-62	stem_cells	SLC2A1
1.00044477856205E-59	1.21296465076215	1	0.826	1.97167656959009E-55	stem_cells	VIM
1.19158351570964E-59	0.860952117950643	0.535	0.109	2.34837279276057E-55	stem_cells	ADM
1.47715070002665E-59	0.608561164045279	1	0.998	2.91116859961252E-55	stem_cells	RPL41
3.42708282703851E-59	0.609434557257256	0.619	0.154	6.75409483552749E-55	stem_cells	CASP7
2.31548469745719E-57	0.711460547098557	0.71	0.209	4.56335724174862E-53	stem_cells	SPAG4
9.80294464706764E-56	0.564633374710777	1	0.998	1.93196433104409E-51	stem_cells	RPL31
1.12573309762104E-55	0.497460255189087	1	0.998	2.21859478879155E-51	stem_cells	RPL35A
1.77046506156073E-54	0.527283222550154	1	1	3.48923254332389E-50	stem_cells	RPL13
3.04702755020133E-54	0.574663767420803	1	0.999	6.00508189593679E-50	stem_cells	RPS18

7.35531115408049E-53	0.616749582182697	0.994	0.989	1.44958472224618E-48	stem_cells	NPM1
4.99714949212476E-52	0.804020203681976	0.742	0.271	9.84838291907948E-48	stem_cells	PLOD2
5.27807021007884E-52	0.864377336267267	0.871	0.432	1.04020207700234E-47	stem_cells	P4HA1
1.16641415019801E-51	0.470546150283485	1	0.997	2.29876900721023E-47	stem_cells	RPL21
1.09324545977373E-50	0.483527314203788	1	0.996	2.15456815212207E-46	stem_cells	RPL9
3.70215831163558E-50	0.779714411874147	1	0.993	7.29621360057141E-46	stem_cells	ENO1
3.88003640935094E-50	0.498990826029009	1	0.999	7.64677575554882E-46	stem_cells	RPS15A
5.36484984857933E-50	0.526736150106154	1	0.999	1.05730460815801E-45	stem_cells	RPL7
1.42131985962386E-49	0.514969716691688	1	0.995	2.80113717934671E-45	stem_cells	RPL36
3.48670495521364E-49	0.499007812168142	1	1	6.87159812573505E-45	stem_cells	RPS19
5.73930687997399E-49	0.514348738432574	1	0.997	1.13110259990527E-44	stem_cells	RPL5
3.59604626854513E-48	0.522337417242754	1	0.997	7.08708798604874E-44	stem_cells	RPS8
1.90983607376843E-47	0.706475279938447	0.994	0.951	3.76390493418282E-43	stem_cells	ZFAS1
5.69213371999177E-47	0.446420694111023	1	0.999	1.12180571353598E-42	stem_cells	RPS27
1.2749063461665E-46	0.439669294057021	1	0.996	2.51258542702494E-42	stem_cells	RPS29
2.9012073790529E-46	0.426745156243833	1	0.999	5.71769950263746E-42	stem_cells	RPS14
8.45234934513182E-46	0.778688877172967	0.852	0.304	1.66578900893858E-41	stem_cells	HES1
2.42672484106741E-45	0.460038903693688	1	0.997	4.78258931677564E-41	stem_cells	RPL39
6.60253198574764E-45	0.654631398534076	1	0.986	1.30122700375115E-40	stem_cells	ALDOA
7.6562024801908E-45	0.434084997722131	1	1	1.508884384796E-40	stem_cells	RPS23
1.29178074661243E-44	0.470882866559025	1	0.997	2.54584149542378E-40	stem_cells	RPS27A
1.57431999676522E-44	0.443955843290733	1	1	3.10266984962489E-40	stem_cells	RPS2
1.72955597153543E-44	0.513927907634011	1	0.996	3.40860890870202E-40	stem_cells	RPS12
4.34700160065309E-44	0.423566248429181	1	0.999	8.5670707545671E-40	stem_cells	RPL32
4.77834170505954E-44	1.0873553747212	0.961	0.646	9.41715583233135E-40	stem_cells	FOS
6.33515289023249E-44	0.412733348963522	1	0.999	1.24853193160702E-39	stem_cells	RPL34
8.02249823505822E-44	0.504812822292909	0.458	0.105	1.58107395216527E-39	stem_cells	ESPN
1.01230631176351E-43	0.787521954939318	0.561	0.159	1.99505327922354E-39	stem_cells	ZFP36
4.56219594848503E-43	0.73217255522657	0.806	0.378	8.9911757752743E-39	stem_cells	INSIG2
5.87013517902919E-43	0.450122034085345	1	0.996	1.15688624108307E-38	stem_cells	RPL26
4.01667895414379E-42	0.450388045890142	1	0.999	7.91607088282659E-38	stem_cells	RPS3A
5.90523964268419E-42	0.448151456792128	1	0.998	1.1638046287802E-37	stem_cells	RPL10A
1.04814801926193E-41	0.41150096448709	1	0.999	2.06569011636141E-37	stem_cells	RPL3
1.15755680124603E-41	0.792003290767777	0.942	0.524	2.28131294389567E-37	stem_cells	PTH2
2.05423965040811E-41	0.448769934783282	1	0.997	4.0484955030243E-37	stem_cells	RPL30
5.07101680671082E-41	0.601884878233793	0.742	0.288	9.99395992266568E-37	stem_cells	EMP3

5.53676861145617E-41	0.485357138291838	1	0.997	1.09118635794578E-36	stem_cells	RPLP0
6.72957641215386E-41	0.776843061658034	0.897	0.599	1.32626491930728E-36	stem_cells	SNHG7
3.08109980435995E-40	0.442240034296484	1	0.998	6.07223149443258E-36	stem_cells	RPS7
5.10621549126818E-40	0.452341267798857	1	0.996	1.00633294901913E-35	stem_cells	RPS17
8.0468752735395E-40	0.516181815878437	0.69	0.248	1.58587817890916E-35	stem_cells	FKBP10
1.019735165514E-39	0.764765559149871	0.974	0.483	2.009694064195E-35	stem_cells	ZFP36L1
1.08698981438388E-39	0.421081286017832	0.426	0.098	2.14223952618776E-35	stem_cells	MDFI
2.43947064295157E-39	0.760508169139452	0.942	0.522	4.80770874312895E-35	stem_cells	TTYH1
3.10122989946296E-39	0.458030998478947	1	0.998	6.1119038858616E-35	stem_cells	RPS24
5.69707319590584E-39	0.594127057904836	0.652	0.221	1.12277918544912E-34	stem_cells	STC2
5.96387583730217E-39	0.676864889471821	0.594	0.207	1.17536065001551E-34	stem_cells	ZFP36L2
7.61449716284014E-39	0.464920620366912	1	0.994	1.50066510085253E-34	stem_cells	RPS20
8.57517264181855E-39	0.467523416213325	1	0.994	1.6899950242496E-34	stem_cells	RPL12
3.43731720012906E-37	0.41667041527781	1	0.999	6.77426473801435E-33	stem_cells	RPS15
4.23101917247487E-37	0.795596769859095	0.935	0.55	8.33849258511347E-33	stem_cells	EGR1
6.85438902400119E-37	0.707667795487063	0.69	0.283	1.35086298885015E-32	stem_cells	DDIT3
8.66597568600859E-37	0.470932504031022	1	0.999	1.70789048819857E-32	stem_cells	RPS6
9.33593477480798E-37	0.67482292956253	0.974	0.699	1.83992602541916E-32	stem_cells	FAM162A
2.74157432484221E-36	0.523002180652145	0.484	0.133	5.40309467939902E-32	stem_cells	EGR2
1.36558449358865E-35	0.577645149095339	0.71	0.303	2.69129391996452E-31	stem_cells	CDCA7L
1.7734131976337E-35	0.561978231841783	1	0.997	3.49504272989651E-31	stem_cells	EIF1
6.57083917013807E-35	0.637971873635276	0.981	0.749	1.29498098365081E-30	stem_cells	LMAN1
4.65723596503309E-34	0.665766189683438	1	0.889	9.17848063988721E-30	stem_cells	BNIP3
9.49573149297882E-33	0.469947633025536	0.658	0.253	1.87141876263627E-28	stem_cells	AK4
3.68048456440336E-32	0.831177652775781	0.923	0.752	7.25349897952615E-28	stem_cells	DDIT4
9.22213144242256E-32	0.435038997149455	0.994	0.985	1.81749766467264E-27	stem_cells	RPL36A
1.04110654632446E-31	0.702108443925639	0.974	0.644	2.05181278149625E-27	stem_cells	SFRP2
2.73673842004498E-31	0.701786639476783	0.903	0.495	5.39356407822465E-27	stem_cells	SPP1
1.00220892322097E-30	0.62629198917451	0.903	0.573	1.97515334588389E-26	stem_cells	NPC2
1.04701970279832E-30	0.484123604422494	0.994	0.89	2.06346643027493E-26	stem_cells	RPL17
6.731832237041E-30	0.542169858477775	0.703	0.319	1.32670949727604E-25	stem_cells	TIMP1
1.66540879880465E-29	0.840613685662336	0.884	0.541	3.2821876606842E-25	stem_cells	JUNB
3.45410787386705E-29	0.460253285471862	1	0.998	6.80735579781718E-25	stem_cells	FTL
5.85873311553102E-29	0.72049350374087	0.961	0.754	1.15463912240885E-24	stem_cells	IER2
9.43441615347494E-29	0.558600854717945	0.942	0.829	1.85933473552684E-24	stem_cells	CCNG1
4.01158154083963E-28	0.4502805428948	0.555	0.219	7.90602490068674E-24	stem_cells	CMBL

6.73615704504571E-28	0.640190447989034	0.91	0.541	1.32756183043761E-23	stem_cells	SOX2
8.75480601853914E-28	0.537424234065376	0.748	0.39	1.72539717013369E-23	stem_cells	NUDT4
1.3155070530782E-27	0.601502746132573	0.619	0.247	2.59260130020651E-23	stem_cells	FOSB
2.99169969667063E-27	0.619985933296654	0.839	0.564	5.89604176219848E-23	stem_cells	EPB41L4A-
5.76904081697109E-27	0.430714788510074	0.987	0.964	1.13696256420866E-22	stem_cells	EIF3E
1.02828901060486E-26	0.664531595701687	0.955	0.757	2.02655198210005E-22	stem_cells	DKK 3.00
2.09659167105562E-26	0.481748743976213	0.652	0.296	4.13196286531643E-22	stem_cells	PLA2G16
6.68372532842484E-26	0.437400322742041	0.652	0.279	1.31722858772597E-21	stem_cells	VSX2
8.12876005833901E-26	0.45864135018494	0.652	0.289	1.60201603229745E-21	stem_cells	CDH11
8.80558544179484E-26	0.447315061677368	0.981	0.92	1.73540477886893E-21	stem_cells	EEF1D
2.67609224809629E-25	0.491123516640224	0.987	0.903	5.27404260254816E-21	stem_cells	C4orf3
3.6374421650779E-25	0.455256377999377	0.903	0.743	7.16867101893552E-21	stem_cells	IMPDH2
6.66107759498825E-25	0.488321254193129	0.987	0.965	1.31276517242028E-20	stem_cells	PGK 1.00
8.98515609343261E-25	0.483711769731571	0.665	0.291	1.7707945628937E-20	stem_cells	COL2A1
1.11701180891546E-24	0.534712880161376	0.929	0.783	2.20140687301058E-20	stem_cells	C6orf48
1.97734813371896E-24	0.475767904664363	0.935	0.811	3.89695770193332E-20	stem_cells	AC090498.
1.02568923882322E-23	0.599217715377384	0.903	0.597	2.0214283518728E-19	stem_cells	CYP1B1
2.36750337857929E-23	1.0017007283071	0.742	0.406	4.66587565850407E-19	stem_cells	CYP26A1
6.391061110083016E-23	0.412207686377862	0.735	0.354	1.25955032175161E-18	stem_cells	PLPP3
8.12175876658473E-23	0.67291445416429	0.865	0.639	1.60063621771852E-18	stem_cells	GPI
8.46423919010057E-23	0.768740298510723	0.613	0.278	1.66813225958502E-18	stem_cells	CYR61
1.19066517878656E-22	0.446140000968752	0.91	0.712	2.34656293435256E-18	stem_cells	RSL1D1
2.34951929082048E-22	0.538656256249581	0.755	0.519	4.63043261834901E-18	stem_cells	SNHG8
1.22686022088094E-21	0.54557682065704	0.858	0.652	2.41789612331217E-17	stem_cells	SLC3A2
1.3391143910732E-21	0.483162315048431	0.723	0.358	2.63912664192706E-17	stem_cells	SPARC
1.72219491478493E-21	0.428963059931672	0.89	0.668	3.39410173805814E-17	stem_cells	QPRT
3.72139011245266E-20	0.60139319000255	0.929	0.776	7.33411563362171E-16	stem_cells	NEAT1
3.88426094105512E-20	0.483116928588187	0.548	0.256	7.65510146263144E-16	stem_cells	HLA-B
4.0370406158388E-20	0.441045061173744	0.942	0.816	7.95619964569511E-16	stem_cells	BTG1
8.62412050711451E-20	0.620790812460634	0.51	0.218	1.69964166954213E-15	stem_cells	LAMP5
1.25641174311505E-19	0.42096921080622	0.471	0.197	2.47613626333114E-15	stem_cells	CLRN1
1.64912141414722E-18	0.504117442150949	0.826	0.569	3.25008848300135E-14	stem_cells	NR2F1
4.09706044745948E-18	0.416565985381075	0.71	0.405	8.07448672985314E-14	stem_cells	RHOC
8.48446363904978E-18	0.429326031283402	0.968	0.764	1.67211809398393E-13	stem_cells	PRDX6
1.8122949795717E-17	0.794553044559105	0.723	0.46	3.5716709457399E-13	stem_cells	HSPB1
5.600335339328E-17	0.484385873539845	0.465	0.205	1.10371408867476E-12	stem_cells	PLK2

5.62461871528052E-17	0.424833383304525	0.832	0.626	1.10849985640749E-12	stem_cells	PNRC1
5.6993070907443E-17	0.458284613175961	0.284	0.088	1.12321944144389E-12	stem_cells	TRIB3
7.35984173920231E-17	0.537640450788067	0.652	0.411	1.45047760996199E-12	stem_cells	HILPDA
9.75579992952015E-17	0.407812796932079	0.742	0.484	1.92267305010983E-12	stem_cells	MYADM
1.13605091437702E-16	0.412093785283506	0.671	0.411	2.23892914205423E-12	stem_cells	TAF1D
3.2908210360562E-16	0.453467920029592	0.432	0.191	6.48555009785955E-12	stem_cells	APOE
3.7380817210291E-16	0.696804710888032	0.91	0.795	7.36701145580415E-12	stem_cells	JUN
8.39729866029222E-16	0.583045279334468	0.419	0.179	1.65493961997039E-11	stem_cells	ATF3
3.29184093565238E-15	0.435155595706156	0.529	0.269	6.48756011598372E-11	stem_cells	HLA-DRB1
3.98257580537189E-15	0.52397715329344	0.787	0.55	7.84886039722692E-11	stem_cells	HERPUD1
1.21440204967507E-13	0.446208568031257	0.684	0.471	2.39334355949963E-09	stem_cells	SLC16A1
4.53958342162456E-13	0.522808451778494	0.632	0.427	8.94661100733769E-09	stem_cells	SQSTM1
5.4423529753697E-12	0.459202949621829	0.677	0.412	1.07257892438586E-07	stem_cells	ID3
8.34396441610571E-12	0.511028101125693	0.4	0.192	1.64442850712611E-07	stem_cells	PLP1
1.44512206349179E-10	0.435651393829041	0.671	0.445	2.84804656272963E-06	stem_cells	ID1

SupTable 4 GFP DEG10

p_val	avg_logFC	pct.1	pct.2	p_val_adj	cluster	gene
7.9755606001145E-273	1.40687509154545	0.994	0.774	1.52412963068188E-268	progenitors	SFRP2
2.49792717412938E-215	1.10792614355096	0.979	0.679	4.77353882976125E-211	progenitors	CCND1
1.85787725777464E-183	1.02937240932241	0.917	0.527	3.55040343960734E-179	progenitors	IFITM3
7.4066933197728E-179	0.819761985581814	0.976	0.648	1.41541909340858E-174	progenitors	ZFP36L1
9.07551000912606E-155	0.884976464884904	0.994	0.326	1.79432996274399E-150	progenitors	IFITM2
5.76141481742139E-154	0.799704968799598	0.94	0.567	1.10100637160923E-149	progenitors	SPP1
6.64350211498513E-148	0.840515644141872	0.996	0.969	1.26957325417366E-143	progenitors	TUBA1B
4.98192161231705E-75	0.875412079859905	0.733	0.414	9.52045220113788E-71	progenitors	ID3
3.7046619019519E-64	0.798452198708058	0.521	0.202	7.07960889463007E-60	progenitors	TOP2A
1.85546245477534E-31	0.814642413278677	0.935	0.873	3.54578875107567E-27	progenitors	HIST1H4C
7.2954676474322E-155	1.59801553415597	0.866	0.05	1.39416386742429E-150	existing_progenitors	VSX1
1.03911716785467E-64	2.12932606929404	0.896	0.173	1.98575290777027E-60	existing_progenitors	NEUROD1
1.24149239692652E-47	1.40548563638122	0.985	0.295	2.37249197052657E-43	existing_progenitors	GADD45A
1.46083426287943E-43	2.63111846143287	1	0.588	2.79165427636259E-39	existing_progenitors	HES6
4.82477763184945E-39	1.56099638527471	1	0.999	9.2201500544643E-35	existing_progenitors	CKB
1.08268544410143E-38	1.41338645627875	0.985	0.386	2.06901188367782E-34	existing_progenitors	TOP2A
1.41196897993069E-34	1.47472975445024	1	0.82	2.69827272064755E-30	existing_progenitors	HMGB2
6.04793414891691E-34	1.62890152812534	0.925	0.393	1.15576021585802E-29	existing_progenitors	UBE2C
1.2588052172725E-31	1.47249990993975	0.94	0.46	2.40557677020775E-27	existing_progenitors	UBE2S
2.45762647695137E-19	1.52401547361851	1	0.909	4.69652419745406E-15	existing_progenitors	HIST1H4C
1.58465566595118E-106	1.23781838970503	0.781	0.136	3.02827697763271E-102	neuroblasts	RASD1
2.07794986521511E-86	1.76935434095007	0.907	0.315	3.97096219242608E-82	neuroblasts	RGS16
5.83735191721759E-83	1.80571880822077	0.861	0.28	1.11551795138028E-78	neuroblasts	GADD45A
1.36643906209204E-71	1.45433707165045	0.993	0.805	2.61126504765789E-67	neuroblasts	SH3BGRL3
1.95708713178716E-71	1.03370974860396	1	0.992	3.73999350884525E-67	neuroblasts	RBP1
9.30910987572058E-66	1.86753029882987	0.967	0.577	1.7789708972502E-61	neuroblasts	HES6
4.03321739470783E-65	1.6520567018224	0.695	0.195	7.70747844128665E-61	neuroblasts	RP3-395M20.12
1.00948029377479E-52	2.70905334751122	0.596	0.163	1.92911684140362E-48	neuroblasts	GAL
8.11922275965311E-46	1.39163024172413	0.894	0.589	1.55158346936971E-41	neuroblasts	TRH
1.3582387027706E-34	1.21826979255327	0.384	0.089	2.59559416099461E-30	neuroblasts	CLDN5
0	2.53809497444755	0.891	0.016	0	photoreceptors	DCT
0	1.79281106208741	0.832	0.018	0	photoreceptors	PRDM1
1.79493797776546E-196	1.98740664572594	0.653	0.024	3.4301264755098E-192	photoreceptors	RCVRN
6.4160580545524E-183	1.75792736202719	0.792	0.049	1.22610869422496E-178	photoreceptors	GNB3
1.03472421379948E-112	1.62778005261522	0.871	0.125	1.9773579725708E-108	photoreceptors	SEPT4
9.85220748449355E-109	1.98729829403436	0.95	0.161	1.88275685028672E-104	photoreceptors	NEUROD1
5.41587624456727E-93	1.97736147740527	0.931	0.216	1.0349739503368E-88	photoreceptors	PHLDA1
2.98941308612055E-92	1.66753426505955	0.812	0.126	5.71276840757638E-88	photoreceptors	SSTR2

2.79256254814977E-90	2.32822297749944	1	0.301	5.33658702951421E-86	photoreceptors	FAM57B
2.79670025374746E-65	1.84728491349718	1	0.537	5.3444941849114E-61	photoreceptors	PCBP4
6.83826479193271E-283	1.74475653920269	0.876	0.063	1.30679240173834E-278	rgc	NEFM
1.21117925290698E-253	1.60314977443565	0.742	0.043	2.31456355230524E-249	rgc	ELAVL4
4.21051803814329E-197	1.61871436608795	0.732	0.07	8.04629997089184E-193	rgc	NEFL
4.54528126733512E-169	1.86078476725769	0.919	0.178	8.68603250187741E-165	rgc	SNCG
bioRxiv preprint doi: https://doi.org/10.1101/2020.10.27.258125 ; this version posted November 9, 2020. The copyright holder for this preprint (which was not certified by peer review) is the author/funder. All rights reserved. No reuse allowed without permission.						
6.25881677744711E-100	2.59361590262807	0	0.001	1.11926776854106E-99C	rgc	NSG1
7.88674169471337E-143	2.46425886392925	0.952	0.331	1.50715633785973E-138	rgc	GAP43
5.18627711382802E-142	1.94591534625095	0.603	0.068	9.91097556452535E-138	rgc	PRPH
1.27579741404468E-132	1.6192275686326	0.967	0.338	2.43804885823938E-128	rgc	TAGLN3
1.28574486485278E-130	2.21079637469672	0.995	0.426	2.45705843673367E-126	rgc	STMN2
4.61190659072856E-99	1.58325292053938	0.976	0.644	8.81335349488229E-95	rgc	TUBB2A
2.34856100902955E-258	1.9415508564384	0.652	0.011	4.48810008825547E-254	hc/ac	TFAP2A
4.01413646679045E-123	1.76249219831456	0.957	0.132	7.67101478803654E-119	hc/ac	ONECUT2
3.97561951181722E-99	1.3497925095472	0.707	0.076	7.59740888708271E-95	hc/ac	HMP19
1.20881240855296E-61	1.22079022460648	0.63	0.099	2.31004051274471E-57	hc/ac	ONECUT1
4.59065478460819E-60	2.12190030735959	1	0.451	8.77274129338626E-56	hc/ac	STMN2
2.15654880866339E-52	1.73862906000784	1	0.977	4.12116477335574E-48	hc/ac	SOX4
3.08417096870498E-45	1.21129892303644	1	0.876	5.89385072119522E-41	hc/ac	MLLT11
1.0126107081594E-36	1.22880326073114	0.967	0.848	1.93509906329262E-32	hc/ac	AP1S2
2.81432353183936E-32	1.20097554358389	0.924	0.587	5.37817226934501E-28	hc/ac	ID2
4.6942112596226E-32	1.27061487486526	0.837	0.419	8.9706377171388E-28	hc/ac	STMN4
5.23425939472817E-151	1.14155452016634	0.995	0.915	1.00026697033255E-146	stem_cells	SLC2A1
1.87761454988888E-140	1.08937888613719	0.834	0.299	3.58812140483764E-136	stem_cells	STC2
2.77590027316862E-136	1.18549703280372	0.968	0.789	5.30474542202523E-132	stem_cells	GPI
1.39749757548281E-129	0.956761975856372	0.91	0.461	2.67061786674765E-125	stem_cells	INSIG2
8.21286962102296E-124	1.14328670467328	0.985	0.768	1.56947938457749E-119	stem_cells	DDIT4
8.63568118614085E-124	0.933003209699659	0.971	0.694	1.65027867467152E-119	stem_cells	P4HA1
1.38799681730411E-120	0.918667371961046	0.787	0.263	2.65246191786815E-116	stem_cells	NRN1
5.60507060033651E-114	0.958886841325971	0.895	0.507	1.07112899172431E-109	stem_cells	PLOD2
1.43866432066906E-95	1.0879783356735	0.861	0.559	2.74928751679858E-91	stem_cells	HILPDA
1.14892702959881E-80	0.938827359825493	0.802	0.476	2.19559955356332E-76	stem_cells	HERPUD1

SupTable 5 AEP DEG10

p_val	avg_logFC	pct.1	pct.2	p_val_adj	cluster	gene
6.39573942155995E-271	1.80017474019716	0.953	0.315	1.17182737681821E-266	progenitors	IFITM3
2.77180252852078E-262	1.95164088218322	0.984	0.575	5.07849659275577E-258	progenitors	SFRP2
2.73807012392059E-253	1.44337180480181	0.96	0.328	5.0166920810473E-249	progenitors	ZFP36L1
9.51532528948643E-242	1.43313963944759	0.885	0.206	1.7433978995397E-237	progenitors	IFITM2
9.4886297721164E-238	1.27200952559519	0.999	0.866	1.7385067468463E-239	progenitors	VIM
1.79464429574571E-226	1.17531169252608	0.965	0.36	3.28814727866529E-222	progenitors	TTYH1
4.16180920452147E-224	1.41824425120026	0.972	0.448	7.62526682452424E-220	progenitors	CCND1
1.58397835401464E-215	1.21337205474433	0.862	0.205	2.90216514022563E-211	progenitors	SPARC
5.96497905353651E-190	1.35613068953389	0.938	0.485	1.09290346218896E-185	progenitors	CYP1B1
3.85262260187086E-164	1.30534936143499	0.8	0.222	7.05877513114779E-160	progenitors	CYP26A1
3.24944976314277E-76	1.20598430460788	0.59	0.075	5.95364185603018E-72	existing_progenitors	VSX1
7.1348673247806E-57	1.29987975957748	0.902	0.316	1.3072503912463E-52	existing_progenitors	TOP2A
1.07542437130816E-55	1.22589353178636	0.861	0.28	1.97039253311082E-51	existing_progenitors	UBE2C
6.48330311191483E-49	1.1991704912128	0.934	0.517	1.18787079616503E-44	existing_progenitors	SMC4
4.20441488419837E-43	1.38336128533363	1	0.997	7.70332895082825E-39	existing_progenitors	CKB
2.04891166895415E-41	1.21864140609545	0.967	0.931	3.7540159598578E-37	existing_progenitors	HMGN2
1.16260164382321E-40	1.39816044459392	0.91	0.677	2.13011873181288E-36	existing_progenitors	HMGB2
1.12278064821554E-35	2.31057854494181	0.836	0.665	2.05715870366051E-31	existing_progenitors	HES6
6.20041520861325E-29	1.65828612519295	0.656	0.293	1.13604007452212E-24	existing_progenitors	NEUROD1
4.90825008538755E-25	1.61095769030704	0.91	0.904	8.99289580644707E-21	existing_progenitors	HIST1H4C
3.80238631583176E-148	1.92035935445039	0.938	0.367	6.96673220786695E-144	neuroblasts	RGS16
7.52013513064403E-101	1.2576381383528	0.984	0.886	1.3778391586366E-96	neuroblasts	SH3BGRL3
2.11331468448761E-93	1.24191233140106	0.954	0.603	3.87201516491819E-89	neuroblasts	CXCR4
2.00740780047695E-77	1.16832909368441	0.801	0.37	3.67797257203388E-73	neuroblasts	GADD45A
2.6701594327663E-72	0.985456908782068	0.889	0.655	4.89226611271441E-68	neuroblasts	PLEKHA1
2.72740805013327E-68	1.03216913098815	0.961	0.72	4.99715702945417E-64	neuroblasts	MIAT
2.39716675218779E-61	0.953813717715007	0.404	0.081	4.39208892335848E-57	neuroblasts	NPTX2
7.17348557059775E-47	1.123359176442	0.485	0.165	1.31432602624492E-42	neuroblasts	RP3-395M20.12
5.71905669120376E-33	0.912768028476612	0.811	0.644	1.04784556696235E-28	neuroblasts	DDIT4
2.2780986964826E-15	2.18878439106377	0.352	0.189	4.17393243169542E-11	neuroblasts	GAL
1.32281477626319E-238	2.24286358839265	0.768	0.014	2.42366123306941E-234	photoreceptors	DCT
1.9255751452955E-164	1.75679765800481	0.695	0.025	3.52803878121042E-160	photoreceptors	PRDM1
3.83865615277828E-151	1.45688916442888	0.817	0.046	7.03318580312036E-147	photoreceptors	OTX2
6.20711003228119E-138	1.74044750000154	0.476	0.01	1.13726670011456E-133	photoreceptors	RCVRN
2.7800971429975E-104	1.45588816611958	0.707	0.059	5.09369398540002E-100	photoreceptors	GNB3
1.00597507140801E-60	1.82815049566438	0.878	0.218	1.84314752583376E-56	photoreceptors	PHLDA1
2.88033389114746E-56	1.48515343225882	0.939	0.272	5.27734775536037E-52	photoreceptors	GADD45G
1.81538136733053E-50	1.98287380925581	0.963	0.432	3.32614174122299E-46	photoreceptors	FAM57B

5.6333511734969E-47	1.66329792428303	0.878	0.291	1.0321426020081E-42	photoreceptors	NEUROD1
6.67364050599618E-37	1.32535107851136	0.805	0.27	1.22274441350862E-32	photoreceptors	SSTR2
4.12885434629089E-294	1.74139838543831	0.892	0.081	7.56488693327417E-290	rgc	ELAVL4
7.36627409341882E-278	1.71048945121131	0.949	0.136	1.3496487393962E-273	rgc	NEFM
1.34088353486753E-257	1.67410573149885	0.875	0.118	2.45676681258428E-253	rgc	NEFL
6.14578460448607E-253	2.39383643489055	0.974	0.277	1.12603065523394E-248	rgc	NSG1
9.416705822245E-256	2.91472061525060885	0.985	0.206	2.5626943808561E-245	rgc	GAP43
2.18222751118301E-215	1.70725969084125	0.963	0.285	3.99827724598952E-211	rgc	SNCG
5.70669595896323E-213	2.0146760642284	0.719	0.075	1.04558083360124E-208	rgc	PRPH
1.03206708508868E-194	1.56429345706391	0.881	0.221	1.89095331329947E-190	rgc	RTN1
8.30031088456194E-184	1.47628228700844	0.982	0.667	1.52078296026944E-179	rgc	TUBB2A
7.7158900020107E-177	1.51416014880798	1	0.618	1.4137053661684E-172	rgc	STMN2
1.1103731610065E-251	2.12263183380489	0.768	0.014	2.03442570559611E-247	hc/ac	TFAP2A
4.54344425863255E-198	1.09574466629866	0.632	0.012	8.32449857066657E-194	hc/ac	PRDM13
5.13187294689624E-76	1.62828437612529	0.884	0.205	9.4026176133033E-72	hc/ac	HMP19
9.04150578804771E-74	1.54629631306233	0.979	0.282	1.6565846904861E-69	hc/ac	ONECUT2
1.39108178050353E-63	1.45040152226063	0.863	0.229	2.54874003823858E-59	hc/ac	ONECUT1
4.26516611959661E-56	1.57486074155381	1	0.97	7.8146373643249E-52	hc/ac	SOX4
1.98117270771394E-52	1.21846345379997	0.874	0.332	3.62990463507348E-48	hc/ac	TRIB1
5.73623597848123E-48	1.49272513533908	0.968	0.86	1.05099315597733E-43	hc/ac	AP1S2
4.46012231278163E-46	1.31429875353724	1	0.688	8.1718361014785E-42	hc/ac	STMN2
1.05670246841988E-39	1.23876554334889	0.947	0.459	1.9360902626389E-35	hc/ac	ID2
4.32921057014761E-39	1.09116962446826	1	0.994	7.93197960662446E-35	stem_cells	ENO1
5.49339183605781E-34	1.2821501454216	0.988	0.721	1.00649925220251E-29	stem_cells	SLC2A1
7.77217718296961E-34	1.01791220033394	0.915	0.444	1.42401830346369E-29	stem_cells	P4HA1
1.39434675614325E-32	0.897913705579275	1	0.973	2.55472212660566E-28	stem_cells	ALDOA
5.34358631991486E-30	1.01166162914946	1	0.93	9.790518855348E-26	stem_cells	PGK 1.00
2.24724302531134E-29	1.02904775671633	1	0.827	4.11739867097544E-25	stem_cells	BNIP3
2.55877799433127E-29	0.995095245716952	0.976	0.67	4.68819304121375E-25	stem_cells	FAM162A
5.68503236876911E-28	1.10359464079105	0.976	0.619	1.04161163060588E-23	stem_cells	GPI
4.7025008989883E-11	0.932198958555707	0.756	0.468	8.61592214712636E-07	stem_cells	CYP26A1
6.12133792825982E-10	1.07289940316878	0.805	0.655	1.12155153521576E-05	stem_cells	LDHA

SupTable 6 NEP DEG10

p_val	avg_logFC	pct.1	pct.2	p_val_adj	cluster	gene	
0	2.15040505118418	0.999	0.526		0	progenitors	SFRP2
0	1.84620823017618	0.853	0.252		0	progenitors	CYP26A1
0	1.7779501569875	0.996	0.312		0	progenitors	ZFP36L1
0	1.69432772775035	0.962	0.278		0	progenitors	IFITM3
bioRxiv preprint doi: https://doi.org/10.1101/2020.10.27.358135 ; this version posted November 9, 2020. The copyright holder for this preprint (which was not certified by peer review) is the author/funder. All rights reserved. No reuse allowed without permission.							
0	1.58805350397293	0.997	0.472		0	progenitors	CCND1
0	1.5118992094342	1	0.769		0	progenitors	VIM
0	1.51158747141804	0.95	0.478		0	progenitors	CYP1B1
0	1.50081898363016	0.886	0.111		0	progenitors	HES1
0	1.43894021706406	0.987	0.366		0	progenitors	TTYH1
1.0584002645718E-208	1.47309084340855	0.776	0.286	2.08589524141811E-204	progenitors	ID3	
9.39016262972125E-122	1.5665779818246	0.91	0.233	1.85061325106546E-117	existing_progenitors	NUSAP1	
5.89479884790682E-113	1.66641195406698	0.938	0.268	1.16174695694548E-108	existing_progenitors	TOP2A	
1.29350913432114E-98	1.67066088043172	0.91	0.27	2.5492478019201E-94	existing_progenitors	CENPF	
1.086617967745E-93	1.89557367559608	0.994	0.623	2.14150669083185E-89	existing_progenitors	HMGB2	
2.50334683364065E-91	1.405817569228	0.96	0.422	4.93359593973899E-87	existing_progenitors	CKS1B	
1.38952887466771E-88	1.39020620894491	0.994	0.903	2.73848350619513E-84	existing_progenitors	HMGN2	
7.82767250167975E-83	1.85265267079734	1	0.794	1.54267769663105E-78	existing_progenitors	HES6	
1.97289656102834E-79	1.85868819317848	0.876	0.344	3.88818454247465E-75	existing_progenitors	UBE2C	
7.0043335639928E-69	1.48098372730913	0.904	0.419	1.3804140587917E-64	existing_progenitors	PTTG1	
4.84999865374688E-42	1.78719991772938	0.944	0.735	9.55837734680436E-38	existing_progenitors	HIST1H4C	
1.16930187145625E-188	0.966624036001392	0.985	0.957	2.30446012826598E-184	neuroblasts	SH3BGRL3	
2.30946768397378E-182	1.15929408515216	0.956	0.733	4.55149891157552E-178	neuroblasts	CXCR4	
7.04199761050279E-179	0.955966843545263	0.984	0.837	1.38783688907789E-174	neuroblasts	MIAT	
1.44450092859416E-135	1.01847166776057	0.849	0.536	2.84682243007337E-131	neuroblasts	GADD45A	
9.45647113032676E-101	1.06573669165747	0.765	0.507	1.8636813303648E-96	neuroblasts	RGS16	
1.70931757053462E-74	0.813698539051603	0.852	0.734	3.36872306800962E-70	neuroblasts	DDIT4	
4.89795774625378E-61	0.946739111301297	0.864	0.788	9.65289512631695E-57	neuroblasts	HES6	
1.12755056010244E-33	1.00097391371338	0.405	0.254	2.22217664384989E-29	neuroblasts	RP3-395M20.12	
2.11577992763031E-21	0.700450123851411	0.391	0.252	4.16977908137382E-17	neuroblasts	IGFBP5	
1.02459238475717E-07	1.5069924112315	0.287	0.233	0.00201926667187942	neuroblasts	GAL	
0	2.42896721596791	0.832	0.041		0	photoreceptors	DCT
0	1.42077576520909	0.864	0.096		0	photoreceptors	OTX2
0	1.39708500678511	0.586	0.026		0	photoreceptors	PRDM1
2.27127159864859E-285	1.72244069569183	0.801	0.115	4.47622206661664E-281	photoreceptors	GNB3	
4.08309335937793E-217	1.7301652160062	0.72	0.117	8.04696039266203E-213	photoreceptors	C8orf46	
8.37752023354786E-212	1.48042568102138	0.895	0.271	1.65104168762761E-207	photoreceptors	SEPT4	
7.21606404542176E-198	1.82800223735372	0.552	0.065	1.42214190207172E-193	photoreceptors	RCVRN	
3.77906501604816E-187	1.58681037681391	0.987	0.673	7.44778133362771E-183	photoreceptors	FAM57B	

1.57294965357472E-176	1.51786999689233	0.869	0.296	3.09996917726505E-172	photoreceptors	PHLDA1
9.21728351610386E-25	1.48935056516302	0.545	0.347	1.81654223535375E-20	photoreceptors	CRABP2
0	1.67866507543497	0.985	0.59	0	rgc	GAP43
0	1.62664244202391	0.915	0.36	0	rgc	NSG1
0	1.40049703856269	0.937	0.429	0	rgc	RTN1
0	1.17520642487855	0.907	0.292	0	rgc	ELAVL4
bioRxiv preprint doi: https://doi.org/10.1101/2020.10.27.258135 ; this version posted November 9, 2020. The copyright holder for this preprint (which was not certified by peer review) is the author/funder. All rights reserved. No reuse allowed without permission.	0	0	0	0	rgc	TUBB2A
0	1.11760455903467	0.998	0.827	0	rgc	STMN2
1.87768401855086E-243	1.12692275958606	0.743	0.214	3.70053966376003E-239	rgc	NEFM
1.30313699795126E-232	1.1381549245492	0.711	0.208	2.56822239556234E-228	rgc	NEFL
1.11683555681864E-194	1.2404999457904	0.788	0.385	2.20105951537818E-190	rgc	SNCG
2.16620330274188E-139	1.36607779037133	0.461	0.122	4.2691534690437E-135	rgc	PRPH
1.43951936272422E-250	1.78941831362287	0.619	0.021	2.83700476005688E-246	hc/ac	TFAP2A
1.07916254507875E-179	1.16821826326153	0.571	0.03	2.1268135438412E-175	hc/ac	PRDM13
2.8293086949641E-61	1.16167923360779	0.944	0.44	5.57600157603524E-57	hc/ac	ONECUT2
1.16228379969261E-60	1.07143760136788	1	0.988	2.2906289124342E-56	hc/ac	SOX4
1.57431637321431E-47	1.43905447292851	0.841	0.39	3.10266270833077E-43	hc/ac	ID2
1.21972883458479E-46	0.971662459931208	0.778	0.289	2.40384158719971E-42	hc/ac	LINC00599
1.65626261443858E-46	0.930895015971393	0.468	0.098	3.26416236053555E-42	hc/ac	PROX1
7.29033246405269E-46	1.03334028832232	0.873	0.41	1.4367787220155E-41	hc/ac	HMP19
9.2672618918328E-46	1.14788890128705	0.968	0.874	1.82639197364241E-41	hc/ac	AP1S2
9.68404134892103E-35	0.984539251362921	0.667	0.272	1.90853086904536E-30	hc/ac	ONECUT1
1.68248737987099E-66	1.39239449977265	0.981	0.754	3.31584612824975E-62	stem_cells	SLC2A1
1.00044477856205E-59	1.21296465076215	1	0.826	1.97167656959009E-55	stem_cells	VIM
1.19158351570964E-59	0.860952117950643	0.535	0.109	2.34837279276057E-55	stem_cells	ADM
4.99714949212476E-52	0.804020203681976	0.742	0.271	9.84838221907948E-48	stem_cells	PLOD2
5.27807021007884E-52	0.864377336267267	0.871	0.432	1.04020207700234E-47	stem_cells	P4HA1
4.77834170505954E-44	1.0873553747212	0.961	0.646	9.41715583233135E-40	stem_cells	FOS
4.23101917247487E-37	0.795596769859095	0.935	0.55	8.33849258511347E-33	stem_cells	EGR1
3.68048456440336E-32	0.831177652775781	0.923	0.752	7.25349897952615E-28	stem_cells	DDIT4
1.66540879880465E-29	0.840613685662336	0.884	0.541	3.2821876606842E-25	stem_cells	JUNB
2.36750337857929E-23	1.0017007283071	0.742	0.406	4.66587565850407E-19	stem_cells	CYP26A1